TECHNISCHE UNIVERSITÄT MÜNCHEN

TUM School of Life Sciences

The role of long noncoding RNA *Ctcflos* in the orchestration of transcription and alternative splicing programs in thermogenic adipogenesis

Andrea Daniela Bast-Habersbrunner

Vollständiger Abdruck der von der TUM School of Life Sciences der Technischen Universität München zur Erlangung des akademischen Grades einer

Doktorin der Naturwissenschaften
(Dr. rer. nat)

genehmigten Dissertation.

Vorsitzende:	Prof. Dr. Nina Henriette Uhlenhaut
Prüfer der Dissertation:	Prof. Dr. Martin Klingenspor
	Prof. Dr. Alexander Bartelt
	Prof. Dr. Jörg Heeren

Die Dissertation wurde am 06.09.2021 bei der Technischen Universität München eingereicht und durch die TUM School of Life Sciences der Technischen Universität München am 19.11.2021 angenommen.

TABLE OF CONTENTS

ABBREVIATIONS

ABSSQ	Abdominal Subcutaneous
ADINR	Adipogenic Differentiation Induced Noncoding RNA
ADIPOQ	Adiponectin
AGPAT2	1-Acylglycerol-3-Phosphate-O-Acyltransferase 2
AIR	Antisense lncRNA
AKS	Arginine Kinase
ANOVA	Analysis of Variance
ASO	Antisense Oligonucleotide
ATF4	Activating Transcription Factor 4
ATGL	Adipose Triglyceride Lipase
ATP	Adenosine Triphosphate
ATP5K/S	ATP Synthase Subunit E/S
BAT	Brown Adipose Tissue
BCA	Bicinchoninic Acid
BLNC1	Brown fat lncRNA 1
BMI	Body Mass Index
BRB-seq	Bulk-RNA Barcoding and Sequencing
Brite	Brown-in-White
BSA	Bovine Serum Albumine
C/EBPα/β/δ	CCAAT/Enhancer-Binding Protein α/β/δ
cAMP	cyclic Adenosine Monophosphate
CAS9	CRISPR associated protein 9
cDNA	complementary Deoxyribonucleic Acid
CELF1	CUGBP Elav-Like Family Member 1
CETP	Cholesteryl Ester Transfer Protein
CIDEA	Cell death-Inducing DNA Fragmentation Factor alpha-like Effector A
CL	CL316243
CLK1	CDC-Like Kinase 1
COX4/7a1/8b	Cytochrome C Oxidase 4/7a1/8b
CPAT	Coding Potential Assessment Tool
CPC2	Coding Potential Calculator 2
CRE	cAMP Response Element
CREB	cAMP Response Element Binding protein
CRISPRa(SAM)	Clustered Regulators Interspaced Short Palindromic Repeats activating (Synergistic Activation Mediator)
CTBP1,2	C-terminal Binding Protein 1,2
CTCFL	CCCTC-Binding Factor (Zink Finger Protein)-like
CTCFLOS	CCCTC-Binding Factor (Zink Finger Protein)-like, Opposite Strand
DAPI	4’,6-Diamidin-2-Phenylindol
dCAS9	dead Cas9
DDBJ	Databank of Japan
DEPC	Diethyl Pyrocarbonate
DMEM	Dulbecco's Modified Eagle Medium
DMSO	Dimethylsulfoxid
DNA	Deoxyribonucleic Acid
dsiRNAs	dicer-substrate short interfering RNA
EBF1/2	Early B Cell Factor 1/2
EDTA	Ethylenediaminetetra-Acetic Acid
EGR1	Early Growth Response 1
EHMT1	Euchromatic Histone Methyltransferase 1
ELAVL1/2/3	ELAV (embryonic lethal, abnormal vision)-Like Protein 1/2/3
ELOVL3	Elongation of Very Long Chain Fatty Acids (FEN1/Elo2, SUR4/Elo3, yeast)-like 3

ENCODE	Encyclopedia of DNA Elements
ESE/ESS	Exonic Splicing Enhancer/Silencer
EV	Empty Vector
eWAT	epididymal White Adipose Tissue
FABP4	Fatty Acid Binding Protein 4
FANTOM	Functional Annotations of the Mammalian Genome
FBS	Fetal Bovine Serum
FCCP	Carbonyl Cyanide-p-Trifluoromethoxyphenylhydrazone
FDR	False Discovery Rate
FGFR2	Fibroblast Growth Factor 2
FIRRE	Functional Intergenic Repeating RNA Element
FHL1	Four and a Half LIM Domains Protein 1
FTO	Fat Mass and Obesity Associated
tGFP	turbo Green Fluorescent Protein
GO	Gene Ontology
GTF2B	General Transcription factor 2B
gWAT	gonadal White Adipose Tissue
H19	H19 imprinted maternally expressed transcript
HNRNP /U/R	Heterogeneous Nuclear Ribonucleoprotein /U/R
HOTAIR	Hox Transcript Antisense Intergenic RNA
HSF1	Heatshock Protein 1
HSL	Hormone Sensitive Lipase
iBAT	inguinal Brown Adipose Tissue
IBMX	Isobutylmethylxanthine
IGG	Immunglobulin G
IMM	Inner Mitochondrial Membrane
IMPA2	Inositol Monophosphatase 2
IMS	Intermembrane Space
INSR	Insulin Receptor
ISE/ISS	Intronic Splicing Enhancer/Intronic Splicing Inhibitor
iWAT	inguinal White Adipose Tissue
KD	Knockdown
KLF4	Kruppel-like Factor 4
KO	Knockout
LINC00473	Long Intergenic Non-protein Coding RNA 473
LPIN1	Lipin 1
LNA	Locked Nucleic Acid
LNC-BATE1/10	Brown Adipose Tissue Enriched Long Non-Coding RNA 1/10
lncRNA	long noncoding RNA
MAP4K4	Mitogen-Activated Protein Kinase Kinase Kinase Kinase 4
MAPK /9	Mitogen-Activated Protein Kinase /9
MBD1	Methyl-CpG-Binding Domain Protein 1
MBNL1	Muscleblind Like Splicing Regulator 1
MEF2C	Myocyte Enhancer Factor 2C
miRNA	micro RNA
MRLN	Myoregulin
mRNA	messenger RNA
mTOR	mechanistic Target of Rapamycin Kinase
MXD1	MAX Dimerization Protein 1
NBEA	Neurobeachin
NC	Nontargeting/Negative Control
NCOR	Nuclear Receptor Corepressor
NDUFA3/S4	NADH:Ubiquinone Oxidoreductase Subunit A3/S4
NDUFAF5	NADH:Ubiquinone Oxidoreductase Complex Assembly Factor 5

NEAT1	Nuclear Paraspeckle Assembly Transcript 1
NFE2L1	Nuclear Factor Erythroid 2 Like 1
NFIA	Nuclear Factor I/A
NOVA1	NOVA Alternative Splicing Regulator 1
NR4A1	Nuclear Receptor Subfamily 4 Group A Member 1
NRG4	Neuregulin 4
ODC	Oxodicarboxylate Carrier
OE	Overexpression
ORO	Oil Red O
p38MAPK	p38 Map Kinase
PAM	Protospacer Adjacent Motif
PARAL1	PPARG Activating RBM14 Associated lncRNA 1
PBP-FUS	RNA-Binding Protein Fused in sarcoma
PBS	Phosphate Buffered Saline
PBST	Phosphate Buffered Saline with Tween
PC	Phase Contrast
PCA	Principle Component Analysis
PCK1	Phosphoenolpyruvate Carboxykinase 1
PCR	Polymerase Chain Reaction
PDE3B	Phosphodiesterase 3B
PEG	Paternally Expressed Genes
PGC1α	Peroxisome Proliferative Activated Receptor γ, Coactivator 1 α
PI3K	Phosphatidylinositol 3-Kinase
piRNA	piwi-associated RNA
PKA	Protein Kinase A
PKCD	Protein Kinase C δ
PPARα/γ	Peroxisome Proliferator Activated Receptor α/γ
PPM1G	Protein Phosphatase, Mg2+/Mn2+ dependent 1G
PRDM16/3	PR Domain Containing 16/3
PREF1	Preadipocyte Factor 1
PTBP1	Polypyrimidine Tract-Binding Protein 1
PYCARD-AS1	PYCARD Antisense RNA 1
qPCR	quantitative Polymerase Chain Reaction
RACE	Rapid Amplification of cDNA Ends
RAP1	Regulated in AdoPogenesis
RAR /β	Retinoid Acid Receptor /β
RBM4/41	RNA Binding Motif Protein 4/41
RBP /J/FUS	RNA Binding Protein /J/Fused in Sarcoma
RIPA	Radio Immunoprecipitation Assay
RMRP	RNA component of Mitochondrial RNAase P
RNA	Ribonucleic Acid
RNAi	RNA interference
RNP	Ribonucleoprotein
Rosi	Rosiglitazone
RPKM	Reads Per Kilobase Per Million Mapped Reads
rRNA	ribosomal RNA
RXRα	Retinoid X Receptor α
SCLAV	Supraclavicular
SD	Standard Deviation
SDHB	Succinate Dehydrogenase Complex, Subunit B, Iron Sulfur
SDS-PAGE	Sodium Dodecyl Sulfate Polyacrylamide Gel Electrophoresis
SFPEL-LPI	Sequence-based Feature Projection Ensemble Learning method-LncRNA-Protein Interaction
sgRNA	single guide RNA

SIRT1	Sirtuin 1
siRNA	small interfering RNA
snoRNA	small nucleolar RNA
sn-RNA	small nuclear RNA
sn-RNP	small nuclear RNP
SRA	Steroid Receptor RNA Activator
SREBF1	Sterol Regulatory Element Binding Transcription Factor 1
SRP40	SR Protein 40
SRPK	SR Protein Kinase
SR-protein	Serine and Arginine-rich Protein
SRSF1/2/5/10	Serine and Arginine-rich Splicing Factor 1/2/5/10
SSC	Saline Sodium Citrate
STE	Sucrose Tris EDTA
SUS	Shortest Unique Sequence
SVF	Stromal Vascular Fraction
TCA	Tricarboxyclic Acid
TF	Transcription Factor
THRβ	Thyroid Hormone Receptor β
TLE3	Transducing-Like Enhancer Protein 3
TOST	Two-One-Sided-T-Test
tRNA	transfer RNA
TSS	Transcriptional Start Site
TUG1	Taurine Upregulated Gene 1
UCP1	Uncoupling Protein 1
UCSC	University of California Santa Cruz
UQCRQ	Ubiquinol-Cytochrome C Reductase, Complex III Subunit VII
UTR	Untranslated Region
VP64	Viral Protein 64
WAT	White Adipose Tissue
WT	Wildtype
XIST	Inactive X Specific Transcripts
YBX1	Y-box Protein 1
ZFP423/516/521	Zink Finger Protein 423/516/521

LIST OF FIGURES

Main Figures

LIST OF TABLES

Main Tables

Supplemental Tables

ABSTRACT

Intensified research into adipose tissue biology, driven by the continuously aggravating obesity pandemic, revealed a profound cellular plasticity and functional diversity of this organ. Thermogenic brown and brown-in-white (brite) adipocytes attain special attention as they involve the capacity to dissociate chemical energy as heat and thus stand in contrast to the predominant energy storing purpose of white adipocytes. In order to evaluate the contribution of thermogenic adipocytes to whole body energy homeostasis, metabolic health and their envisioned use as obesity treatment strategy, it is pivotal to gain a profound understanding of the regulatory routes that govern their development and function. To this end, the so far established, yet incomplete network of protein regulators needs to be complemented by a recently recognized class of potent modulators, the long noncoding RNAs (lncRNAs). LncRNAs are non-protein coding RNA transcripts of at least 200 nucleotides length that have longtime been regarded as transcriptional junk, but in fact comprise a variety of biological functionalities.

In this context, the present thesis utilized the naturally varying, adipocyte-intrinsic propensities of different inbred mouse strains for brite adipocyte recruitment in white adipose tissue (WAT) (browning) to identify lncRNAs of functional relevance in this process. Comparative transcriptome analyses of I) mature brite adipocytes across the five mouse strains, II) differentiated brite adipocytes and undifferentiated cells, and III) mature brite and mature white adipocytes revealed 189 positively regulated lncRNAs of interest. Among them, lncRNA *CCCTC-binding factor (zinc finger protein)-like, opposite strand* (*Ctcflos*) stood out as the top candidate, being additionally induced during brown adipose tissue (BAT) activation and WAT browning *in vivo*. *Ctcflos* could be characterized as non-protein coding, polyadenylated, multi-isoform RNA that is retained in the nucleus and predominantly expressed in adipose tissues. Accordingly, *Ctcflos* loss-of-function studies validated its essential contribution to brite adipogenesis, as *Ctcflos* deficient cells exhibited impaired thermogenic marker gene expression, mitochondrial biogenesis and Uncoupling Protein 1 (UCP1)-mediated uncoupled respiratory capacity. Mechanistic studies revealed *Ctcflos* to act as pleiotropic regulator that orchestrates thermogenic gene expression on two levels. It is essential I) for the transcriptional recruitment of the early core thermogenic regulation program and II) for the modulation of alternative splicing to drive brite adipogenesis. These activities were showcased in *Ctcflos*-dependent transcription and thermogenesis promoting alternative splicing of key browning factor *PR domain containing 16* (*Prdm16*) and adipogenesis-related lncRNA *Nuclear paraspeckle assembly transcript 1* (*Neat1*). Beyond this, genome-wide analyses demonstrated further extensive modulatory influence of *Ctcflos* on both regulatory levels, affecting numerous adipose- and mitochondria-related factors.

Conclusively, the present thesis established a resource for the identification of functional lncRNA regulators in thermogenic adipogenesis. With the characterization of *Ctcflos* it further provides molecular inside into the mechanistic versatility of lncRNAs, acting coordinatively at multiple regulatory levels of gene expression, including transcriptional and post-transcriptional levels. On a broader scale, the present thesis thus emphasizes lncRNAs as critical components in the gene expression regulatory network. A profound understanding of this will be essential for a complete comprehension of thermogenic adipogenesis.

ZUSAMMENFASSUNG

Ausgehend von der weltweit steigenden Prävalenz von Übergewicht, hat vermehrtes wissenschaftliches Interesse an der Fettgewebsbiologie und –pathologie ein neues Licht auf die zelluläre und funktionelle Vielfalt dieses Organs geworfen. Dabei kommt thermogenen braunen und beigen (brite) Adipozyten besondere Aufmerksamkeit zu. Im Gegensatz zur Energie speichernden Funktion weißer Fettzellen besitzen sie die Fähigkeit chemische Nahrungsenergie in Wärme umzuwandeln. Um den Beitrag dieser thermogenen Fettzellen zur Energiehomöostase des Menschen, zu seiner metabolischen Gesundheit und zu ihrem möglichen Einsatz in der Übergewichtsbehandlung bewerten zu können, ist es unerlässlich zu verstehen, wie ihre Entwicklung und Funktion reguliert werden. Das bislang etablierte, aber noch unvollständige Netzwerk regulatorischer Proteine sollte hierzu durch eine weitere Gruppe wirkungsvoller Regulatoren, die langen nicht kodierenden RNAs (lnkRNAs), ergänzt werden. LnkRNAs sind nicht-Protein-kodierende RNA Transkripte von mindestens 200 Nukleotiden Länge, die zunächst als transkriptioneller Ausschuss betrachtet wurden, sich aber im letzten Jahrzehnt als vielfältige Modulatoren zahlreicher biologischer Prozesse erwiesen haben.

Vor diesem Hintergrund nutzt die vorliegende Arbeit die unterschiedliche Fähigkeit verschiedener Mausstämme, beige Fettzellen in weißem Fettgewebe zu rekrutieren (Bräunen), um für diesen Prozess relevante lnkRNAs zu identifizieren. In einer vergleichenden Transkriptomanalyse von I) reifen beigen Adipozyten der fünf Mausstämme, II) differenzierten beigen Adipozyten und proliferierenden Zellen, sowie III) reifen beigen und reifen weißen Fettzellen konnten 189 positiv regulierte lnkRNAs identifiziert werden. Unter ihnen erschien lnkRNA *CCCTC-binding factor (zinc finger protein)-like, opposite strand* (*Ctcflos*) von höchstem Interesse. Die Expression von *Ctcflos* wird sowohl während der Entwicklung beiger Adipozyten *in vitro* reguliert, als auch durch die Aktivierung braunen Fettgewebes und durch das Bräunen weißen Fettgewebes *in vivo* aktiviert. *Ctcflos* konnte als nicht-protein kodierende, polyadenylierte RNA mit verschiedenen Isoformen identifiziert werden, die im Zellkern lokalisiert und vorwiegend in Fettgeweben exprimiert ist. Dementsprechend konnte in *Ctcflos Knockdown* Studien validiert werden, dass *Ctcflos* eine essentielle Funktion in der beigen Adipogenese und ihrer thermogenen Funktion zukommt. *Ctcflos*-defiziente Zellen wiesen eine beeinträchtigte Expression thermogener Markergene, eine reduzierte Mitochondrienbiogenese und eine verminderte Uncoupling Protein 1 (UCP1)-vermittelte entkoppelte Atmung auf. Mechanistische Studien zeigten, dass *Ctcflos* dabei die Expression thermogener Faktoren auf zwei verschiedenen Ebenen koordiniert. Es agiert I) auf transkriptioneller Ebene, um das frühe thermogene Regulationsprogramm zu rekrutieren und II) als Modulator alternativen Spleißens, um die beige Adipogenese zu fördern. Diese Aktivitäten zeigten sich beispielhaft in der *Ctcflos*-abhängigen Transkription und dem Spleißen des Browning-Faktors *PR domain containing 16* (*Prdm16*) und der Adipogenese-assoziierten lnkRNA *Nuclear paraspeckle assembly transcript 1* (*Neat1*). Darüber hinaus weisen genomweite Analysen auf einen weitreichenden modulatorischen Einfluss von *Ctcflos* auf beiden Ebenen hin, der sich auf zahlreiche Adipozyten- und Mitochodrien-bezogene Faktoren auswirkt.

Zusammenfassend stellt die vorliegende Arbeit eine Ressource für die Identifizierung funktioneller lnkRNA-Regulatoren in der thermogenen Adipogenese dar. Mit der Charakterisierung von *Ctcflos* liefert sie zudem einen Einblick in die mechanistische Vielseitigkeit von lnkRNAs, die koordinativ auf verschiedenen regulatorischen Ebenen der Genexpression wirken können, einschließlich der transkriptionellen und post-transkriptionellen Ebene. Im weiteren Sinne betont die vorliegende Arbeit somit die Bedeutung von lnkRNAs als kritische Komponenten im regulatorischen Netzwerk der Genexpression. Ein fundiertes Verständnis darüber wird notwendig sein, um die thermogene Adipogenese vollständig zu verstehen.

1 INTRODUCTION

The predominant perception of adipose tissue in biology and biochemistry experienced a great change during the last decades from a mere black and white image to a multicolored picture of cellular and functional diversity. Originally regarded as rather uniform organ with sole purpose of energy storage, adipose tissue is nowadays classified into different subtypes comprising white, brown, beige/brite ('brown-in-white') and pink adipocytes that comply a variety of functions, including lipid storage, hormone production, signaling and thermogenesis (Giordano *et al*, 2014; Giralt & Villarroya, 2013; Kershaw & Flier, 2004). In times of the world-wide burden of increasing obesity, thermogenic brown and brite adipocytes stepped into the focus of research, as they can utilize nutritional energy to produce heat and thus act as energy sink, involved in blood glucose and lipid clearance (Bartelt *et al*, 2011; Chondronikola *et al*, 2014; Chondronikola *et al*, 2016; Olsen *et al*, 2019; Stanford *et al*, 2013; Yoneshiro *et al*, 2013). Transforming energy storing white into energy dissipating brite fat cells in a process called browning evolved as a promising strategy to control energy homeostasis. This vision presupposes a profound understanding of the regulatory mechanisms that drive brite adipocyte development and thermogenic function.
In this regard, a newly recognized class of potent regulatory molecules, the long noncoding RNAs (lncRNAs) recently revolutionized the conception of regulatory circuits in cellular differentiation, forcing to rethink the canonical focus on protein regulators. This group of long non-protein coding RNAs, which was previously regarded as transcriptional junk, revealed to possess expansive and versatile regulatory functions in a variety of biological processes (Kung *et al*, 2013). Currently, we are just starting to grasp their role in thermogenic adipocytes. The present thesis contributes to provide further insides into this question.

1.1 WHITE, BRITE AND BROWN ADIPOCYTES IN THE LIGHT OF THE GLOBAL BURDEN OF OBESITY

Mammalian adipose tissue is not a uniform organ but comprises different types of fat cells, including white, brite and brown adipocytes. The metabolic activity of brown and brite adipocytes stands in contrast to that of white adipocytes, as they do not store energy in the form of triglycerides but dissipate it in the form of heat. This thermogenic capacity relies on the Uncoupling Protein 1 (UCP1). UCP1 is a transmembrane protein located in the inner mitochondrial membrane of brown and brite adipocytes. Upon β-adrenergic stimulation of the cells, free fatty acids from lipolytic release activate UCP1 to short circuit the respiratory chain proton gradient across the membrane, which normally powers ATP synthesis. In the attempt to re-establish the electrochemical gradient, compensatory substrate catabolism is induced to fuel the respiratory chain (Cannon & Nedergaard, 2004; Nicholls & Locke, 1984; Nicholls & Rial, 1999). In the net equation, chemical energy of fatty acids and glucose are thus converted into thermal energy.

When fully activated, brown and brite adipocytes share similar phenotypical and biochemical characteristics with multilocular and mitochondrial-rich morphology, high *Ucp1* gene expression and thermogenic activity (Himms-Hagen *et al*, 2000; Li *et al*, 2014b; Shabalina *et*

al, 2013). Despite these resemblances, they constitute distinct types of fat cells. While brown adipocytes are generated during embryogenesis in defined depots and permanently express UCP1, brite adipocytes develop postnatally within white adipose tissue (WAT) and possess a reversible phenotype: UCP1 expressing brite adipocytes are not inherently present within WAT depots but emerge in response to cold-induced sympathetic or agonistic stimulation of β_3-adrenergic receptors, which is referred to as 'browning' of WAT (Bartelt & Heeren, 2014; Cousin *et al*, 1992; Himms-Hagen *et al.*, 2000; Schulz & Tseng, 2013; Young *et al*, 1984). Whether the emergence of brite adipocytes is achieved by trans-differentiation of existing mature white adipocytes or by de novo development from a subset of WAT residing progenitor cells, is still a matter of debate. Experimental evidence for both scenarios might propose a combination of both procedures (Barbatelli *et al*, 2010; Himms-Hagen *et al.*, 2000; Kozak & Koza, 2010; Lee *et al*, 2015; Rosenwald *et al*, 2013). In reverse to this recruitment, UCP1 expression disappears again when mice are returned to a warm environment, attributing certain white fat a convertible phenotype as energy storing organ in unstimulated conditions and energy dissipating organ when stimulated (Loncar, 1991; Rosenwald *et al.*, 2013). This convertible phenotype varies between distinct mouse strains and among white fat depots, with low browning characteristics of visceral gonadal WAT (gWAT) and high browning propensity of inguinal WAT (iWAT) (Guerra *et al*, 1998; Koza *et al*, 2000; Kozak & Koza, 2010; Li *et al*, 2019). In addition to their distinct development, brite adipocytes also possess a unique gene expression profile divergent from that of white and brown adipocytes, further establishing them as a discrete type of fat cell (Wu *et al*, 2012).

The thermogenic, energy dissipating phenotype of brown and brite adipocytes gains particular interest considering the continuously increasing world-wide burden of obesity. Overweight and obesity, which are the result of a long-term shift of the energy balance towards increased energy intake or decreased energy expenditure, present the major risk factor of several metabolic diseases like diabetes mellitus type 2, fatty liver, dyslipidemia, hypertension and arteriosclerosis. Obesity treatment still largely depends on the reduction of energy intake as numerous attempts to develop pharmacological treatment strategies that are safe, efficient and long-lasting, remained unsuccessful (Müller *et al*, 2018). In this regard, the discovery that considerable amounts of brown fat are not only present in rodents and human newborns for body temperature defense, but can also be detected in adults, raised the idea to utilize its energy expending capacity in the treatment of obesity (Saito *et al*, 2009; van Marken Lichtenbelt *et al*, 2009; Virtanen *et al*, 2009). This strategy evolved to be even more promising with the notion that equivalent to the murine browning process, thermogenic adipocytes can also be recruited in WAT of humans (Herz & Kiefer, 2019; Sharp *et al*, 2012; Wu *et al*, 2013). Accordingly, thermogenic adipocytes have been inversely related with body mass index (BMI), energy expenditure, blood glucose and lipid control in mouse and human (Bartelt *et al.*, 2011; Bordicchia *et al*, 2012; Cederberg *et al*, 2001; Cypess *et al*, 2009; Hanssen *et al*, 2015; Ouellet *et al*, 2012). The relatively limited amounts of brown fat in humans (300 ml (Gerngroß *et al*, 2017)) and especially in obese (Ouellet *et al*, 2011), however, provoked skepticism in its biological relevance and therapeutic potential. Arguing against this concern, it has to be taken into account that BAT functions on both sides of the energy balance. It affects not only energy

dissipation through adaptive thermogenesis, but also modulates energy intake in a gut-secretin-BAT-brain axis that induces satiation (Li *et al*, 2018), rendering it more efficient in the rebalancing of energy homeostasis. Moreover, activation of BAT could be especially useful in combination with other obesity treatment strategies by counteracting the reduction of basal metabolic rate that usually accompanies weight loss and hampers reduced weight maintenance (especially in thrifty phenotypes) (Major *et al*, 2007). Beyond this, the recruitment of thermogenic brite adipocytes in WAT provides a powerful means to extend the thermogenic capacity beyond the local boundaries of brown fat. Especially regarding the increased amounts of WAT in obesity, a redirection of the organs activity from mere energy storage towards energy dissipation could present a powerful way to restore energy balance and to prevent or alleviate metabolic comorbidities.

1.2 REGULATORY CIRCUITS IN THERMOGENIC ADIPOCYTE DIFFERENTIATION – ESTABLISHED REGULATORS AND FUTURE DISCOVERY POTENTIAL

An essential prerequisite for the envisioned employment of thermogenic adipocytes in the anti-obesity treatment is a fundamental understanding of the regulatory circuits that govern their development and thermogenic function. The differentiation of brite and brown preadipocytes into mature thermogenic cells is driven by highly complex transcriptional networks, which are subject of past and ongoing research. A considerable number of involved transcription factors (TFs), co-regulators and chromatin modifiers have been identified with more and more novel factors joining (Li *et al.*, 2019; Pradhan *et al*, 2017). Persisting gaps, however, still express the need for further investigation. The differentiation process of brown and brite adipocytes involves a general adipogenesis program complemented by thermogenesis specific gene expression networks.

General adipogenesis, which lays the basis for the development into lipid loaded fat cells, is largely coordinated by the TFs CCAAT/enhancer-binding protein β (C/EBPβ) and C/EBPδ, which form heterodimers and induce transcription of adipogenic master regulator *Peroxisome proliferator activated receptor γ* (*Pparγ*) and C/*ebpα*. These two TFs, in turn, mutually regulate their own transcription and that of numerous other genes involved in lipid storage, fatty acid synthesis and glucose metabolism (Rosen & MacDougald, 2006).

On top, several TFs and co-regulators drive the thermogenic specification of the cells. Among them PPARγ, Early B cell factor 2 (EBF2), PR domain containing 16 (PRDM16) and Peroxisome proliferative activated receptor γ, coactivator 1 α (PGC1α) emerged as central coordinators of the thermogenic differentiation process in both brown and brite adipocytes. Besides its role in general adipogenesis, PPARγ also acts as a master TF in brown, brite and white adipocyte differentiation. In brown and brite in contrast to white adipogenesis, the transcriptional activity of PPARγ thus needs to be directed towards thermogenic genes (Pradhan *et al.*, 2017). In this respect, EBF2 acts as early effector that initiates thermogenic gene expression independent of general adipogenesis. The helix-loop-helix TF binds to promoter or enhancer regions of thermogenic genes and guides and enables their subsequent transcriptional activation by PPARγ (Rajakumari *et al*, 2013). This might be mediated via EBF2 interaction with

brown fat-associated chromatin remodelers (Shapira *et al*, 2017). In this way, EBF2 induces expression of a series of thermogenic and mitochondrial but not general adipogenic genes, including *Prdm16* and *Pgc1α*. Accordingly, EBF2 overexpression reprogramed fibroblasts into brown fat cells and induced browning of iWAT, while EBF2 knockout (KO) severely impaired BAT development and β-adrenergic agonist-induced iWAT browning (Rajakumari *et al.*, 2013; Stine *et al*, 2016). With transcriptional induction of *Prdm16*, EBF2 induces a master transcriptional co-regulator in thermogenic differentiation that at least partially mediates the function of EBF2 in brite and brown fat cells (Rajakumari *et al.*, 2013). PRDM16 physically interacts with TFs, including C/EBPβ, PPARγ, PPARα, Zink finger protein 516 (ZFP516) and PGC1α, and stimulates their activity to induce transcription of thermogenic genes (Dempersmier *et al*, 2015; Seale *et al*, 2008; Seale *et al*, 2007). In parallel, it represses myogenic and white fat selective gene expression by recruiting histone methyl transferases to respective gene loci either directly by interacting with Euchromatic histone methyltransferase 1 (EHMT1) or indirectly by complexing with corepressor C-terminal binding protein 1,2 (CTBP1,2), which in turn recruits repressive histone modifiers (Harms *et al*, 2014; Kajimura *et al*, 2008; Ohno *et al*, 2013). Additionally, it induces expression of a downstream miRNA cluster (*miR-193-365*), which is also involved in negative regulation of myogenic gene expression (Sun *et al*, 2011). In white adipocytes, in contrast, Transducing-like enhancer protein 3 (TLE3) competes with PRDM16 for PPARγ binding to prohibit thermogenic cell fate (Villanueva *et al*, 2013). In accordance with this range of functionalities, the KO of *Prdm16* in all fat cells during late adipose tissue development completely impaired brite fat function and entailed adipose tissue inflammation and induction of visceral fat-selective genes (Cohen *et al*, 2014). Similarly, deletion of *Prdm16* together with its homolog *Prdm3* in developing brown fat resulted in early and severe deficit in BAT formation (Harms *et al.*, 2014). Transgenic *Prdm16* overexpression (OE) in all murine fat cells, in contrast, led to the appearance of multilocular brown-like adipocytes in WAT (Seale *et al*, 2011; Seale *et al.*, 2007). PRDM16 thus functions as a cell-autonomous key regulator in brown and brite adipogenesis that is required and sufficient for thermogenic differentiation. While PRDM16 function is prominent during early cell commitment and beginning differentiation, PGC1α acts as master regulator of mitochondrial biogenesis and thermogenic gene expression in late brite differentiation and mature brown adipocyte activation (Harms & Seale, 2013). Activated via the cAMP-PKA-p38MAPK pathway, it interacts with PPARγ, PPARα, Thyroid hormone receptor (THR) and Retinoid acid receptor (RAR) to specify their target genes and to enhance their transcription efficiency (Harms & Seale, 2013; Hondares *et al*, 2006; Puigserver *et al*, 1998; Wulf *et al*, 2008). Accordingly, loss of PGC1α in white fat impaired expression of thermogenic and mitochondrial genes (Kleiner *et al*, 2012), while forced expression of PGC1α in white adipocytes had the opposite effect (Tiraby *et al*, 2003). Beyond this, several further factors are involved in the regulation of thermogenic differentiation through modulating transcription rates or activity states of the named core thermogenic coordinators, generating a complex gene regulatory network (Klingenspor *et al*, 2017; Pradhan *et al.*, 2017) (Fig. 1).

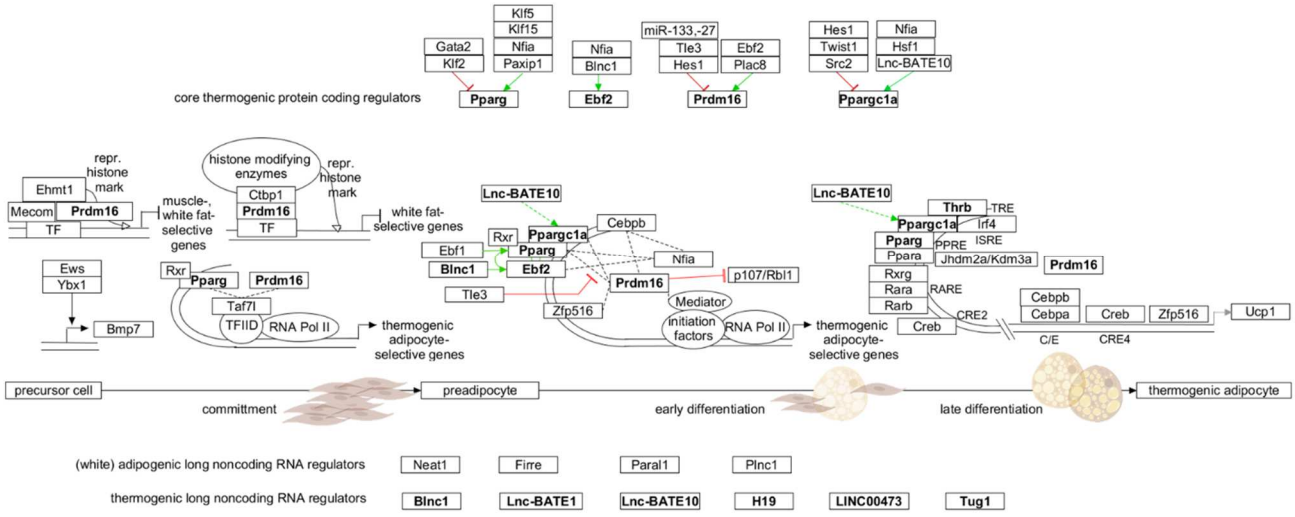

Figure 1: The core thermogenic gene transcription machinery. Overview of the components of the core thermogenic gene expression network, comprising key protein coding factors involved in commitment, early and late differentiation of brite and brown adipocytes, as well as adipogenesis related lncRNAs. Visualization by Path Visio software, red t-bars represent inhibitory effects, green arrows represent activating effects.

In the context of these regulatory circuits, the present thesis utilizes the capacity of thiazolidendiones such as rosiglitazone to induce brite adipocyte differentiation of precursor cells derived from the stroma vascular fraction of the murine iWAT depot (Oeckl *et al*, 2020; Petrovic *et al*, 2010). Rosiglitazone acts as PPARγ agonist and operates synergistically with PRDM16 in the induction of browning. This is likely mediated via PRDM16 protein stabilization and extension of its half-life time (Ohno *et al*, 2012) as well as by SIRT1-mediated PPARγ deacetylation, which promotes PRDM16 recruitment to PPARγ and induction of its thermogenic target genes (Qiang *et al*, 2012). Activation of MAPK and PI3K pathways by rosiglitazone might further be involved (Fayyad *et al*, 2019).

Ongoing research continuously complements the thermogenic regulatory network with more novel factors. In this regard, non-protein coding molecules, including micro RNAs, circular RNAs and long noncoding RNAs, which revealed to possess high regulatory potential, were included in the search for thermogenic modulators. While a considerable number of miRNAs had been associated with brown and brite differentiation within the last decades (Gharanei *et al*, 2020), there is still a large gap of knowledge on the contribution of lncRNAs in this process, with only a few factors, such as *Brown fat lncRNA 1* (*Blnc1*), *Brown adipose tissue enriched long non-coding RNA 1/10 (Lnc-BATE1/10)*, *H19 imprinted maternally expressed transcript* (*H19*), *Long intergenic non-protein coding RNA 473* (*LINC00473*) and *Taurine upregulated gene 1* (*Tug1*) being characterized (Fig. 1) (Alvarez-Dominguez *et al*, 2015a; Bai *et al*, 2017; Schmidt *et al*, 2018; Tran *et al*, 2020; Zhang *et al*, 2020; Zhao *et al*, 2014). Investigations into this group of regulatory molecules thus provides a large potential for the discovery of yet unknown thermogenic effectors and thus for the complementation of our understanding of brite adipocyte development.

1.3 LONG NONCODING RNAS - A LONGTIME NEGLECTED CLASS OF POTENT REGULATORS

Enhanced efforts in the elucidation of the human genome, coupled to the recent availability of high throughput sequencing technologies, brought surprising new insights into the genome composition and its functional transcription. The Encyclopedia of DNA Elements (ENCODE) project concluded that 74.7% of the human genome are processed into primary transcripts. Exons of protein coding genes, however, only cover 2.94% of the genome, indicating pervasive transcription into non-protein coding RNA (Djebali *et al*, 2012; The-ENCODE-Project-Consortium, 2012). Further challenging the previously protein-centered view on cellular function, it is not the number of protein coding genes but the relative amount of non-protein coding DNA sequence that correlates with organismal complexity (Taft *et al*, 2007). These observations drastically changed the perception of non-protein coding RNAs from mere transcriptional junk towards significant functional and regulatory entities.

Non-protein coding transcripts include housekeeping RNAs such as transfer RNAs (tRNAs), small nuclear RNAs (snRNAs), small nucleolar RNAs (snoRNAs) and ribosomal RNAs (rRNAs), as well as regulatory RNAs including micro RNAs (miRNAs), *piwi*-associated RNAs (piRNAs) and long noncoding RNAs (lncRNAs) (Zhang *et al*, 2019). LncRNAs are defined as transcripts of more than 200 nucleotides length that are not translated into proteins (Geisler & Coller, 2013). Due to this rough definition, varying annotation strategies and quality metrics, the number of recorded lncRNAs differs between databases. The GENCODE databank currently includes 17944 human (version 38) and 13188 murine (version M27) lncRNA genes (Frankish *et al*, 2019) with increasing trend, while LNCipedia lists 49372 high-confidence lncRNA genes in human (version 5.2) (Volders *et al*, 2019). Similar as messenger RNAs (mRNAs), lncRNAs are usually transcribed by RNA polymerase II, they can be processed by 5' capping, poly-adenylation and alternative splicing. LncRNAs, however, possess on average less exons and their expression strength is clearly lower compared to protein coding genes (Hezroni *et al*, 2015; Statello *et al*, 2021). LncRNA genes are mostly classified according to their genomic location relative to nearby protein coding genes into intergenic, intronic, divergent, sense and antisense lncRNAs (Fig. 2) (Zhao & Lin, 2015). Following transcription and processing, lncRNAs can either stay in the nucleus, translocate into the cytoplasm or reside in both cell compartments. Within nucleus and cytoplasm they can further associate with subnuclear structures such as nuclear speckles and paraspeckles or with cytosolic organelles such as mitochondria, lipid droplets the endoplasmic reticulum, ribosomes and exosomes, respectively (Bridges *et al*, 2021; Chen, 2016; Nakagawa *et al*, 2012; Statello *et al.*, 2021; Tran *et al.*, 2020; Wang *et al*, 2018; Zeng *et al*, 2018).

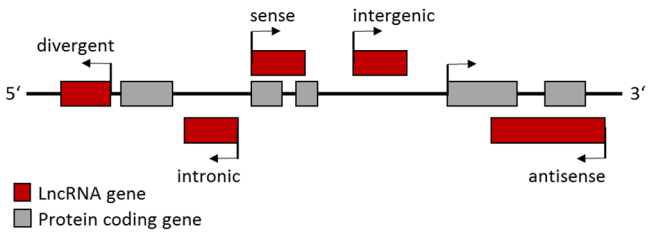

Figure 2: Classification of lncRNAs by their genomic location relative to nearby protein coding genes. LncRNA genes are presented in red, protein coding genes are presented in grey. Modified from (Zhao & Lin, 2015).

Searching for reasons of the superiority of noncoding RNAs over proteins as drivers of organismal complexity, some unique properties of lncRNAs and RNA in general need to be strengthened (Fig. 3) (Geisler & Coller, 2013). (I) Firstly, lncRNAs are highly tissue- and developmental stage specifically expressed, fostering their regulatory influence on cell identity and differentiation (Derrien *et al*, 2012). (II) Furthermore, as RNA they can be rapidly recruited and depleted again by transcription and RNA degradation without the need for more time-consuming translation into proteins. This renders them flexible effectors that can be transiently available specifically in times of need. (III) Additionally, RNA molecules can bind other nucleic acids (DNA and RNA) efficiently by simple base pairing. Proteins, in contrast, require more complex nucleic acid recognition sites that need to be encoded on far more genomic sequence space. (IV) LncRNAs are thereby not limited by a one dimensional structure, as they can also fold into complex three dimensional molecules, which provides versatile recognition and interaction possibilities. (V) Lastly, RNAs are more tolerant to mutations, as they do not need to maintain amino acid coding potential. This allows evolutionary innovation without loss of function (Geisler & Coller, 2013).

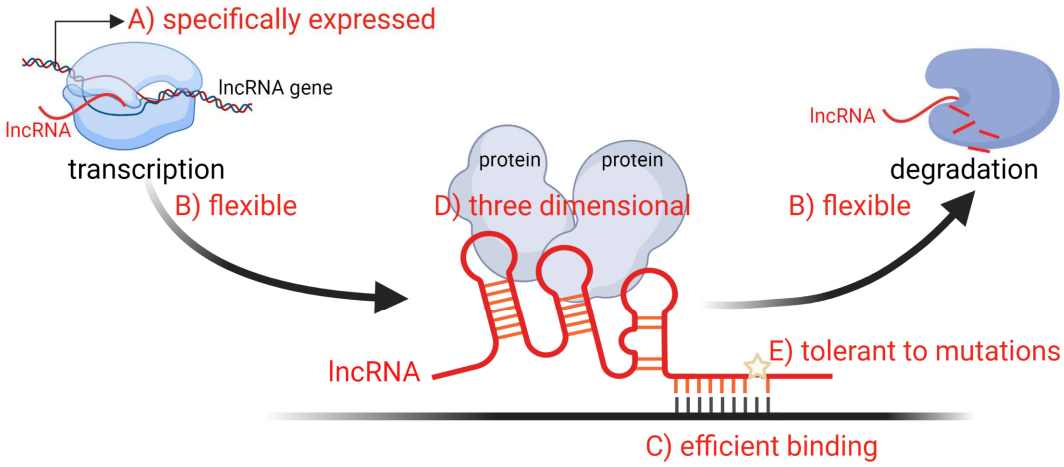

Figure 3: Unique properties of RNA. Summary of specific characteristics of lncRNA molecules providing the basis for their versatile regulatory potential. Created with BioRender.com.

Equipped with these characteristics, lncRNAs can act as potent regulatory molecules by various distinct mechanisms. (I) With their ability to interact with both, proteins and nucleic acids, they can act as guides that recruit regulatory factors to defined sites on the DNA or to other RNA transcripts. Guided regulators can be chromatin modifiers, TFs, splicing factors or other RNA binding proteins, which hence modulate chromatin accessibility, transcription rate or RNA processing of their respective lncRNA-defined targets (Marchese *et al*, 2017; Plath *et al*, 2002; Singer *et al*, 2019). (II) With their similarity to DNA and other RNA molecules, they can mimic binding sites of TFs, RNA binding proteins or miRNAs, hijacking them from their actual targets (Bai *et al.*, 2017; Cesana *et al*, 2011; Kino *et al*, 2010). Also RNA polymerase II can be directly bound by lncRNAs to inhibit transcription (Mariner *et al*, 2008), and transport factors can be occupied to prevent nuclear localization of TFs (Willingham *et al*, 2005). (III) Comparable to co-regulators, folded lncRNAs can modulate the activity of interacting regulators, such as TFs or chromatin modifiers. Depending on the type of interaction, their activities can be enhanced or reduced (Feng *et al*, 2006; Wang *et al*, 2008). (IV) Interacting

with two or more protein factors simultaneously, lncRNAs can act as scaffolds that provide the platform for higher order protein complex formation or to facilitate protein-protein interaction (Tsai *et al*, 2010; Yap *et al*, 2010). (V) Moreover, lncRNAs themselves can function as repressors by binding and blocking target DNA sites or RNA transcripts for regulation by other factors. Formation of a lncRNA-DNA triplex structure for instance can inhibit the assembly of the pre-initiation complex (Martianov *et al*, 2007), lncRNA binding to pre-mRNA can prevent splicing of defined introns (Krystal *et al*, 1990) and lncRNA interaction with mature transcripts can mask miRNA binding sites to prevent their silencing (Faghihi *et al*, 2010). (VI) Finally, the transcription process of lncRNAs itself can modify the local chromatin structure, either by RNA polymerase activity alone or by chromatin modifiers bound to its carboxy-terminal domain (Kornienko *et al*, 2013). With these versatile mechanistic activities, lncRNAs can act as potent modulators of the gene expression machinery, comprising epigenetic regulations, transcription, pre-mRNA processing and stability, mRNA degradation and translation. Accordingly, they emerge as important players in a multitude of biological processes including cell fate decision and cellular differentiation (Schmitz *et al*, 2016).

Brown and brite adipogenesis and thermogenesis also depend on lncRNA activity. Several lncRNAs have been associated with thermogenic fat cells, with continuously more novel factors joining. Only for a few lncRNAs, however, the molecular mechanism could be clarified. LncRNA *Blnc1*, for instance, that is conserved in mouse and human, is required for and drives brown and brite adipogenesis (Zhao *et al.*, 2014). It forms a ribonucleoprotein complex with EBF2, supported by Heterogeneous nuclear ribonucleoprotein (HNRNPU), to enhance thermogenic gene expression. In a positive feedback loop, this complex in turn promotes transcription of *Blnc1*, forming a self-enforcing regulatory circuit (Mi *et al*, 2017; Zhao *et al.*, 2014). *Lnc-BATE1* is a brown and brite adipocyte expressed lncRNA that is enriched during thermogenic adipogenesis. *Lnc-BATE1* and HNRNPU also interact in a ribonucleoprotein complex and both are required for BAT development and physiology (Alvarez-Dominguez *et al.*, 2015a). *Lnc-BATE10*, which is needed for full brown fat differentiation and white fat browning, protects *Pgc1α* from CUGBP Elav-like family member 1 (CELF1) binding. CELF1 is a RNA binding protein that binds to 3'UTRs of target mRNAs, such as *Pgc1α*, to promote their degradation. *Lnc-BATE10* also possesses binding sites for CELF1, decoys it and thus prevents its negative impact on *Pgc1α* (Bai *et al.*, 2017). The maternally expressed, imprinted lncRNA *H19* is involved in the regulation of brown adipogenesis, oxidative metabolism and mitochondrial biogenesis and is inversely correlated with human BMI (Schmidt *et al.*, 2018). *H19* interacts with Methyl-CpG-binding domain protein 1 (MBD1) to repress the expression of some paternally inherited genes (PEG) that are mainly downregulated during brown adipogenesis. The *H19*-MBD1 complex is thus proposed as "BAT-selective PEG gatekeeper" (Schmidt *et al.*, 2018). *LINC00473* is attributed a role in energy metabolism of human thermogenic adipocytes (Tran *et al.*, 2020). It shuttles out of the nucleus and localizes to the interphase between mitochondria and lipid droplets, where it is supposed to play a role in the coupling of lipolysis and mitochondrial respiration (Tran *et al.*, 2020). LncRNA *TUG1* induces thermogenic gene expression likely through downregulation of *miR-204* transcription, counteracting the miRNA's negative influence on *Sirt1* transcript levels. *TUG1* overexpression

hence increased SIRT1 and in dependence of this also ATGL, PPARγ, PGC1α and UCP1 expression (Zhang *et al.*, 2020). Beyond these factors, further lncRNAs have been associated with thermogenic adipogenesis including positive and negative regulators (Chen *et al*, 2019; Cui *et al*, 2016; Liu *et al*, 2020; Wang *et al*, 2020; Xiong *et al*, 2018; You *et al*, 2018).

Considering their molecular characteristics, their diverse functionalities and the increasing rate of discovery, lncRNAs arose as effective regulatory molecules, which provide strong detection potential. Identifying functional lncRNAs in thermogenic fat cells will thus make an important contribution to our yet incomplete understanding of brite and brown adipocyte development and physiology.

1.4 GENE TRANSCRIPTION AND ALTERNATIVE SPLICING AS IMPORTANT REGULATORY LAYERS DURING CELLULAR DIFFERENTIATION

To investigate and understand the role of lncRNAs in thermogenic adipocyte development, it is important to recognize cell fate and cellular differentiation as a complex, multilayered and interconnected process. Several regulatory layers, including chromatin accessibility, transcription, pre-mRNA splicing, processing, nuclear export, mRNA stability and translation cooperate to build up a cell type characteristic machinery, which defines morphology and function of the respective cell.

Among these steps, the modulation of transcription and alternative splicing present powerful means to shape cellular gene expression. Time-specific transcriptional induction or repression of defined genes and dynamic adaptations of the transcription strength largely determine the cellular equipment during cell development. Accordingly, transcription levels of cell type characteristic marker genes often serve to evaluate the state and direction of differentiation. Alternative splicing, which describes the processing of the same gene into distinct transcript isoforms, usually receives less attention. However, different transcript isoforms of the same gene can give rise to proteins with divergent functionalities. Additionally, isoform profiles of a given gene can be adapted during cellular differentiation in a cell type- and time-specific manner (Lin *et al*, 2014; Singer *et al.*, 2019). Alternative splicing thus provides a further layer of functional modulation of the cellular machinery and influences cell fate and cellular differentiation. Since transcriptome profiling is often not deep enough to distinguish distinct isoforms, this regulatory layer mostly remains unnoticed, although it harbors valuable information for the understanding of the differentiation process.

In the context of the multilayered regulation of cellular differentiation, the varied functionalities of lncRNAs are of high interest. LncRNAs have been described to be implicated in every step of gene expression (Chen & Zhang, 2016) and even the same lncRNA can be involved on more than one regulatory level (Goldfarb & Cech, 2017; Miao *et al*, 2019; Noh *et al*, 2016). Additionally, the great diversity of lncRNA interactions with other RNA species and proteins allow them to form regulative networks with other gene expression modulators. LncRNAs thus possess a coordinative potential in cellular differentiation, by orchestrating distinct levels of gene expression (Chen & Zhang, 2016; Fatica & Bozzoni, 2014). Also in brown

and brite adipogenesis it is thus of high interest to uncover the regulatory routes and coordinative properties of functional lncRNAs to understand the thermogenic regulatory network.

1.5 A COMPARATIVE MODEL OF INBRED MOUSE STRAINS TO UNCOVER NOVEL REGULATORS IN BRITE ADIPOGENESIS

The pivotal first step to determine functional lncRNAs comprises their filtering among the great number of expressed candidates. This in turn demands an effective selection method that filters lncRNAs with regulatory potential. In this regard, it is of interest that different inbred mouse strains possess a varying propensity to recruit brite adipocytes within iWAT (Guerra *et al.*, 1998; Koza *et al.*, 2000; Li *et al.*, 2019). BL/6J and SWR/J mouse strains have a low, while A/J, AKR/J and 129S6 mice have a high browning capacity, as exhibited by corresponding strength of *Ucp1* expression (Li *et al.*, 2019). Several cell-external conditions could be responsible for this variation *in vivo*, including different strengths in sympathetic innervation, a varying degree of angiogenesis, differences in endocrine stimuli or progenitor cell abundance. The strain-specific browning variation, however, is maintained in cultured primary adipocytes of iWAT and thus appears largely independent of the named extrinsic cues. Also paracrine and autocrine signal variations could be excluded as browning determinants. The strain-dependent browning propensity is thus mainly dictated by cues intrinsic to the progenitor cells, determined by the respective genetic background (Li *et al*, 2014a). As such, it provides a valuable model that fades out external noise and allows to uncover the key cellular drivers of browning. Contrasting gene knockout-based studies on the browning process, it employs the naturally occurring phenomenon of genetic and phenotypic variation among the mouse strains and might thus imply higher physiological relevance (Li *et al.*, 2019).

The model was applied previously in a systems-genetics approach, which performed transcriptome analysis on iWAT derived precursor cells and differentiated brite adipocytes of the five mouse strains (Li *et al.*, 2019). In combination with a BL/6J-129S6-F1-hybrid system and the BXD mouse genetic reference panel, several known and novel browning regulatory genes were identified, validated and integrated into a comprehensive network. Among further TF-encoding genes, as well as metabolism-, mitochondria- and signaling-related genes, *Fhl1*, *Mxd1* and *Zfp521* could be revealed as functional browning regulators. Comprehensive network analyses on the identified factors achieved to define an extensive regulatory network that coordinates white fat browning (Li *et al.*, 2019). This clearly supports the discovery potential provided by the comparative mouse strain model and encourages to apply these resources for the elucidation of lncRNAs in the regulation of white fat browning.

1.6 AIMS OF THE THESIS

In the context of the persistently increasing prevalence of obesity and its associated health burdens, it is the aim of the present thesis to advance the yet incomplete comprehension of thermogenic adipogenesis. This shall be achieved by changing the perspective from the canonical focus on protein regulators towards the potent and versatile regulatory class of noncoding RNAs, the contribution of which remains largely unexplored.

An established, powerful selection model that exploits the varying, adipocyte-intrinsic propensities of different inbred mouse strains for white fat browning, will serve as a tool to identify lncRNA candidates of putative functional relevance in this process. This shall provide the source for the selection of a promising individual lncRNA candidate that will be evaluated experimentally. Its regulation during thermogenic adipocyte differentiation will be assessed in rosiglitazone-induced brite adipogenesis *in vitro* as well as during cold-mediated iBAT activation and iWAT browning *in vivo*. Knockdown studies will serve to validate the lncRNA's role in the browning process and investigate its contribution to brite adipocyte characteristic gene expression and thermogenic function. The differentiation process will thereby be regarded as complex, multilayered procedure that requires precise spatial and temporal coordination of the multiple steps of gene expression, including chromatin remodeling, gene transcription, splicing, RNA transport, stability and translation. Which of these routes are targeted by the lncRNA candidate will be subject of investigation. Beyond this, explorative experimental and computational investigations shall further approach the lncRNA's mechanism on molecular level.

With this strategy, the present project aims to shed light on the functional contribution of lncRNA regulators in the browning process, i) providing a source for the identification of functional lncRNAs and ii) giving an exemplary insight into the versatile routes of lncRNA-mediated coordination of thermogenic gene expression.

2 MATERIAL AND METHODS

2.1 ANIMALS

Male mice of the following strains 129S6sv/ev, A/J, AKR/J, SWR/J, C57BL6/J and 129/SvImJ (UCP1-KO mice and wild-type littermates) were bred at the SPF facility of the Technical University of Munich registered at the local authorities according the German Animal Welfare Act. Mice were group-housed in individually ventilated cages at room temperature (23°C ± 1°C), 55% relative humidity, 12/12 hour light/dark cycle (5:00 am/pm CET) with ad libitum access to water and food (regular chow diet V1124-3M-Z; ssniff Spezialdiäten GmbH, Germany). At the age of 5-6 weeks they were used for whole organ extraction or preparation of primary cell cultures of inguinal white and brite or interscapular brown adipocytes. Animal studies that were conducted previous to this work and provided material or data were performed according to the German Animal Welfare based on approved licenses.

2.2 CELL CULTURE

2.2.1 Primary cell culture of inguinal white and interscapular brown adipocytes

Primary cell cultures were prepared from inguinal white and interscapular brown adipose tissue depots of 5-6 week old male mice. Fat depots of at least two mice were dissected and gathered in pre-warmed phosphate buffered saline (PBS) containing Gentamycin and Penicillin/Streptomycin (0.4% (v/v) each). Tissues were rinsed with a small volume of isolation medium (Tab. 1) and cut into small pieces using surgical scissors. The minced tissues were digested in 7 ml of collagenase-containing isolation medium for 45 min at 37°C under continuous orbital shaking (120 rpm). Every 10 min, additional manual shaking supported the digestion yield. The emerging cell suspension was subsequently filtered through a 250 µm pore-size nylon mesh to remove remaining undigested tissue. Centrifugation at 250 *g* for 5 min was applied to pellet the stromal vascular fraction (SVF) and to separate it from the floating fraction of mature adipocytes. To complete the separation, the tubes were shaken to disrupt the floating pellet and centrifuged again at 250 *g* for 5 min. The mature adipocyte containing supernatant was removed, the SVF pellet was re-suspended in 7 ml wash buffer (Tab. 1) and centrifuged again at 500 *g* for 5 min. After discarding the supernatant, the pellet was re-suspended in 1 ml pre-warmed culture medium containing Amphotericin B (Tab. 1), passed through a 40 µm cell strainer to generate a singularized cell suspension and diluted in an appropriate volume of culture medium with Amphotericin B. The cells were seeded into 12-well culture plates, evenly distributed and cultured at 37°C and 5% CO_2.

At the following day, culture medium was removed and the cells were washed twice with pre-warmed PBS to remove cell debris. Fresh culture medium was added and changed every second day until the cells reached sub-confluence. Differentiation was induced with induction medium (Tab. 1) for 2 days and continued for the following seven days with differentiation medium (Tab. 1) that was changed every second day. Brown and brite adipocytes were induced and differentiated in the presence, white adipocytes in absence of rosiglitazone. For

knockdown studies, cells were subjected to reverse transfection at day 4 of proliferation, at day 1 of differentiation or at day 5 of differentiation.

Table 1: Media composition for primary cell isolation and culture.

medium	compound	amount
isolation medium	1xHBSS	
	BSA	3.5%
	glucose	0.55 mM
	collagenase A	1 mg/ml
wash medium	1xHBSS	
	BSA	3.5%
culture medium	DMEM	80% (v/v)
	FBS	20% (v/v)
	gentamycin	0.4% (v/v)
	penicillin/streptomycin	0.4% (v/v)
	amphotericin B	0.2% (v/v)
induction medium	DMEM	90% (v/v)
	FBS	10% (v/v)
	gentamycin	0.4% (v/v)
	penicillin/streptomycin	0.4% (v/v)
	insulin	850 nM
	T3	1 nM
	IBMX	500 µM
	indometacin	125 µM
	dexamethason	1 µM
	(rosiglitazone	1 µM)
differentiation medium	DMEM	90% (v/v)
	FBS	10% (v/v)
	gentamycin	0.4% (v/v)
	penicillin/streptomycin	0.4% (v/v)
	insulin	850 nM
	T3	1 nM
	(rosiglitazone	1 µM)

2.2.2 LNA Gapmer ASO- and siRNA-mediated knockdown in primary adipocytes

The knockdown of targeted lncRNA and mRNA transcripts was performed by reverse lipofection of locked nucleic acid (LNA) Gapmer antisense oligonucleotides (ASOs) (Quiagen), small interfering RNAs (siRNAs) (Eurofins), or dicer-substrate short interfering RNAs (dsiRNAs) (IDT). Transfection mixes were prepared by adding the lipofection reagent (Lipofectamin RNAiMax, Thermo Scientific) and the respective interfering DNA/RNA to reduced serum medium (OptiMEM). The compounds were gently mixed and pre-incubated for 25 min on the target well format (XF96-well cell culture microplate for subsequent Seahorse respirometry; 24-well plate for lncRNA knockdown experiments by LNA Gapmer ASOs; 12-well plate for mRNA knockdown experiments by siRNA or dsiRNA) (Tab. 2). Depending on the experimental design, primary adipocytes were washed with prewarmed PBS and trypsinized from their

original plates after I) proliferation into sub-confluence, II) at day 1 of differentiation or III) at day 5 of differentiation to modulate gene expression in proliferating pre-adipocytes, during early differentiation or in differentiated mature adipocytes, respectively. Trypsinized cells were collected, pelleted and resuspended in an appropriate volume of induction medium for design I), or differentiation medium for designs II) and III), devoid of antibiotics (Tab. 2 (*cell suspension*)). The cell suspensions were added on top of the pre-incubated transfection mixes and incubated for 24 hours. On the following day, cells were either directly harvested (24 hour effect investigations) or supplied with fresh medium containing antibiotics and incubated for another 48 h before cell harvest (72 hours effect investigations). Sequences of LNA Gapmer ASOs, siRNAs and dsiRNAs are listed in the key resources table.

Table 2: Procedural details for LNA Gapmer ASO-, siRNA- or dsiRNAs-mediated knockdown experiments. Upper table: Volumes of transfection mix components, volume of cell suspension and final total volume (data per well). Lower table: Approximate amount of cells used for reverse transfection experiments in terms of number of wells of original culture plate transferred to a defined number of wells on the transfection plate).

	OptiMEM	RNAiMax	ASO/siRNA/dsiRNA [100 µM stock]	cell suspension	total volume
per well of a 96-well Seahorse pl.	15 µl	0.45 µl	0.045 µl for [50 nM final conc.]	75 µl	90 µl
per well of a 24-well pl.	100 µl	3 µl	0.3 µl for [50 nM final conc.]	500 µl	600 µl
per well of a 12-well pl.	200 µl	6 µl	0.6 µl for [50 nM final conc.]	1000 µl	1200 µl

original cell culture plate	transfection cell culture plate
3 wells of a 6 well plate	64 wells on a XF96 well Seahorse plate
1 well of a 12 well plate	2 wells of a 24 well plate
1 well of a 12 well plate	1 well of a 12 well plate

2.2.3 Culture of C3H10T1/2-CRISPRa(SAM) cells

The Clustered Regulators Interspaced Short Palindromic Repeats activating (Synergistic Activation Mediator) (C3H10T1/2-CRISPRa(SAM)) stable cell line was generated and kindly provided by the group of Associate Professor Dr. Brice Emanuelli (University of Copenhagen, Faculty of Health and Medical Sciences, The Novo Nordisk Foundation Center for Basic Metabolic Research, Section on Integrative Physiology) (Lundh *et al*, 2017). The CRISPRa(SAM) system provides the opportunity to activate the expression of endogenous genes by bringing transcriptional activators into contact with gene promoters. The system is composed of I) an inactivated version of CRISPR associated protein 9 (dead Cas9 (dCas9)) coupled to transcriptional activator Viral Protein 64 (VP64) and II) single guide RNAs (sgRNAs) that are also coupled to transcriptional activators P65 and Heat Shock Factor 1 (HSF1) via two MS2 stem loops (Fig. 4). The target specific sgRNAs recruit dCas9 to the promoter of the gene of interest by complementary base pairing. In the presence of the transcriptional activators, gene expression is induced.

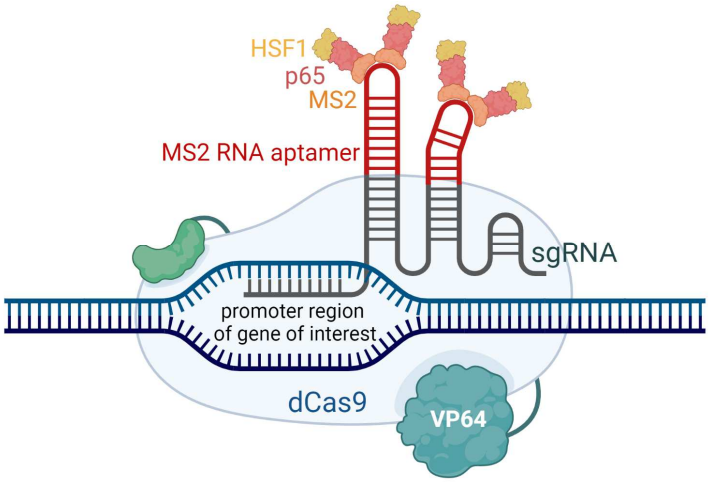

Figure 4: Components of the CRISPRa(SAM) system for overexpression of endogenous genes. Functionally inactivated dCas9 coupled to transcriptional activator VP64 and sgRNA with MS2 RNA aptamers, coupled to transcriptional activators p65 and HSF1 via MS2 tags. Created with BioRender.com.

C3H10T1/2-CRISPRa(SAM) cells were proliferated in culture medium containing DMEM (80%), FBS (20%) and penicillin/streptomycin (1%) that was refreshed every other day. At sub-confluence the cells were induced for two days and subsequently differentiated using the same media compositions as in primary adipocyte culture (Tab. 1).

2.2.4 SgRNA-mediated overexpression in C3H10T1/2-CRISPRa(SAM) cells

For *Ctcflos* overexpression by the CRISPRa(SAM) system, sgRNAs were designed, cloned into sgRNA(MS2) vector backbones (according to a protocol by S. Konermann, Zhang lab 2014 (Konermann *et al*, 2015; Shalem *et al*, 2014) and reverse transfected into C3H10T1/2-CRISPRa(SAM) cells at beginning differentiation.

For sgRNA design and cloning, 20 bp sequences upstream of the transcriptional start site (TSS) of *Ctcflos* isoform 1 that locate in direct neighborhood to a protospacer adjacent motif (PAM) sequence were selected by hand (Sequences of *Ctcflos* sgRNAs are listed in the key resources table). Forward and reverse oligos containing the chosen 20 bp sequence and defined overhangs (Fig. 5) were ordered (Eurofins Genomics), annealed and 5' phosphorylated (in a 10 µl reaction containing 1 µl of each oligo (100 µM), 1 µl of T4 ligase buffer (NEB), 0.5 µl T4 PNK (NEB) and nuclease-free water) (using the following temperature program: 37°C for 30 min, 95°C for 5 min, ramp to 25°C by decreasing temperature by 5°C/min).

Target sequence: 1 2 3 4 5 6 7 8 9 10 11 12 13 14 15 16 17 18 19 20 NGG-PAM

Oligo 1 → 5' – **CACCG**NNNNNNNNNNNNNNNNNNN - 3'

3' - **C**NNNNNNNNNNNNNNNNNNN**CAAA** – 5' ← Oligo 2

Figure 5: Design of sgRNA oligonucleotides. Sequences of sgRNA-oligonucleotides (Oligo) 1 and 2, defined overhangs are highlighted in red, the targeted sequence corresponding to the promoter region of the target gene is encoded by N for any type of nucleotide.

In a golden gate reaction, annealed oligos were introduced into the sgRNA(MS2) cloning backbone (Addgene) (Fig. S1) (in a 25 µl reaction containing 1 µl of diluted oligo anneal (1:10), 1 µl of backbone vector (25 ng/µl), 1 µl of BbsI restriction enzyme (NEB), 0.125 µl of T7 ligase (Enzymatics), 0.125 µl BSA (20 ng/µl) and 12.5 µl 2x rapid ligase buffer (Enzymatics)) (using the following temperature program: 15 cycles of 37°C for 5 min and 20°C for 5 min). 2 µl of the golden gate reaction were transformed into competent *E.coli DH5α* (NEB). Single colonies, grown overnight at 37°C on ampicillin containing agar plates, were further proliferated overnight in liquid cultures at 37°C with shaking (180 rpm) before the plasmids were isolated using PureYield™ Plasmid Miniprep System (Promega) and sequenced to confirm successful cloning.

At day 1 of differentiation, the sgRNA(MS2) vectors were introduced into C3H10T1/2-CRSPRa(SAM) cells by reverse lipofection onto 24-well plates. Transfection mixes were prepared by combining the lipofection reagent (Lipofectamin RNAiMax, Thermo Scientific) (3 µl) and the sgRNA(MS2) vectors (250 ng) in 100 µl reduced serum medium (OptiMEM). The compounds were gently mixed and pre-incubated for 20 min on the 24-well plate. Meanwhile, C3H10T1/2-CRISPRa(SAM) cells at day 1 of differentiation were washed with pre-warmed PBS, trysinized from their plates, collected, pelleted by centrifugation at 400 *g* for 4 min and resuspended in an appropriate volume of differentiation medium without antibiotics. 250000 cells within 400 µl were added on top of the transfection mix and incubated for 48 hours before harvest.

2.3 RNA ISOLATION

2.3.1 Total RNA isolation of cultured cells and murine tissues

Total RNA of adipocyte cell cultures and murine tissues was isolated using the SV Total RNA Isolation System (Promega) adapted to the isolation from fat rich material. Frozen cell cultures were scraped from the plate and lysed in TRIsure (Bioline) (200 µl/well for a 12-well plate), murine tissues were homogenized in TRIsure (1 ml) using an Ultra-Turrax D-1 disperser (Miccra GmbH). The lysates were centrifuged at 2500 *g* for 5 min. In case of a floating fat layer only the lower fraction was extracted, mixed with Chlorophorm in a TRIsure:Chlorophorm ratio of 5:1, rigorously shaken by hand for 15 sec, incubated for 2-3 min and centrifuged at 12000 *g* for 15 min to separate the RNA containing aqueous upper phase from protein and DNA accumulating interphase and lower phenol-chlorophorm organic phase, respectively. The upper aqueous phase was extracted, mixed with ethanol (75% in DEPC treated water) (100 µl for 12-well plate cell cultures; 500 µl for tissue samples) and transferred to a spin column provided by the kit system. According to the manufacturer's instructions, the columns were centrifuged at 12000 *g* for 1 min to let the RNA attach to the column. Subsequently, they were washed with 600 µl ethanol-containing wash buffer (centrifugation 12000 *g*, 1 min), treated with DNase (40 µl Yellow Core Buffer + 5 µl $MnCl_2$ (0.09 M) + 5 µl DNase I enzyme) for 15 min for on-column genomic DNA degradation, washed again with 600 µl wash buffer (centrifugation 12000 *g*, 1 min) and a second time with 250 µl wash buffer (centrifugation 12000 *g*, 2 min). Finally, the RNA was eluted from the column in nuclease free water (25 µl for

24-well plate adipocyte samples or 50 µl for tissue samples) (centrifugation 12000 *g*, 1 min). For higher RNA yields the elution procedure was repeated a second time with the eluate, RNA concentration was measured spectrophotometrically by the InfiniteM2000 NanoQuant (Tecan) and RNA samples were stored at -80°C.

2.3.2 Fractionated isolation of nuclear, cytosolic and mitochondrial RNA

Nuclear, cytosolic and mitochondrial RNA fractions were separated by density centrifugation. Cells grown on 6-well plates were washed three times with PBS and scraped from the plates in 1 ml PBS. Cells of nine wells were pooled and pelleted by centrifugation at 1000 *g* for 5 min. The cell pellet was carefully resuspended in 1 ml cold high salt cell disruption buffer (KCl (10 mM), $MgCl_2$ (1.5 mM), Tris (20 mM), pH 7.5) and incubated for 10 min on ice. After swelling to around three times of their original size, the cells were homogenized in a dounce homogenizer (type B pestle, 0.0005-0.0025 in.) by 15 strokes, mixed with Triton X-100 (0.1%) and centrifuged at 1000 *g* for 5 min to separate pelleted cell nuclei and other organelles from the cytosolic supernatant fraction. After harvesting the cytosolic fraction, the pellet was resuspended in STE buffer (Sucrose (250 nM), Tris (5 mM), EDTA (2 mM), pH7.4) to further separate in a second centrifugation step at 1000 *g* for 3 min mitochondrial (supernatant) and nuclear (pellet) fractions. Finally, RNA of the three fractions was isolated using TRIsure and the SV Total RNA Isolation System (Promega) as described above for total RNA extraction.

2.3.3 Poly-A RNA enrichment

Poly-A RNA enrichment from total RNA was performed with the PolyATtract® mRNA Isolation System (Promega) according to the manufacturer's instructions using biotinylated poly-dT primers that bind to transcript poly-A tails and can be captured by streptavidin-coupled paramagnetic particles. 500 mg of total RNA, isolated from mature brite adipocytes or iBAT, as described above, was brought to a final volume of 500 µl with nuclease-free water and heated up to 65°C for 10 min. 3 µl of biotinylated poly-dT primers and 13 µl of 20x saline sodium citrate (SSC) were added, mixed gently and incubated at room temperature for annealing while cooling down. The paramagnetic particles were prepared by washing three times in 300 µl of 0.5x SSC using a magnetic stand and resuspending in 100 µl of 0.5x SSC. Subsequently, the annealing reaction of RNA and primers was incubated with the paramagnetic beads for 10 min with inversion every 2 min for gentle mixing. The paramagnetic particles with the attached poly-A RNA fraction were captured using a magnetic stand, the supernatant containing the non-poly-adenylated part of RNA was removed and the particles were washed four times with 300 µl of 0.1x SSC. Lastly, the paramagnetic particles were resuspended in 100 µl of nuclease free-water to elute the poly-A RNA from the beads, the beads were magnetically captured and the eluted poly-A RNA was harvested. To complete the elution, this step was repeated a second time with 150 µl of nuclease-free water.

2.4 cDNA SYNTHESIS, qPCR AND PCR

Reverse transcription of RNA into complementary deoxyribonucleic acid (cDNA) was performed using the SensiFAST™ cDNA Synthesis kit (Bioline). The reaction mixture was

composed of 500 ng RNA, 2 µl of oligo-dT and random hexamer primer-containing TransAmp buffer and 0.5 µl of reverse transcriptase in a final volume of 10 µl. The reaction was conducted with the following temperature program (Tab. 3).

Table 3: Temperature program for cDNA synthesis.

	temperature	duration
annealing	25°C	10 min
rev. transcr.	42°C	15 min
inctivation	85°C	5 min
cooling	4°C	--

Quantitative determination of the transcript abundance of individual genes of interest was conducted by quantitative real-time Polymerase Chain Reaktion (qPCR) using the SensiMix SYBR® No-ROX Kit system (Bioline). During qPCR, DNA amplification from the cDNA template, using gene specific primers, can be monitored in real time by photometric detection of a fluorescent signal that emerges, when SybrGreen intercalates into the newly formed double-stranded DNA (dsDNA). With ongoing cycles of amplification the signal increases until it exceeds background fluorescence, which is referred to as cycle threshold (Ct-value). With more cDNA template the threshold is reached earlier. In comparison with a standard curve, the Ct-value thus provides information on the relative transcript abundance in the original sample. QPCR analysis thus allows quantitative comparison of a defined transcript between samples. (Expression levels of different transcripts amplified by distinct primer pairs, in contrast, cannot be compared due to varying primer binding efficiencies. Furthermore, distinct transcript isoforms that are amplified by the same pair of primers cannot be distinguished in qPCR.)

For preparation of the standard curve, a small fraction of all cDNA samples were pooled and serially diluted (1:2) in eight steps. 1 µl of standards or 1 µl of samples (diluted 1:10) were added onto a 384-well plate (4titude) into a 11.5 µl reaction mix containing 6.25 µl of 2x SensiMix SYBR No-ROX master mix, 0.03125 µl of 100 µM forward and reverse primers each and 5.19 µl nuclease-free water. Standards were prepared in duplicates, samples in triplicates. LightCycler 480 II (Roche) was used for the PCR reaction and fluorescence detection using the following temperature program (Tab. 4):

Table 4: Temperature program for qPCR.

		temperature	duration
initial denaturation		95°C	6 min
	denaturation	97°C	10 sec
45 cycles	annealing	53°C	15 sec
	extension	72°C	20 sec
melting curve			
cooling		4°C	--

With use of the standard curve, transcript levels were determined and expressed relative to the expression of the housekeeping gene *General transcription factor 2b* (*Gtf2b*) to normalize for differences in cell number or processing between samples.

Qualitative analysis of gene expression was done by regular PCR using ImmoMix™ (Bioline), followed by gel electrophoresis. A gene of interest is amplified from the cDNA template in a PCR reaction using gene specific primers and DNA polymerase. PCR products are separated by size on an agarose gel and visualized by the DNA intercalating dye HDGreen™ Plus (Intas). In contrast to qPCR analysis, this method allows the separate visualization and direct comparison of size-distinct transcript isoforms amplified by the same pair of primers. This proved useful in the present thesis for alternative splicing analysis.

For the PCR reaction, 1 µl of cDNA sample (diluted 1:10) was added into a 19 µl reaction mix composed of 1 µl of 10 µM forward and reverse primers each, 10 µl 2x ImmoMix master mix and nuclease free water. The PCR reaction was conducted in a thermal cycler using the following program (Tab. 5).

Table 5: Temperature program for PCR reactions.

*The annealing temperature was set 2°C below the melting temperature of the respective primers.

		temperature	duration
initial denaturation		95°C	10 min
40 cycles	denaturation	95°C	30 sec
	annealing	*	15 sec
	extension	72°C	15 sec
Final extension		72°C	2 min
cooling		4°C	--

PCR products were loaded together with DNA gel loading dye onto an HDGreen Plus containing agarose gel (1-2% depending on PCR fragment size), separated electrophoretically next to a DNA size marker and visualized under UV light.

2.5 RNA SEQUENCING

2.5.1 Re-analysis of transcriptome data of undifferentiated and differentiated brite adipocytes of five inbred mouse strains

Identification of browning-related lncRNAs

LncRNAs of relevance in iWAT browning were identified from a transcriptome data set of proliferating and mature differentiated (w/o rosiglitazone) primary adipocytes, derived from iWAT of five inbred mouse strains (C57BL/6J, 129S6sv/ev, A/J, AKR/J, SWR/J). The dataset was published previously where it served for the identification of protein-coding browning regulators (Li *et al.*, 2019) (https://www.ebi.ac.uk/arrayexpress/experiments/E-MTAB-8344/ (Li Y, 2019)). For the identification of lncRNAs of potential functional relevance in brite adipogenesis, sequenced tags were mapped against the GRCm38/mm10 genome assembly. Uniquely identified hits were assigned to transcripts of the ElDorado database, a Genomatix

genome annotation, based on publicly available reference assemblies, including Refseq, Ensembl and GenBank, by scanning sequenced tags for the shortest unique sequences (SUS) defining a specific position in the target genome. LncRNAs were extracted from alignments against the GenBank and analyzed for differential expression using the Genomatix DESeq2 pipeline. Transcript coverage rates were assigned in reads per kilobase per million mapped reads (RPKM). Criteria set for the selection of brite adipogenesis relevant lncRNAs included correlation with *Ucp1* >0.6 or <-0.6 in differentiated adipocyte samples across the five mouse strains, significant regulation during differentiation of 129S6 iWAT derived adipocytes with log2 fold change >1 or <-1 and significant regulation in response to rosiglitazone treatment of 129S6 iWAT derived adipocytes with log2 fold change >0.585 or <-0.585.

Heatmap generation

For heatmap generation, transcript level count data were normalized using the regularized logarithm transformation, subset to those lncRNAs identified as being of functional relevance as described above, row-mean centered and clustered using hierarchical clustering.

Principal component analysis and hierarchical clustering of the lncRNA transcriptome

Principal component analysis and hierarchical clustering were performed on all lncRNAs that exceeded a mean read number of 3 across all samples in the transcriptome analysis described above. The R function prcomp (with centering and scaling) and the factoextra R package were used for principal component analysis. For hierarchical clustering the distance matrix of the lncRNA expression data was computed and hierarchical clustering was conducted with dist (with scaling) and hclust R functions, respectively.

LncRNA-mRNA co-expression network analysis

The principle of gene network analysis was previously described (Bai *et al.*, 2017). Transcript level count data were normalized by regularized logarithm transformation and confined to the transcripts of putative functional relevance according to their correlation with Ucp1, regulation during differentiation and in response to rosiglitazone, as described above. The GeneNet R package was used to calculate partial correlations and FDR for all pairs of transcripts. Partial correlations with FDR <5% were used to create a graph with vertices representing transcripts and edges representing significant correlations. Networks of commonly regulated transcripts were determined using the fast greedy modularity optimization algorithm (igraph R package). Those mRNAs, lacking a direct link to a lncRNA, were excluded from the analysis and the remaining mRNAs with direct link to a lncRNA were subjected to GO analysis using parent-child algorithm (topGO R package).

2.5.2 Transcriptome analysis of *Ctcflos* KD and control adipocytes

The effects of *Ctcflos* deficiency were analyzed on transcriptome-wide level to obtain a comprehensive view of knockdown-dependent transcriptional changes, using bulk-RNA barcoding and sequencing (BRB-seq) by the group of Prof. Dr. Bart Deplancke (Laboratoty of Systems Biology and Genetics, EPFL) (Alpern *et al*, 2019). For this purpose, *Ctcflos* was knocked down at day 1 or at day 5 of brite adipocyte differentiation and total RNA samples of KD and control cells were harvested after 24 hours and after 72 hours. All samples were tested for

RNA integrity using RNA 6000 Nano kit (Agilent) and reverse transcribed by SuperScriptTM II Reverse Transcriptase (Lifetech) using specific barcoded oligo-dT primers. Sample pools were purified by DNA clean and concentrator kit (Zymo Research), followed by exonuclease I treatment (NEB) and second strand synthesis by nick translation (Alpern *et al.*, 2019) to generate double stranded (ds) cDNA. cDNA was purified with AMPure magnetic beads (30 µl, 0.6x) (Beckman Coulter) and eluted in water (20 µl). Libraries were prepared by tagmentation of full-length ds cDNA (5 ng) with Tn5 enzyme (1 µl, 11 µM) and amplified (15 cycles). AMPure beads (Beckman Coulter) were used to size-select fragments of 200-1000 bp in two rounds (0.5x beads and 0.7x beads, respectively). Libraries were profiled with the High Sensitivity NGS Fragment Analysis Kit (Advanced Analytical), measured with the Qubit dsDNA HS Assay Kit (Invitrogen), pooled and sequenced on the Illumina NextSeq 500 platform with custom primer and High Output v2 kit (75 cycles) (Illumina). Sequenced tags were aligned to the NCBI Reference Sequence Database and differential expression analysis was performed with DESeq2 using Genomatix Software Suite.

Gene ontology analysis

For functional predictions, differentially regulated genes were subjected to gene ontology (GO) analysis. Overrepresented GO terms associated with the regulated genes were identified using InCroMAP software (Wrzodek *et al*, 2013).

2.5.3 Global analysis of *Ctcflos*-dependent alternative splicing in brite adipogenesis

The analysis of *Ctcflos* KD-dependent changes in transcript splicing patterns was based on a deep RNA sequencing approach that delivered exon-spanning reads to reconstruct and quantify specific transcript isoforms using the SGSeq algorithm (Goldstein *et al*, 2016). For this analysis, total RNA harvested after 24 hours post *Ctcflos* KD at day 1 of brite adipocyte differentiation was subjected to deep sequencing using Illumina HiSeq 4000 platform (Helmholtz Center Munich). Libraries of 6 samples were pooled into one sequencing lane and sequenced in 150 bp paired-end reads, ~40 mio reads per sample. Reads were aligned to the GRCm38 genome assembly by STAR_2.5.3a. The obtained BAM files were used to construct splice graphs based on Gencode vM21 exon annotation using SGSeq algorithm (Goldstein *et al.*, 2016). Splice events, detected based on splice junction spanning reads, were further tested for differential occurrence in *Ctcflos* KD and control samples using DEXSeq (Anders *et al*, 2012).

Enrichment analyses for RNA binding protein (RBP) motifs

Enrichment analysis of RNA binding protein motifs among differentially spliced transcripts was performed by Transcript Set Motif Analysis Tool (Transite) (https://transite.mit.edu/, 06.11.2019) (Krismer et al., 2019). RBM41 binding sites within *Ctcflos* tr1 were identified using RBPmap (http://rbpmap.technion.ac.il/ 03.03.2020) (Paz et al, 2014).

2.6 RESPIROMETRY

UCP1 activity of brite and brown adipocytes under control and *Ctcflos*-deficient conditions was assessed by the measurement of oxygen consumption rates by microplate based respirometry using the XF96 Extracellular Flux Analyzer (Seahorse Bioscience) as described previously (Li *et al*, 2017; Oeckl *et al.*, 2020). The respiration analysis is based on the real-time measurement of oxygen concentrations in the medium directly above a cell monolayer by oxygen-sensitive fluorescent sensors. Changes in the oxygen concentration over time and in response to successively injected effectors provide information about different mitochondrial respiratory states (Fig. 6): Measurement of basal oxygen consumption is followed by oligomycin injection, which blocks ATP synthase and thus allows to determine respiration induced by the basal leakage of protons across the inner mitochondrial membrane. Injection of isoproterenol leads to activation of UCP1, enabling the measurement of UCP1-mediated uncoupled respiration, stimulated by the influx of protons through UCP1. Injection of FCCP, a strong chemical uncoupler, induces maximal respiration, and finally, antimycin A inhibits respiratory chain complex III to quantify non-mitochondrial oxygen consumption, which is subtracted from all other respiration rates. The measurement is performed in the presence of bovine serum albumin (BSA) to buffer excess free fatty acids, which would contribute to non-specific uncoupling and confound the quantification of UCP1-dependent respiration.

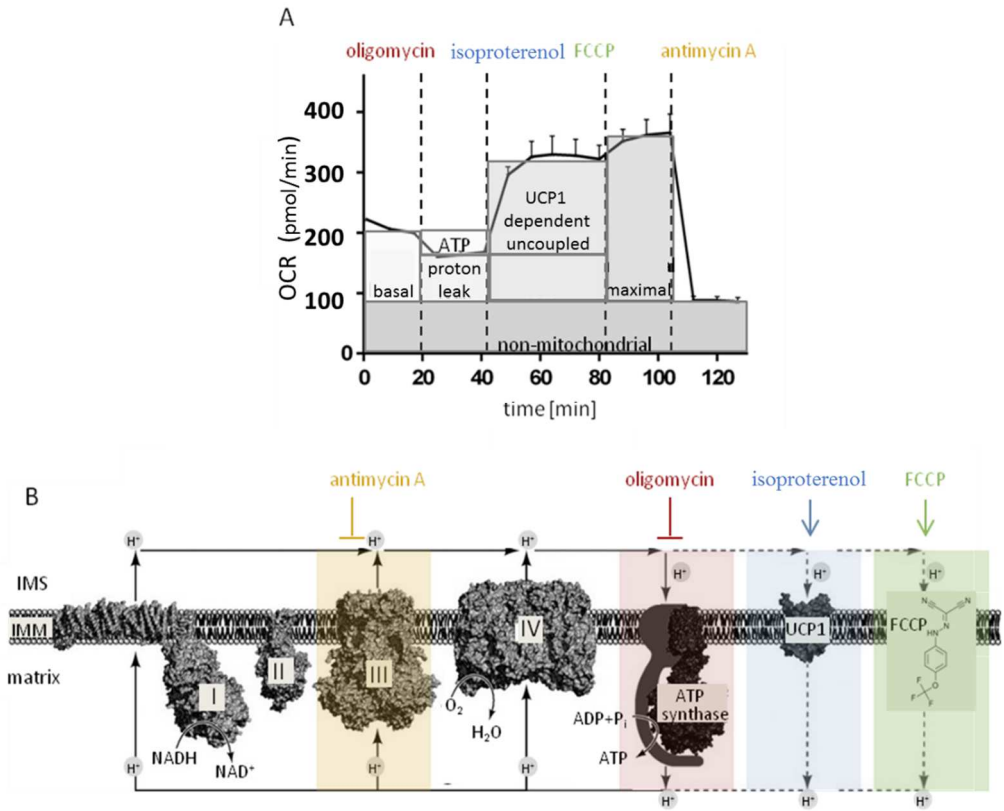

Figure 6: General procedure of respiration measurements. (A) Respiration profile of a typical seahorse measurement, showing the change of oxygen consumption over time in response to injected substances depicted in colors. **(B)** Respiratory chain with highlighted target sites of the injected substances. Intermembrane space (IMS), inner mitochondrial membrane (IMM). Modified from (Divakaruni & Brand, 2011).

For the comparison of respiration profiles of *Ctcflos* KD and control cells, primary brite adipocyte were cultured on 6-well plates. During the *Ctcflos* KD procedure at day 1 or day 5 of differentiation, the cells were reverse transfected onto the seahorse plate, as described above, and further differentiated for 72 hours. On the day before the measurement, the sensor cartridge was hydrated for around 16 hours with 200 µl per well of XF96 Calibrant buffer at 37°C in a non-CO_2 incubator. On the measurement day, the adipocytes were first washed with pre-warmed seahorse assay medium without BSA (Tab. 6) and then incubated with seahorse assay medium containing 2% BSA (Tab. 6) at 37°C in the non-CO_2 incubator for 1 hour.

Table 6: Composition of the seahorse assay medium.

compound	amount
DME (base)	
glucose	25 mM
sodium pyruvate	2 mM
glutmax	2 mM
NaCl	31 mM
phenol red	15 mg/l
(essentialy fatty acid free BSA	2%)
pH	7.4

In the meantime, the four injection ports of the sensor cartridge were loaded with the injection reagents in seahorse assay medium without BSA at 10x concentrations to achieve the final concentrations of oligomycin (5 µM), isoproterenol (5 µM), FCCP (1-5 µM) and antimycin A (5 µM) after injection. Finally, the sensor cartridge and the cell plate were subjected to the Seahorse analyzer and the measurement was conducted in repeating loops of injection, mixing and measuring (Tab. S1).

2.7 IMMUNOBLOT ANALYSIS

Protein expression was analyzed by sodium dodecyl sulfate polyacrylamide gel electrophoresis (SDS-PAGE), followed by electroblotting and immunological protein detection on a nitrocellulose membrane (Li-Cor). In this procedure, proteins are extracted from cultured cells, separated according to size in an electric field, transferred to a membrane, detected by a protein-specific primary antibody and visualized by a fluorescently-labeled secondary antibody.

For protein extraction, frozen cells were lysed in radio immunoprecipitation assay (RIPA) buffer (NaCl (150 mM), Tris-HCl (50 mM), EDTA (1 mM), NP-40 (1%) and Na-deoxycholat (0.25%)) during shaking for 15 min at 4°C. Centrifugation at 14000 *g* at 4°C for 15 min subsequently separated the solubilized protein fraction from cell nuclei and cell debris. The protein containing supernatant was harvested and protein concentration was determined by the Pierce bicinchoninic acid (BCA) protein assay (Thermo Scientific) according to the manufacturer's instructions: Protein samples were diluted (1:5) and bovine serum albumin (BSA) protein standards of varying concentrations were prepared for a standard curve. 10 µl of samples and standards were incubated on a 96-well plate with 200 µl of BCA working reagent (composed of 50 parts 'Reagent A' + 1 part 'Reagent B') for 30 min at 37°C.

Absorbance was measured at 562 nm using the InfiniteM2000 NanoQuant (Tecan), and protein concentration was determined.

30 µg of protein lysate together with 2x sample buffer (Tris-HCl, glycerin, SDS, bromophenol blue), containing 5% β-mercaptoethanol, were heated up to 95°C for 5 min for protein denaturation. Subsequently, protein samples and protein ladder were size separated by electrophoresis in a 12.5% sodium dodecyl polyacrylamide gel (70 Volt followed by 100 Volt). Separated proteins were electroblotted onto a nitrocellulose membrane (Li-Cor) in a Trans-Blot SD Semi-Dry Transfer cell (Bio-Rad) (1 mA/1 cm^2). The membrane was blocked at 4°C overnight by BSA and treated with the primary antibody against UCP1 (rabbit anti-UCP1, 1:10000, Abcam), against COX4 (rabbit anti-COX4, 1:5000, Abcam) or against β-Actin (mouse anti-Actinb, 1:5000, EMD Millipore) by orbital shaking for 1.5 hours at room temperature. Fluorophore-conjugated secondary antibody (goat anti-rabbit IRDye 800 CW or donkey anti-mouse IRDye 680, 1:20000, Li-Cor) was applied for another 1.5 hours orbital shaking at room temperature and fluorescent signals were detected by Odyssey fluorescent imager (Licor Biosciences).

2.8 IMMUNOCYTOCHEMISTRY

Immunocytochemistry served to visualize and quantify splicing factor SC35 as well as UCP1 within primary brite adipocyte cultures. In this procedure, cell fixation and permeabilization is followed by immunological protein detection using protein-specific primary antibodies and visualization by fluorophore-coupled secondary antibodies. Compared to immunoblot analysis, this strategy provides additional information on subcellular localization of the protein of interest and on the distribution of its expression within the cell population.

Primary brite adipocytes derived from iWAT of 129S6 mice were reverse transfected during *Ctcflos* KD on day 1 of differentiation into 8-well chambers (flexiPERM® slide, Sarstedt) placed on a microscopic slide (SuperFrost™ Microscope slides, Thermo Scientific). To make sure that the *Ctcflos* KD effects observed after 24 hours on transcript level are translated onto protein level, the immunocytochemistry analysis was started 48 hours post KD. The cells were washed two times with PBS and fixed with cooled ethanol (95%) and glacial acetic acid (5%) at -20°C for 10 min. After another three washes with PBS, the cells were permeabilized by TritonX-100 (0.3%) for 10 min, washed again three times with PBST and blocked with donkey serum (10%) in PBST containing TritonX-100 (0.3%) for 2 hours. Three washes with PBST were followed by primary antibody incubation targeting SC35 (mouse anti-SC35, 1:100, Abcam) or targeting UCP1 (rabbit anti-UCP1, 1:200, Abcam) in PBST with TritonX-100 (0.3%) and donkey serum (1%) overnight. Cells were washed five times with PBS and treated with the respective fluorophore coupled secondary antibodies (Alexa Fluor 647 donkey anti-mouse IgG, Invitrogen, or Alexa Fluor 546 donkey anti-rabbit IgG, Life Technologies, both diluted 1:500 in PBST with donkey serum (1%)) for 1.5 hours. After five washing steps with PBST, the slides were mounted with Vectashield Mounting Medium containing DAPI for nuclear counterstain (Vector Labs), sealed with a cover slip (VWR) and nail polish and visualized with 60x oil immersion objective in a confocal laser-scanning microscope (Olympus FluoView FV10i). Quantification of fluorescent signals was performed by ImageJ software.

2.9 MITO TRACKER STAINING

The impact of *Ctcflos* KD (day 1 of differentiation) on mitochondrial biogenesis was investigated by mitochondrial staining using MitoTracker™ Deep Red 633 (Invitrogen). This involves a fluorescent dye that selectively accumulates within the mitochondrial matrix and covalently binds to mitochondrial proteins.

As described above for immunocytochemistry, primary brite *Ctcflos* KD and control adipocytes, which were reverse transfected onto 8-well chamber microscopic slides, were subjected to Mito Tracker staining 48 hours after the KD. The cells were washed with PBS and treated with Mito Tracker staining solution (100 nM in DMEM) at 37°C for 30 min. After washing with DMEM, they were fixed with formaldehyde (3.7% in DMEM) at 37°C for 10 min, mounted with Vectashield Mounting Medium containing DAPI for nuclear counterstain (Vector Labs) and sealed with a cover slip and nail polish. The fluorescent signal was visualized using a 60x oil immersion objective in a confocal laser-scanning microscope (Olympus FluoView FV10i) and quantified by ImageJ software.

2.10 LIPID DROPLET STAINING AND QUANTIFICATION

Lipid droplet staining of *Ctcflos* KD (day 1 of differentiation) and control primary brite adipocytes was performed by use of a hydrophobic dye 'Oil Red O' (Sigma-Aldrich) that accumulates within lipid droplets and thus visualizes them. After extraction, it can be quantified photometrically.

Prior to the staining, the cells were washed with PBS and fixed with formaldehyde (3.7%) for 1 hour. Oil red O (0.3%) in isopropanol was added for 1 hour at room temperature for the staining, the cells were washed two times and covered with PBS for microscopic viewing and picture taking (10x and 32x objectives). For quantification of the lipid droplet accumulated Oil Red O dye, the cells were washed three times with isopropanol (60%) for 5 min each and incubated with isopropanol (100%) for 5 min for Oil Red O extraction. 80% of the extraction volume was transferred to a Nunc 96-well plate (VWR) and absorbance was measured at 492 nm in the Infinite M200 Microplate reader (Tecan). Absorbance of a blanc sample (100% isopropanol) was subtracted from absorbance of the samples.

Lipid droplet numbers and size distributions were determined by automated digital image analysis (Wimasis).

2.11 LIPOLYSIS ASSAY

Lipolysis rates of *Ctcflos* KD (day 1 of differentiation) and control primary brite adipocytes were determined by the measurement of glycerol release under basal and isoproterenol-stimulated conditions using Free Glycerol Reagent (Sigma-Aldrich). In coupled enzyme reactions, involving glycerol kinase, glycerol phosphate oxidase and peroxidase, a quinoneimine dye is produced in direct proportion to the free glycerol concentration in the sample and measured photometrically.

48 hours after the KD, the cells were washed with PBS, pretreated for 1 hour and then incubated for another hour w/o isoproterenol (0.5 µM) in DMEM with glucose (1 g/l) and BSA (2%), pH 7.4. The incubation medium was harvested and the cells were frozen for protein concentration determination for data normalization. On a 96-well plate 10 µl of the incubation medium were combined with 100 µl of free glycerol reagent and incubated by gentle shaking at room temperature in the dark for 15 min. The dye production was measured at 540 nm in the Infinite M200 Microplate reader (Tecan) and normalized by protein concentration.

2.12 LENTIVIRAL OVEREXPRESSION

Rescue experiments of *Ctcflos* KD effects were conducted by the combination of lentiviral overexpression of *Prdm16* in proliferating primary brite adipocytes and KD of *Ctcflos* at beginning differentiation.

For cloning of the lenitviral *Prdm16* overexpression (OE) vector, the *FLAG-Prdm16* (short isoform) open reading frame was PCR amplified from MSCV-Prdm16 (Fig. S2) (gift of Bruce Spiegelman to Addgene, http://n2t.net/addgene:15504 ; RRID:Addgene_15504) (Seale *et al.*, 2007) using Phusion® High-Fidelity DNA polymerase (Thermo Scientific) and target-specific primers extended for restriction enzyme (PmeI and EcoRI) recognition motifs. The amplification product was separated from the donor backbone on an agarose gel and purified (Wizard® SV Gel and PCR Clean-Up System, Promega). The purified *FLAG-Prdm16* product and the lentiviral overexpression pCDH-PGK receiver vector (Addgene) (Fig. S3) were digested with PmeI and EcoRI (NEB) at 37°C for 30 min, followed by inactivation at 65°C for 20 min. The cut vector backbone and *FLAG-Prdm16* inserts were again separated on an agarose gel, purified and ligated by T4 DNA ligase (NEB) in a ratio of 1:3 at 16°C overnight, followed by heat inactivation at 65°C for 10 min. The ligated lentiviral pCDH-PGK-FLAG-Prdm16 overexpression vector was transformed into NEB® Stable competent *E.coli* cells by a heat-shock. Plasmids were purified from bacterial colonies, which had been grown overnight on ampicillin containing agar plates and further proliferated in liquid cultures, using PureYield™ Plasmid Miniprep System (Promega). Plasmids were control digested and sent for DNA sequencing to validate the cloning result.

For virus production, the cloned pCDH-PGK-FLAG-Prdm16 vector (6 µg) or pCDH-PGK-tGFP vector (6 µg), as control, were co-transfected together with second-generation packaging plasmids psPAX2 (4.5 µg) (Fig. S4) (Addgene) and pMD2.*G* (1.5 µg) (Fig. S5) (Addgene) into 50% confluent HEK 293T cells on 10 cm culture plates using PolyFect transfection reagent (Qiagen). Virus containing supernatant was harvested from two plates on the following three days, passed through a 0.45 µm polyether-sulfone membrane filter and added to polyethylene glycol (PEG-*it*™ Virus precipitation solution, System Biosciences) for virus concentration. After overnight precipitation, the virus was pelleted by centrifugation at 1500 *g* for 30 min at 4°C (supernatant aspiration) and 1500 *g* for 5 min at 4°C (supernatant aspiration). The virus was resuspended in 140 µl PBS and the virus titer was determined based on the quantification of the p24 viral capsid protein using One-Wash™ Lentivirus TiterKit HIV-1 p24 Elisa Assay (Origene).

Primary proliferating iWAT preadipocytes remained untreated or were transduced at 50% confluence with lentivirus (*FLAG-Prdm16* overexpression virus or *tGFP* overexpression virus as control) (multiplicity of infection (MOI) 500 or 800) using polybrene (8 µg/ml) for 24 hours. At 80% confluence, the cells were induced for two days and *Ctcflos* was knocked down at the first day of differentiation as described above. The cells were harvested after 72 hours for RNA isolation and gene expression analysis by qPCR. In the comparison of FLAG-RRDM16 with tGFP overexpressing adipocytes, gene transcript levels were normalized to *fatty acid binding protein 4* (*Fabp4*) in order to normalize for the slightly decreased differentiation rate in the tGFP cells. As second control, FLAG-PRDM16 overexpressing adipocytes were compared to virus-untreated cells with equivalent differentiation rate (transcript levels normalized to *Gtf2b*).

2.13 SPLICING INHIBITION

Splicing was inhibited in primary brite adipocytes at the first day of differentiation using isoginkgetin (Tocris), a membrane-permeable natural inhibitor that prevents the assembly of the spliceosomal A complex during pre-mRNA splicing.

10 nM, 15 nM or 20 nM isoginkgetin diluted in DMSO or a corresponding amount of DMSO alone, as control, was added to the differentiation medium of the cells and incubated for 48 hours. The cells were washed and harvested for RNA isolation and qPCR analysis.

2.14 CODING POTENTIAL DETERMINATION

Protein coding potentials were evaluated by three different publicly available software tools, Coding Potential Calculator 2 (CPC2) (Kang *et al*, 2017), Coding Potential Assessment Tool (CPAT) (Wang *et al*, 2013b) and lncScore (Zhao *et al*, 2016). For CPC2 default setting were used for the run, LncScore was run using the hexamer and training data distributed with the software and CPAT was executed via the web interface. The threshold for protein coding propability was set to 0.4, with lower scores being judged as non-protein coding. For additional evaluation, RNA sequences were *in silico* translated and blasted against the RefSeq protein database using blastx with restriction to the plus strand.

2.15 EQUIVALENCE TESTING

In order to investigate whether the impact of *Ctcflos* KD on *Ucp1* gene transcription is dependent or independent of *Prdm16*, *Ctcflos* and *Prdm16* single KD effects on *Ucp1* were compared to the effect size of their double knockdown. For this purpose, the different KD groups (*Ctcflos* single KD, *Prdm16* single KD and *Ctcflos*+*Prdm16* double KD) were tested for equivalence by Two-One-Sided-t-tests (TOST) Equivalence Testing for dependent t-tests implemented in the R function TOSTpaired.raw (significance level α=0.1). In this test, upper and lower equivalence bounds are defined as the smallest effect sizes that would be regarded as interesting. If the actually observed effect size does not exceed these bounds downwards or upwards, it is too small to be considered and the compared groups can be regarded as equivalent.

For the comparison of *Ctcflos* single KD or *Prdm16* single KD with their double KD, respectively, equivalence bounds (±0.18) and (±0.33) were set based on the multiplicative gene interaction model, which postulates that the effect size of a double KD of two genes would be equal to the multiplication of the single KD effects, if the genes worked completely independent of each other (Costanzo *et al*, 2019). Equivalence bounds were thus defined as the delta between the remaining *Ucp1* expression of the single KD and this theoretically calculated value for the double KD (Form. 1). A smaller difference between single and double KD point towards an epistasis/ interaction between the two genes.

Formula 1: Calculation of equivalence bounds for TOST equivalence testing

Equivalence bounds for the comparison of *Ctcflos* single KD with *Ctcflos-Prdm16* double KD

= rem. rel. *Ucp1* expr. in *Ctcflos* KD – (rem. rel. *Ucp1* expr. in *Ctcflos* KD **x** rem. rel. *Ucp1* expr. in *Prdm16* KD)

= 0.36 – (0.36 **x** 0.51)

= **0.18** (Equivalence bounds: **± 0.18**)

Equivalence bounds for the comparison of *Prdm16* single KD with *Ctcflos-Prdm16* double KD

= rem. rel. *Ucp1* expr. in *Prdm16* KD – (rem. rel. *Ucp1* expr. in *Ctcflos* KD **x** rem. rel. *Ucp1* expr. in *Prdm16* KD)

= 0.51 – (0.36 **x** 0.51)

= **0.33** (Equivalence bounds: **± 0.33**)

The actual difference in *Ucp1* transcript levels between *Ctcflos* or *Prdm16* single KD and *Ctcflos-Prdm16* double KD was compared to these equivalence bounds in the TOST test.

2.16 COMPUTATIONAL PREDICTIONS

Approaching the mechanism of *Ctcflos* activity in brite adipogenesis, a series of *in silico* predictions were performed to investigate putative *Ctcflos* binding sites on DNA, the *Ctcflos* secondary structure, enrichment of RNA binding protein (RBP) motifs in *Ctcflos*-dependently spliced transcripts and *Ctcflos*-protein interactions. All analyses present theoretical approaches that can provide useful starting points for future investigations but warrant further experimental evaluation.

For the identification of DNA loci that could be targeted by *Ctcflos* through complementary base pairing, the *Ctcflos* isoform 1 transcript sequence was blasted against the murine genome (GRCm38) using the Ensembl BLAT function. For the identification of blast-hits of interest, they were investigated for the co-localization with areas of high *Ctcflos*-dependent transcriptional regulation. For this purpose, the mean percentage of all *Ctcflos*-dependently regulated genes (up-regulated, down-regulated and both) was calculated and blotted within frames of 10 Mbs stepping along the entire mouse genome in 1000 bp intervals. Blast hits, co-localizing with areas of either strong positive or strong negative *Ctcflos*-dependent transcriptional regulation, were pointed out.

Putative transcription factor (TF) binding sites within the *Ctcflos* isoform 1 sequence were identified by the Genomatix MatInspector algorithm, which provides and ranks TF matrix families and the corresponding TFs within a given sequence (Quandt *et al*, 1995).

Ctcflos secondary structure was predicted by the RNAfold web server (Vienna RNA Web Services Institute for Theoretical Chemistry) (http://rna.tbi.univie.ac.at/cgi-bin/RNAWebSuite/RNAfold.cgi) (Gruber *et al*, 2008) with minimum free energy and partition function, as well as avoidance of isolated base pairs.

Ctcflos-dependently spliced transcripts were analyzed for the enrichment of motifs of gene expression modulating RNA binding proteins (RBPs) using the Transite analysis platform (https://transite.mit.edu) (Krismer *et al*, 2019). Transite Set Motif analysis was performed with a matrix-based analysis approach searching for RBP motifs I) in the 3'UTRs or II) in the mature mRNA sequences based on the Transite motif database (p-value adjustment by Benjamini-Hochberg).

Sequence-based feature projection ensemble learning method-lncRNA-protein interaction (SFPEL-LPI), a machine learning algorithm, was applied for the prediction of *Ctcflos* interaction with proteins (www.bioinfotech.cn/SFPEL-LPI) (Zhang *et al*, 2018). The prediction is based on the extraction of lncRNA and protein sequence-based features, their comparison to other lncRNAs and proteins and interaction predictions using known lncRNA-protein interactions.

2.17 STATISTICAL ANALYSIS AND DATA PRESENTATION

In the present thesis, data are either presented in bar charts as means ± SD or in point diagrams showing means and individual values. Significance of differences for single comparisons were assessed by paired or unpaired two-tailed Student's t test. One-way or two-way analysis of variance (ANOVA) with Šídák *post hoc* test were applied for the comparison of two or more groups. Correlations are given with Pearson correlation coefficients. Statistical significance is considered for p-values below 0.05. The statistical analysis was predominantly conducted by prism 6 software (GraphPad).

3 RESULTS

Different inbred mouse strains vary in their propensity to recruit brite adipocytes in inguinal white adipose tissue (iWAT) in response to cold or β-adrenergic receptor stimulation. This diverging capacity for iWAT browning can be deduced to cell intrinsic cues, since it is mirrored *in vitro* in primary brite adipocytes, devoid of systemic influences (Li *et al.*, 2019). High expression levels of key thermogenic marker *Ucp1* report strong browning potentials of adipocytes derived from 129S6, A/J and AKR/J mouse strains, while low *Ucp1* transcription levels reveal weak browning capacities of cells originating from BL/6J and SWR/J mice (Fig. 7 A) (Li *et al.*, 2019). Comparative transcriptome analyses using this previously established five mouse strain-model set the basis for the identification of long noncoding RNAs (lncRNAs) of regulatory potential in brite adipogenesis within the present thesis. Parts of the below presented results were published (Bast-Habersbrunner *et al*, 2021).

3.1 REGULATION OF LONG NONCODING RNAS DURING BRITE ADIPOGENESIS ALONG WITH PROTEIN CODING GENES

The transcriptomes of undifferentiated preadipocytes and rosiglitazone-differentiated mature brite adipocytes (derived from all five mouse strains) as well as non-rosiglitazone differentiated mature white adipocytes (originating from 129S6 mice) included 5741 transcribed lncRNAs with a mean read number over all samples of ≥3 (Fig. 7 A). In principal component analysis (PCA) and hierarchical clustering the identified lncRNA transcriptome clearly separated undifferentiated from differentiated adipocyte samples, denoting profound transcriptional regulation of lncRNAs during brite adipogenesis (Fig. 7 B and C). Increasing distances among the mouse strains in differentiated compared to undifferentiated adipocytes further point towards a switch from a relatively common lncRNA expression pattern to a more strain-specific signature along the differentiation process (Fig. 7 B). Both observations are consistent with the scenario that lncRNAs are functionally involved in the browning process and may contribute to the strain-specific browning propensity.

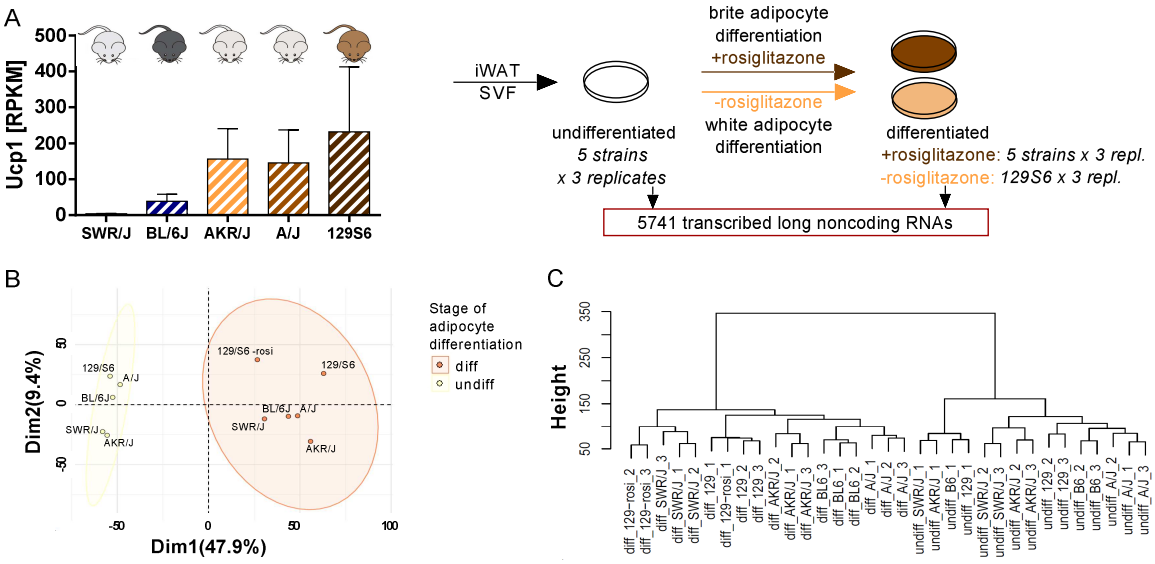

Figure 7: Long noncoding RNAs are regulated during brite adipogenesis. (A) Experimental design of comparative transcriptome analysis. Primary preadipocytes and differentiated adipocytes ((w/o) rosiglitazone), isolated from iWAT of five inbred mouse strains of varying browning propensity, were subjected to RNA sequencing to identify regulated lncRNAs. The differential browning propensity was evaluated based on *Ucp1* transcript levels in RPKM (reads per kilobase per million mapped reads). Mean values ± SD, n=3 (biological replicates) (Data ref: Array Express E-MTAB-8344, 2019) (Li Y, 2019). **(B)** Principal component analysis of the lncRNA transcriptome of undifferentiated and differentiated adipocyte samples, n=3 (biological replicates). **(C)** Hierarchical clustering of the lncRNA transcriptome of undifferentiated and differentiated adipocyte samples, n=3 (biological replicates), euclidean distance. Modified from (Bast-Habersbrunner *et al.*, 2021).

To narrow down those lncRNAs of potential functional involvement in brite adipogenesis, three selection criteria were set, filtering for lncRNAs that **i)** correlate with browning marker *Ucp1* in differentiated adipocytes across the five mouse strains (Pearson r >0.6 for positive correlation; Pearson r <-0.6 for negative correlation), **ii)** are significantly regulated during the course of brite adipocyte differentiation in the 129S6 strain with the strongest browning capacity (log2 fold change (differentiated: undifferentiated) >1 for up- and <-1 for downregulation, respectively) and **iii)** respond to rosiglitazone treatment in adipocytes of the 129S6 strain (log2 fold change (with rosiglitazone: without rosiglitazone) >0.585 for induced and <-0.585 for repressed lncRNAs, respectively). This led to the identification of **189 positively regulated** lncRNAs, which follow the trend of browning propensity across the mouse strains (positive correlation with *Ucp1*), are induced during brite adipogenesis in cells of the 129S6 strain (upregulation differentiated: undifferentiated) and are increased in mature brite compared to white adipocytes (upregulation with rosiglitazone: without rosiglitazone) (Fig. 8 A and C); as well as **103 negatively regulated** lncRNAs that oppose the browning trend among the mouse strains (negative correlation with *Ucp1*), are repressed during 126S6 brite adipogenesis (downregulation differentiated: undifferentiated) and are decreased in brite compared to white adipocytes (downregulation with rosiglitazone: without rosiglitazone) (Fig. 8 A and D). Applying the same three selection criteria to protein coding genes, accordingly identified 2165 positively and 2375 negatively regulated transcripts (Fig. 8 B, E and F).

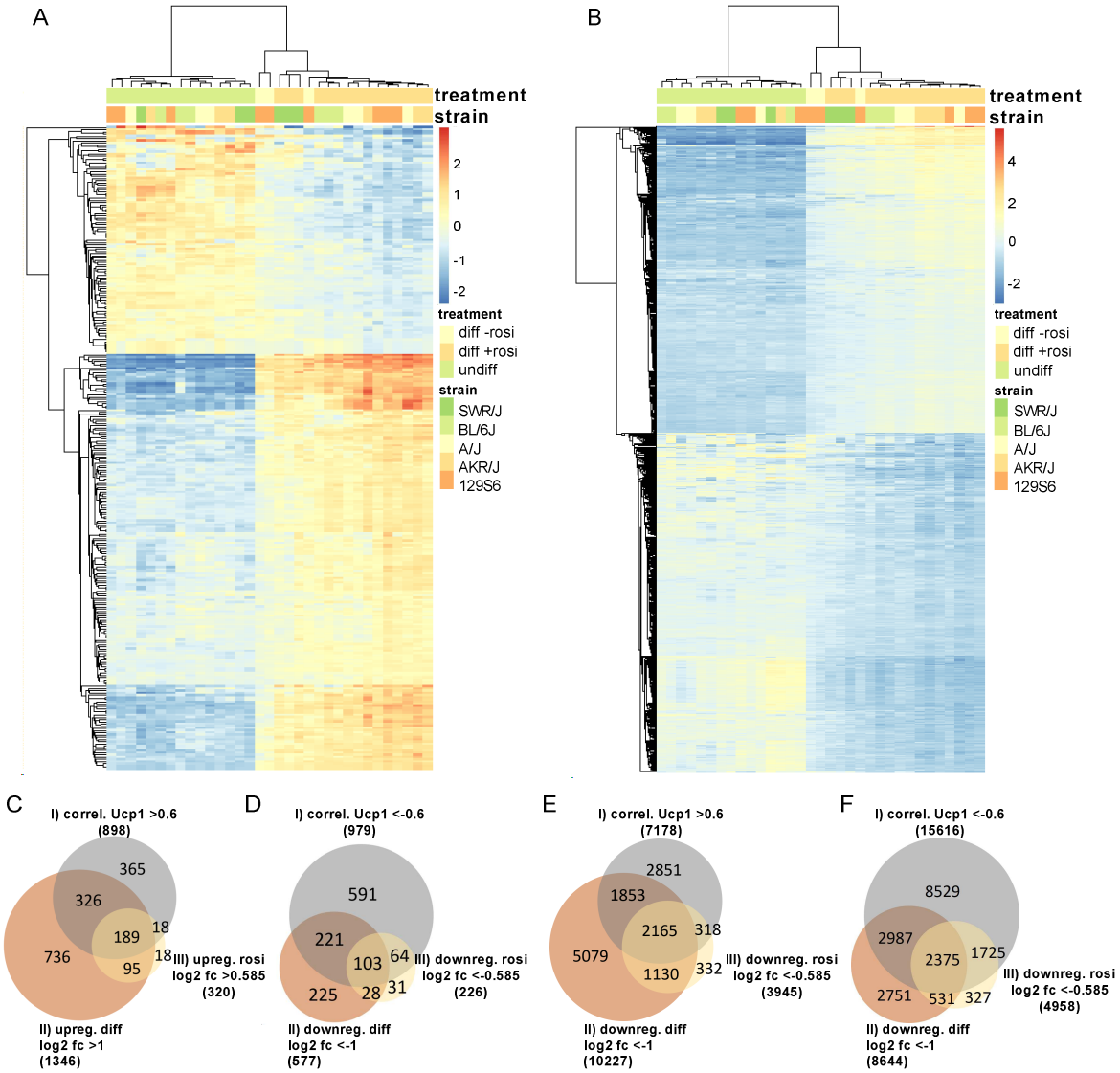

Figure 8: Comparative transcriptome analysis reveals positive and negative lncRNA and protein coding regulators in brite adipogenesis. (A, B) Heat maps of **(A)** lncRNAs and **(B)** protein coding genes, regulated in primary iWAT-derived adipocytes according to the defined three selection criteria (correlation with *Ucp1* across the five mouse strains, regulation during brite differentiation and by rosiglitazone treatment of 129S6 derived adipocytes). Displayed are row-wise centered log2 normalized counts, n=3 (biological replicates). **(C-F)** Venn diagrams of **(C)** positively and **(D)** negatively regulated lncRNAs, as well as **(E)** positively and **(F)** negatively regulated protein coding genes, n=3 (biological replicates). Modified from (Bast-Habersbrunner *et al.*, 2021).

Comparing long noncoding and protein coding transcripts, their strength of regulation and also the overall proportion of positively regulated lncRNAs (3.3%) was similar to that of positively regulated protein coding genes (3.8%) (Tab. 7). The percentage of negatively modulated lncRNAs (1.8%), in contrast, was exceeded by that of protein coding transcripts (4.1%), stressing the role of lncRNAs as potential inducers rather than repressors of brite adipogenesis (Tab. 7). Positively regulated lncRNAs were therefore chosen for most further analyses.

Table 7: Numerical overview of regulated lncRNAs and protein coding genes.
Absolute numbers and relative portions of regulated lncRNAs and protein coding genes.

	correl. Ucp1 - reg. diff - reg. rosi				
nr. of regulated	**pos.-up-up**	**neg.-down-down**	**pos.-down-up**	**neg.-up-down**	**total nr.**
lnc RNAs	189	103	0	6	5741
%	**3.3%**	**1.8%**	**0**	**0.1%**	**100%**
coding genes	2165	2375	9	290	57676
%	**3.8%**	**4.1%**	**0.02%**	**0.5%**	**100%**

Gene ontology (GO) term analysis of the filtered protein coding genes strongly suggested involvement of positively regulated transcripts in fatty acid metabolism, mitochondrial functions, respiratory chain and thermogenesis (Fig. 9 A), while negatively regulated transcripts were associated with cell division, cell migration and angiogenesis (Fig. 9 B). This supports that the selection strategy effectively filters for protein coding factors associated with the regulation of brite adipogenesis and that it might accordingly provide the potential to identify lncRNAs involved in that process.

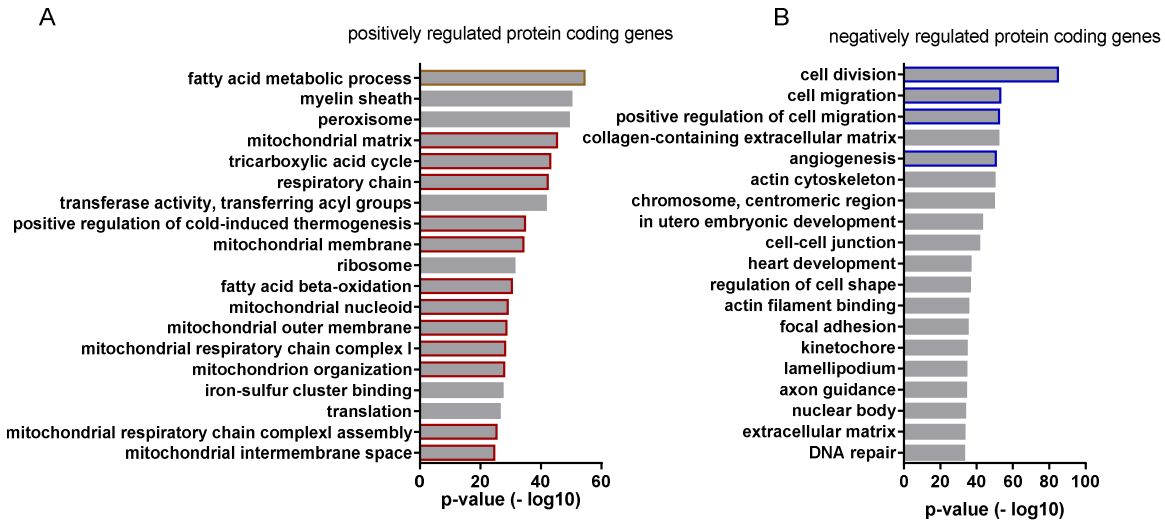

Figure 9: Regulated protein coding genes are associated with adipogenic and thermogenic functions.
GO term analysis of **(A)** positively and **(B)** negatively regulated protein coding genes, according to the above defined three selection criteria.

Owing to their predominantly poor conservation and the fact that they are up to date only marginally studied, it is more difficult to generally annotate functions to a defined group of lncRNAs. Nevertheless, it was proposed that lncRNA functions can be deduced from their correlation with mRNAs in context of a dynamic physiological process (Bai *et al.*, 2017; Cabili *et al*, 2011). Overrepresented GO terms of those mRNAs directly connected to at least one lncRNA within a correlation network cluster point towards the potential lncRNA functions. This strategy was used to deduce the biological functions of the here identified, positively regulated lncRNAs during brite adipogenesis. For this aim, lncRNA-mRNA correlations were calculated and translated into a lncRNA-mRNA correlation network. The network was clustered, unveiling three co-expression groups. GO terms of all lncRNA-connected mRNAs suggest involvement of lncRNAs of cluster 1 and 2 in lipid metabolism and electron transport

chain, while lncRNAs in cluster 3 are connected to tricarboxyclic acid (TCA) cycle function (Fig. 10).

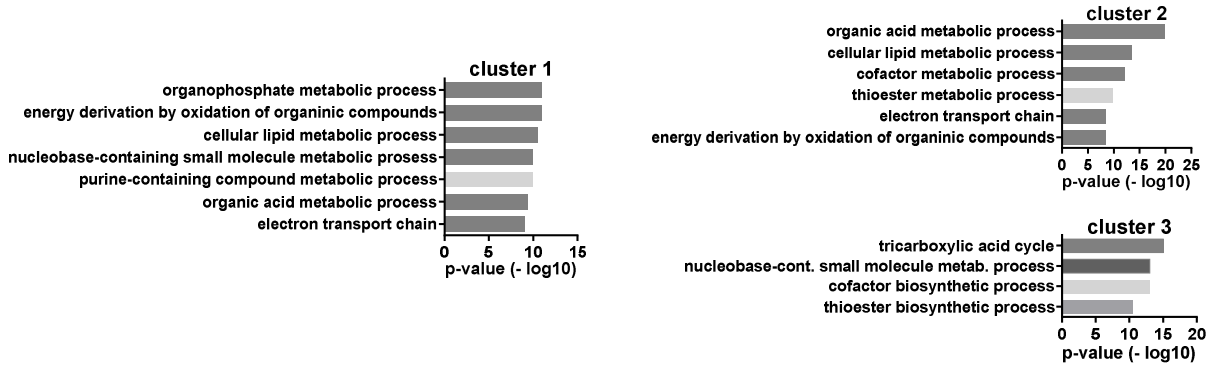

Figure 10: LncRNA-co-expressed mRNAs are associated with lipid and energy metabolic processes. GO term analyses of different mRNA clusters derived from a lncRNA-mRNA co-expression network (according to (Bai *et al.*, 2017)) that point towards lncRNA associated cellular processes. Positively regulated lncRNAs were included in the analysis. Modified from (Bast-Habersbrunner *et al.*, 2021).

3.2 THE TOP CANDIDATE REGULATED IN BRITE ADIPOGENESIS AND BROWN FAT THERMOGENESIS - LONG NONCODING RNA *CTCFLOS*

In a second step of selection, the above identified positively regulated lncRNAs were further narrowed down to thermogenesis-associated transcripts in order to reveal the candidates of strongest regulatory potential in both, brite adipocyte development **and thermogenic function**. For this, the selected lncRNAs were tested for their response to cold-induced stimulation of interscapular brown adipose tissue (iBAT) *in vivo*, constituting a state of full thermogenic activity. Only seven of the positively regulated lncRNAs were also significantly upregulated more than two fold (log2 fold change >1) in iBAT of BL/6J mice in response to six hours cold (4°C) exposure (Fig. 11 A and B). Among them, the three transcripts with the strongest thermogenic activity-associated regulation all constituted isoforms of lncRNA *CCCTC-binding factor (zink finger protein)-like, opposite strand* (*Ctcflos*) (also *1300015D01ik*), which was thus ranked as top candidate and chosen for further in depth analyses.

Side note to Fig. 11:

Besides Ctcflos, also the other four lncRNAs could present promising candidates for future investigation (Fig. 11 B). For example, the genetic location of AK087872 close to brown fat signaling factor Neuregulin 4 (Nrg4) might hint towards a putative functional implication in thermogenic adipocytes (Blüher, 2019).

A

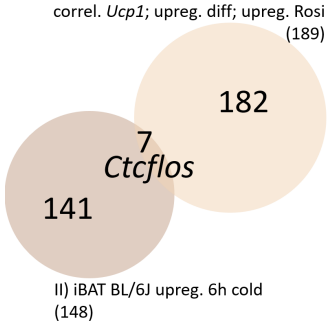

B

			brite adipocytes		iBAT
Symbol	Accn	correl Ucp1	upreg diff [log2 fc]	upreg rosi [log2 fc]	upreg 6h cold [log2 fc]
Ctcflos					
1300015D01Rik	AK041254 (tr 1)	0,89	8,45	0,66	1,87
1300015D01Rik	AK079954 (tr 3)	0,79	7,22	0,63	1,58
1300015D01Rik	AK005014 (tr 4)	0,85	7,74	0,87	1,37
AK087872	AK087872	0,87	3,72	1,36	1,31
4930534D22Rik	AK090212	0,64	1,36	0,86	1,14
A930026I22Rik	AK020893	0,76	2,42	1,01	1,13
Gm15834	AK053027	0,86	1,9	1,12	1,02

Figure 11: *Ctcflos* stands out as strongest regulated lncRNA in brite adipogenesis *in vitro* and during iBAT activation *in vivo*. (A) Venn diagram of lncRNAs positively regulated during brite adipogenesis *in vitro* and induced by cold-stimulated activation of iBAT *in vivo*. Seven lncRNAs are upregulated in both conditions. **(B)** Table of the seven co-regulated lncRNAs. The top three regulated transcripts present isoforms of lncRNA *Ctcflos*. (Bast-Habersbrunner *et al.*, 2021).

Validating its ranking as the top candidate, *Ctcflos* met the selection criteria as depicted from the RNA transcriptome data and confirmed by qPCR (Fig. 12). (I) *Ctcflos* expression in mature brite adipocytes correlates with *Ucp1* transcript levels across the five mouse strains. In accordance with *Ucp1*, it is strongly expressed in cells derived from the strains with high browning potential (129S6, AKR/J, A/J) and it is less abundant in those of low browning capacity (BL/6J, SWR/J) (Fig. 12 A). (II) In the course of 129S6 derived brite adipocyte differentiation its transcription is strongly induced 280-fold in RNA sequencing (Fig. 12 B) and 860-fold in qPCR analysis (Fig. 12 C). (III) *Ctcflos* is higher expressed in brite compared to white adipocytes differentiated in the presence and absence of rosiglitazone, respectively (1.54-fold in RNA sequencing (Fig. 12 D) and 1.59-fold in qPCR analysis (Fig. 12 E)), supporting its specific activity in thermogenic adipocytes. Finally, (IV) *Ctcflos* transcription is activated in iBAT of BL/6J mice in response to cold (3.81-fold after 6 hours) (Fig. 12 F). The induction of *Ctcflos* is strongest after 6 hours and correlates with *Ucp1* transcript levels across different durations of cold exposure (0, 6, 24 and 48 hours) (Fig. 12 G).

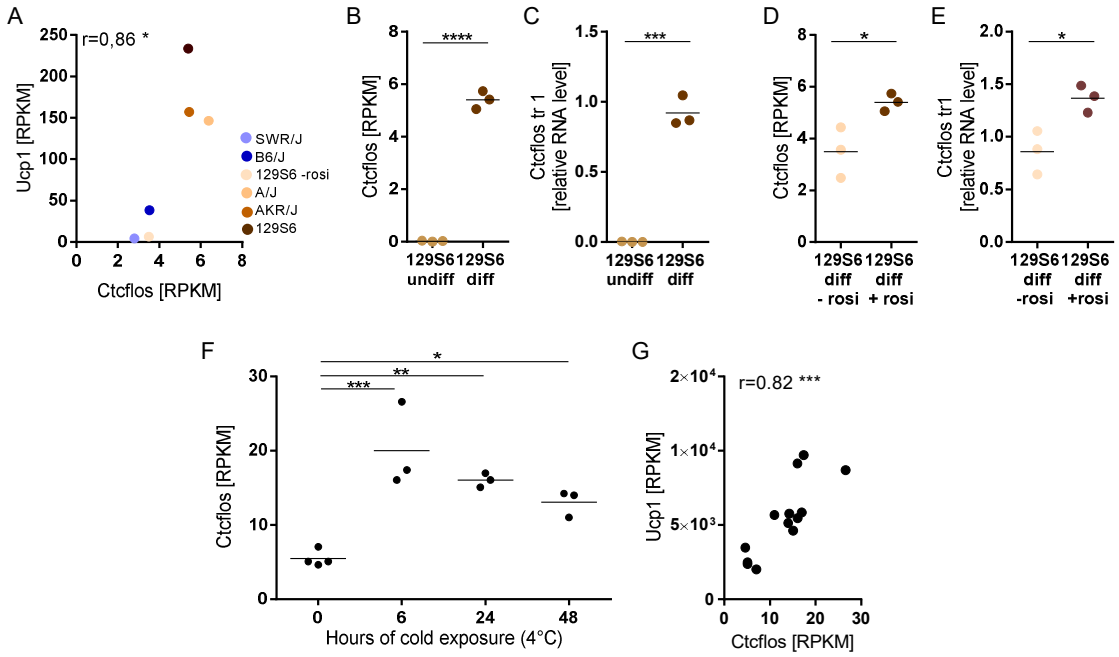

Figure 12: *Ctcflos* meets the defined selection criteria for positively regulated lncRNAs during brite adipogenesis and iBAT activation. (A) Correlation of *Ctcflos* with *Ucp1* transcript levels across differentiated primary brite adipocytes derived from iWAT of the five inbred mouse strains (transcript levels in RPKM, assessed by RNA sequencing). Mean values, n=3 (biological replicates), Pearson correlation. **(B, C)** *Ctcflos* transcript levels in differentiated brite compared to undifferentiated primary adipocytes derived from iWAT of 129S6 mice. **(B)** Transcript levels in RPKM, assessed by RNA sequencing **(C)** *Ctcflos* isoform 1 transcript levels relative to *Gtf2b*, assessed by qPCR. Mean and individual values, n=3 (biological replicates), unpaired t tests. **(D, E)** *Ctcflos* transcript levels in differentiated brite compared to differentiated white primary adipocytes derived from iWAT of 129S6 mice. **(D)** Transcript levels in RPKM, assessed by RNA sequencing. **(E)** *Ctcflos* isoform 1 transcript levels relative to *Gtf2b*, assessed by qPCR. Mean and individual values, n=3 (biological replicates), unpaired t tests. **(F, G)** Regulation of *Ctcflos* and *Ucp1* by cold-induced iBAT stimulation in C57BL/6J mice *in vivo* (Data ref. (Maurer S, 2018)). **(F)** *Ctcflos* transcript levels in iBAT of 0, 6, 24 or 48 hours cold (4°C) exposed C57BL/6J mice (transcript levels in RPKM, assessed by RNA sequencing). Mean and individual values, n=3-4 (biological replicates), one-way ANOVA (Šídák-test). **(G)** Correlation of *Ctcflos* with *Ucp1* transcript levels across the different durations of cold exposure (transcript levels in RPKM, assessed by RNA sequencing). Individual values. Pearson correlation. *p<0.05, **p<0.01, ***p<0.001, ****p<0.0001. Modified from (Bast-Habersbrunner *et al.*, 2021).

In support of the *in vitro* data on *Ctcflos* modulation during brite adipogenesis, it is also induced during iWAT browning *in vivo*. *Ctcflos* transcript levels are elevated in parallel to the cold-induced occurrence of thermogenic adipocytes in iWAT (as indicated by increased *Ucp1* abundance) in BL/6J mice kept at 5°C for one week, compared to age and weight matched mice housed at room temperature and thermoneutrality (Fig. 13).

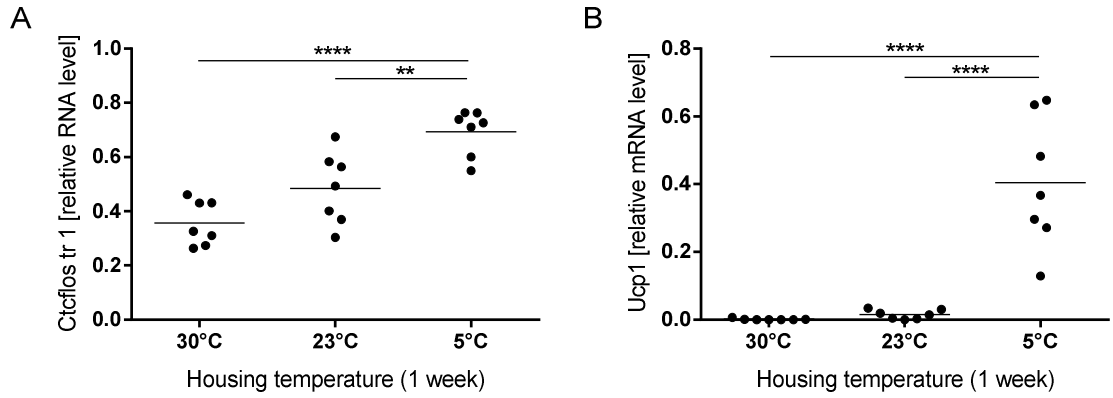

Figure 13: *Ctcflos* is induced during cold-mediated iWAT browning *in vivo*. (A) *Ctcflos* isoform 1 and **(B)** *Ucp1* transcript levels relative to *Gtf2b* in iWAT of C57BL/6J mice housed at 5°C for one week, compared to age and weight matched mice housed at 30°C or 23°C, assessed by qPCR. Mean and individual values, n=7 (biological replicates), one-way ANOVA (Šídák-test). **p<0.01, ****p<0.0001. Modified from (Bast-Habersbrunner *et al.*, 2021).

Together, these data confirm the strong regulation of the top candidate *Ctcflos* during brite adipocyte differentiation *in vitro* as well as iBAT activation and iWAT browning *in vivo* and thus support its responsiveness to the recruitment of thermogenic functionality.

3.3 CHARACTERIZATION OF LNCRNA *CTCFLOS*

The *Ctcflos* gene is encoded on chromosome 2: (173,110,818-173,133,204), partially overlapping at its 5' end with *Ctcfl* on the opposite strand. The Ensembl genome assembly (GRCm39) annotates four different isoforms for *Ctcflos*, ranging between 469 bp and 3476 bp in length; the DNA Databank of Japan (DDBJ) annotates three isoforms (Tab. 8).

Table 8: *Ctcflos* isoforms. *Ctcflos* isoform IDs in the Ensembl genome assembly and DNA Databank of Japan (DDBJ) and isoform lengths.

Ensembl	DDBJ	in the following referred to as	length
ENSMUST00000144256.1	AK041254	isoform1/transcript1 (tr1)	1237bp
ENSMUST00000142165.1	---	Isoform2/transcript2 (tr2)	469bp
ENSMUST00000142207.7	AK079954	Isoform3/transcript3 (tr3)	918bp
ENSMUST00000153523.1	AK005014	Isoform4/transcript4 (tr4)	3476bp

Using transcript specific primers, the presence of all four Ensembl-annotated *Ctcflos* isoforms could be confirmed in mature brite adipocytes (Fig. 14 A and B). Detailed analysis of the brite adipocyte transcriptome data, however, revealed read mapping throughout the *Ctcflos* locus, involving introns and extending beyond the 3' end of the transcripts (Fig. 14 C). This might be partially explained by reads mapping to unprocessed pre-RNAs, the clear allocation of reads beyond the annotated transcript boundaries, however, suggests incomplete isoform annotation. *De novo* reconstruction of *Ctcflos* transcripts based on the brite cell RNA sequencing data using String Tie, accordingly predicted prolonged exons for isoforms 1, 3 and 4 as well as a new isoform with joint exons of isoform 2 and 4 (Fig. 14 D). A 3' rapid amplification of cDNA ends (RACE) PCR could further clarify the sequences of *Ctcflos* transcripts in brite cells in future analysis.

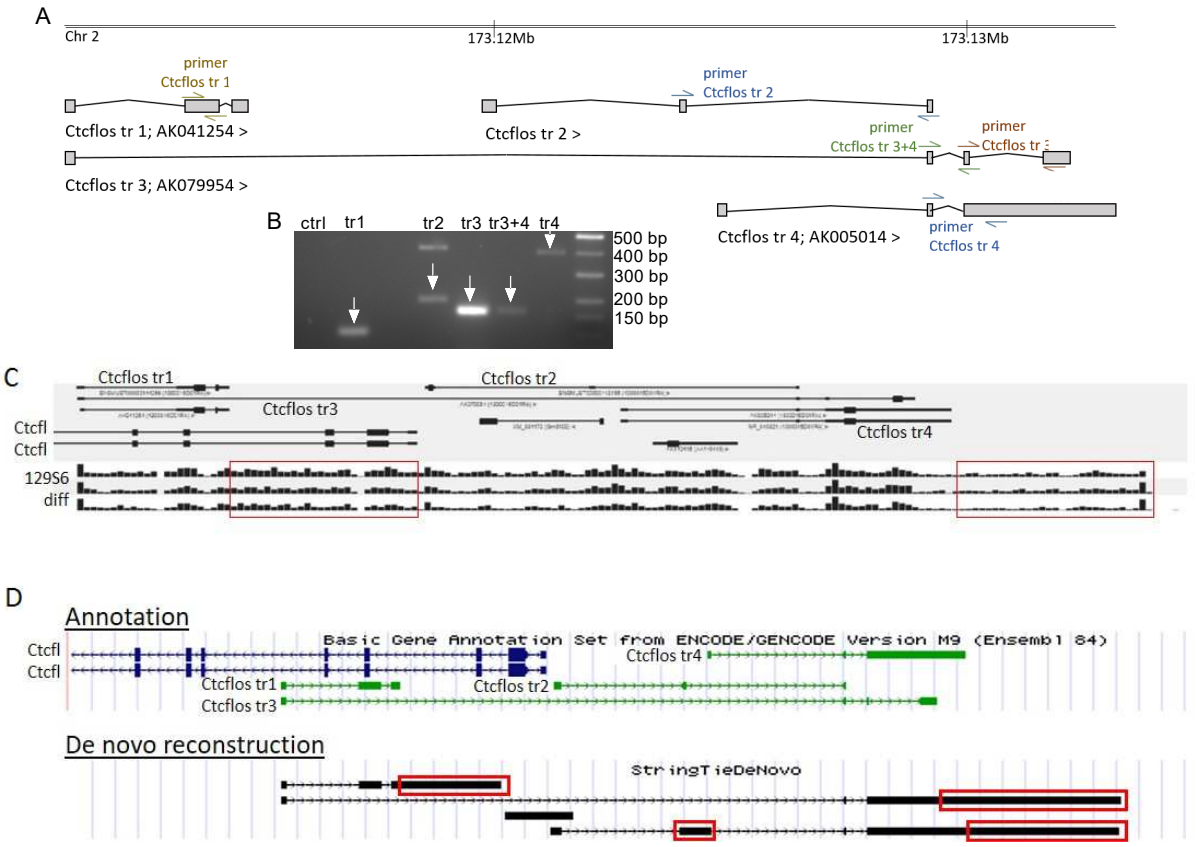

Figure 14: The *Ctcflos* isoform profile requires thorough revision. (A) *Ctcflos* locus, displaying location and structure of annotated *Ctcflos* isoforms according to the Ensembl genome assembly (GRCm39). Brown, blue and green marks display binding sites for primers used in isoform specific PCR (see (B)). **(B)** Gel picture of *Ctcflos* isoforms expressed in differentiated primary brite adipocytes, amplified by PCR using isoform specific primers (see (A)). **(C)** Read mapping to the *Ctcflos* locus in RNA sequencing of brite adipocytes at the third day of differentiation (Genomatix Software Suite). Red boxes highlight read mapping outside of annotated *Ctcflos* exon boundaries, n=3 (biological replicates) **(D)** Comparison of Ensembl annotated and *de novo* reconstructed *Ctcflos* isoform transcripts predicted from RNAseq read mapping using StringTie *de novo* reconstruction. Red boxes highlight prolonged 3' ends of *Ctcflos* exons. Modified from (Bast-Habersbrunner *et al.*, 2021).

Concerning post-transcriptional processing, lncRNAs can either be polyadenylated, as the majority of mRNAs, or remain unprocessed at their 3' ends, lacking a poly A tail. *Ctcflos* could be assigned to the group of polyadenylated lncRNAs, as its transcripts were primarily detectable in the poly A RNA fraction of brite and brown adipocytes, similar as polyadenylated positive control *Ucp1* (Fig. 15). Poly A-negative control *45S ribosomal RNA* (*45SrRNA*), in contrast, was diminished in the poly A RNA fraction (Fig. 15).

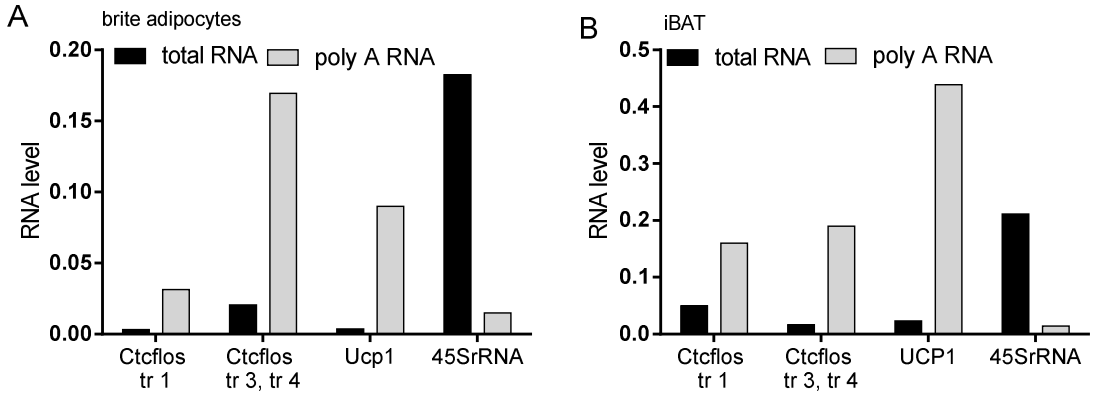

Figure 15: *Ctcflos* lncRNA is polyadenylated. *Ctcflos*, *Ucp1* and *45SrRNA* transcript abundance in total RNA and the poly A RNA fraction of **(A)** differentiated primary brite adipocytes and **(B)** iBAT tissue of 129S6 mice, assessed by qPCR, n=1 (biological replicate). Modified from (Bast-Habersbrunner *et al.*, 2021).

To determine the distribution of *Ctcflos* expression within the murine organism, several tissues were analyzed for *Ctcflos* transcript abundance. This revealed predominant transcription of *Ctcflos* in adipose tissues, including iBAT, iWAT and gWAT in descending order, following the trend of *Ucp1* abundance (Fig. 16 B). Minor *Ctcflos* transcript levels were detectable in liver and muscle. Further supporting the dominance of *Ctcflos* expression in thermogenic fat cells, the BioGPS database also states clear dominance of *Ctcflos* in brown adipose tissue compared to a wide range of different tissues and cell lines (Fig. 16 A) (Wu *et al*, 2009).

Following their transcription, lncRNAs can either be retained in the nucleus, exported to the cytosol or present in both compartments. The subcellular localization helps to narrow down the lncRNA's functional mechanism. Comparing nuclear, cytosolic and mitochondrial RNA fractions of primary brite adipocytes demonstrated dominant retention of *Ctcflos* in the nucleus (Fig. 16 C). As positive and negative controls nuclear *45SrRNA* and cytosolic *12SrRNA* were primarily detected in the nuclear and cytosolic fraction, respectively (Fig. 16 B).

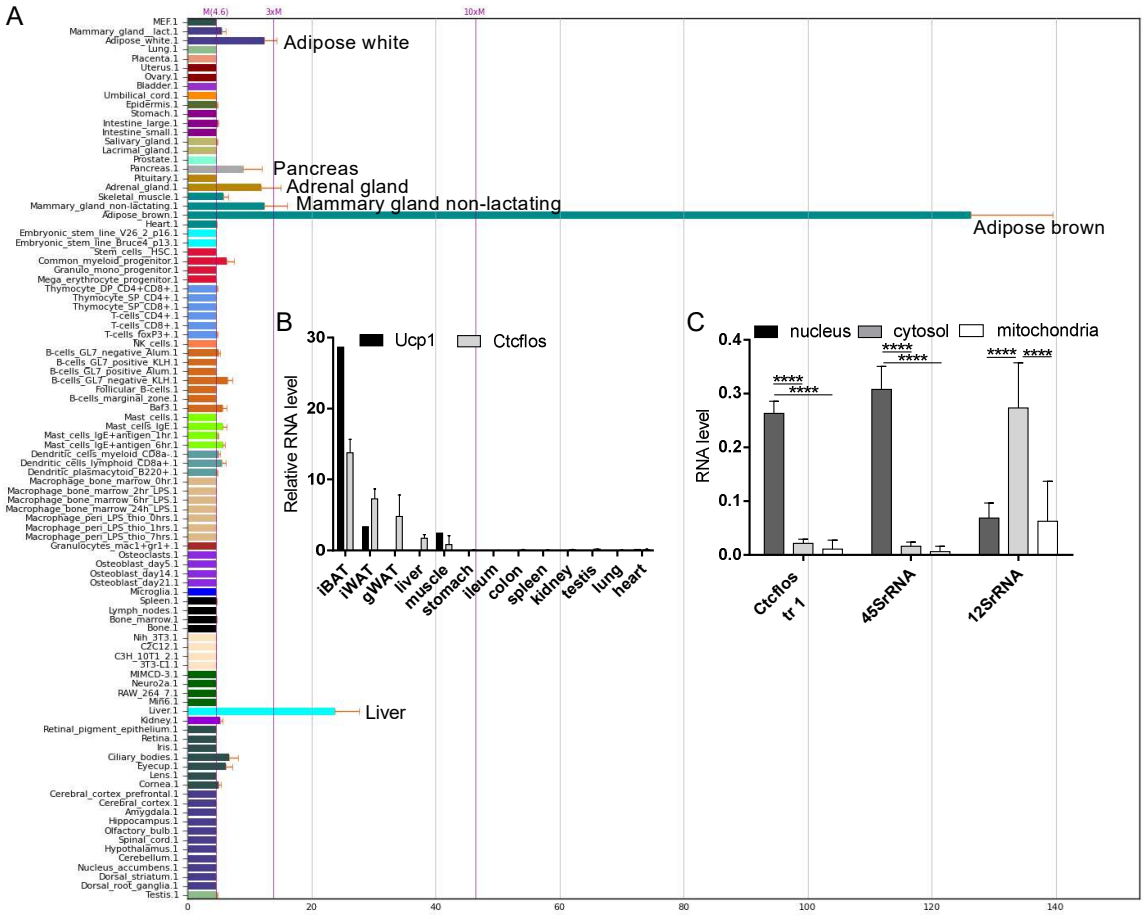

Figure 16: *Ctcflos* is predominantly expressed in adipose tissues and enriched in cell nuclei. (A) Overview of *Ctcflos* expression in different tissues and cell types by BioGPS (normalized expression levels ± SEM) (Wu *et al.*, 2009). **(B)** *Ctcflos* and *Ucp1* transcript levels relative to *Gtf2b* in different tissues of 129S6 mice, assessed by qPCR. Mean values ± SD, n=3 (biological replicates) for *Ctcflos*, n=1 (biological replicate) for *Ucp1*. **(C)** *Ctcflos*, *45SrRNA* and *12SrRNA* transcript levels relative to *Gtf2b* in nuclear, cytosolic and mitochondrial sub-fractions of primary brite adipocytes derived from iWAT of 129S6 mice, assessed by qPCR. Mean values ± SD, n=6 (biological replicates), two-way ANOVA (Tukey-test), ****p<0.0001. Modified from (Bast-Habersbrunner *et al.*, 2021).

Previously, lncRNAs that were annotated as noncoding transcripts, such as *Myoregulin*, were shown to actually encode for small peptides in *in vitro* translation experiments (Anderson *et al*, 2015). To evaluate whether *Ctcflos* is correctly annotated as noncoding RNA, the protein coding potential of *Ctcflos* was assessed using three independent, publicly available software tools: Coding potential calculator (CPC2) (Kang *et al.*, 2017), Coding potential assessment tool (CPAT) (Wang *et al.*, 2013b) and lncScore (Zhao *et al.*, 2016). With calculated protein coding probability scores below the cut off of 0.4, *Ctcflos* transcripts were evaluated as non-protein coding (Fig. 17 A). As controls, *Neat1*, an established lncRNA, was similarly evaluated as non-protein coding, while *Ucp1* was reliably predicted to encode a protein. *Myoregulin*, however, was also mainly judged as non-protein coding, revealing a limited sensitivity of the applied algorithms (Fig. 17 A). For additional validation, the *Ctcflos* isoforms were therefore *in silico* translated and blasted against the RefSeq protein database to test for the presence of any corresponding protein or peptide that could be encoded by *Ctcflos* RNAs. This analysis could not detect any significant match for the four *Ctcflos* isoforms, supporting that *Ctcflos* lacks protein coding potential and is correctly annotated as noncoding RNA (Fig. 17 B).

A

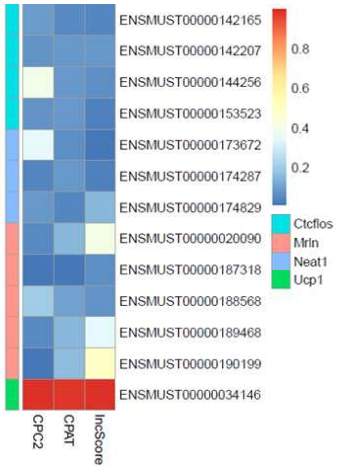

B

searched transcript	protein hit	ID proetin hit	% identity	length	mismatch	gapopen	e-value
Ctcflos ENSMUST00000144256	Arhgef40	NP_937892	25,243	103	56	4	**2,8**
		NP_001139394					
		NP_001139393					
Ctcflos ENSMUST00000142165	Tpm3	NP_001139393	25,455	55	41	0	**4,7**
		NP_001240667					
		NP_001280678	25,455	55	41	0	**5**
		NP_001258693					
Ctcflos ENSMUST00000142207	Cflar	XP_006495698	28,571	56	38	1	**4,8**
		XP_017169048					
		XP_011236725					
		XP_011236724					
		XP_011236723					
		XP_011236722					
Ctcflos ENSMUST00000153523	Tas2r115	NP_996903	32,609	46	30	1	**5,9**
Ucp1 ENSMUST00000034146	Slc25a14	NP_001277633	34,276	283	171	6	**1,25E-49**

Figure 17: *Ctcflos* can be confirmed as noncoding RNA. (A) Protein coding potential scores of *Ctcflos*, *Myoregulin* (*Mrln*), *Nuclear Paraspeckle Assembly Transcript 1* (*Neat1*) and *Ucp1* by publicly available machine learning algorithms: Coding potential calculator 2 (CPC2) (Kang *et al.*, 2017), Coding potential assessment tool (CPAT) (Wang *et al.*, 2013b) and lncScore (Zhao *et al.*, 2016). **(B)** *In silico* translation of *Ctcflos* transcript isoforms, followed by alignment against the NCBI protein database, to test for the presence of corresponding *Ctcflos*-derived peptides. Modified from (Bast-Habersbrunner *et al.*, 2021).

In contrast to protein coding genes, inter-species conservation is less pronounced among lncRNAs that are often species-specifically expressed. For the examination of murine *Ctcflos* conservation in the human genome, the human locus between *Ctcfl* and *Pck1*, which flank the murine *Ctcflos* gene, were searched for lncRNA annotations. Functional Annotations of the Mammalian Genome (FANTOM) predicted one human lncRNA upstream of *Pck1* (Fig. 18 A). Alignment of the human lncRNA sequence against all murine *Ctcflos* transcripts, however, did not show considerable matches (Fig. 18 B). Similarly, alignment of the murine *Ctcflos* sequences against the human genome and transcriptome by Ensembl BLAT and BLASTN, respectively, did not reveal considerable alignments with putative human lncRNA genes (data not shown). On the level of primary nucleotide sequence, *Ctcflos* thus seems not to be conserved in the human genome. The lack of sequence conservation, however, does not strictly entail a lack of functional conservation. For several lncRNAs the RNA structure, rather than the nucleotide sequence, constitutes the functional unit and evolutionary constraint (Johnsson *et al*, 2014). Analysis of *Ctcflos* secondary structure and comparison to the human lncRNA structures might thus present another reasonable approach to identify human lncRNAs of putative similar functionality.

Figure 18: *Ctcflos* is not conserved in the human genome. (A) Human gene locus between *Ctcfl* and *Pck1*, comprising a short lncRNA in between. **(B)** Alignments of the in (A) highlighted human lncRNA sequence with those of the murine *Ctcflos* transcripts. *Ctcflos* transcripts served as templates, grey areas in the human lncRNA illustrate sequence matches, red areas display sequence deviations. Modified from Peer Review (Bast-Habersbrunner *et al.*, 2021).

In summary, *Ctcflos* can be characterized as polyadenylated, nuclear retained, non-protein coding RNA that is transcribed into different isoforms, mainly expressed in adipose tissue and not conserved in humans on the level of nucleotide sequence.

3.4 THE ROLE OF *CTCFLOS* IN BRITE ADIPOCYTE DIFFERENTIATION AND THERMOGENIC FUNCTION

The proposed role of lncRNA *Ctcflos* in the browning process was experimentally evaluated by *in vitro* knockdown (KD) experiments in brite adipocytes. Continuous monitoring of *Ctcflos* expression along the course of brite adipocyte proliferation, induction and differentiation revealed sensible time points for the KD: *Ctcflos* expression starts to significantly increase during the induction of brite cell differentiation in the presence of rosiglitazone and experiences a second boost of transcription reaching the fifth day of differentiation, before levelling off in a plateau (Fig. 19 A). KD of *Ctcflos* at these two stages of differentiation allows investigation of *Ctcflos* functionality, both during early onset of brite adipogenesis (KD at day 1 of differentiation (diff), followed by analysis at day 4 diff) and in mature brite cells (KD at day 5 diff, followed by analysis at day 8 diff) (Fig. 19 B).

The KD experiments were conducted by locked nucleic acid (LNA) Gapmer antisense oligonucleotides (ASOs) that were preferred over RNA interference (RNAi), since they were shown previously to achieve stronger KD efficiencies of specifically nuclear located transcripts. The ribose rings at the LNA Gapmer ASO flanks are locked in an optimal conformation for Watson-Crick binding, which shall enhance their thermal stability and target affinity to attain specific and efficient target degradation. To further reduce the risk of off-targeting, six distinct ASOs were used, targeting three different isoforms of *Ctcflos*: ASO1, 3 and 4 for the KD of *Ctcflos* transcript 1 (tr1) and ASO2, 5 and 6 for KD of *Ctcflos* transcripts 3 and 4 (tr3, 4) (Fig. 19 C). Another ASO without any cellular target served as negative control (NC).

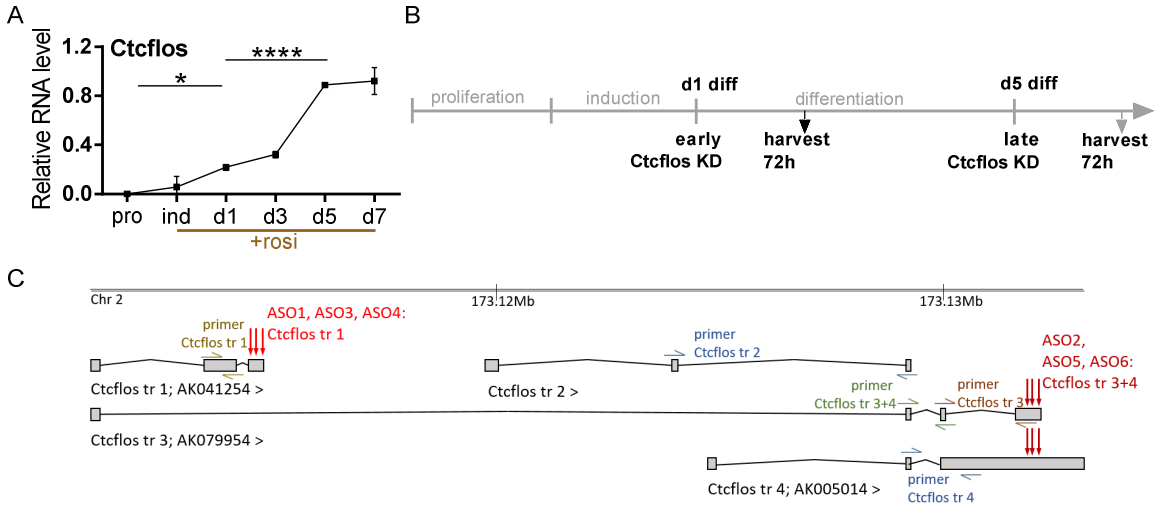

Figure 19: *Ctcflos* knockdown was performed at beginning and during late brite adipocyte differentiation. (A) Time course of relative *Ctcflos* expression across proliferation, induction and differentiation of primary brite adipocytes derived from iWAT of 129S6 mice (transcript levels relative to *Gtf2b*), assessed by qPCR. Mean ± SD, n=3 (technical replicates), one-way ANOVA, one representative experiment of three biological replications with comparative results (Fig. S6). **(B)** Design of *Ctcflos* KD experiments. KD of *Ctcflos* either at day 1 of differentiation followed by harvest 72 hours later, or KD of *Ctcflos* at day 5 of differentiation followed by harvest after 72 hours. **(C)** *Ctcflos* locus with annotated *Ctcflos* transcripts. Red arrows mark target sites of LNA Gapmer ASOs for *Ctcflos* KD. *p<0.05, ****p<0.0001. Modified from (Bast-Habersbrunner *et al.*, 2021).

3.4.1 Thermogenic marker gene expression in differentiating *Ctcflos*-deficient brite adipocytes

KD of *Ctcflos* at the first day of differentiation (Fig. 20 A) efficiently reduced *Ctcflos* transcript levels to 20-35% (tr1) and 11-15% (tr3 and 4), respectively (Fig. 20 B and C). Expression analysis of *Ucp1*, a key marker of thermogenic adipocytes, served to evaluate the impact of early *Ctcflos* deficiency on brite adipogenesis. *Ctcflos* KD entailed a pronounced reduction of *Ucp1* pre-mRNA, mRNA and protein levels, especially in response to *Ctcflos* tr1 deficiency (ASO1) (Fig. 20 D-H). The observation that already pre-mature *Ucp1* transcripts are downregulated, suggests that *Ucp1* expression is affected on the level of *Ucp1* gene transcription, rather than RNA processing, nuclear export or translation (Fig. 20 E). *Ucp1* mRNA was reduced to 31% by ASO1-6 in the mean (Fig. 20 D), which translated for ASO1 in significantly decreased protein abundance, as visualized and quantified in Western Blot and immunofluorescent analysis (Fig. 20 F-H). UCP1 protein expressing adipocytes (visualized by strong red immunofluorescent signals) are less abundant in *Ctcflos* deficient cells (Fig. 20 G and H). Transcription of *Cell death-inducing DNA fragmentation factor alpha-like effector A* (*Cidea*) and *Cytochrome c oxidase subunit 7a1* (*Cox7a1*) as further brite and brown adipocyte markers was also affected, further supporting that early *Ctcflos* KD impairs the brite adipocyte differentiation process (Fig. 20 I). For additional evaluation of the role of *Ctcflos* in the browning process, preliminary efforts were made towards overexpression of endogenous *Ctcflos* in C3H10T1/2 cells using the CRISPRa(SAM) system. Induction of *Ctcflos* could be achieved only in individual samples and thus requires further optimization and reproduction (Fig. 20 J (green) and K). Nevertheless, in the samples of elevated *Ctcflos* transcript levels also *Ucp1* tended to be increased (Fig. 20 L).

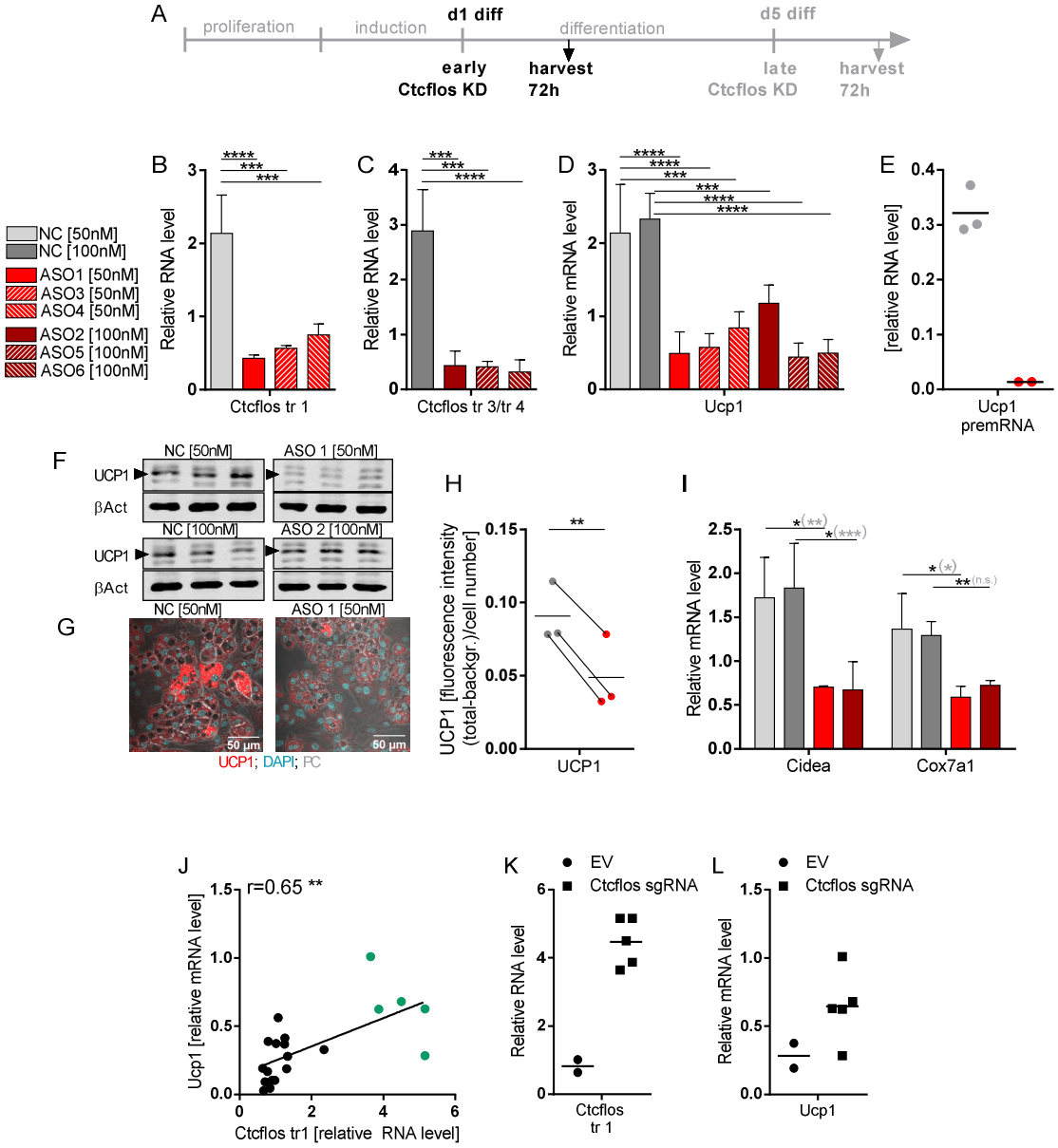

Figure 20: *Ctcflos* deficiency impairs brite adipogenic gene expression. (A) Design of the *Ctcflos* KD experiment. KD of *Ctcflos* at day 1 of differentiation of primary brite adipocytes derived from iWAT of 129S6 mice, followed by harvest after 72 hours. **(B, C)** Efficiency of *Ctcflos* KD by **(B)** LNA Gapmer ASO1, 3 and 4, targeting *Ctcflos* transcript 1 and **(C)** LNA Gapmer ASO2, 5 and 6, targeting *Ctcflos* transcripts 3 and 4, compared to non-targeting controls (NC) (transcript levels relative to *Gtf2b*), assessed by qPCR. Mean values ± SD, n=3 (biological replicates), one-way ANOVA (Šídák-test). **(D-H)** Impact of *Ctcflos* KD on UCP1 expression **(D)** *Ucp1* mRNA levels relative to *Gtf2b* in response to *Ctcflos* tr1 KD (ASO1, 3, 4), tr3 and 4 KD (ASO2, 5, 6) compared to non-targeting controls, assessed by qPCR. Mean values ± SD, n=3-4 (biological replicates), one-way ANOVA (Šídák-test). **(E)** *Ucp1* pre-mRNA transcript levels relative to *Gtf2b* in response to *Ctcflos* tr1 KD (ASO1) compared to non-targeting controls, assessed by qPCR. Mean and individual values, n=2-3 (biological replicates). **(F)** Western Blot analysis of UCP1 protein in response to *Ctcflos* tr1 KD (ASO1), tr3 and 4 KD (ASO2) compared to non-targeting controls. Actin-β as loading control, arrow heads mark UCP1 specific bands. **(G)** Immunocytochemistry of UCP1 protein in response to *Ctcflos* tr1 KD (ASO1) compared to non-targeting control. UCP1 (red), DNA stained by DAPI (green), phase contrast (PC) (grey). **(H)** Quantification of UCP1 fluorescent signal from immunocytochemistry analysis. Whole image fluorescence intensity subtracted by background and normalized to cell number. Mean and individual values, n=3 (biological replicates (with 7-8 analyzed images for each biological replicate)), paired t-test. **(I)** *Cell death-inducing DNA fragmentation factor*

alpha-like effector A (*Cidea*) and *Cytochrome c oxidase subunit 7a1* (*Cox7a1*) transcript levels relative to *Gtf2b* in *Ctcflos* tr1 KD (ASO1), tr3 and 4 KD (ASO2) compared to non-targeting controls, assessed by qPCR. Mean values ± SD, n=3 (biological replicates), unpaired t test or in grey parenthesis one-way ANOVA (Šídák-test). Preliminary data of **(J)** correlation between *Ctcflos* and *Ucp1* transcript levels relative to *Gtf2b* across empty vector (EV) control or *Ctcflos* sgRNA transfected (day 1 diff) C3H10T1/2-CRISPRa(SAM) cells, assessed by qPCR. Individual samples with successful *Ctcflos* overexpression are highlighted in green. Individual values, n=20 (combined technical replicates of two experiments), Pearson correlation. **(K)** *Ctcflos* and **(L)** *Ucp1* transcript levels relative to *Gtf2b* of those five samples with successful *Ctcflos* overexpression, assessed by qPCR. Mean and individual values n=2-5 (technical replicates). *p<0.05, **p<0.01, ***p<0.001, ****p<0.0001. Modified from (Bast-Habersbrunner *et al.*, 2021).

3.4.2 Thermogenic function of differentiating *Ctcflos*-deficient brite adipocytes

The decreased expression levels of brite adipocyte marker genes in *Ctcflos* KD cells further entailed a pronounced impairment of their thermogenic capacity. The respiration profile of *Ctcflos* deficient adipocytes was clearly shifted towards **I)** moderately lower basal oxygen consumption and **II)** profoundly decreased UCP1-dependent uncoupled respiration in response to isoproterenol-mediated β-adrenergic stimulation (Fig. 21 A-C).

I) The slight reduction in basal oxygen consumption by ASO1-mediated KD suggests impaired mitochondrial biogenesis that might come along as a consequence of restrained brite adipogenesis. Reduced mitochondrial staining by MitoTracker and decreased abundance of respiratory chain complex 4 (Cytochrome c oxidase 4 (COX4)) protein confirmed this (Fig. 21 D-F).

II) *Ctcflos* KD by ASO1 and ASO2 strongly affects isoproterenol-stimulated UCP1-mediated uncoupled respiration. The effect size on isoproterenol-respiration clearly exceeds that on basal respiration, indicating that it cannot merely be explained by the observed reduced mitochondrial content. Importantly, the effect is present in brite adipocytes of wild type (WT) mice but absent in cells of UCP1 KO mice, confirming that *Ctcflos* is required for specifically **UCP1**-mediated thermogenesis (Fig. 21 G-I). The rate of UCP1-uncoupled respiration is thereby determined by two factors, the abundance of UCP1 protein and the extent of its activation by lipolytically released free fatty acids. Glycerol release, as measure for the rate of lipolysis in response to isoproterenol, is only mildly affected in *Ctcflos* KD cells, pointing out that impaired *Ucp1* gene expression, rather than its activation, is responsible for the deficient thermogenic potential (Fig. 21 J).

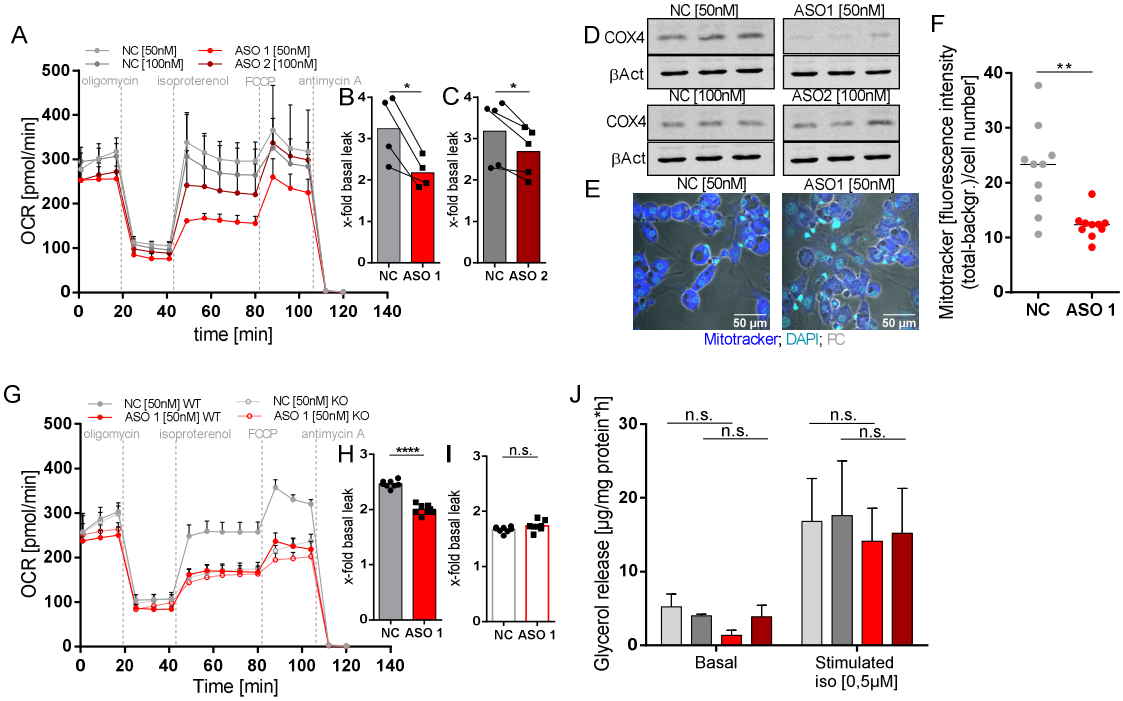

Figure 21: *Ctcflos* deficiency affects brite adipocyte thermogenic function. (A-C) Impact of *Ctcflos* KD at day 1 of differentiation on brite adipocyte respiratory capacity after 72 hours. **(A)** Time course of oxygen consumption rates in primary brite adipocytes derived from iWAT of 129S6 mice, comparing *Ctcflos* tr1 KD (ASO1), tr3 and 4 KD (ASO2) with their non-targeting controls, measured by microplate-based respirometry (Seahorse XF96 Analyzer). Oxygen consumption is recorded under basal conditions and in response to successive injection of oligomycin (5 µM), isoproterenol (1.5 µM), FCCP (1 µM) and antimycin A (5 µM) to determine basal leak, UCP1-dependent uncoupled, maximal and non-mitochondrial respiration, respectively. Mean values ± SD, n=4-5 (biological replicates). **(B, C)** Quantification of isoproterenol-stimulated UCP1-mediated uncoupled respiration, expressed as fold of basal leak respiration. Mean and individual values, n=4 (biological replicates), paired t test. **(D-F)** Impact of *Ctcflos* KD on mitochondrial biogenesis. **(D)** Western Blot analysis of Cytochrome C Oxidase subunit 4 (COX4) protein level in *Ctcflos* tr1 KD (ASO1), tr3 and 4 KD (ASO2) compared to non-targeting controls. Actin-β as loading control. **(E)** Mito Tracker stained brite adipocytes in response to *Ctcflos* tr1 KD (ASO1) compared to non-targeting controls. Mito Tracker (blue), DNA stained by DAPI (green), phase contrast (PC) (grey). **(F)** Quantification of Mito Tracker staining as whole image fluorescence intensity subtracted by background and normalized to cell number. Mean and individual values, n=10 (technical replicates), the experiment was repeated a second time (Fig. S7) for a total of two biological replicates, unpaired t test. **(G)** Time course of oxygen consumption rates in primary brite adipocytes derived from iWAT of wildtype (WT) and UCP1 knockout (KO) 129/SvImJ mice, comparing *Ctcflos* tr1 KD (ASO1) with non-targeting controls, measured by microplate-based respirometry (Seahorse XF96 Analyzer) as described above for (A). Mean values ± SD, n=7 (technical replicates). **(H, I)** Quantification of isoproterenol-stimulated UCP1-mediated uncoupled respiration, expressed as fold of basal leak respiration. Mean and individual values, n=7 (technical replicates), unpaired t tests. **(J)** Lipolysis rates in response to *Ctcflos* tr1 KD (ASO1), tr3 and 4 KD (ASO2) compared to non-targeting controls. Basal and isoproterenol (0.5 µM)-stimulated glycerol release. Mean values ± SD, n=4 (biological replicates), two-way ANOVA (Šídák-test). n.s. $p>0.05$, *$p<0.05$, **$p<0.01$, ****$p<0.0001$. Modified from (Bast-Habersbrunner *et al.*, 2021).

Excursion 1:

FCCP needs to be titrated to evaluate the maximal respiratory capacity of *Ctcflos* deficient adipocytes:

Following the measurement of isoproterenol stimulated UCP1-dependent oxygen consumption, FCCP is injected to determine the maximal respiratory capacity. FCCP, as chemical uncoupler, enables proton conductance across the inner mitochondrial membrane to completely uncouple nutrient oxidation from ATP synthesis. Consequently, respiratory chain activity is increased to its maximal capacity for compensation, providing a readout for respiratory chain abundance. In *Ctcflos* deficiency induced by ASO1, this maximal respiration in response to FCCP (1 µM) seemed to be considerably reduced, providing the impression of substantially decreased respiratory equipment of the cells (Fig. 21 A). In this context, however, it has to be kept in mind that the measurement is performed in the presence of bovine serum albumin (BSA), which allows the determination of specifically UCP1-mediated respiration by binding excess free fatty acids that can contribute to uncoupling and thus obscure the UCP1 effect. BSA, however, also binds FCCP, reducing its activity. Under conditions of reduced lipolytic activity, less BSA is occupied by free fatty acids, allowing stronger interaction with FCCP and resulting in an underestimation of maximal respiratory capacity. Although lipolysis is only diminished by trend in *Ctcflos* KD cells, FCCP was titrated to exclude any bias through capturing by BSA. Elevating FCCP concentration to 5 µM could indeed increase maximal respiration levels, approaching the control (Fig. E1). The residual impact is explainable by the mildly impaired mitochondrial biogenesis in *Ctcflos* deficient adipocytes.

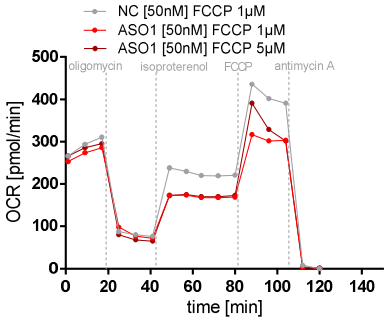

Figure E1: FCCP titration in respirometry. Time course of oxygen consumption rates of *Ctcflos* tr1 KD (ASO1) and control brite adipocytes with two different FCCP concentrations.

3.4.3 Modulation of cell morphology of differentiating *Ctcflos*-deficient brite adipocytes

Besides impaired thermogenic gene expression and thermogenic function, *Ctcflos* KD also entailed subtle changes on morphological level. *Ctcflos* deficiency induced a mild shift in lipid droplet size distribution towards enlarged lipid droplets (Fig. 22 A and B). Droplets with a diameter of more than 40 µm tended (statistically non-significant) to be more abundant in the KD cells (Fig. 22 C). The total number of lipid droplets slightly decreased (Fig. 22 D), while the overall lipid content of the cells was not significantly reduced (Fig. 22 E and F). *Ctcflos* KD adipocytes thus maintained the ability to differentiate into lipid loaded adipocytes but tended to deviate from the brite adipocyte typical multilocular cell morphology.

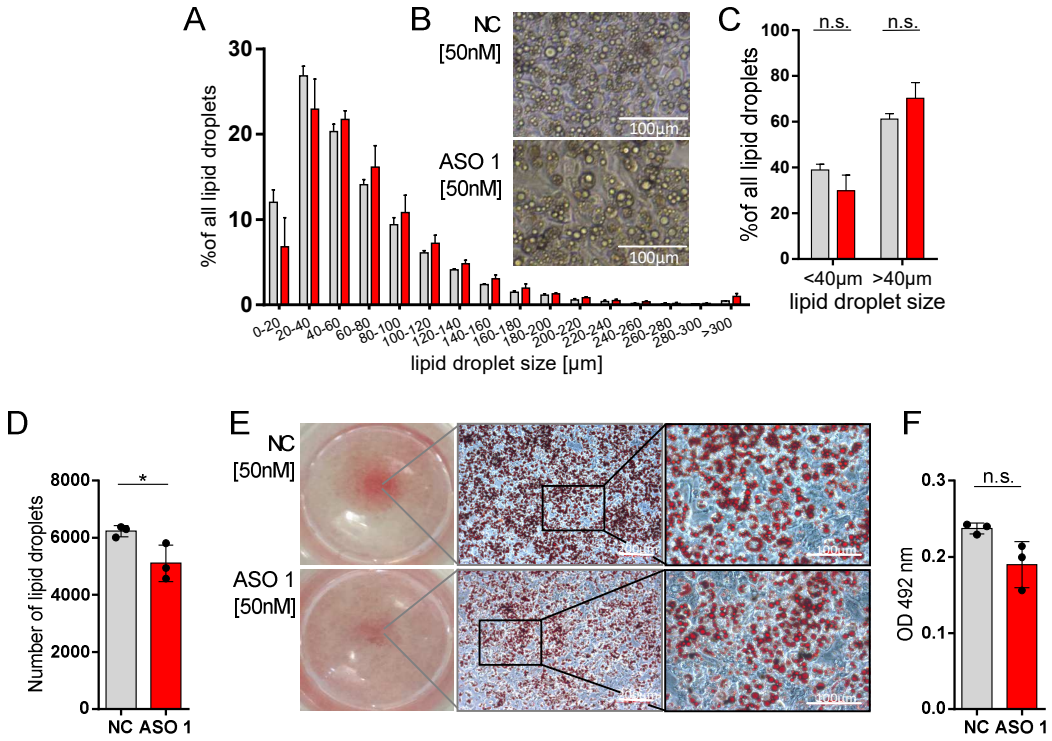

Figure 22: *Ctcflos* deficiency slightly alters brite adipocyte cell morphology. (A-C) Impact of *Ctcflos* tr1 KD (ASO1) at day 1 of differentiation compared to non-targeting control treatment on lipid droplet morphology of brite adipocytes. **(A)** Lipid droplet size distribution in *Ctcflos* KD and control cells, lipid droplets in different size categories as percentage of all lipid droplets, assessed by digital image analysis (Wimasis). Mean ± SD, n=3 (biological replicates). **(B)** Microscopic image section of *Ctcflos* KD and control adipocytes. **(C)** Percentage of lipid droplets below and above 40 µm cutoff. Mean ± SD, n=3 (biological replicates), two-way ANOVA (Šídák-test). **(D)** Total number of lipid droplets, assessed by digital image analysis (Wimasis). Mean ± SD, n=3 (biological replicates), unpaired t test. **(E, F)** Oil red O staining of lipid droplets of *Ctcflos* tr1 KD (ASO1), tr3 and 4 KD (ASO2) compared to non-targeting control cells. **(E)** Images of entire stained wells (left), microscopic images (10x objective) (middle), microscopic image (32x objective) (right). **(F)** Quantification of extracted Oil red O stain by absorbance measurement at 492 nm subtracted by background. Mean and individual values, n=3 (technical replicates), unpaired t test. N.s. p>0.05 *p<0.05. Modified from (Bast-Habersbrunner *et al.*, 2021).

3.4.4 The role of *Ctcflos* in mature brite adipocytes

The second boost of *Ctcflos* expression during late brite adipocyte differentiation proposes a functional relevance of *Ctcflos* also in mature brite cells. Accordingly, KD of *Ctcflos* at day 5 of differentiation, when it reaches its maximal transcript levels, also compromised brite marker gene expression and UCP1-dependent thermogenesis, though with slightly alleviated impact sizes (Fig. 23).

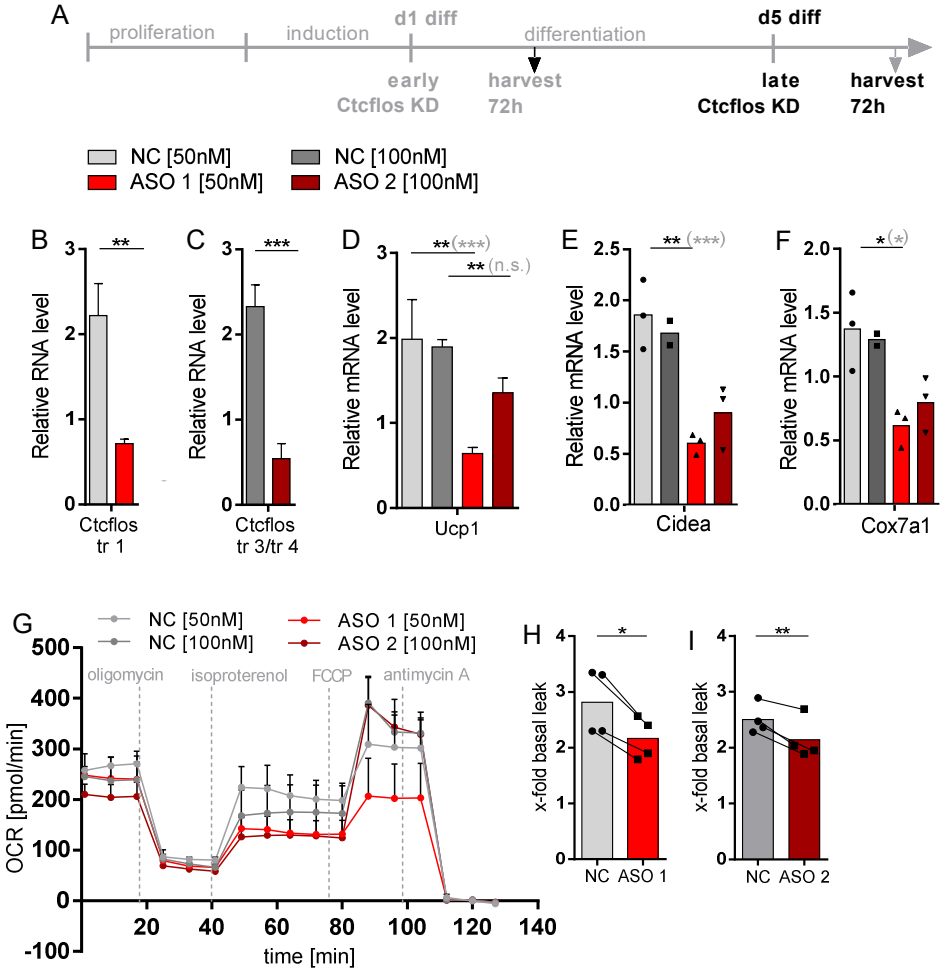

Figure 23: *Ctcflos* is required to maintain the brite adipocyte phenotype. (A) Design of the *Ctcflos* KD experiment. KD of *Ctcflos* at day 5 of differentiation of primary brite adipocytes derived from iWAT of 129S6 mice, followed by harvest 72 hours later. **(B, C)** Efficiency of *Ctcflos* KD by **(B)** LNA Gapmer ASO1, targeting *Ctcflos* transcript 1 and **(C)** LNA Gapmer ASO2, targeting *Ctcflos* transcripts 3 and 4 compared to non-targeting controls (transcript levels relative to *Gtf2b*), assessed by qPCR. Mean values ± SD, n=3 (biological replicates), unpaired t tests. **(D)** *Ucp1* mRNA levels relative to *Gtf2b* in response to *Ctcflos* tr1 KD (ASO1), tr3 and 4 KD (ASO2) compared to non-targeting controls, assessed by qPCR. Mean values ± SD, n=3 (biological replicates), unpaired t tests or in grey parenthesis one-way ANOVA (Šídák-test). **(E)** *Cidea* and **(F)** *Cox7a1* transcript levels relative to *Gtf2b* in response to *Ctcflos* tr1 KD (ASO1), tr3 and 4 KD (ASO2) compared to non-targeting controls. Mean and individual values, n=2-3 (biological replicates), for groups with n=3: unpaired t tests or in grey parenthesis one-way ANOVA (Šídák-test). **(G)** Time course of mature brite adipocyte oxygen consumption rates, comparing *Ctcflos* tr1 KD (ASO1), tr3 and 4 KD (ASO2) with their non-targeting controls, measured by microplate-based respirometry (Seahorse XF96 Analyzer). Mean values ± SD, n=4-5 (biological replicates). **(H, I)** Quantification of isoproterenol-stimulated UCP1-mediated uncoupled respiration, expressed as fold of basal leak respiration. Mean and individual values, n=4 (biological replicates), paired t tests. N.s. p>0.05, *p<0.05, **p<0.01; ***p<0.001. Modified from (Bast-Habersbrunner *et al.*, 2021).

3.4.5 Functional specificity of *Ctcflos* for thermogenic adipogenesis

As described above, *Ctcflos* expression is not restricted to brite adipocytes but distributed across different types of adipose tissue, with high abundance in iBAT and considerable expression in iWAT. The role of *Ctcflos* was therefore additionally investigated in primary brown and white adipocytes derived from these tissues. Early KD of *Ctcflos* in differentiating brown adipocytes, especially by ASO1, severely affected *Ucp1* gene transcription and thermogenic function similar to the KD impact in brite adipocytes, proposing a requisite contribution of *Ctcflos* isoform 1 also to brown adipogenesis (Fig. 24 A-D). *Ctcflos* deficiency in differentiating white adipocytes, cultured in the absence of rosiglitazone, in contrast, had minor impacts on white fat marker gene expression, indicating a vast dispensability of *Ctcflos* in white adipocyte development (Fig. 24 E).

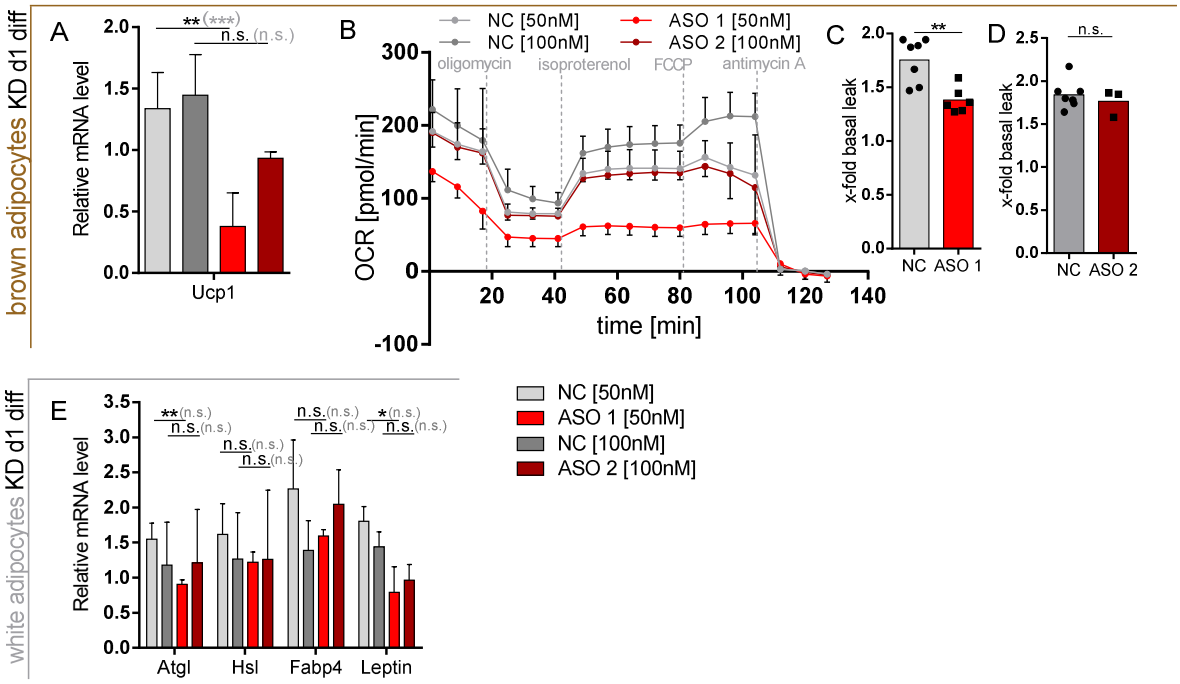

Figure 24: *Ctcflos* is specifically needed for thermogenic gene expression. (A-D) Impact of *Ctcflos* KD on differentiating primary brown adipocytes derived from iBAT of 129S6 mice (*Ctcflos* KD at day 1 of differentiation, harvest after 72 hours). **(A)** *Ucp1* mRNA levels relative to *Gtf2b* in response to *Ctcflos* tr1 KD (ASO1), tr3 and 4 KD (ASO2) compared to non-targeting controls, assessed by qPCR. Mean values ± SD, n=3-4 (biological replicates), unpaired t tests or in grey parenthesis one-way ANOVA (Šídák-test). **(B)** Time course of differentiating brown adipocyte oxygen consumption rates, comparing *Ctcflos* tr1 KD (ASO1), tr3 and 4 KD (ASO2) with their non-targeting controls, measured by microplate-based respirometry (Seahorse XF96 Analyzer). Mean values ± SD, n=3-7 (technical replicates). **(C, D)** Quantification of isoproterenol-stimulated UCP1-mediated uncoupled respiration, expressed as fold of basal leak respiration. Mean and individual values, n=3-7 (technical replicates), unpaired t tests. **(E)** Impact of *Ctcflos* KD on differentiating primary white adipocytes derived from iWAT of 129S6 mice and induced in the absence of rosiglitazone (*Ctcflos* KD at day 1 of differentiation, harvest after 72 hours). *Adipose triglyceride lipase* (*Atgl*), *Hormone sensitive lipase* (*Hsl*), *Fatty acid binding protein 4 (Fabp4)* and *Leptin* transcript levels relative to *Gtf2b* in *Ctcflos* tr1 KD (ASO1), tr3 and 4 KD (ASO2) compared to control samples, assessed by qPCR. Mean values ± SD, n=3 (biological replicates), unpaired t tests, or in grey parenthesis two-way ANOVA (Šídák-test). N.s. p>0.05, *p<0.05, **p<0.01; ***p<0.001. Modified from (Bast-Habersbrunner *et al.*, 2021).

In summary, the presented KD experiments confirm an essential functionality of lncRNA *Ctcflos* specifically in thermogenic programming. Especially *Ctcflos* isoform 1 is essential for the recruitment of transcriptional and functional characteristics in developing brite and brown adipocytes and for the maintenance of the thermogenic phenotype in mature adipocytes, without affecting general adipogenesis or white adipocyte differentiation.

3.5 *CTCFLOS*-DEPENDENT TRANSCRIPTION AND ALTERNATIVE SPLICING IN BRITE ADIPOCYTES

The phenotypic characterization of *Ctcflos* deficiency revealed profound deviations from regular brite cell development and function, suggesting wide-ranging alterations in cellular gene expression. To obtain a comprehensive overview of these changes and to explore the regulatory routes of *Ctcflos* activity in brite adipogenesis, whole transcriptomes of *Ctcflos* KD and control cells were profiled by RNA sequencing. As *Ctcflos* isoform 1 KD had a greater impact at beginning differentiation, the transcriptome analysis mainly concentrated on the KD by ASO1 at day 1 of differentiation. Going beyond a single snapshot of transcription, the cells were analyzed at two consecutive time points, 24 hours and 72 hours after *Ctcflos* KD to monitor acute and adaptive changes, respectively (Fig. 25 A). Gene expression modulations 24 hours after *Ctcflos* KD, comprising 780 up- and 657 downregulated transcripts (DESeq2, adj. p-value<0.05, log2 fold change ≥1 or ≤-1), provide insights into the molecular basis of *Ctcflos* function and its proximal regulatory modules (Fig. 25 B and D). Transcriptome changes after 72 hours, including 692 enriched and 715 reduced transcripts (DESeq2, adj.p-value<0.05, log2 fold change≥1 or ≤-1), inform about more distal regulatory modules of *Ctcflos* and serve to validate and complement the *Ctcflos* KD phenotype (Fig. 25 C and E).

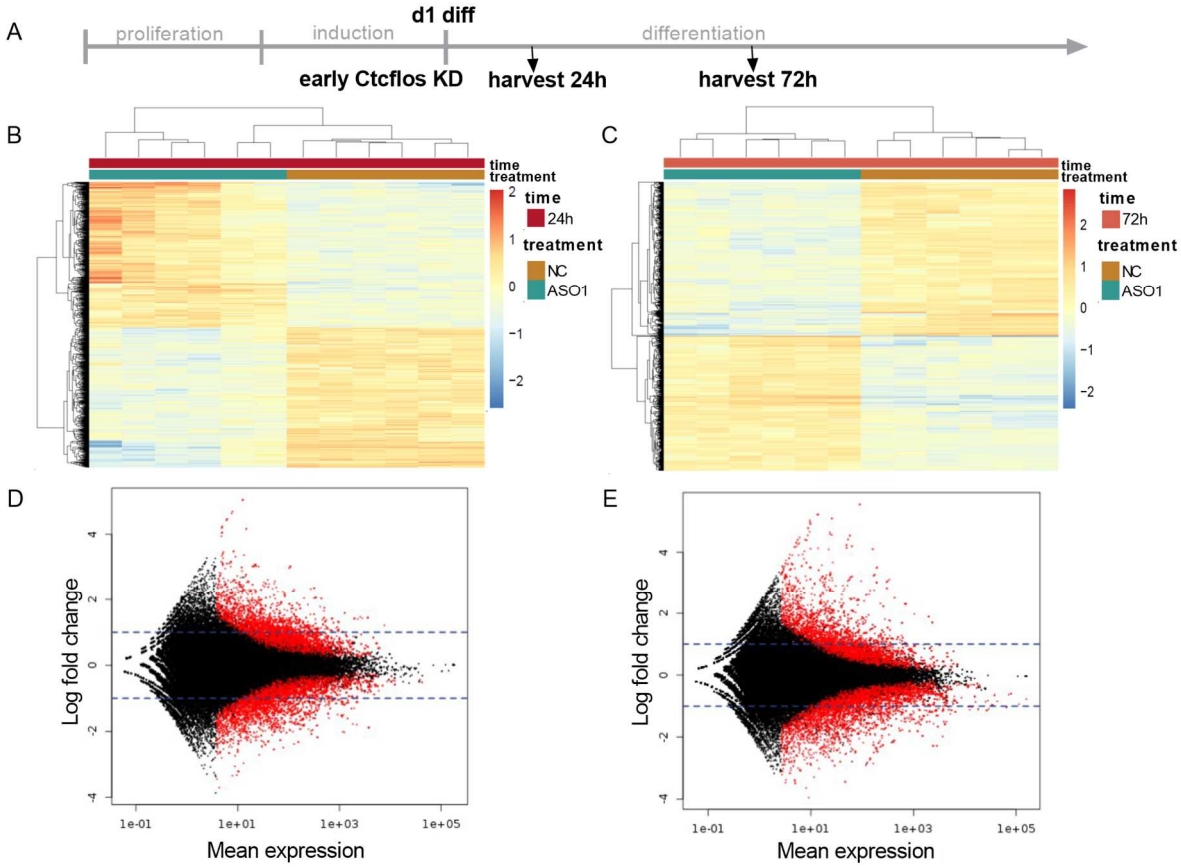

Figure 25: Whole transcriptome analysis provides a global overview of *Ctcflos* KD effects. (A) Experimental setup of two-time point transcriptome analysis of primary brite adipocytes derived from iWAT of 129S6 mice. *Ctcflos* tr1 was knocked down (ASO1) or cells were treated with non-targeting control at beginning differentiation, RNA was harvested after 24 hours and 72 hours and subjected to transcriptome analysis. **(B, C)** Heat maps of differentially expressed genes between *Ctcflos* KD and control cells (DESeq2, adj.p-value<0.05, log2 fold change ≥1 or ≤-1) **(B)** 24 hours and **(C)** 72 hours after

the KD. Row-wise centered log2 normalized counts are displayed. **(D, E)** MA plots, showing mean expression and fold change of all determined genes, comparing *Ctcflos* KD and control cells **(D)** 24 hours and **(E)** 72 hours after the KD. Significantly differentially expressed genes are highlighted in red. Modified from (Bast-Habersbrunner *et al.*, 2021).

3.5.1 Confirmation of the experimentally observed *Ctcflos* KD phenotype by global transcriptome analysis

Consistent with the experimental characterization of *Ctcflos* KD, global transcriptome analysis similarly revealed pronounced reduction of *Ucp1* gene transcription 72 hours after *Ctcflos* KD. This was accompanied by downregulation of other brite marker genes, including *Cidea*, *Cox7a1* (for ASO1 and ASO2 mediated KD) as well as *PPARγ coactivator 1α* (*Pgc1α*) and *Elongation of very long chain fatty acids (FEN1/Elo2, SUR4/Elo3, yeast)-like 3* (*Elovl3*) (for ASO1 mediated KD) (Fig. 26 A). Several GO terms associated with mitochondrial respiration and thermogenesis, fatty acid and carbohydrate metabolism, as well as brown fat cell differentiation were overrepresented among downregulated transcripts (72 hours post KD), further supporting compromised brite adipocyte development (Fig. 26 B). Decreased transcription of multiple subunits of all respiratory chain complexes is consistent with the observed reduction of the respiratory capacity of *Ctcflos* KD cells (Fig. 26 C and D). Across a range of general adipogenesis markers, in contrast, only few factors were affected, again substantiating the specific activity of *Ctcflos* in thermogenic gene programming and less in adipogenesis *per se* (Fig. 26 E).

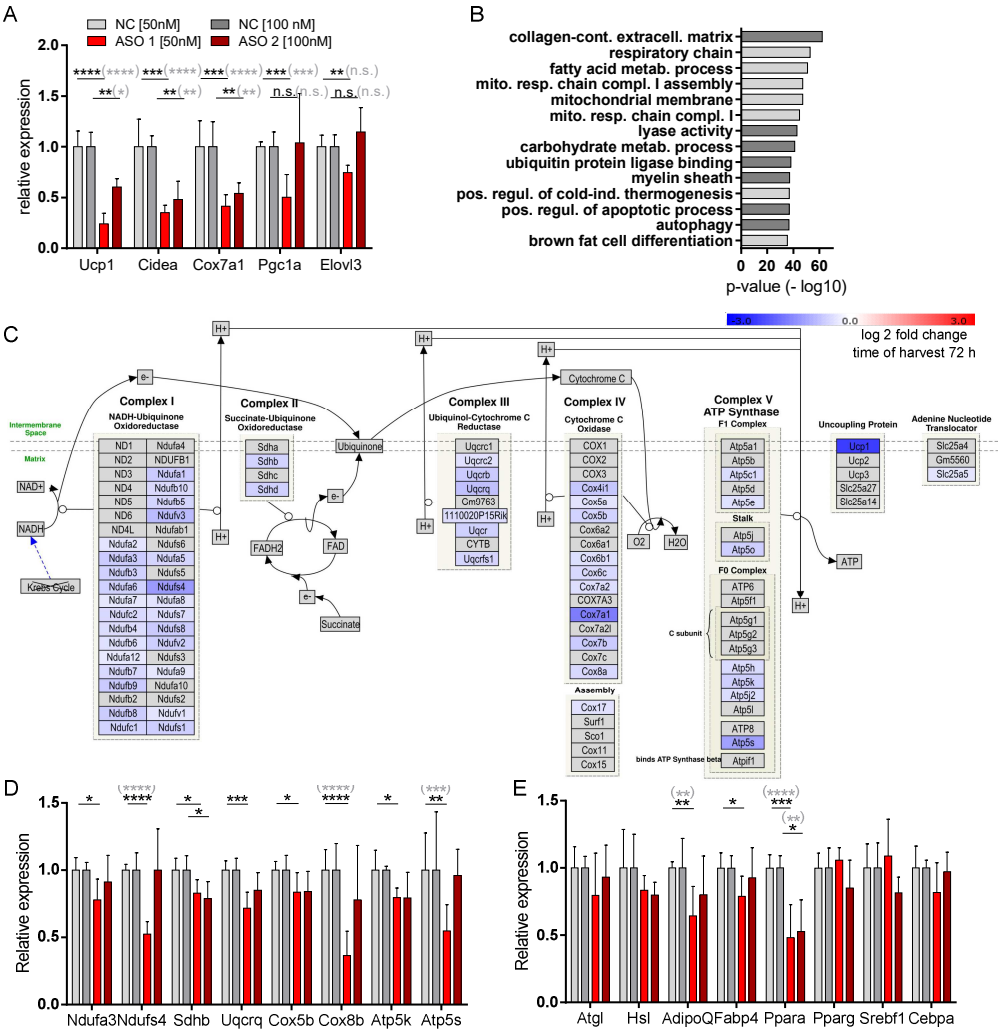

Figure 26: Global transcriptome profiling confirms the observed *Ctcflos* KD phenotype. Transcriptome profiling of primary brite adipocytes 72 hours after *Ctcflos* tr1 KD (ASO1), tr3 and 4 KD (ASO2) compared to non-targeting controls. **(A)** Relative expression levels of brite adipocyte marker genes: *Ucp1*, *cell death-inducing DNA fragmentation factor alpha-like effector A* (*Cidea*), *cytochrome c oxidase subunit 7a1* (*Cox7a1*), *peroxisome proliferator activated receptor γ coactivator 1α* (*Pgc1α*) and *elongation of very long chain fatty acids-like 3* (*Elovl3*). Transcript levels in RPKM. Mean values ± SD, n=6 (biological replicates), unpaired t tests or in grey parenthesis two-way ANOVA (Šídák-test). **(B)** GO term analysis of downregulated genes. Hypergeometric test. **(C)** *Ctcflos* KD-dependent transcriptional impact on components of the respiratory chain. Visualization by Path Visio software, the color code displays log2 fold changes of gene transcript levels 72 hours after the KD. **(D)** Relative expression levels of selected respiratory chain complex subunits: *NADH:ubiquinone oxidoreductase subunit A3* (*Ndufa3*), *NADH:ubiquinone oxidoreductase core subunit S4* (*Ndufs4*), *succinate dehydrogenase complex, subunit B, iron sulfur* (*Sdhb*), *ubiquinol-cytochrome c reductase, complex III subunit VII* (*Uqcrq*), *cytochrome c oxidase subunit 5B* (*Cox5b*), *cytochrome c oxidase subunit 8B* (*Cox8b*), *ATP synthase subunit E* (*Atp5k*), *ATP synthase subunit S* (*Atp5s*). Mean values ± SD, n=6 (biological replicates), unpaired t tests or in grey parenthesis two-way ANOVA (Šídák-test). **(E)** Relative expression levels of general adipogenic marker genes: *Adipose triglyceride lipase* (*Atgl*) and *Hormone sensitive lipase* (*Hsl*), *Adiponectin* (*AdipoQ), Fatty acid binding protein 4* (*Fabp4*), *Peroxisome proliferator activated receptor α* (*Pparα*), *Peroxisome proliferator activated receptor γ* (*Pparγ*), *Sterol regulatory element binding transcription factor 1* (*Srebf1*), *CCAAT/enhancer binding protein α* (*C/ebpα*). Mean values ± SD, n=6 (biological replicates), unpaired t tests or in grey parenthesis two-way ANOVA (Šídák-test). N.s. p>0.05, *p<0.05, **p<0.01, ***p<0.001, ****p<0.0001, for (D and E) no * indicate nonsignficant changes (not depicted in the graphs due to visibility reasons). Modified from (Bast-Habersbrunner *et al.*, 2021).

3.5.2 Routes of *Ctcflos* regulatory activity in brite adipogenesis

The development of pluripotent precursor cells into functionally specified mature adipocytes demands complex re-organization of the cellular machinery. Gene expression is reprogrammed on a broad scale to adapt to the requirements of brite cell thermogenic functionality. The regulation of gene expression occurs on several levels, comprising epigenetic modulations, transcription, RNA processing, nuclear export and translation. LncRNAs have been shown to act at any of these steps via a variety of different mechanisms. Interestingly, a single lncRNAs can perform different functions, allowing it to intervene at more than one level of gene expression. This provides lncRNAs the potential to efficiently coordinate gene programming during cellular differentiation. Further in depth analyses, presented in the following, aim to understand in which ways lncRNA *Ctcflos* contributes to brite adipogenesis and on which regulatory levels it modulates cellular programming during thermogenic differentiation.

3.5.2.1 *Ctcflos*-dependent regulation of the core thermogenic transcription program

In search of the routes of *Ctcflos*-dependent regulation of brite adipogenesis, more detailed analyses of *Ctcflos* KD-induced transcriptome changes revealed extensive modulations in the core thermogenic transcription regulatory program (Fig. 27). Among the widely established transcriptional regulators that drive commitment of precursor cells into thermogenic preadipocytes and their early and late differentiation into mature thermogenic adipocytes, several key factors were affected by *Ctcflos* KD. These profound changes in the central thermogenic transcription program most likely causally contribute to impaired brite adipogenesis of *Ctcflos* KD cells. Importantly, the applied two time point strategy of transcriptome analysis provided further information on the chronology of *Ctcflos* KD-induced modulations. Some key brite regulators, including *Prdm16*, *Pparγ*, *Nuclear factor I/A* (*Nfia*) and *Early B cell factor 1* (*Ebf1*) were less transcribed directly (24 hours) after *Ctcflos* KD (Fig. 27 color code within left part of the gene box). As these factors are affected rapidly, they potentially present proximal regulatory modules of *Ctcflos*. Later (72 hours) after the KD, transcript levels of several *Ucp1* gene regulatory element binding factors and co-regulators comprising *Peroxisome proliferator activated receptor α* (*Pparα*), *Thyroid hormone receptor β* (*Thrβ*), *CCAAT/enhancer binding protein β* (*C/ebpβ*), *Retinoid acid receptor β* (*Rarβ*) and *PPARγ coactivator 1α* (*Pgc1α*) were reduced, possibly as a consequence of the early (24 hours) changes. Together, these changes finally converged in reduced *Ucp1* gene transcription. The formation of the core transcription regulatory network, which programs thermogenic adipocyte differentiation, thus depends on the early presence of *Ctcflos*, establishing transcriptional modulations as one major route of *Ctcflos* activity in brite adipogenesis.

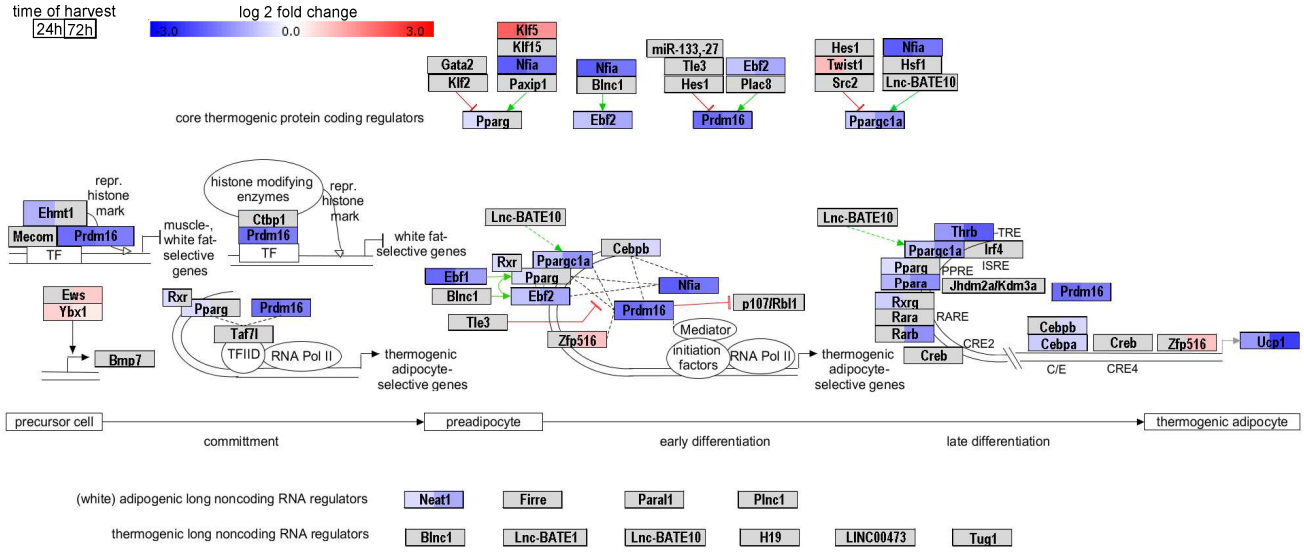

Figure 27: *Ctcflos* KD affects the core thermogenic gene transcription machinery. *Ctcflos* KD-dependent transcriptional impact on components of the core thermogenic gene expression network, comprising key protein coding factors involved in commitment, early and late differentiation of brite and brown adipocytes, as well as adipogenesis related lncRNAs. Visualization by Path Visio software, the color code displays log2 fold changes of gene transcript levels 24 hours (left part of the box) and 72 hours (right part of the box) after the KD. Red t-bars represent inhibitory effects, green arrows represent activating effects. Modified from (Bast-Habersbrunner *et al.*, 2021).

Transcriptional regulation of *Prdm16*

With the modulation of *Prdm16* transcription, which was confirmed by qPCR analysis (Fig. 28 A), *Ctcflos* possesses the capacity to control an early key regulator of brite gene transcription that is well established to be required and sufficient to promote the differentiation of thermogenic adipocytes (Seale *et al.*, 2007). PRDM16 acts as a co-regulator that physically interacts with thermogenic TFs to stimulate brown and brite selective gene transcription (Seale *et al.*, 2008; Seale *et al.*, 2007). Large parts of the *Ctcflos* KD impact on the brite transcription regulatory network after 72 hours, could thus occur as consequence of early downregulation of *Prdm16*. Consistently, downstream targets of PRDM16, including *Pparα*, *C/ebpβ*, *Ebf2* and *Pgc1α*, were also affected in *Ctcflos* KD cells in chronological succession to reduced *Prdm16* transcription (Fig. 27). The transcription regulatory function of *Ctcflos* in brite gene programming could thus in part be mediated via PRDM16.

To further investigate the hypothesized function of PRDM16 as downstream mediator of *Ctcflos* activity in brite cells, single and joint KD effects of *Ctcflos* and *Prdm16* were compared in a multiplicative effect model, adopted from the concept of genetic interaction (Costanzo *et al.*, 2019). According to this adapted model, the impact size of a double knockdown of two independently acting factors can be estimated from the multiplication of their single KD effects. Any deviation from this points towards an interaction between the investigated factors, such as sharing a common signaling pathway. Accordingly, the experimentally observed impact on *Ucp1* gene transcription in combined *Ctcflos* and *Prdm16* deficiency (residual *Ucp1* expression: 0.26 (26%)) was less severe than theoretically calculated by multiplication of the single KD effects (0.36 (36%)) for *Ctcflos* KD x 0.51 (51%) for *Prdm16* KD = 0.18 (18%) residuel *Ucp1* expression) (Fig. 28 B-D). This suggests that *Ctcflos* and PRDM16 do not function independently of each other, but share common regulatory routes in brite adipogenesis. Notably, the effect size of the double KD resembles that of *Ctcflos* single KD (Fig. 28 E), but is not similar to that of *Prdm16* single KD (Fig. 28 F). This proposes an asymmetric interaction, in which *Ctcflos* KD effects mask that of *Prdm16*, indicating that *Ctcflos* signaling in brite adipogenesis involves the modulation of *Prdm16* transcript levels, but comprises further pathways of regulation.

The interaction between *Ctcflos* and *Prdm16* was additionally evaluated in rescue experiments by *Prdm16* overexpression. *Ctcflos* was knocked down in *Prdm16* overexpressing cells, and the resulting phenotype was compared to that of GFP overexpressing control and GFP overexpressing *Ctcflos* KD cells (Fig. 28 G-J). The reduction of *Ucp1* gene expression in *Ctcflos* KD-GFP cells compared to control-GFP adipocytes was abolished by *Prdm16* overexpression in *Ctcflos* KD cells (Fig. 28 I). Comparing *Ctcflos* KD with their corresponding non-targeting control cells, showed that *Ctcflos* KD had a smaller impact on *Ucp1* gene transcription in *Prdm16* compared to GFP overexpressing cells (Fig. 28 J, K). This further argues for the involvement of *Prdm16* in *Ctcflos* functionality in brite adipogenesis. The small residual impact of *Ctcflos* KD on *Ucp1* expression that remained despite *Prdm16* overexpression (Fig. 28 J), again hints towards additional regulatory routs of *Ctcflos* beyond the modulation of *Prdm16*. Since GFP overexpressing cells showed slightly decreased differentiation rates compared to *Prdm16* overexpressing adipocytes, the data were normalized to *fatty acid binding protein 4* (*Fabp4*),

as its expression strength mirrors the differentiation state. Additionally, the experiment was repeated, comparing *Prdm16* overexpressing to virus-untreated control cells with equivalent differentiation rates, revealing comparable results (Fig. S8).

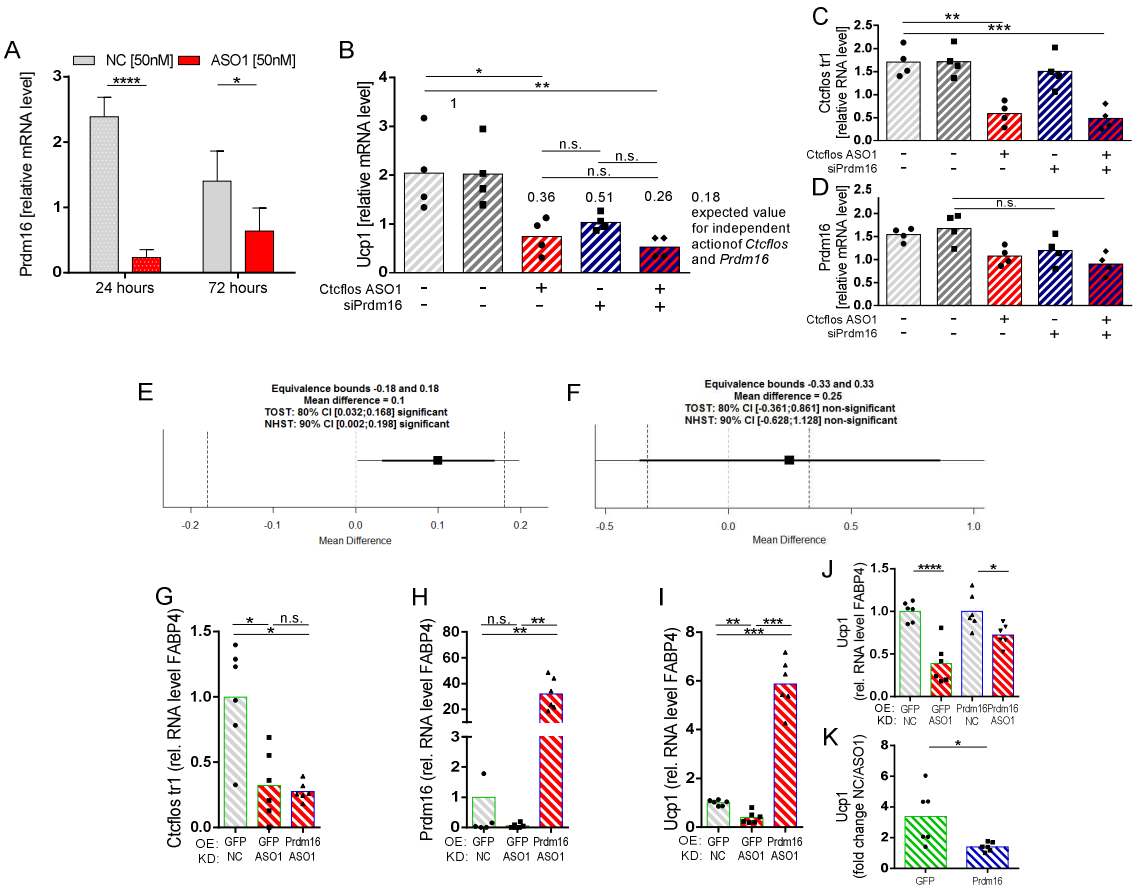

Figure 28: *Prdm16* is involved in downstream mediation of *Ctcflos* activity in brite adipogenesis. (A) *PR domain containing 16* (*Prdm16*) transcript levels relative to *Gtf2b*, 24 and 72 hours after the knockdown of *Ctcflos* tr1 (ASO1) compared to control cells, assessed by qPCR. Mean values ± SD, n=3 (biological replicates), two-way ANOVA (Šídák-test). **(B)** *Ucp1*, **(C)** *Ctcflos* and **(D)** *Prdm16* transcript levels relative to *Gtf2b* in single and double KD of *Ctcflos* tr1 and *Prdm16* by ASO1 and siPRDM16, respectively, compared to non-targeting controls, assessed by qPCR. Mean and individual values, n=4 (biological replicates), one-way ANOVA (Šídák-test). **(E, F)** Paired TOST-Equivalence tests comparing *Ucp1* transcript levels of **(E)** *Ctcflos* single KD with *Ctcflos*+*Prdm16* double KD and **(F)** *Prdm16* single KD with *Ctcflos*+*Prdm16* double KD, with significance level alpha set to 0.1. Equivalence bounds were set based on the multiplicative gene interaction model. **(G-K)** Rescue of *Ctcflos* KD impact on *Ucp1* gene transcription by *Prdm16* overexpression. **(G)** *Ctcflos* tr1, **(H)** *Prdm16* and **(I, J)** *Ucp1* transcript levels relative to *Fabp4* in primary iWAT cells infected with *Prdm16*- or *turbo green fluorescent protein* (*GFP*)-expressing viral particles at the second day of proliferation, followed by reverse transfection at the first day of differentiation using non-targeting control or *Ctcflos* tr1-targeting ASO1. Gene expression analyzed 72 hours later by qPCR. Mean and individual values. Each graph presents pooled data from two experiments with slightly varying virus titers. RM One-way ANOVA (Tukey-test). **(K)** Fold change of *Ucp1* transcript levels between non-targeting control and Ctcflos tr1 KD (ASO1) among *GFP* and *Prdm16* overexpressing cells. Mean and individual values. Unpaired t test. N.s. p>0.05, *p<0.05, **p<0.01, ***p<0.001, ****p<0.0001. Modified from (Bast-Habersbrunner *et al.*, 2021).

Transcriptional regulation of *Neat1*

Beyond the well-established protein coding regulatory factors of brite gene programming, intensified research in the field of noncoding RNA within the last few years also uncovered several lncRNAs of significant regulatory involvement in adipogenesis. The canonical adipogenic regulatory network could thus be complemented by a few long noncoding regulatory modules (Fig. 27). Among them *Blnc1*, *lncBATE1*, *lncBATE10* and *H19* were shown to be implicated in brite and/or brown adipogenesis (Alvarez-Dominguez *et al.*, 2015a; Bai *et al.*, 2017; Schmidt *et al.*, 2018; Zhao *et al.*, 2014), *Plnc1*, *Steroid receptor RNA activator* (*SRA*), *PPARγ-activator RBM14-associated lncRNA* (*Paral1*), *Functional intergenic repeating RNA element* (*Firre*) *(also lnc-RAP1)* and *Neat1* were associated with white adipogenesis (Cooper *et al*, 2014; Firmin *et al*, 2017; Gernapudi *et al*, 2016; Sun *et al*, 2013; Xu *et al*, 2010; Zhu *et al*, 2019). *Ctcflos* KD hardly affected any of these long noncoding regulators, except for profound transcriptional downregulation of *Neat1* 72 hours after *Ctcflos* KD (Fig. 27 and Fig. 29). *Ctcflos* thus operates largely independent of these previously characterized lncRNA regulators of brite and brown adipogenesis. *Neat1* was so far only characterized as an essential component in white adipogenesis, its role in thermogenic adipocytes was not clarified (Gernapudi *et al.*, 2016). To investigate whether *Ctcflos* KD-induced *Neat1* deficiency could contribute to compromised brite adipocyte differentiation, *Neat1* regulation and *Neat1* KD effects in brite adipocytes were explored in a small side project (see Excursion 2). Collectively, the experiments demonstrated that *Neat1* short isoform is strongly induced during brite adipogenesis and required for normal brite adipocyte differentiation with full activation of *Ucp1* gene transcription and recruitment of thermogenic capacity. Compromised expression of *Neat1* might thus also contribute to the *Ctcflos* KD phenotype.

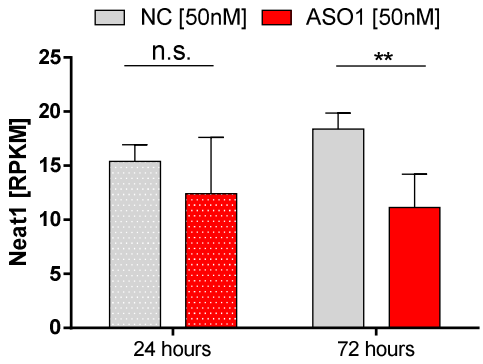

Figure 29: *Ctcflos* KD impairs lncRNA *Neat1* gene transcription. *Neat1* transcript levels in RNA sequencing of primary brite adipocytes derived from iWAT of 129S6 mice, 24 hours and 72 hours after *Ctcflos* tr1 KD (ASO1) compared to non-targeting controls (transcript levels in RPKM). Mean ± SD, n=6 (biological replicates), two-way ANOVA (Šídák-test). N.s. $p>0.05$, **$p<0.01$.

In summary, the presented data demonstrate a profound influence of *Ctcflos* on transcriptional regulatory circuits that drive brite adipogenesis. On the one hand, this is partially based on the capacity of *Ctcflos* to modulate key gatekeeper *Prdm16* that largely governs brite gene programming. On the other hand, it might involve lncRNA *Neat1*-dependent activities in the browning process and comprise additional pathways of transcriptional regulation beyond this.

Excursion 2:

A small side project on adipogenesis-associated lncRNA *Neat1* explored its transcriptional regulation during thermogenic adipogenesis and assessed its requirement for this process in KD studies. During the course of iWAT derived primary brite adipocyte differentiation *in vitro*, *Neat1* expression was significantly induced, reaching a profound mean transcription level of 880 RPKM (Fig. E2 A). Likewise, cold-induced iBAT activation *in vivo* was accompanied by an increase in *Neat1* expression, which was maximal after 6 hours of exposure to 4°C (Fig. E2 B) and correlated with the stimulation of *Ucp1* transcription across increasing durations of cold exposure (Fig. E2 C).

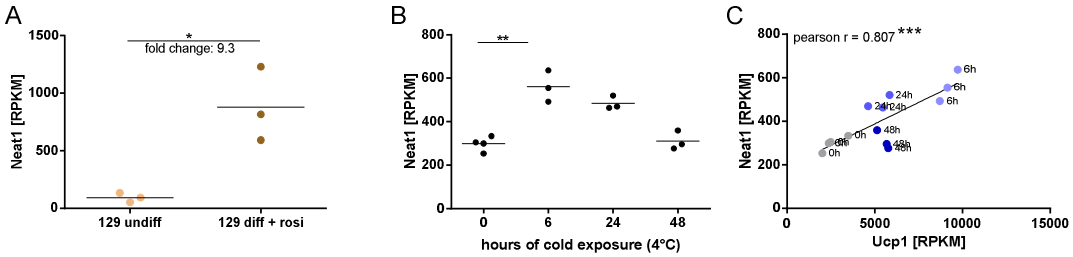

Figure E2: LncRNA *Neat1* is positively regulated during thermogenic adipogenesis. (A) *Neat1* transcript levels in differentiated brite compared to undifferentiated primary adipocytes derived from iWAT of 129S6 mice. Transcript levels in RPKM, assessed by RNA sequencing. Mean and individual values, n=3 (biological replicates), unpaired t test. **(B)** *Neat1* transcript levels in iBAT of 0, 6, 24 or 48 hours cold (4°C) exposed C57BL/6J mice (transcript levels in RPKM), assessed by RNA sequencing (Data ref. (Maurer S, 2018)). Mean and individual values, n=3-4 (biological replicates), one-way ANOVA (Šídák-test). **(C)** Correlation of *Neat1* with *Ucp1* transcript levels across the different durations of cold exposure (transcript levels in RPKM), assessed by RNA sequencing. Individual values. Pearson correlation. *p<0.05, **p<0.01, ***p<0.001.

LncRNA *Neat1* can be processed into a long or into short isoforms (Fig. E3 A). For the study of their putative functional contribution in brite adipogenesis, they were knocked down at beginning differentiation (day 1 diff) (Fig. E3 B) using LNA Gapmer ASOs targeting either *Neat1* long isoform alone (ASO long) or *Neat1* long and short isoforms in combination (ASO all) (Fig. E3 A, C and D). This demonstrated that the combined knockdown of *Neat1* short and long (ASO all) but not of *Neat1* long (ASO long) alone impaired *Ucp1* gene expression (Fig. E3 E) and UCP1-mediated uncoupled respiration (Fig. E3 F and G), attributing specifically *Neat1* short isoforms an implication in brite adipocyte development.

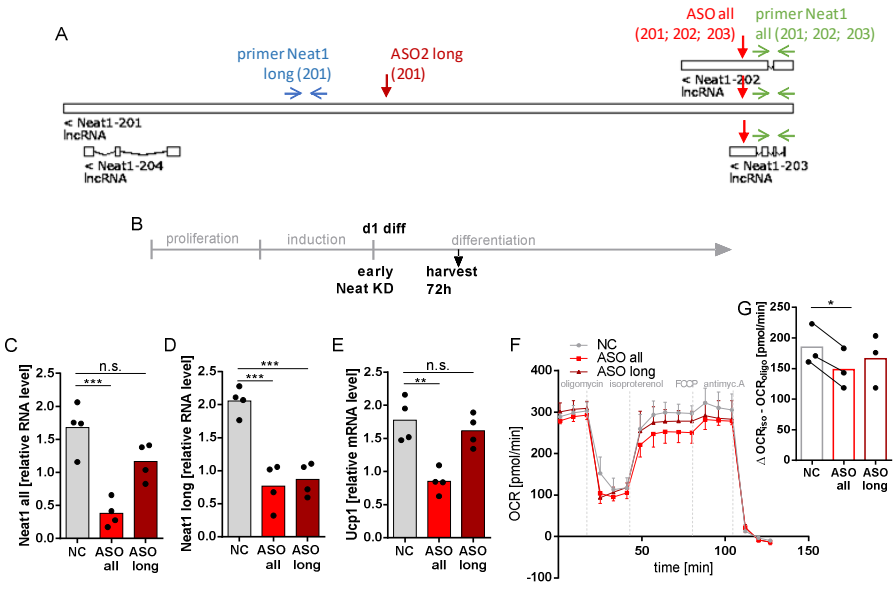

Figure E3: *Neat1* short isoforms are required for regular brite adipogenesis. (A) *Neat1* locus with annotated *Neat1* isoforms. Blue and green arrows mark primer binding sites for qPCR analysis, red arrows mark target sites of LNA Gapmer ASOs **(B)** Design of the *Neat1* KD experiments. KD of *Neat1* at day 1 of differentiation of primary

brite adipocytes derived from iWAT of 129S6 mice, followed by harvest 72 hours later. **(C, D)** Efficiency of *Neat1* KD by ASO all and ASO long on **(C)** total *Neat1* expression and **(D)** *Neat1* long expression compared to non-targeting controls (transcript levels relative to *Gtf2b*), assessed by qPCR. Mean and individual values, n=4 (biological replicates), one-way ANOVA (Šídák-test). **(E)** *Ucp1* mRNA levels relative to *Gtf2b* in response to *Neat1* short+long KD (ASO all) and *Neat1* long KD (ASO long) compared to non-tageting control, assessed by qPCR. Mean and individual values, n=4 (biological replicates), one-way ANOVA (Šídák-test). **(F)** Time course of differentiating brite adipocyte oxygen consumption rates, comparing *Neat1* short+long KD (ASO all) and *Neat1* long KD (ASO long) with non-targeting control, measured by microplate-based respirometry (Seahorse XF96 Analyzer). Mean values ± SD, n=3 (bio logical replicates). **(G)** Quantification of isoproterenol-stimulated UCP1-mediated uncoupled respiration, expressed as delta between highest respiration rate under isoproterenol-induced and oligomycin-dependent respiration. Mean and individual values, n=3 (biological replicates), paired t tests. N.s. $p>0.05$, *$p<0.05$, **$p<0.01$; ***$p<0.001$.

3.5.2.2 *Ctcflos*-dependent modulation of alternative splicing programs

As mentioned above, cellular programming is coordinated on several regulatory levels that can all be targeted by lncRNAs. In this context, transcriptome profiling strongly pointed towards the involvement of *Ctcflos* in further regulatory routes beyond transcriptional modulation. In immediate response to *Ctcflos* KD, multiple factors associated with the splicing process were transcriptionally upregulated. GO term analysis of genes enriched by *Ctcflos* KD accordingly revealed enrichment for terms of molecular functions and structures related to splicing, including ‘mRNA processing’, ‘RNA splicing’, ‘nuclear speck’ and ‘spliceosomal complex’ (Fig. 30 A). This seemed to be a proximal effect of *Ctcflos* deficiency (after 24 hours, data in dark grey) as it was less pronounced 72 hours after the KD (data in light grey). A closer insight into the components of the splicing machinery confirmed comprehensive transcriptional upregulation of multiple subunits of all spliceosomal complexes and of numerous splicing factors (Fig. 30 E, right part of the gene boxes). This clearly opposed the trend of regulation during brite cell differentiation that involved broad downregulation of spliceosomal components (Fig. 30 E left part of the gene boxes) and splicing factors on transcriptional level (Tab. 9). Among the two dominant families of splicing factors, *Serine/arginine-rich proteins* (*SR-proteins*) and *Heterogeneous nuclear ribonucleoproteins* (*Hnrnps*), 84% and 94% were downregulated during brite adipogenesis, while 58% and 66% were upregulated in response to *Ctcflos* KD, respectively. Additionally, in an explorative experiment, general inhibition of splicing by isoginkgetin, largely attenuated thermogenic differentiation, while it had a minor impact on general adipogenesis, as quantified by reduced *Ucp1* per *Fabp4* mRNA transcription levels (Fig. 30 B-D).

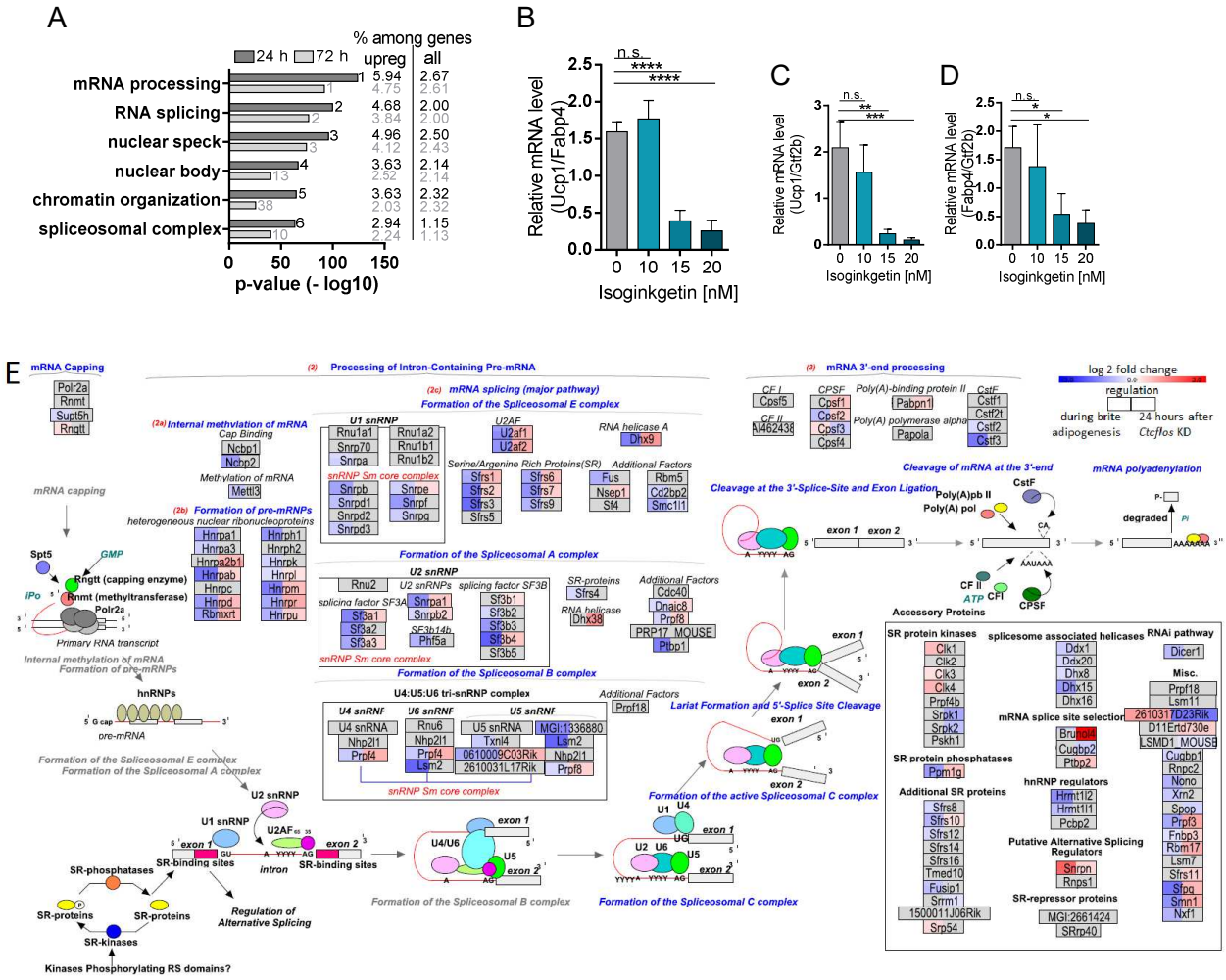

Figure 30: *Ctcflos* KD modulates the splicing machinery. (A) GO term analysis of genes upregulated in response to *Ctcflos* tr1 KD (ASO1). In dark gray, negative log10 p-values of overrepresented GO terms 24 hours after KD and percentages of genes belonging to the respective GO terms among upregulated and among all genes. Small numbers next to the bars show rank positions of GO terms. In light grey, corresponding values for the same GO terms after 72 hours, hypergeometric test. **(B-D)** Impact of splicing inhibition by different concentrations of general splicing inhibitor isoginkgetin on brite adipogenesis, **(B)** expressed as *Ucp1* relative to *Fabp4* mRNA levels, **(C)** *Ucp1* relative to *Gtf2b* and **(D)** *Fabp4* relative to *Gtf2b*. Mean values ± SD, n=3 (biological replicates), one-way ANOVA (Šídák-test). **(E)** Transcriptional changes of components of the splicing machinery and splicing regulatory factors during brite adipocyte differentiation and in direct response to *Ctcflos* tr1 KD (ASO1) (day 1 of differentiation). Visualization by Path Visio software, the color code displays log2 fold changes of gene transcript levels comparing undifferentiated and differentiated primary brite adipocytes of 129S mice (left part of the box) and in direct (24 hours) response to *Ctcflos* KD. N.s. p>0.05, *p<0.05, **p<0.01, ***p<0.001, ****p<0.0001. Modified from (Bast-Habersbrunner *et al.*, 2021).

Table 9: Regulation of splicing factors during brite adipogenesis and in response to *Ctcflos* KD. Log2 fold change, adjusted p-value and direction of regulation of *SR-proteins* and *Hnrnps*, comparing mature with undifferentiated primary brite adipocytes derived from iWAT of 129S6 mice and in response to *Ctcflos* tr1 KD (ASO1) (KD at day 1 of differentiation, harvest after 24 hours).

		diff 129 - undiff 129			Ctcflos KD d1 diff (24 hours)		
splicing factor	**Accn**	**log2 fc**	**adj. p-value**	**regulation**	**log2 fc**	**adj. p-value**	**regulation**
Srsf3	NM_013663	-1,73	1,22E-14	down			
Srsf3	NR_036613	-1,5	1,46E-12	down			
Srsf2	NM_011358	-1,52	1,67E-10	down	0,52	2,51E-02	up
Srsf7	NR_036615	-1,26	5,42E-10	down	0,55	9,44E-03	up
Srsf7	NM_146083	-1,26	7,47E-10	down	0,55	9,95E-03	up
Srsf7	NM_001195485	-1,26	7,84E-10	down	0,54	9,98E-03	up
Srsf7	NM_001195487	-1,26	8,31E-10	down	0,54	9,98E-03	up
Srsf7	NM_001195486	-1,25	9,74E-10	down	0,55	9,59E-03	up
Srsf6	NM_026499	-1	5,61E-09	down	0,74	3,24E-03	up
Srsf1	NM_173374	-0,98	1,30E-06	down			
Srsf9	NM_025573	-0,88	1,83E-06	down			
Srsf9	NR_036616	-0,88	2,09E-06	down			
Srsf1	NM_001078167	-0,91	7,89E-06	down	0,8	2,52E-03	up
Srsf10	NM_010178	-0,77	8,79E-05	down			
Srsf10	NM_001080387	-0,66	2,59E-04	down			
Srsf4	NM_020587	-0,44	2,15E-02	down			
Srsf11	NM_001093752				0,53	5,52E-04	up
Srsf11	NM_001093753				0,53	6,97E-04	up
Srsf11	NM_026989				0,52	1,01E-03	up
regulated proportion				84%			58%
Hnrnpm	NM_029804	-1,5	1,70E-19	down	0,73	3,58E-03	up
Hnrnpm	NM_001109913	-1,48	6,21E-19	down	0,74	3,32E-03	up
Hnrnph1	NM_021510	-1,24	5,89E-16	down			
Hnrnpab	NM_001048061	-1,6	2,17E-14	down	0,49	3,85E-02	up
Hnrnpab	NM_010448	-1,6	3,21E-14	down	0,49	3,75E-02	up
Hnrnpr	NM_028871	-1,01	1,13E-09	down	0,95	2,12E-03	up
Hnrnpd	NM_001077265	-1,12	2,60E-09	down	0,78	4,35E-04	up
Hnrnpd	NM_007516	-1,12	2,69E-09	down	0,77	6,29E-04	up
Hnrnpd	NM_001077266	-1,11	4,24E-09	down	0,78	4,35E-04	up
Hnrnpd	NM_001077267	-1,11	4,53E-09	down	0,77	6,29E-04	up
Hnrnpa0	NM_029872	-1,08	5,69E-08	down			
Hnrnpu	NM_016805	-0,92	6,29E-07	down	0,53	5,90E-03	up
Hnrnpf	NM_001166431	-0,86	1,50E-06	down	0,48	2,36E-03	up
Hnrnpf	NM_001166430	-0,86	1,50E-06	down	0,48	2,36E-03	up
Hnrnpa1	NR_002885	-1,11	4,51E-06	down			
Hnrnpf	NM_001166427	-0,84	1,79E-05	down	0,48	2,57E-03	up
Hnrnpf	NM_001166428	-0,83	2,26E-05	down	0,48	2,57E-03	up
Hnrnpf	NM_001166429	-0,82	2,84E-05	down	0,48	2,57E-03	up
Hnrnpf	NM_133834	-0,82	3,39E-05	down	0,48	2,57E-03	up
Hnrnpf	NM_001166432	-0,81	3,50E-05	down	0,48	2,57E-03	up
Hnrnpa1	NM_001039129	-0,96	5,73E-05	down			
Hnrnpa1	NM_010447	-1,03	1,56E-04	down			
Hnrnpdl1	NM_016690	-0,73	3,38E-04	down	0,73	8,98E-03	up
Hnrnpk	NM_025279	-0,52	4,98E-03	down			
Hnrnpul1	NM_144922	-0,42	7,49E-03	down			
Hnrnpll	NM_144802	-0,43	1,01E-02	down			
Hnrnpul2	NM_001081196	-0,37	1,20E-02	down			
Hnrnpul1	NM_178089	-0,42	1,53E-02	down			
Hnrnpa3	NM_146130	-0,56	2,04E-02	down			
Hnrnpl	NM_177301	-0,4	2,59E-02	down	0,33	3,29E-02	up
Hnrnpa2b1	NM_182650				1,09	1,79E-06	up
Hnrnpa2b1	NM_016806				0,75	4,16E-04	up
regulated proportion				94%			66%

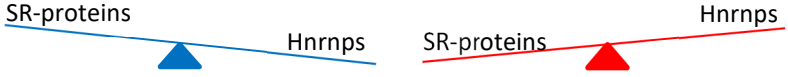

Alternative splicing constitutes a mechanism that generates distinct transcripts from the same gene. A large proportion of human genes can be processed into different isoforms that can have varying or even opposite functions (Modrek & Lee, 2003; Pan *et al*, 2008). Alternative splicing patterns can differ between cell types and are dynamically regulated during differentiation, providing cellular plasticity and adaptability. Targeted and timed modulation of alternative splicing can thus contribute to direct cell fate and function. With the implied involvement of *Ctcflos* in the regulation of alternative splicing, it is thus equipped with a further efficient mechanism to fine tune cellular functionality during brite cell differentiation.

Notably, several genes with isoforms of varying functionality in thermogenic adipocyte differentiation were previously identified, including *Prdm16* (Lin, 2015a). Also *Neat1* was characterized in the present thesis to be transcribed into isoforms of distinct implication in brite adipogenesis. Being already targeted by *Ctcflos* regulation on transcriptional level, these two genes were therefore additionally investigated in terms of their alternative splicing profiles in *Ctcflos* deficiency.

Alternative splicing of *Prdm16*

Prdm16 pre-mRNA can be spliced into two main protein coding transcripts that vary in the utilization of exon 16 and different stop codons in exon 17, resulting in a length difference of 172 bp. *Prdm16* short isoform (ENSMUST00000105636.8, 8426 bp) skips exon 16 and uses an earlier stop codon, while *Prdm16* long isoform (ENSMUST00000030902.13, 8598 bp) includes exon 16 and is terminated at a later stop codon (Fig. 31 A). During brite cell development the two isoforms are differentially regulated. *Prdm16* long remains at a low expression level throughout brite adipogenesis, while *Prdm16* short transcription is significantly induced, reaching its strongest expression at the onset of differentiation (Fig. 31 B).

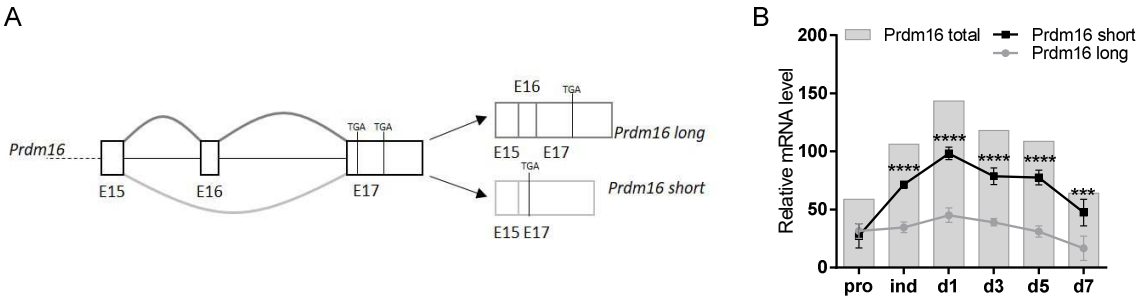

Figure 31: *Prdm16* isoforms are differentially regulated during brite adipogenesis. (A) Splice graph of *Prdm16* and resulting *Prdm16* long and short isoforms. **(B)** Time course of *Prdm16* total, long and short isoform expression relative to *Gtf2b* during brite adipogenesis, assessed by qPCR using isoform specific primers. Mean values ± SD, one representative replicate of two experiments with comparable results (Fig. S9), Two-way ANOVA (Šídák-test). ***p<0.001, ****p<0.0001. Modified from (Bast-Habersbrunner *et al.*, 2021).

Consistent with its prominence in brite adipocytes, *Prdm16* short was previously reported to exert a stronger effect on enhancing the thermogenic gene program and energy expenditure in brown adipocytes (Chi & Lin, 2018). Thus not only absolute *Prdm16* abundance, but also its relative isoform composition influences thermogenic programming. The observed shift in the *Prdm16* isoform profile towards *Prdm16* short during brite adipogenesis can thus further

support the differentiation process. Importantly, it is observed here that this process depends on *Ctcflos*. Comparing the relative abundances of the two isoforms in *Ctcflos* KD and control cells (using an exon 16 spanning primer pair that amplifies both isoforms (*Prdm16* long in an upper band (348 bp), *Prdm16* short in a lower band (173 bp))), revealed that the brite characteristic alternative splicing profile of *Prdm16* is vastly lost in *Ctcflos* deficiency (Fig. 32 A (orange primers) and B). *Prdm16* short transcription is decreased in the absence of *Ctcflos*, considerably reducing its dominance over *Prdm16* long isoform (Fig. 32 C). In isoform specific qPCR analyses (using forwards primers located within exon 16 or reaching from exon 15 into exon 17 to amplify *Prdm16* long and short, respectively (Fig. 32 A (blue primers))), it was further confirmed that total *Prdm16* transcription is predominantly reduced at the expense of *Prdm16* short, while *Prdm16* long expression remained largely unaffected (Fig. 32 D-F (24 hours after KD) and I-K (72 hours after KD)). The fold change of transcript levels between control and *Ctcflos* KD cells was higher for Prdm16 short than for *Prdm16* long isoform (Fig. 32 G and H (24 hours after KD), L and M (72 hours after KD)). This specific impact on the processing of *Prdm16* short was present directly after *Ctcflos* KD (24 hours, significant for ASO1) and maintained during differentiation (72 hours, significant for ASO1 and ASO2). The missing shift of *Prdm16* alternative splicing towards the thermogenesis promoting isoform profile thus likely contributed to the *Ctcflos* KD phenotype. Consistently, there is a strong positive correlation between the relative abundance of *Prdm16* short and *Ucp1* transcript levels across all samples (control and *Ctcflos* KD samples) (Fig. 32 N). Among control cells the correlation persisted, but it was absent among *Ctcflos* KD samples, strengthening the *Ctcflos* dependency of this relation.

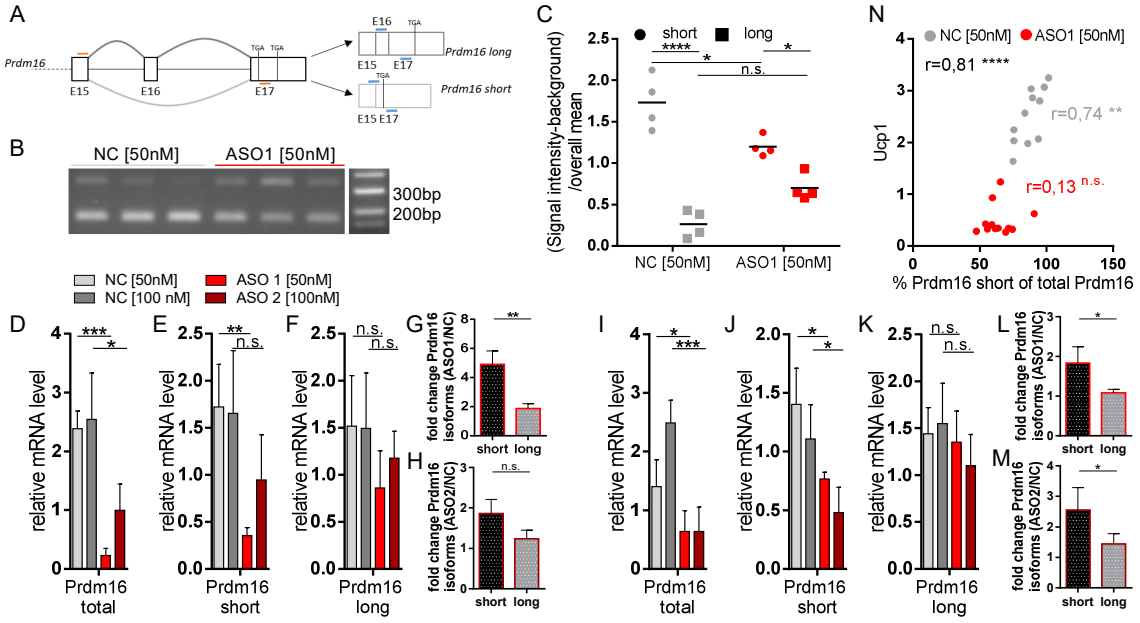

Figure 32: *Ctcflos* modulates *Prdm16* alternative splicing. Impact of *Ctcflos* KD at beginning differentiation of primary brite adipocytes derived from iWAT of 129S6 mice on the alternative splicing profile of *Prdm16*. **(A)** Splice graph of *Prdm16* and resulting *Prdm16* long and short isoforms. Primers used to amplify both *Prdm16* isoforms at once by PCR are displayed in orange, primers used to amplify specifically Prdm16 short and *Prdm16* long, respectively, are displayed in blue**. (B)** Gel picture of PCR products using exon 16 spanning primers to detect *Prdm16* long (upper band (348 bp)) and *Prdm16* short (lower band (173 bp)) comparing *Ctcflos* tr1 KD (ASO1) and non-targeting control samples. **(C)**

Quantification of signal intensities of PCR gel picture subtracted by background and normalized to overall mean signal intensity of the respective biological replicate. Mean and individual values, n=4 (biological replicates), two-way ANOVA (Šídák-test). **(D)** *Prdm16* total, **(E)** *Prdm16* short and **(F)** *Prdm16* long transcript levels relative to *Gtf2b* 24 hours after *Ctcflos* KD, comparing *Ctcflos* tr1 KD (ASO1) and tr3, 4 KD (ASO2) with non-targeting control samples, assessed by qPCR, Mean values ± SD, n=3-4 (biological replicates), unpaired t tests. **(G, H)** Fold change of *Prdm16* short and *Prdm16* long comparing **(G)** ASO1 to NC and **(H)** ASO2 to NC 24 hours after *Ctcflos* KD, n=3-4 (biological replicates), unpaired t tests. **(I)** *Prdm16* total, **(J)** *Prdm16* short and **(K)** *Prdm16* long transcript levels relative to *Gtf2b* 72 hours after *Ctcflos* KD, comparing *Ctcflos* tr1 KD (ASO1) and tr3, 4 KD (ASO2) with non-targeting control samples, assessed by qPCR, Mean values ± SD, n=3-4 (biological replicates), unpaired t tests. **(L, M)** Fold change of *Prdm16* short and *Prdm16* long comparing **(L)** ASO1 to NC and **(M)** ASO2 to NC 72 hours after *Ctcflos* KD, n=3-4 (biological replicates), unpaired t tests. **(N)** Correlation of *Prdm16* short and *Ucp1* expression levels across *Ctcflos* tr1 KD (ASO1) and non-targeting control samples and within both groups. Pearson correlation. N.s. p>0.05, * p<0.05, **p<0.01, ***p<0.001, ****p<0.0001. Modified from (Bast-Habersbrunner *et al.*, 2021).

Together, this demonstrates that beyond the control of overall *Prdm16* transcript abundance, *Ctcflos* additionally regulates its relative isoform composition to further fine tune its functionality towards thermogenic adipogenesis.

Alternative splicing of *Neat1*

Similar to *Prdm16*, lncRNA *Neat1* was shown in the present thesis to be transcribed into isoforms of divergent implication in brite adipogenesis (Fig. E3). For *Neat1*, mainly a long and short isoforms can be distinguished (Fig. 33 A and Fig. E3 A). *Neat1* short, but not long isoform, was primarily upregulated during brite cell differentiation and required for full *Ucp1* transcription and thermogenic function (Fig. 33 B and Fig. E3 C-G) (refer to Excursion2).

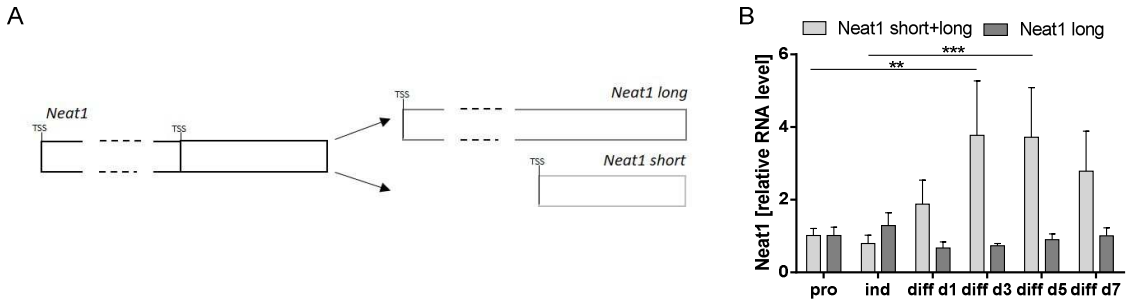

Figure 33: LncRNA *Neat1* isoforms are differentially regulated during brite adipogenesis. (A) Splice graph of *Neat1* and resulting *Neat1* long and short isoforms. **(B)** Time course of *Neat1* total (short+long) and long isoform expression relative to *Gtf2b* during brite adipogenesis, assessed by qPCR. Mean values ± SD, n=3 (technical replicates), two-way ANOVA (Šídák-test). **p< 0.01, ***p< 0.001.

As for *Prdm16*, this browning-characteristic *Neat1* splicing was examined for *Ctcflos* dependency. Total *Neat1* transcripts were by trend downregulated in response to *Ctcflos* KD (at day 1 of differentiation) in qPCR analysis (Fig. 34 A). Specific quantification of *Neat1* long, in contrast, revealed profound transcriptional induction (Fig. 34 B). Considering the *Ctcflos* KD impact on total *Neat1* as sum of the KD effects on *Neat1* short and *Neat1* long, this proposes a profound downregulation of the short *Neat1* isoforms, which opposes its preferred splicing

during brite differentiation. The brite-characteristic *Neat1* splicing thus depends on the presence of *Ctcflos*. These data support that also *Neat1* expression is modulated by *Ctcflos* on both, the level of transcription and RNA processing towards increased *Neat1* short isoform abundance, which was shown to be the isoform of prime importance in brite adipogenesis (Fig. E3 C-G).

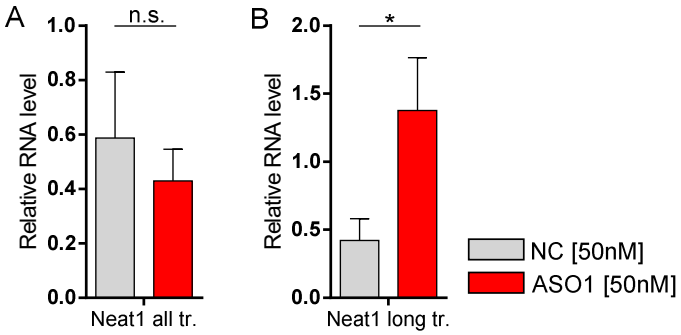

Figure 34: *Ctcflos* modulates *Neat1* alternative splicing. (A) *Neat1* total (short+long) and **(B)** *Neat1* long transcript levels relative to *Gtf2b* 24 hours after *Ctcflos* tr1 KD (ASO1) (KD day1 diff) compared to non-targeting control samples, assessed by qPCR. Mean ± SD, n=3 (biological replicates), unpaired t-tests. N.s. p>0.05, *p<0.05.

Global analysis of alternative splicing

To explore the extent of *Ctcflos*-dependent alternative splicing modulation beyond *Prdm16* and *Neat1*, splicing events were systematically profiled in differentiating brite adipocytes and in response to *Ctcflos* KD (KD on day 1 of differentiation, analysis after 24 hours, when changes in the splicing machinery were strongest pronounced). For this purpose, control and *Ctcflos* KD samples were deep sequenced with >40 mio reads per sample (150 bp, paired-end) and analyzed for differential splice events using the SGSeq algorithm (Goldstein *et al.*, 2016). Splice junction spanning reads thereby served to identify and quantify splice events, revealing 455 transcripts with differential splice patterns between *Ctcflos* KD and control cells (Fig. 35 A). Importantly, around one third of them (149 transcripts) were previously determined as putative candidates of browning regulation, supporting that the *Ctcflos*-dependent changes of alternative splicing profiles can be of relevance in brite adipogenesis. Numerous factors involved in adipogenesis, lipid metabolism, mitochondrial function and splicing itself were among the differentially spliced genes, including transcript isoforms that were already characterized by other studies to possess varying functionalities in adipogenesis (*Insr*, *Pparγ*, *Mapk9*, *Mbnl1* and *Rbm4*) (Fig. 35 B) (Cooper *et al.*, 2014; Entingh *et al*, 2003; Hung & Lin, 2020; Lin *et al.*, 2014).

With the impact of *Ctcflos* on *Rbm4* alternative splicing, it affects a reported effector in thermogenic brown adipogenesis, which itself operates as transcriptional regulator and modulator of adipocyte-specific splicing events. RBM4 induces isoform shifts of several adipogenesis-related factors, including *Pparγ*, *Insr*, *Nova1*, *Mbnl1*, *Prdm16*, *Pref1*, *Mef2c*, *Fgfr2*, *Map4k4* to foster thermogenic adipocyte development (Chi & Lin, 2018; Hung & Lin, 2020; Lin, 2015b; Lin *et al*, 2016a; Lin *et al*, 2016b; Lin *et al.*, 2014; Peng *et al*, 2018).

Interestingly, there is quite some overlap between RBM4 affected genes and *Ctcflos* targets for transcriptional and splicing modulation, placing *Ctcflos* activity upstream of an established splicing regulatory network in thermogenic adipogenesis (Fig. 35 C). How *Ctcflos*-dependent splicing of *Rbm4* affects its functionality and whether *Ctcflos* includes *Rbm4* as a downstream mediator, warrants further investigation.

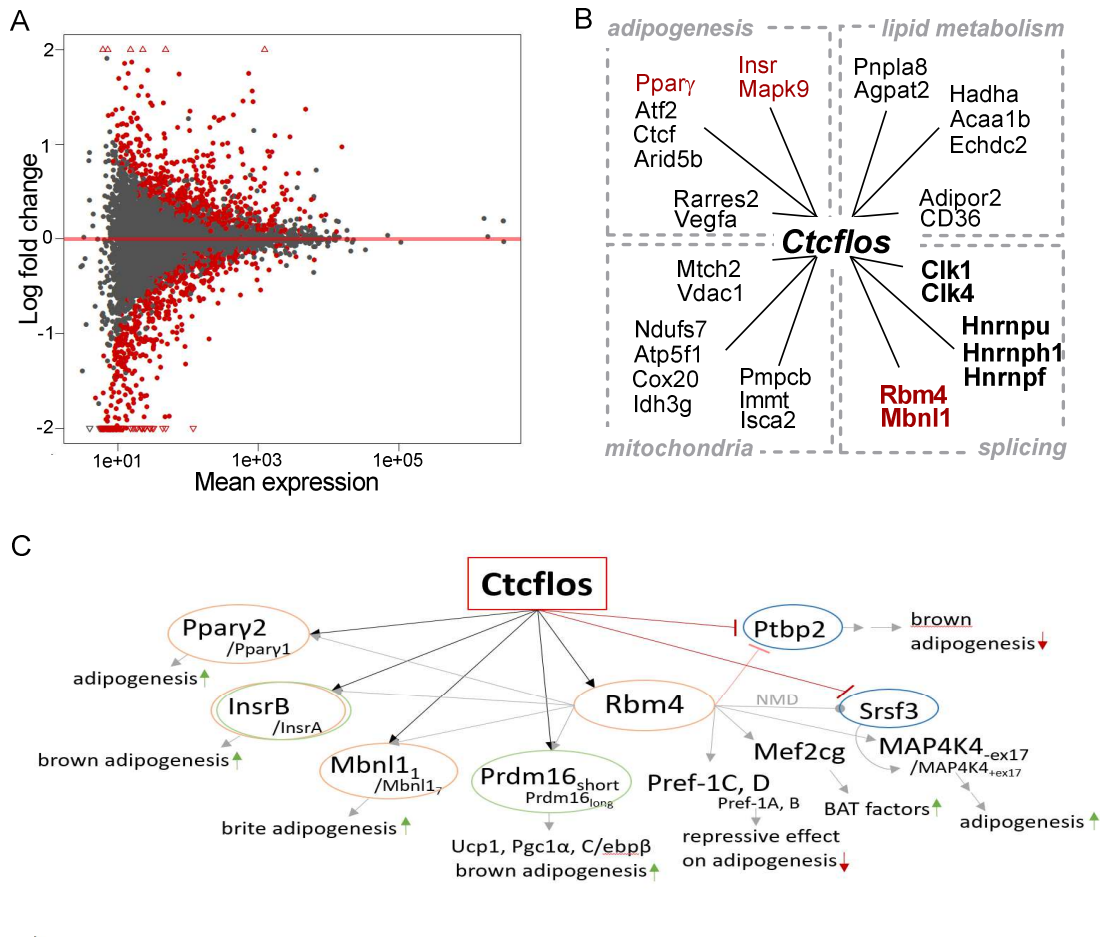

Figure 35: *Ctcflos* modulates alternative splicing during brite adipogenesis on a broad scale. Global transcriptome analysis of *Ctcflos* tr1 KD impact on alternative splicing (KD day 1 of differentiation, analysis after 24 hours)**. (A)** MA-plot of differential alternative splicing analysis using SGSeq algorithm comparing *Ctcflos* tr1 KD (ASO 1) with non-targeting controls. Each data point depicts a splice event. Splice events of differential abundance are colored in red. **(B)** Overview of selected genes involved in adipogenesis, lipid metabolism, mitochondria or splicing, with differential splicing profiles between *Ctcflos* tr1 KD (ASO 1) and control samples. Genes previously described to be spliced into alternative isoforms of varying function in brown adipogenesis are marked in red. **(C)** Reported targets of RBM4-regulated alternative splicing and transcription in brown adipose tissue (Chi & Lin, 2018; Hung & Lin, 2020; Lin, 2015b; Lin *et al.*, 2016a; Lin *et al.*, 2016b; Lin *et al.*, 2014; Peng *et al.*, 2018). Yellow circles mark genes that were identified by deep sequencing to be differentially spliced also by *Ctcflos* tr1 KD, green circles mark genes for which *Ctcflos*-dependent alternative splicing was confirmed experimentally, blue circles highlight genes that are transcriptionally regulated by *Ctcflos*. Modified from (Bast-Habersbrunner *et al.*, 2021).

For validity testing of the SGSeq analysis, the identified splicing of *Insulin receptor* (*Insr*) was chosen for experimental verification. Two isoforms can be processed from *Insr* pre-mRNA, that vary in the utilization of exon 11 (ENSMUSE00001381444; 36 bp), $Insr_{+ex11}$ and $Insr_{-ex11}$. SGSeq analysis predicted lower exon 11 inclusion in *Ctcflos* KD adipocytes (Fig. 36 A). Consistent with this, PCR experiments confirmed a decreased $Insr_{+ex11}/Insr_{-ex11}$ ratio, which

becomes significant 72 hours after *Ctcflos* KD (Fig. 36 B-E). The isoform switch towards $Insr_{+ex11}$ that can be observed during brite adipogenesis for control cells (when comparing isoform profiles at day 4 of differentiation (Fig. 36 G data for NC) with those of day 1 (Fig. 36 F data for NC)), is less pronounced in *Ctcflos* KD cells (Fig. 36 G and F data for ASO1). Also a previous publication reported an isoform shift towards dominance of $Insr_{+ex11}$ during the course of brown adipocyte differentiation, which induces hyperphosphorylation of p38-MAPK and promotes brown adipogenesis (Lin *et al.*, 2014). The experimental reproducibility of *Ctcflos*-associated *Insr* splicing and the accordance with published data strengthens the reliability of the SGSeq prediction.

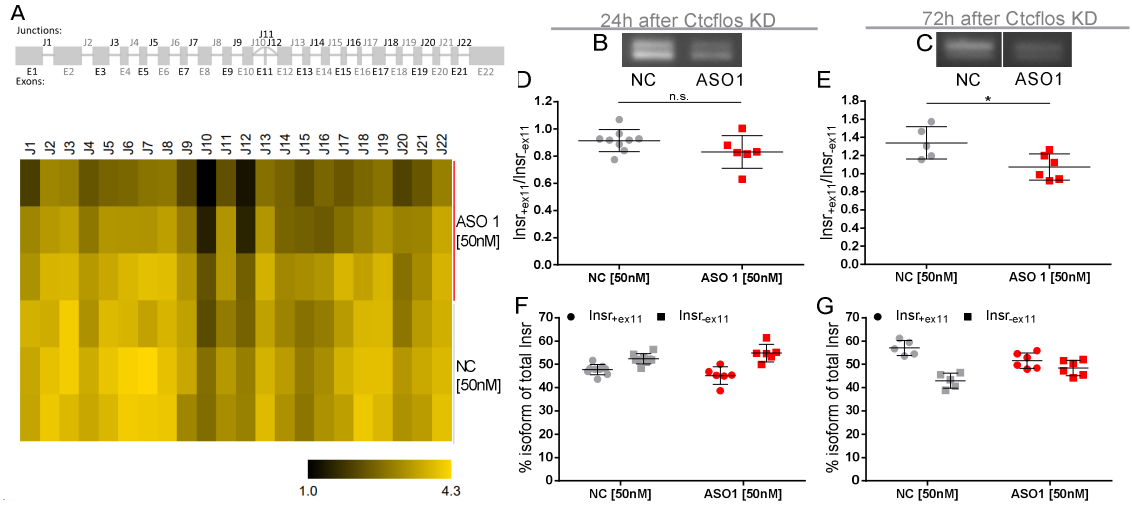

Figure 36: SGSeq-predicted splicing of *Insr* is validated experimentally. (A) Splice graph (upper panel) and exon junction heatmap (lower panel) of *Insulin receptor* (*Insr*) comparing *Ctcflos* tr1 KD (ASO1) and non-targeting controls in transcriptome wide splicing analysis by SGSeq algorithm (Goldstein et al., 2016). The splice graph displays *Insr* exons and alternative exon junctions. In the heatmap usage of exon junctions is quantified from junction spanning reads. **(B, C)** PCR gel pictures of *Insr*+ex11 (upper band) and *Insr*-ex11 (lower band) in non-targeting control and *Ctcflos* tr1 KD (ASO1) samples**, (B)** 24 hours or **(C)** 72 hours after the KD. **(D, E)** Ratio of *Insr*+ex11 to *Insr*-ex11 in non-targeting control and *Ctcflos* tr1 KD (ASO1) samples, **(D)** 24 hours or **(E)** 72 hours after the KD, quantified from PCR signals. Mean and individual values, n=5-9 (technical replicates), unpaired t tests. **(F, G)** Percentage of *Insr*+ex11 and *Insr*-ex11 of total *Insr* in non-targeting control and *Ctcflos* tr1 KD (ASO1) samples, **(F)** 24 hours or **(G)** 72 hours after the KD quantified from PCR signals. Mean and individual values, n=5-9 (technical replicates). N.s. $p>0.05$, *$p<0.05$. Modified from (Bast-Habersbrunner *et al.*, 2021).

Side note

The experimentally determined impact of *Ctcflos* on *Prdm16* and *Neat1* alternative splicing is not predicted in the transcriptome wide splicing analysis. Specifically extracting the coverage data of splice junction spanning reads for *Prdm16*, indicate that the sequencing depth was not sufficient to evaluate its splicing profile. Across all samples, only 1 to 5 reads spanned across the alternatively spliced exon 16. An even deeper sequencing strategy would thus be required to identify all differential splice events and to fully grasp the dimensions of *Ctcflos*-associated alternative splicing in brite adipogenesis.

In summary, the in depth characterization of *Ctcflos* KD effects on global level, as well as on the individual targets *Prdm16* and *Neat1*, uncovered two regulatory routes of *Ctcflos* to modulate target gene expression in quantity and quality. It established *Ctcflos* as transcriptional and alternative splicing regulator that acts upstream of established (Prdm16) and novel (Neat1) effectors in brite adipogenesis.

3.5.3 Mechanisms of *Ctcflos*-dependent transcription and alternative splicing regulation

The identification of *Ctcflos* activity in transcriptional and alternative splicing regulation during brite adipogenesis raises the question of the molecular mechanism(s) that convey these functionalities. LncRNAs have been attributed various different functions and mechanistic activities in past studies. This mechanistic versatility of lncRNAs renders it specifically challenging to narrow down the precise molecular operation of *Ctcflos*. The following sections approach this question from different angles and develop perspectives that could present the starting point for future mechanistic investigations.

3.5.3.1 Possible mechanisms of *Ctcflos*-mediated regulation of transcription

Among the described mechanisms mediating transcriptional regulation, lncRNAs can act on genes *in cis* or *in trans*, they can operate as guides or hijackers of chromatin modifiers and transcription factors or serve as scaffolds for regulatory protein complexes.

Gene transcription regulation *in cis* or *in trans*

Several lncRNAs have been reported to modulate transcription of genes in close proximity to their own gene locus *in cis*. In case that this affects a prominent regulatory factor, cellular functionality can be shaped on a broad scale. To investigate this scenario for *Ctcflos*, its direct neighbor genes were analyzed for transcriptional modulation in *Ctcflos* deficiency and for their own regulatory potential in brite adipogenesis. This will evaluate whether they could act as direct *Ctcflos* mediators of the above described transcriptional changes in the thermogenic gene program.

In upstream direction, the *Ctcflos* locus partially overlaps with *Ctcfl* gene and promoter sequences on the opposite strand (Fig. 37 A). During brite adipogenesis, *Ctcfl* expression is slightly upregulated, though it reaches only a low level at the onset of differentiation (d1) when *Ctcflos* activity is most prominent (Fig. 37 B). In qPCR analysis *Ctcfl* was not significantly affected in *Ctcflos* deficiency and KD of *Ctcfl* had no impact on *Ucp1* gene transcription, excluding *Ctcfl* as direct target and mediator of *Ctcflos* activity (Fig. 37 C and D).

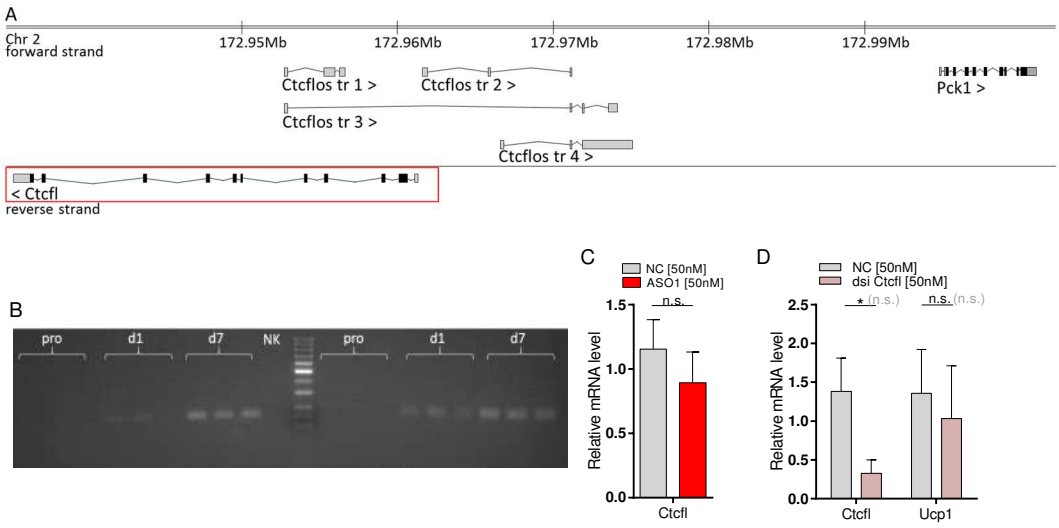

Figure 37: *Ctcflos* acts independent of its upstream neighbor *Ctcfl*. (A) Gene locus of *Ctcflos* and its up- and downstream neighbors *Ctcfl* and *Pck1*. **(B)** Gel picture of *Ctcfl* PCR products amplified from

proliferating, differentiating and mature brite adipocytes, n=2 (biological replicates). **(C)** *Ctcfl* transcript levels relative to *Gtf2b* in *Ctcflos* tr1 KD (ASO1) compared to non-targeting control cells (KD day1 diff, harvest after 24 hours), assessed by qPCR. Mean ± SD, n=3 (biological replicates), unpaired t test. **(D)** *Ctcfl* and *Ucp1* transcript levels relative to *Gtf2b* in *Ctcfl* KD (dsi *Ctcfl*) compared to non-targeting controls (KD day1 diff, harvest after 72 hours), assessed by qPCR. Mean ± SD, n=3 (biological replicates), unpaired t tests or in grey parenthesis two-way ANOVA (Šídák-test). N.s. p>0.05, *p<0.05. Modified from (Bast-Habersbrunner *et al.*, 2021).

The *Ctcflos* downstream neighbor *Pck1* is clearly expressed in differentiating brite adipocytes and downregulated in response to early *Ctcflos* deficiency (Fig. 38 A-E). Notably, *Pck1* expression was induced during brite adipogenesis, it was higher expressed in brite compared to white adipocytes and correlated with *Ucp1* across the five mouse strains, proposing a putative regulatory function in browning (Fig. 38 B-D). Knockdown of *Pck1*, however, had no impact on *Ucp1* gene transcription, excluding also *Pck1* as downstream mediator of *Ctcflos* activity and proposing its transcriptional activity *in trans* rather than *in cis* (Fig. 38 F).

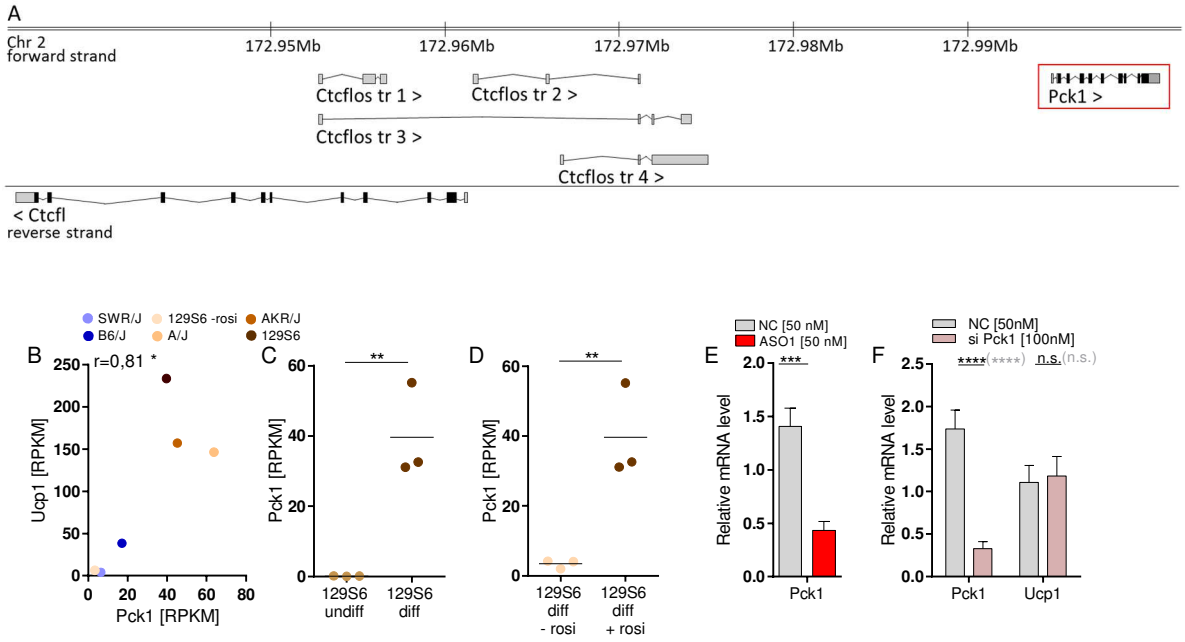

Figure 38: *Ctcflos* acts independent of its downstream neighbor *Pck1*. (A) Gene locus of *Ctcflos* and its up- and downstream neighbors *Ctcfl* and *Pck1*. **(B)** Correlation of *Pck1* with *Ucp1* transcript levels across differentiated primary brite adipocytes derived from iWAT of the five inbred mouse strains (transcript levels in RPKM), assessed by RNA sequencing. Mean values, n=3 (biological replicates), Pearson correlation. **(C)** *Pck1* transcript levels in differentiated brite compared to undifferentiated primary adipocytes derived from iWAT of 129S6 mice (transcript levels in RPKM), assessed by RNA sequencing. Mean and individual values, n=3 (biological replicates), unpaired t test. **(D)** *Pck1* transcript levels in differentiated brite compared to differentiated white primary adipocytes derived from iWAT of 129S6 mice (transcript levels in RPKM), assessed by RNA sequencing. Mean and individual values, n=3 (biological replicates), unpaired t test. **(E)** *Pck1* transcript levels relative to *Gtf2b* in *Ctcflos* tr1 KD (ASO1) compared to non-targeting control cells (KD day1 diff, harvest after24 hours), assessed by qPCR. Mean ± SD, n=3 (technical replicates), unpaired t test. **(F)** *Pck1* and *Ucp1* transcript levels relative to *Gtf2b* in *Pck1* KD (siPck1) compared to non-targeting control samples (KD day1 diff, harvest after 72 hours), assessed by qPCR. Mean ± SD, n=6 (technical replicates), unpaired t tests or in grey parenthesis two-way ANOVA (Šídák-test). N.s. p>0.05, *p<0.05, **p<0.01, ***p<0.001, ****p<0.0001. Modified from (Bast-Habersbrunner *et al.*, 2021).

Guidance of chromatin modifiers or transcription factors

LncRNAs, which modulate gene transcription in *trans* often act as guides that lead chromatin modifiers or transcription factors to more distant loci. Target DNA sites are recognized through RNA:DNA heteroduplex formation based on sequence similarity (comparable to the activity of sgRNAs in CRISPR systems). Searching for putative target loci for *Ctcflos* binding, the *Ctcflos* isoform 1 cDNA sequence was blasted against the murine genome (GRCm38). This revealed 38 loci that aligned with *Ctcflos* isoform 1 across a length of 18-58 nucleotides (Tab. 10).

Table 10: Murine DNA loci partially aligning with the *Ctcflos* isoform 1 sequence. Results of *Ctcflos* tr1 blast against the murine genome (GRCm38) using Ensembl BLAT function. Additional information on chromosome location of identified loci, association with a single peak of regulated genes 10 Mbp downstream (see Fig. 39) and whether this peak exceeds 8% of regulation.

Genomic Location	Overlapping/ nearby Gene(s)	Query start	Query end	Length	E-val	%identity	not at chr. end	single peak	>8% reg.
2:173113379-173114093	Ctcfl, Ctcflos	189	903	**715**	0,00E+00	**100.00**	yes	yes	
2:173114376-173114709	Ctcfl, Ctcflos	904	1237	**334**	3,40E-187	**100.00**	yes	yes	
2:173110818-173111005	**Ctcfl, Ctcflos**	**1**	**188**	**188**	**9,10E-103**	**100.00**	**yes**	**yes**	**yes**
5:127642123-127642180	Glt1d1	789	846	**58**	7,30E-18	**87.93**	yes	no	
11:96950957-96950997	D030028A08Rik	787	827	**41**	5,80E-12	**90.24**	yes	no	
9:72947196-72947245	Pygo1	808	857	**50**	8,70E-12	**84.00**	yes	no	
2:132465636-132465674	**1700026D11Rik**	**789**	**827**	**39**	**6,70E-11**	**92.31**	**yes**	**yes**	**yes**
5:125727614-125727652	Tmem132b	789	827	**39**	8,80E-11	**89.74**	yes	no	
4:121001232-121001269	**Smap2**	**789**	**827**	**39**	**8,00E-10**	**94.87**	**yes**	**yes**	**yes**
17:80632992-80633025	Map4k3	794	827	**34**	1,70E-09	**94.12**	yes	no	
4:45679551-45679582	**Gm829**	**904**	**935**	**32**	**3,00E-09**	**96.88**	**yes**	**yes**	**yes**
11:94259419-94259456	Wfikkn2 / Gm21885	789	827	**39**	5,10E-09	**92.31**	yes	no	
17:71381168-71381205	Smchd1	789	827	**39**	5,10E-09	**92.31**	yes	no	
12:117220753-117220790	Ptprn2	789	827	**39**	5,10E-09	**92.31**	no	no	
13:58524730-58524764	(Hnrnpk)	815	849	**35**	9,90E-09	**91.43**	yes	no	
2:30572743-30572786	Ier5l/ Cstad	899	941	**44**	1,80E-08	**84.09**	yes	no	
16:18446245-18446279	Txnrd2	789	824	**36**	5,70E-08	**94.44**	yes	no	
5:26594128-26594159	4930584F24Rik	808	839	**32**	1,40E-07	**93.75**	yes	no	
4:43830215-43830247	Olfr156	794	827	**34**	1,70E-07	**94.12**	yes	no	
11:58108568-58108598	Cnot8	795	827	**33**	7,10E-07	**93.94**	yes	no	
4:57339756-57339781	Ptpn3	802	827	**26**	7,50E-07	**100.00**	yes	no	
3:49082197-49082227	**Gm31415**	**899**	**928**	**31**	**3,60E-06**	**96.77**	**yes**	**yes**	**yes**
2:37661129-37661153	Strbp	899	923	**25**	5,90E-06	**100.00**	yes	no	
5:127885285-127885308	Tmem132d	804	827	**24**	1,30E-05	**100.00**	yes	no	
12:111591515-111591538	Mark3	803	826	**24**	1,30E-05	**100.00**	no	yes	
4:129923542-129923564	Adgrb2, Spocd1	804	826	**23**	5,30E-05	**100.00**	yes	no	
7:142408134-142408156	Syt8, Tnni2, Lsp1	805	827	**23**	5,30E-05	**100.00**	no	no	
9:72417792-72417819	Mns1	936	965	**30**	1,40E-04	**93.33**	yes	no	
X:49339642-49339664	Gm14696, Gm14697	921	943	**23**	1,50E-04	**100.00**	yes	no	
9:59891569-59891596	Myo9a, Gm20275	899	925	**28**	1,80E-04	**96.43**	yes	no	
8:121830567-121830588	Galnt2l	906	927	**22**	3,70E-04	**100.00**	no	no	
14:101709693-101709715	Gm49269, Lmp7	905	927	**23**	2,10E-03	**95.65**	yes	no	
15:75315620-75315645	Gm3454	899	923	**26**	2,70E-03	**96.15**	yes	no	
17:83619616-83619635	Kcng3	808	827	**20**	3,80E-03	**100.00**	yes	no	
3:34446786-34446805	Sox2ot	809	828	**20**	3,80E-03	**100.00**	yes	no	
11:6164926-6164945	Nudcd3	815	834	**20**	2,10E-02	**95.00**	yes	no	
11:75382493-75382511	Smyd4	947	965	**19**	3,40E-02	**100.00**	yes	no	
16:38855372-38855389	Gm15802	804	821	**18**	5,70E-02	**100.00**	yes	no	
11:78151807-78151824	Fam222b	808	825	**18**	6,50E-02	**100.00**	yes	no	
9:72417652-72417669	Mns1	808	825	**18**	6,50E-02	**100.00**	yes	no	
2:76225865-76225883	**Pde11a**	**809**	**827**	**19**	**8,90E-02**	**94.74**	**yes**	**yes**	**yes**

To examine the functional relevance of these putative *Ctcflos*-DNA interaction sites, it was investigated whether they co-localize to areas of high density of *Ctcflos*-dependently transcribed genes. For this purpose, the mean percentage of all *Ctcflos* KD regulated genes within frames of 10 Mbs were plotted in 1000 kb intervals along the entire mouse genome (all regulated genes (blue curve), upregulated genes (red curve) and downregulated genes (green curve)) (Fig. 39). Regions of interest were assigned to those loci, where putative binding sites of *Ctcflos* (blast hits (red dots)) co-located with single peaks of positively or negatively regulated genes that exceed 8% of regulation (Fig. 39 (arrows), Tab. 10). Hits at chromosome ends were excluded due to unreliable distortions in the calculation of regulated genes. This identified six blast hits of interest that were subjected to further analysis.

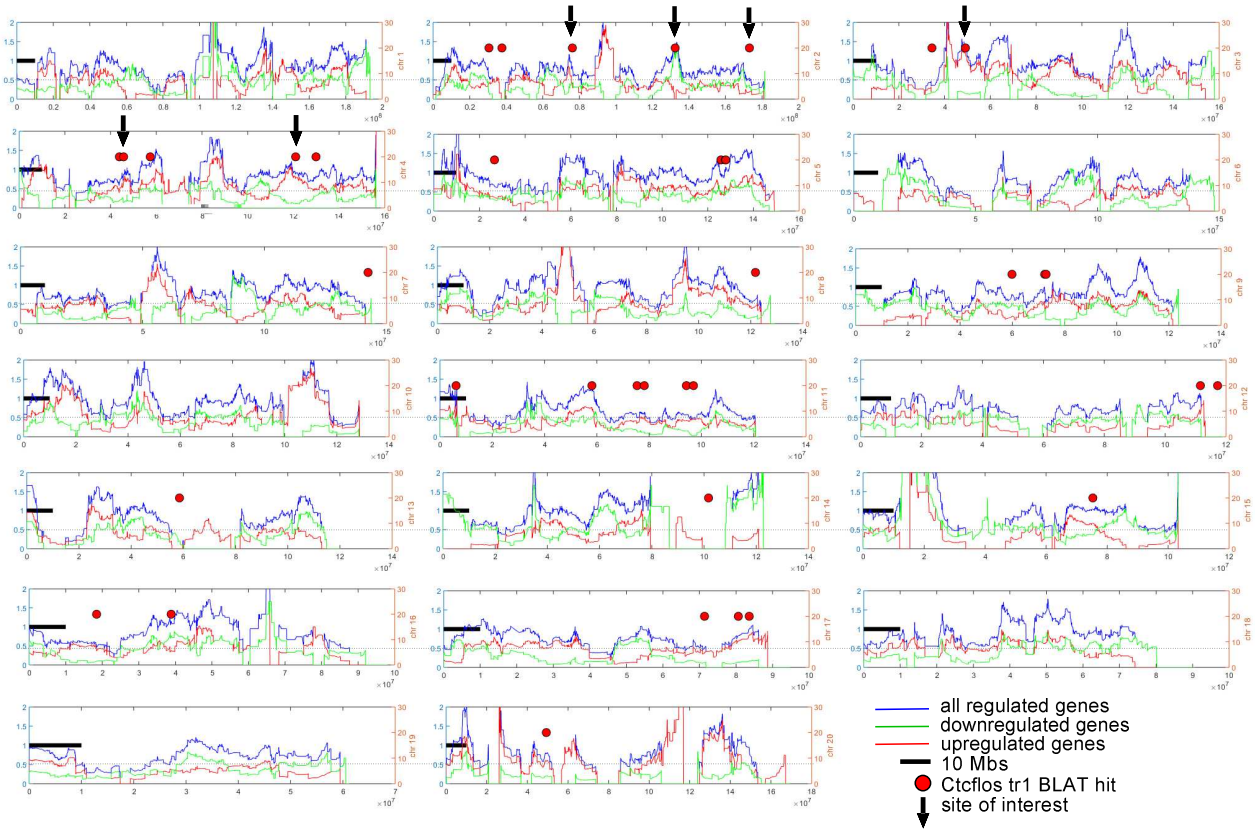

Figure 39: Putative *Ctcflos* DNA binding sites partially overlap with sites of *Ctcflos* KD-induced transcriptional regulation. Location of *Ctcflos* blast hits across the genome (red dots), percentage of all regulated genes (blue curve), upregulated genes (red curve) and downregulated genes (green curve) plotted within frames of 10 Mbs in 1000 kb intervals along the mouse genome. Black arrows depict sites of interest, where *Ctcflos* blast hits co-localize with regions of abundant *Ctcflos* KD-induced positive or negative transcription regulation (single peaks >8% regulation).

To exclude that these putative binding sites hit regions of high positive or negative gene regulation just by chance, 100x6 random regions were chosen within the genome and *Ctcflos*-dependent regulation was quantified at these sites as described above (Fig. 40). The mean percentage of genes regulated at the identified putative *Ctcflos* binding sites significantly exceeded that at the randomly chosen regions, supporting that the transcriptional regulation at the predicted *Ctcflos* binding sites might occur as consequence of *Ctcflos* binding rather than by mere coincidence (Fig. 40).

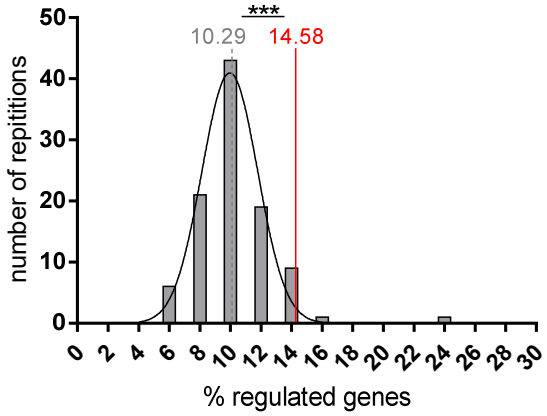

Figure 40: Transcriptional regulation at predicted *Ctcflos* DNA binding sites exceeds regulation at randomly chosen DNA sites. Histogram showing frequency distribution of the mean proportions of strongest regulated genes (either up or down) 10 Mbs downstream of 100x6 randomly chosen DNA sites. Overall mean is depicted in grey. The mean proportion of regulated genes 10 Mbs downstream of the 6 putative *Ctcflos* binding sites of interest is depicted in red. Unpaired t test, ***p<0.001.

A closer look into the regulated genes 10 Mbs downstream of the predicted *Ctcflos* binding sites disclosed some adipose or mitochondrial related genes, including *Kruppel-like factor 4* (*Klf4*), *Y box protein 1* (*Ybx1*), *NADH:ubiquinone oxidoreductase subunit* A5 (*Ndufaf5*), *Neurobeachin* (*Nbea*) and *Arginine Kinase* (*Aks*). Associated GO terms comprised 'ribonucleoprotein complex' (position 4), 'mRNA binding' (position 5), 'transcription regulator complex' (position 8) and 'fat cell differentiation' (position 9) (Tab. S2). Interestingly, the majority of the genes was contrarily regulated in *Ctcflos* deficiency and during brite adipogenesis (Tab. S3).

Hijacking of transcription factors

Beyond their guiding function, lncRNAs are also able to modulate gene transcription *in trans* by acting as decoys that mimic transcription factor binding sequences and sequester transcription factors from their DNA target sites. To investigate whether transcription factors could be trapped by *Ctcflos*, its sequence was analyzed for the presence of transcription factor binding sites using the Genomatix MatInspector algorithm. This predicted the presence of 21 transcription factor binding matrix families spread across the *Ctcflos* isoform 1 sequence (Tab. 11). Several of them constitute binding sites for transcription factors associated with thermogenic gene expression. Notably, their majority was previously established as negative regulators in brown and brite adipogenesis (Activating Transcription Factor 4 (ATF4), Nuclear Receptor 4A1 (NR4A1), Zink Finger Protein 423 (ZFP423) and RNA Binding Protein J (RBPJ) (Bi *et al*, 2014; Kanzleiter *et al*, 2005; Shao *et al*, 2016; Wang *et al*, 2013a)). Hijacking of these transcription factors by *Ctcflos* could thus promote the thermogenic gene transcription program.

Table 11: Transcription factor binding sites within the *Ctcflos* isoform 1 sequence. Transcription factor binding matrix families, their quality rating and corresponding transcription factors (TFs) within *Ctcflos* tr1 sequence, determined by Genomatix MatInspector software. Graphical illustration of spatial distribution of TF binding matrices along *Ctcflos* isoform 1 sequence.

Matrix Family	p-value	binding TFs
V$ZF09	0.000063488	Znf274
V$TCFF	0 .0088307	**Nfe2l1**
V$AARF	0 .00951627	**Atf4**
V$CABL	0 .010224	Abl1
V$PAX9	0 .01775	Pax9
V$BTBF	0 .021504	Zbtb33
V$GABF	0 .025008	(GA boxes)
V$FXRE	0 .026568	Nr1h4, **Rxra**, Rxrb, Rxrg
V$BPTF	0 .0295131	Bptf
V$HASF	0 .0295131	(HIF-1 ancilllary seq fam)
V$PCBE	0 .0351271	Preb
V$DEAF	0 .0357054	Deaf1
V$MITF	0 .0368707	Mitf, Tfe3, Tfeb, Tfec
V$NBRE	0 .0395328	**Nr4a1**, Nr4a2, Nr4a3
V$OAZF	0 .0398319	**Zfp423**
V$MTF1	0 .0413368	Mtf1, Mtf2
V$PTF1	0 .0422471	Ptf1a, **Rbpj**, Rbpjl
V$RU49	0 .0422471	Zscan21
V$ETSF	0 .0443157	Ets1-2, Elk1-4, Etv1-6, and others
V$E4FF	0 .0456291	Dnase1l2, E4f1
V$LTFM	0 .046251	Ltf

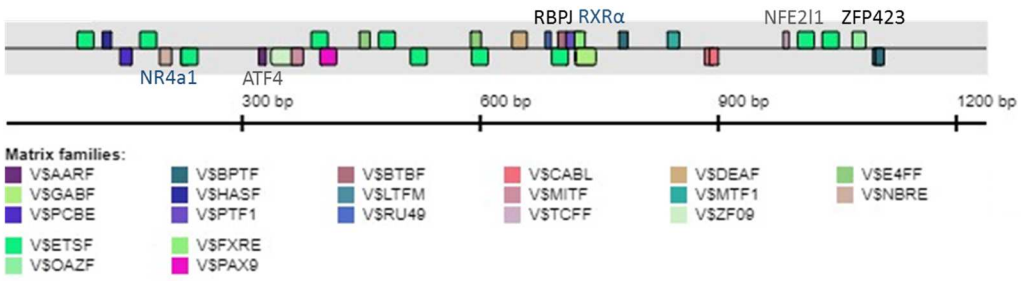

Scaffolding of regulatory protein complexes

In addition to the guidance or hijacking of transcription factors, lncRNAs can also provide a platform for protein complex formation. Largely depending on their secondary structure, lncRNAs can interact with several factors and bring them into spatial proximity. Secondary structure prediction for *Ctcflos* isoform 1 using RNAfold WebServer (Vienna RNA Web Services Institute for theoretical chemistry) (Gruber *et al.*, 2008) proposed extensive base pairing within *Ctcflos* isoform 1 (Fig. 41). Among the identified transcription factors that could bind to *Ctcflos*, there are potential interaction partners such as NR4a1 and Retinoid X Receptor α (RXRα) or Nuclear Factor Erythroid 2 Like 1 (NFE2L1) and ATF4 that could be supported in their interaction through binding to *Ctcflos* (Kanzleiter *et al.*, 2005; Kim *et al*, 2016). Interestingly, the binding sites of NFE2L1 and ATF4 are brought into direct neighborhood in the predicted *Ctcflos* secondary structure, which might approach them for interaction (Fig. 41).

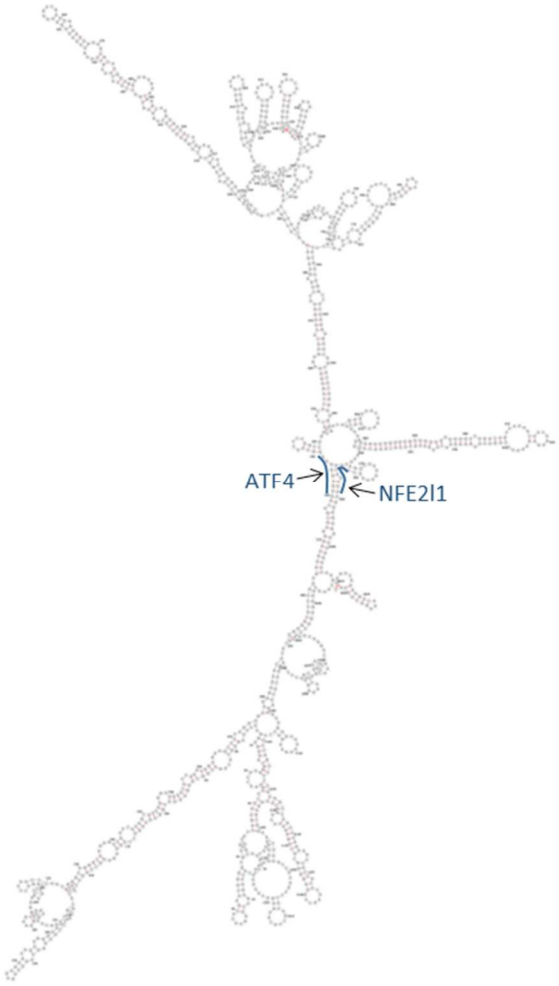

Figure 41: *Ctcflos* is predicted to fold into a complex secondary structure. Secondary structure of *Ctcflos* tr1 predicted by RNAfold WebServer (Vienna RNA Web Services Institute for theoretical chemistry) (Gruber *et al.*, 2008). Locations of ATF4 and NFE2L1 binding sites within the folded *Ctcflos* tr1 structure are highlighted in blue.

3.5.3.2 Possible mechanisms of *Ctcflos*-dependent alternative splicing modulation

Regarding the regulation of pre-mRNA splicing, lncRNAs were also proposed to be involved in various ways. Previously described mechanisms include the interaction of lncRNAs with splicing factors or further RNA binding proteins (RBPs) to modulate their phosphorylation and thus activity state or again to act as hijackers of the named proteins, antagonizing their function in splice site selection and pre-mRNA stability modulation. The question whether *Ctcflos*-dependent alternative splicing could rely on a corresponding mechanistic route was approached by computational predictions from two different angles. I) Differentially spliced transcripts were analyzed for overrepresented RBP motifs and II) *Ctcflos* isoform 1 was investigated for putative protein interaction partners.

RNA binding protein motifs in differentially spliced transcripts

Searching for factors that could convey the observed impact of *Ctcflos* KD on alternative splicing, an enrichment analysis for RBP motifs was performed within 3'UTRs and mRNA sequences of all differentially spliced transcripts, using the Transite analysis platform (Krismer *et al.*, 2019). RNA Binding Motif Protein 41 (RBM41) binding sites (WUACWUU) were prominently overexpressed in the 3'UTRs and also strongly enriched in the mRNA sequences (Fig. 42 A and B). Notably, eight RBM41 binding sites were also present within *Ctcflos* tr1 RNA, providing the possibility for a functional interaction (Tab. S4). Although RBM41 has not yet been associated with thermogenic adipogenesis, the present transcriptome data revealed negative regulation during brite adipocyte differentiation (Fig. 42 C). Consistently, in an explorative experiment mild RBM41 KD-induced *Ucp1* gene expression, suggesting a negative regulatory influence of RBM41 in the browning process (Fig. 42 D). A hijacking function of *Ctcflos* could be envisioned, capturing RBM41 and relieving its negative impact on brite adipogenesis. The implication of RBM41 in splicing regulation, however, remains elusive and would require further investigation. Beyond RBM41, further RNA binding factors overrepresented in the analyses included HNRNPR, Serine/arginine Splicing Factor 1 (SRSF1), YBX1 and ELAV (embryonic lethal, abnormal vision)-like protein 1, 2 and 3 (ELAVL1, 2 and 3), which might also be of interest in the context of splicing or brite adipogenesis.

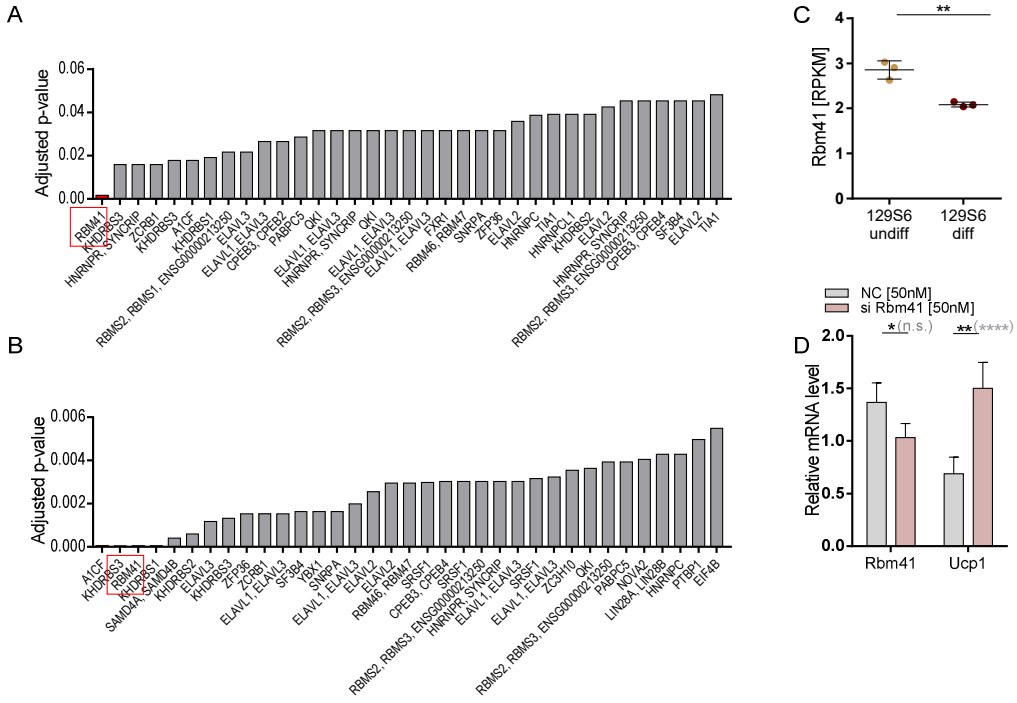

Figure 42: RBM41 binding sites are enriched in *Ctcflos*-dependently spliced transcripts. (A, B) Enrichment analyses of RBP motifs **(A)** within the 3'UTRs and **(B)** within the mRNA sequences of *Ctcflos*-dependently spliced transcripts using Transite matrix-based transcript set motif analysis (Krismer *et al.*, 2019). **(C)** *Rbm41* transcript levels in differentiated brite compared to undifferentiated primary adipocytes derived from iWAT of 129S6 mice (transcript levels in RPKM), assessed by RNA sequencing. Mean and individual values ± SD, n=3 (biological replicates), unpaired t test. **(D)** *Rbm41* and *Ucp1* transcript levels relative to *Gtf2b* in *Rbm41* KD (siRbm41) compared to non-targeting control samples (KD day1 diff, harvest after 72 hours), assessed by qPCR. Mean ± SD, n=4 (technical replicates), unpaired t tests or in grey parenthesis two-way ANOVA (Šídák-test). N.s. $p>0.05$, *$p<0.05$, **$p<0.01$, ****$p<0.0001$.

***Ctcflos* protein interaction partners**

Approaching the regulation of *Ctcflos*-dependent splicing from the opposite angle, interactions between *Ctcflos* isoform 1 and protein factors were predicted *in silico*. Sequence-based feature projection ensemble learning method-lncRNA-protein interaction (SFPEL-LPI), a machine learning algorithm that was reviewed among a number of other tools to possess the highest performance, was used for this purpose (Peng *et al*, 2019; Zhang *et al.*, 2018). In the analysis ELAVL1 ranged at the top position of predicted *Ctcflos* interaction partners with an association score of 0.9985 (scale range 0-1), proposing a high probability of interaction (Tab. 12). ELAVL1 has been identified as negative regulator of WAT browning (Siang *et al*, 2020), it acts as RNA stabilizer, can be involved in splicing regulation (Lebedeva *et al*, 2011; Mukherjee *et al*, 2011) and its binding sites were also overrepresented within *Ctcflos*-dependently differentially spliced transcripts. This clearly renders ELAVL1 a valuable candidate for future experimental analyses of *Ctcflos* interaction partners that could mediate its functionality in alternative splicing regulation during brite adipogenesis. Besides ELAVL1, RNA-binding protein Fused in sarcoma (PBP-FUS), Polypyrimidine tract-binding protein 1 (PTBP1) and SRSF1 were predicted as further putative interaction partners of *Ctcflos* and might also be of interest in terms of alternative splicing regulation in thermogenic adipogenesis (Tab. 12).

Table 12: Predicted *Ctcflos* protein interaction partners. Protein interaction partners of *Ctcflos* tr1 predicted by the machine learning algorithm Sequence-based feature projection ensemble learning method-lncRNA-protein interaction (SFPEL-LPI) (Peng *et al.*, 2019). Protein Uniprot IDs, names and scores (scale 0-1) for interaction with *Ctcflos* isoform1 are listed. Proteins with implication in splicing regulation are highlighted in bold.

Uniprot ID	Protein Name	Score
Q15717	**ELAV-like protein 1**	**0,9985**
O00425	Insulin-like growth factor 2 mRNA-binding protein 3	0,6661
Q9NZI8	Insulin-like growth factor 2 mRNA-binding protein 1	0,5296
Q9Y6M1	Insulin-like growth factor 2 mRNA-binding protein 2	0,5234
P35637	**RNA-binding protein FUS**	**0,4972**
Q13148	TAR DNA-binding protein 43	0,3333
Q9UKV8	Protein argonaute-2	0,3294
P31483	Nucleolysin TIA-1 isoform p40	0,2738
P26599	**Polypyrimidine tract-binding protein 1**	**0,2239**
Q9H9G7	Protein argonaute-3	0,2081
Q9HCK5	Protein argonaute-4	0,2034
Q07955	**Serine/arginine-rich splicing factor 1**	**0,2007**
Q9UL18	Protein argonaute-1	0,1829
Q9HCE1	Putative helicase MOV-10	0,1757
Q8NDV7	Trinucleotide repeat-containing gene 6A protein	0,0895
O43251	RNA binding protein fox-1 homolog 2	0,0123
P25490	Transcriptional repressor protein YY1	0,003
P08047	Transcription factor Sp1	0,0027
P60484	Phosphatidylinositol 3,4,5-trisphosphate 3-phosphatase and dual-specificity protein phosphatase PTEN	0,0025
Q13285	Steroidogenic factor 1	0,0016
Q13127	RE1-silencing transcription factor	0,0015
Q15022	Polycomb protein SUZ12	0,0015

Specified future analyses, such as probe-mediated pull down of *Ctcflos* and identification of its protein-, DNA- or RNA-co-precipitates, could allow for experimental testing of the above proposed regulatory mechanisms.

3.5.3.3 Co-regulation of transcription and alternative splicing

The observation of *Ctcflos* involvement in transcription and alternative splicing regulation initiated successive analyses separately into both directions. However, gene transcription and RNA splicing are in fact tightly coordinated cellular processes that should not be viewed independently. The consolidation of both transcriptome analyses, I) on *Ctcflos*-dependent transcription and II) on alternative splicing, disclosed 152 genes that were co-regulated in both datasets (Fig. 43 A). Similar to the experimentally examined *Ctcflos* targets *Prdm16* and *Neat1*, these genes were differentially transcribed (DESeq2, adj.p-value<0.05, any fold change) and alternatively spliced (SGSeq2, adj.p-value<0.05, any fold change) in *Ctcflos* deficiency. This raises the possibility of a coordinated regulation of both processes. Nuclear speckles, sub-nuclear structures, which function as storage, assembly and modification compartments of both, transcription and splicing factors, are proposed to play a major role in the coordination of the two procedures (Spector & Lamond, 2011). Serine/Arginine-rich splicing factor (SRSF2/SC35) is an established marker for nuclear speckles. Interestingly, immunocytochemical analysis of SC35 revealed elevated fluorescence signals and increased numbers of nuclear speckles per nucleus in *Ctcflos* deficiency (48 hours after *Ctcflos* KD) (Fig. 43 B-D and Fig. S10 A-D), raising the hypothesis of *Ctcflos* activity in association with nuclear speckles to concomitantly coordinate transcription and alternative splicing during brite adipocyte development. In line, SC35 negatively correlated with UCP1 protein abundance across individual *Ctcflos* KD cells (Fig. 43 F and Fig. S10 H-J, N-P), while this relation was absent in control cells (Fig. 43 E and Fig. S10 E-G, K-M), suggesting a causal relation between *Ctcflos* KD-dependent alterations in nuclear speckles and impaired brite adipogenesis. Furthermore, the nuclear speckle associated activation, assembly and translocation processes of splicing- and transcriptions factors are largely governed by phosphorylation and dephosphorylation cycles catalyzed by kinases and phosphatases. In *Ctcflos* deficiency, their abundance is modulated towards reduced *Srpk* kinases and increased *Ppm1g* phosphatase levels (Fig. 30 E).

Following up on the hypothesis of *Ctcflos*-dependent co-regulation of transcription and alternative splicing in association with nuclear speckles, it would be essential to specify the sub-nuclear location of *Ctcflos* in a co-staining with nuclear speckle marker SC35.

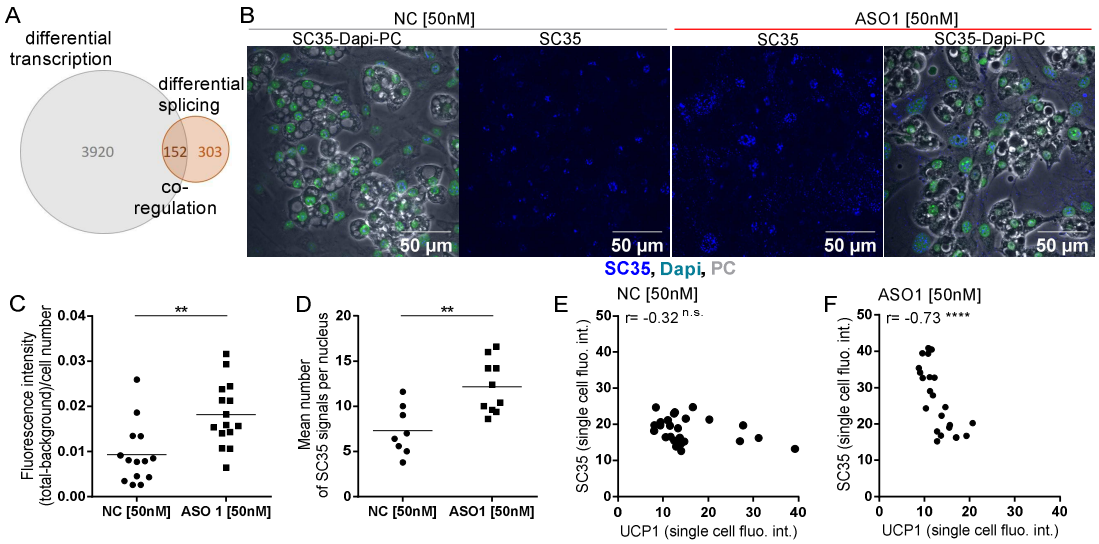

Figure 43: *Ctcflos* deficiency modulates brite adipocyte nuclear speckle morphology. (A) Venn diagram of *Ctcflos*-dependently transcribed and alternatively spliced genes. **(B-F)** Impact of *Ctcflos* tr1 KD (ASO1) on Serine/Arginine rich Splicing factor 2 (SC35/SRSF2) as marker of nuclear speckle abundance (KD day1 diff, harvest after 48 hours, primary brite adipocytes derived from iWAT of 129S6 mice). **(B)** Immunocytochemistry of SC35. SC35 signal (blue) alone (middle images) and SC35 (blue), DNA staining by DAPI (green) and phase contrast (PC) (gray) in combination (outer images). **(C)** Quantification of SC35 fluorescence signal as whole image fluorescence intensity subtracted by background and normalized to total cell number. Mean and individual values, one representative replicate of three experiments with comparative results (see Fig. S10 A and B), unpaired t test. **(D)** Quantification of nuclear speckle number as mean number of SC35 signals per nucleus. Mean and individual values, one representative replicate of three experiments with comparative results (see Fig. S10 C and D), unpaired t test. **(E, F)** Correlation of SC35 and UCP1 fluorescence signals across individual cells in **(E)** control and **(F)** *Ctcflos* tr1 KD (ASO1) cells. Extreme values were excluded to avoid distortion of correlation analysis. One representative replicate of four experiments with comparable results (see Fig. S10 E-P). Pearson correlation. N.s. $p>0.05$, **$p<0.01$, ****$p<0.0001$ Modified from (Bast-Habersbrunner *et al.*, 2021).

In summary, the results presented in this thesis revealed profound regulation of lncRNAs during brite adipogenesis, suggesting their considerable regulatory contribution to the browning process. The top lncRNA candidate *Ctcflos* could be validated as a requisite component in thermogenic adipocyte development and function. Detailed investigations into the regulatory routes of *Ctcflos* revealed it as an essential modulator of transcriptional and post-transcriptional alternative splicing programs in brite adipogenesis. The molecular mechanism of *Ctcflos* activity in brite adipogenesis was approached in a number of explorative computational and experimental analyses, creating hypothesis for future investigations. Jointly, they emphasize the strong discovery potential of the experimental identification of *Ctcflos* interaction partners, DNA, or RNA binding sites and its sub-nuclear location.

4 DISCUSSION

The abiding, pandemic increase of overweight and obesity strongly demands for intensified research to clarify causes and consequences of imbalanced energy homeostasis and to find therapeutic ways to resolve it. In this context, adipose tissue revealed to be a multifaceted organ of different adipose tissue types with a variety of functions. Especially the energy dissipating capacity of thermogenic brown and brite adipocytes, which contrasts to the main energy storing purpose of white adipocytes, is of prominent interest. Accumulating evidence attributes thermogenic adipocytes a potent modulatory role in energy homeostasis and metabolic health (Bartelt *et al.*, 2011; Cypess *et al.*, 2009; Hanssen *et al.*, 2015; Ouellet *et al.*, 2012). In order to evaluate their potential as targets in anti-obesity strategies, it is essential to understand the complex regulatory routes that coordinate their recruitment and thermogenic activity. Our view on cellular differentiation and function that was longtime dominated by protein regulators, however, is recently multiplexed by an additional group of potent regulators, the long noncoding RNAs. They emerged as versatile, efficient and flexible coordinators in a multitude of cellular processes and help to complement our yet incomplete concept of brite adipogenesis. In this regard, the present thesis provides a resource for the disclosure of lncRNAs of functional relevance in brite adipocytes and established lncRNA *Ctcflos* as an integral orchestrator of transcriptional and post-transcriptional alternative splicing programs in thermogenic adipogenesis.

4.1 THE DISCLOSURE OF FUNCTIONAL LNCRNAS RAISES THE NEED FOR POWERFUL SELECTION MODELS

The Encyclopedia of DNA Elements (ENCODE) project taught us that human and murine genomes are extensively transcribed into noncoding RNA transcripts that clearly outnumber protein coding genes (Djebali *et al.*, 2012; The-ENCODE-Project-Consortium, 2012). This includes a high number of lncRNAs (Liu *et al*, 2005). To extract lncRNAs of functional relevance in thermogenic adipogenesis among this vast population, powerful selection models are needed. In this respect, comparative transcriptome analyses of samples representing different levels of thermogenic adipocyte recruitment or activity proved to be valuable approaches. Abundance and activity of thermogenic fat cells can be modulated by cold exposure, β_3-adrenergic receptor agonist treatment and possibly by physical activity (Cousin *et al.*, 1992; De Matteis *et al*, 2013; Guerra *et al.*, 1998; Himms-Hagen *et al.*, 2000; Slocum *et al*, 2013; Young *et al.*, 1984). The propensity for brite adipocyte recruitment by these stimuli varies between adipose tissue depots and different mouse strains.

Several of these conditions were used in previous studies to unveil functional lncRNAs in brown and brite adipocytes: The transcriptome comparison of brown with white adipose tissue, undifferentiated with differentiated brown adipocytes and β_3-adrenergically (CL316243) stimulated with unstimulated WAT revealed lncRNA *Blnc1* among 21 further lncRNA candidates (Zhao *et al.*, 2014). Transcriptome changes in WAT during cold exposure, CL316243 treatment and physical exercise coupled to changes during BAT whitening at thermoneutrality disclosed *lncBATE10* as putative regulator in the browning process (Bai *et*

al., 2017). *De novo* reconstruction of murine iBAT, iWAT and eWAT transcriptomes served to identify novel, tissue specific lncRNAs (Alvarez-Dominguez *et al.*, 2015a).

The present thesis complements this line-up of selection models by exploiting the variable propensity of distinct inbred mouse strains for iWAT browning. The five inbred mouse strains, SWR/J, BL/6J, A/J, AKR/J and 129S6 provide a range of browning propensities, with the first two being rather resistant and the latter three being sensitive to the induction of brite adipogenesis (Kozak & Koza, 2010; Li *et al.*, 2014a; Li *et al.*, 2019; Xue *et al*, 2005). As this phenomenon is maintained on the level of primary adipocytes, devoid of systemic influences, the five mouse strain-*in vitro* model further enables to fade out cell-extrinsic 'noise' such as varying innervation or endocrine signals and to focus on cell-intrinsic regulatory programs that govern brite adipogenesis. Opposed to models that study complex *in vivo* situations, this might provide an advantage to unveil the key cellular regulators. The strain comparison model was established and previously applied in a systems-genetics approach that succeeded to identify novel protein coding regulators in browning, validating the discovery potential of this model (Li *et al.*, 2019). For the identification of long noncoding regulators in the present thesis, lncRNAs were selected based on their correlation with *Ucp1* gene expression across the five mouse strains. Additionally, adipocytes of the 129S6 mouse strain with the highest browning propensity were used to narrow down lncRNAs of interest, according to their regulation during brite adipocyte differentiation and between mature brite and white adipocytes. Notably, while the present thesis relied on the mouse strain with the strongest browning potential (129S6), most other studies focused on BL/6 mice that actually possess a low browning capacity (Bai *et al.*, 2017; Zhao *et al.*, 2014).

4.2 THE LONG NONCODING RNA TRANSCRIPTOME IS STRONGLY REGULATED IN BRITE ADIPOGENESIS AND PRESENTS A VALUABLE SOURCE FOR THE IDENTIFICATION OF NOVEL BROWNING REGULATORS

Comparable to protein coding genes, it was observed here that the long noncoding transcriptome also clearly changes during the course of brite adipogenesis, suggesting that it likewise harbors regulatory factors involved in the coordination of the browning process. Application of the five mouse strain selection system accordingly extracted 189 positively and 103 negatively regulated lncRNA candidates. Besides the here characterized lncRNA *Ctcflos*, this likely includes further lncRNAs of putative functional interest that can be extracted based on their strength of regulation (as done for *Ctcflos*) or their genomic location in relation to functional protein coding genes. LncRNA candidate *B432012C06Rik*, for instance, is located on the opposite strand between *Cidea* and *Impa2*; *AK040824* originates from the *1-acylglycerol-3-phosphate-O-acyltransferase2* (*Agpat2*) locus; *AK044183* overlaps with *Pde3b* on the opposite strand and *AK087872* is located close to brown fat signaling factor *Nrg4*. Especially antisense located lncRNAs, oriented in 'head-to-head' (5'-to-5') direction with a protein coding gene, were shown to often modulate transcription of their neighbor gene (Katayama *et al*, 2005; Villegas & Zaphiropoulos, 2015). They might present candidates of special interest for future analyses. The pool of regulated lncRNAs, identified in the present thesis, can thus serve as starting point for follow-up projects.

Among the regulated lncRNAs, *Ctcflos* stood out as the top candidate by its additional responsiveness to BAT activation in the cold. Despite this strong regulation in thermogenic adipocytes, *Ctcflos* function has not been investigated before. Nevertheless, it also appears in other publicly available datasets to be regulated in association with BAT activation or WAT browning: I) *Ctcflos* isoforms 3 and 4 are also upregulated in the iBAT transcriptome dataset of cold exposed C57BL/6J mice published by (Marcher *et al*, 2015) and II) *Ctcflos* is induced in *early growth response 1* (*Egr1*) knockout mice that are characterized by increased iWAT browning (Milet *et al*, 2017). This fortifies the appearance of *Ctcflos* as top candidate in the present thesis.

4.3 *CTCFLOS* IS A MULTI-ISOFORM, NUCLEAR LOCATED AND PREDOMINANTLY ADIPOSE TISSUE EXPRESSED LONG NONCODING RNA WITH AN ESSENTIAL ROLE IN THERMOGENIC ADIPOGENESIS

Closer characterization of *Ctcflos* lncRNA revealed its transcription into distinct isoforms that are retained in the nuclei of adipocytes and hold a significant role in thermogenic adipocyte development and function.

Although lncRNAs are generally less efficiently spliced compared to protein coding pre-mRNAs, they can also be processed into different isoforms, as it is also the case for *Ctcflos* (Tilgner et al, 2012). These isoforms can either share similar functions or vary in cellular functionality, abundance and even sub-cellular localization (Bridges *et al.*, 2021; Ziegler & Kretz, 2017). Transcript annotations for lncRNAs are, however, in many cases still incomplete. Annotation strategies often have to trade off high throughput against high quality. Automated high throughput annotations allow identification of a large number of transcripts, though often incomplete or fragmented, while manual annotations provide more accurate annotations but in a smaller number (Lagarde *et al*, 2017). Particularly lncRNAs are affected due to their low expression strengths and thus low read coverage in RNA sequencing. In line, *de novo* reconstruction of the murine genome for the discovery of novel lncRNAs revealed that 30% of the transcribed genomic sequence mapped outside of annotated loci (Alvarez-Dominguez *et al*, 2015b). Also for *Ctcflos*, transcript predictions seem to be inconsistent, as they slightly vary between databases, mostly ranging between three (DDBJ, UCSC (RefSeq, GenBank)) and four (ENCODE/GENCODE v.M9 (Ensembl 84)) different transcripts with partially varying exon composition. All exon-intron boundaries except for 5’ and 3’ ends of the Ensembl annotated transcripts could be confirmed. In RNA sequencing, however, read mapping outside of annotated exons, within introns and extending beyond the transcripts 3’ ends, question the completeness of the annotation. Mapping of reads within intronic sequences might indicate the presence of yet unprocessed transcripts. In line with this notion, it was reported that lncRNAs are indeed less efficiently spliced compared to protein coding mRNAs (Melé *et al*, 2017; Tilgner *et al.*, 2012; Zuckerman & Ulitsky, 2019), increasing the incidence of intron retention. The pronounced mapping of reads downstream of the annotated 5’ end of *Ctcflos* transcripts, however, strongly argues for incomplete isoform predictions. Accordingly, String Tie *de novo* reconstruction of the *Ctcflos* locus predicted prolonged 3’ exon boundaries that should be validated experimentally by future 3’ RACE

experiments. Complete knowledge on *Ctcflos* isoform sequences is of pivotal importance to determine the mechanism of *Ctcflos* activity. The lncRNA sequence and its secondary structure harbor information on possible interactions with DNA-, RNA- or protein partners and forms the basis for their experimental exploration in probe based pulldown assays, sub-nuclear localization studies and vector based *Ctcflos* overexpression. *Ctcflos* sequence determination should therefore be treated with high priority in a follow-up project.

Ctcflos expression analysis across a range of murine tissues demonstrated clear predominance of *Ctcflos* abundance in adipose tissues followed by slight expression in liver. This is strongly evidenced by other databases (BioGPS, NCBIGene) that widely agree with the high adipocyte specificity of *Ctcflos* transcription, especially in thermogenic brown adipocytes, and its detectability in liver. Beyond the experimentally examined tissue panel, low levels of *Ctcflos* transcription are reported in mammary and adrenal glands (Wu *et al.*, 2009). Interestingly, transcriptional upregulation of *Ctcflos* in response to hepatic *Reptin* KO, which is characterized by decreased body weight, hypoglycemia and hypolipidemia, associates *Ctcflos* with glucose and lipid metabolism in liver (Javary *et al*, 2018).

Aiming to understand the role of *Ctcflos* in thermogenic adipocytes, its localization was specified on subcellular level. This revealed the exclusive retention of *Ctcflos* in brite adipocyte nuclei and absence in cytosol and mitochondria. The subcellular location of a lncRNA allows a first rough functional classification that can provide orientation for following analyses. Upon transcription, lncRNAs can either stay in the cell nucleus, be exported into the cytosol or reside in both compartments. Within the nucleus, they can further associate with sub-nuclear structures such as nucleoli, nuclear speckles or paraspeckles, while cytosolic lncRNAs can associate with organelles, including mitochondria, lipid droplets, the endoplasmic reticulum or ribosomes (Bridges *et al.*, 2021; Chen, 2016; Nakagawa *et al.*, 2012; Tran *et al.*, 2020; Wang *et al.*, 2018; Zeng *et al.*, 2018). According to their diverse cellular locations, lncRNAs comply various different functions. Even the same lncRNA (e.g. lncRNA *PYCARD antisense RNA 1* (*PYCARD-AS1*)) can exert distinct functionalities when acting in the nucleus or the cytosol, the subcellular microenvironment thus defines lncRNA activity (Bridges *et al.*, 2021; Miao *et al.*, 2019). Generally, nuclear lncRNAs are involved in the modulation of transcriptional programs, in pre-mRNA processing and the spatial organization of sub-nuclear compartments. Cytosolic lncRNAs can be implied in the regulation of mRNA stability and translation or mediate signal transduction pathways (Bridges *et al.*, 2021; Chen, 2016). The presence of *Ctcflos* exclusively in the nucleus of brite adipocytes thus suggested its role in the nuclear steps of thermogenic gene expression, which were set into focus for the functional characterization of *Ctcflos*.

In accordance with the strong regulation of *Ctcflos* during thermogenic adipogenesis, a series of depletion studies demonstrated its requisite role in brite and brown adipocyte development and function. Knockdown experiments were performed at two time points, during early and during late brite cell differentiation that coincide with phases of increasing *Ctcflos* transcript abundance. At both stages of differentiation, *Ctcflos* deficiency impaired brite adipogenesis, attributing *Ctcflos* a role in establishment and maintenance of the thermogenic phenotype. Stronger effect sizes of *Ctcflos* KD at the beginning of differentiation, however, particularly emphasize its contribution to the early switch towards the thermogenic

program. *Ctcflos* major activity thus locates to a critical time window of early cell fate decision along with that of brite master regulators such as *Prdm16*, *Nfia* and *Ebf*. Its function as early effector is evidenced by reduced thermogenic marker gene expression, compromised mitochondrial biogenesis and consequently impaired *Ucp1*-dependent uncoupled respiration in response to *Ctcflos* deficiency at the onset of differentiation. *Ctcflos* thereby acts as specific regulator of the thermogenic gene program without affecting white adipocyte differentiation or general adipogenesis.

With this impact on brite and brown adipocyte gene expression and thermogenic function, *Ctcflos* joins a row of previously characterized lncRNA effectors in thermogenic adipogenesis, including lncRNA *Blnc1*, *lncBATE1*, *lncBATE10*, *H19* and *LINC00473* (Tab. 13) (Alvarez-Dominguez *et al.*, 2015a; Bai *et al.*, 2017; Schmidt *et al.*, 2018; Tran *et al.*, 2020; Zhao *et al.*, 2014).

Table 13: *Ctcflos* in comparison to previously characterized lncRNAs in thermogenic adipogenesis. For each listed lncRNA, information are summarized on the adipose tissue in which it functions, the selection criteria used for its identification, its mechanism of action, the methods (knockdown and/or overexpression) used to evaluate its function and whether its role for UCP1-mediated thermogenic function was assessed. CL316243 (CL), abdominal subcutaneous (AbsSQ), supraclaviclular (Sclav).

lncRNA	adipose tissue of action	selection	mechanism	method of investigation	functional investigation
Blnc1 (Zhao et al. 2014)	brown + brite (nucleus)	reg. in BAT compared to eWAT; during brown adipocyte differentiation; by CL treatment in eWAT	formation of a ribonucleoprotein complex with EBF2 (supported by HNRNPU) > thermogenic gene expression	knockdown + overexpression	no activation of UCP1, no control of free fatty acids
BATE1 (Alvarez-Dominguez et al. 2015)	brown + brite (nucleus+cytosol)	*de novo* reconstruction of iBAT, iWAT, eWAT transcriptomes, identification of tissue specific lncRNAs	not entirely clarified, interaction with HNRNPU	knockdown + overexpression	activation of UCP1 and control of free fatty acids
BATE10 (Bai et al. 2017)	brown + brite (nucleus+cytosol)	reg. in WAT by cold exposure/ CL treatment/ physical exercise; in BAT whitening	hijacking of CELF1 from binding and degradation of Pgc1α	knockdown + overexpression	no determination
H19 (Schmidt et al 2018)	brown (nucleus, cytosol, ribosomes)	reg. in BAT by cold exposure/ HFD feeding	interaction with MBD1 > repression of paternally expressed genes	knockdown + overexpression	no activation of UCP1, no control of free fatty acids
LINC00473 (Tran et al. 2020)	human AbsSQ + Sclav (mitochondrial-lipid droplet interphase)	reg. in human subcutaneous and supraclavicular derived adipocytes in response to norepinephine	coupling of lipolysis and mitochondrial respiration	knockdown + overexpression	activation of UCP1 but no control of free fatty acids
Ctcflos (Bast-Habersbrunner et al. 2021)	brown + brite (nucleus)	correl. with *Ucp1* across mouse strains of varying browning propensity; reg. during brite adipogenesis; by rosiglitazone treatment	not entirely clarified, coordination of transcription and alternative splicing programs in brite adipogenesis	knockdown (preliminary overexpression data)	activation of UCP1 and control of free fatty acids

Except for BAT-selective *H19*, all of the previously characterized lncRNAs act in both, brown and brite adipocytes suggesting, similar as for *Ctcflos*, broader roles in thermogenic programming (Tab. 13). Most of these studies combine knockdown and overexpression as complementary analyses to evaluate lncRNA function (Tab. 13). In the present thesis, uncertainty of the exact transcripts of *Ctcflos* impeded vector mediated overexpression and allowed only limited insights into the consequences of increased *Ctcflos* abundance in CRISPR activation based experiments. As mentioned above, sequence clarification allowing exogenous *Ctcflos* overexpression or further optimization of endogenous *Ctcflos* gene induction will be of great importance in future. Similar to the observations in the present thesis, most of the previously described lncRNAs can also be found (though not always exclusively) in the nucleus (Tab. 13), and their loss clearly affects brite cell marker gene expression. In some of the mentioned studies lipid accumulation seemed to be reduced in lncRNA deficient cells, suggesting an impact on adipogenesis *per se* (Zhao *et al.*, 2014). In these cases it will be of importance to evaluate whether the effect on thermogenic gene expression persists also independent of the impact on general adipogenesis, as it could be affirmed here for *Ctcflos*. Additionally, in some studies it remains unclear to what extent the impaired thermogenic gene expression translates to functional level (Tab. 13). If assessed, oxygen consumption is mostly not measured in states of active UCP1 (e.g. by isoproterenol treatment) and under control of free fatty acid levels, which would be necessary to reliably quantify specifically UCP1-dependent thermogenesis (Li *et al.*, 2014b; Oeckl *et al.*, 2020). In the context of previous studies, the impact of *Ctcflos* in thermogenic adipogenesis thus finds parallels in that of other lncRNAs. Different study designs, however, make it difficult to classify the effect sizes of *Ctcflos* among known lncRNA effectors.

4.4 *CTCFLOS* DRIVES BRITE ADIPOGENESIS THROUGH ORCHESTRATION OF TRANSCRIPTIONAL AND POST-TRANSCRIPTIONAL ALTERNATIVE SPLICING PROGRAMS

In order to understand the regulatory routes of *Ctcflos*, it is essential to recognize brite adipogenesis as a multilayered process. During cellular differentiation, functionally inert precursor cells evolve into specified cell types of defined morphology, protein equipment and biological function. This procedure demands comprehensive reorganization of the cellular machinery, which is only possible by an exact temporal and spatial coordination of each step of gene expression, comprising chromatin organization, gene transcription, post-transcriptional processing and translation.

Among the nuclear steps of gene expression, (I) **gene transcription** largely determines the composition of the cellular machinery, while (II) post-transcriptional processing such as **alternative splicing** enables further fine-tuning of its functionality, together shaping the cellular equipment in **quantity** and **quality**.

(I) The cell type defined pattern and strength of gene **transcription** strongly defines the cellular equipment. It is tightly controlled in a precise interplay of transcriptional activators, repressors and their cofactors. A multitude of these transcriptional regulators have been identified in the modulation of brown and brite adipogenesis, with more and more novel factors joining (Li *et al.*, 2019;

Pradhan *et al.*, 2017; Van Nguyen *et al*, 2020). They regulate transcription rates of several thousand genes to direct cell identity towards that of a thermogenic adipocyte. In this sense, as much as 8391 genes were identified in the present study to be differentially transcribed during brite adipogenesis. Changes on gene transcription level are prominently used as surrogate markers for the progress of brite adipogenesis.

(II) **Alternative splicing**, as another regulatory layer in cellular differentiation, in contrast, is often neglected. Around 95% of human multi-exon genes were reported to be spliced into different isoforms that can convey distinct or even opposite functions, providing another means to precisely adapt to the changing requirements during differentiation and to confer cell type identity (Pan *et al.*, 2008). During differentiation, relative abundances of differentially functional isoforms can be adjusted to the specifications of the respective cell type (Lin *et al.*, 2014) and broadly expressed factors can receive cell type specificity when spliced into a defined isoform, exclusively in a given cell type (Singer *et al.*, 2019). Accordingly, alternative splicing modulations have been observed in the development of numerous cell types and tissues, including smooth muscle cell differentiation, erythropoiesis, liver, heart and brain development as well as T-cell activation (Baralle & Giudice, 2017). Also in adipocyte development and function alternative splicing was established as regulatory theme. High fat diet-induced white adipose tissue expansion entails vast alternative splicing changes, which seem to conflict the thermogenic adipocyte program (Vernia *et al*, 2016). Similarly, brown adipogenesis involves adaptations in alternative splicing patterns, including those of *Insr*, *Mef2c* and *Prdm16* (Chi & Lin, 2018; Lin, 2015b; Lin *et al.*, 2014). Alternative isoforms of varying function have been identified for further adipogenic factors (*Pparγ*, *Pgc1α*, *Pkcd*, *Odc*, *Cetp*, *Mtor*, *Lpin1*, *Ncor, Mapk9*, *Mbnl1*) and adipocyte-related splicing regulators were recognized (Sam68, SRSF10, SRp40, SRSF2+FTO, RBM4a, NOVA) (Cooper *et al.*, 2014; Lin, 2015a; Lin *et al.*, 2014; Vernia *et al.*, 2016), substantiating the regulatory involvement of alternative splicing in adipocyte differentiation. Despite these insights, the extent of its contribution still remains largely unsettled and demands further exploration on the genome-wide scale.

As cellular differentiation is an intricate process that is simultaneously coordinated on several layers, lncRNAs may raise particular interest in their roles as multifunctional regulators. They have been described as modulators in every step of gene expression, comprising epigenetic modulation, control of enhancer activity, transcription, splicing and mRNA stability, miRNA sponging, nuclear mRNA export, translation, protein stability, activity and scaffolding (Geisler & Coller, 2013; Marchese *et al.*, 2017). In fact, lncRNAs unite unique properties, which render them potent and flexible regulators. By rapid generation and degradation they can quickly respond to changing conditions, they can efficiently interact with distinct types of biological molecules (proteins, DNA and RNA) and provide complex three dimensional platforms for protein-protein interactions (Geisler & Coller, 2013). Importantly, with these properties, lncRNAs can act at independent levels of gene expression simultaneously. The same lncRNA

can, for example, modulate gene transcription and mRNA translation of its target gene within the same cell, as it is the case for *PYCARD-AS1* (Miao *et al.*, 2019). LncRNA *RNA component of mitochondrial RNAase P* (*Rmrp*), as another example, is required for RNA processing in the nucleus (Goldfarb & Cech, 2017) as well as DNA replication in mitochondria (Noh *et al.*, 2016). This capacity for gene expression regulation on different levels enhances the potential of lncRNAs to orchestrate the regulatory interplay during differentiation.

Accordingly, also *Ctcflos* was disclosed in the present thesis to operate on two levels of gene expression by adjusting (I) gene transcription and (II) alternative splicing during brite adipocyte development. As discussed above, this provides *Ctcflos* the ability to shape the brite cell machinery in a quantitative and qualitative manner.

(I) In the function of *Ctcflos* as **transcriptional modulator**, KD experiments evidenced that it is required for the formation of the core thermogenic gene transcription program in early brite adipogenesis. In order to go beyond a single snapshot of altered transcription, a two-time point strategy was applied for transcriptome analysis of *Ctcflos* KD adipocytes. This provided valuable insights into the chronology of changes, allowing to distinguish between direct effects of the KD and secondary adaptations. In this respect, *Ctcflos* KD directly affected gene transcription of some proximal gatekeepers of the thermogenic gene transcription program, especially *Prdm16* along with *Nfia*, *Ebf1* and *Pparγ*. Early impairment of these key factors is most likely responsible for the subsequently observed reduced transcription of brown and brite fat selective genes and *Ucp1*. These changes lay the foundation for the observed phenotype of impaired browning, mitochondrial biogenesis and UCP1-mediated uncoupled respiration. *Prdm16*, as prominent and well established effector in thermogenic gene transcription, was chosen to closer examine the hypothesized causal relation between the early *Ctcflos* dependent transcriptional changes and *Ucp1* expression. *Ctcflos*-*Prdm16* combined KD as well as rescue experiments of *Ctcflos* KD coupled to *Prdm16* OE proposed on the one hand that *Ctcflos* activity in brite adipogenesis is mediated to a considerable extent via *Prdm16* transcriptional regulation. At the same time, however, it opened the question for further regulatory pathways of *Ctcflos* to fully explain the observed phenotype. *Ctcflos* dependent regulation of *Nfia* and *Ebf1* might be of interest in this context. Additionally, *Ctcflos* modulates lncRNA *Neat1* transcription. *Neat1*, which is described as modulator of white adipogenesis (Cooper *et al.*, 2014; Gernapudi *et al.*, 2016), was here additionally characterized to be involved in brite adipocyte development and might therefore also be of interest in terms of additional routes of *Ctcflos* activity.

Beyond this transcription regulatory function of *Ctcflos*, its role in alternative splicing modulation needs to be closely regarded to fully grasp its regulatory pathways.

(II) Regarding **alternative splicing regulation**, first hints towards the involvement of *Ctcflos* were obtained from the observation that multiple components of the splicing machinery as well as splicing factors were broadly upregulated in *Ctcflos* deficiency, which opposed their general negative regulation during brite

differentiation. Also the increased abundance of nuclear speckles pointed towards alterations in splicing regulation. Deep global analysis of alternative splicing patterns as well as experimental investigation of isoform profiles of a few candidates, accordingly revealed profound splicing changes in immediate response to the absence of *Ctcflos*. The fact that around one third of the differentially spliced genes were previously evaluated as candidates of browning regulation, supports that the splicing changes might contribute to the impaired browning phenotype and that modulation of alternative splicing presents another regulatory route of *Ctcflos* dependent brite adipogenesis. The differentially processed genes included factors with formally characterized isoforms of varying functionality (*Insr*, *Pparγ*, *Mapk9*, *Mbnl1*) (Cooper *et al.*, 2014; Entingh *et al.*, 2003; Hung & Lin, 2020; Lin *et al.*, 2014) and multiple factors could be functionally associated with adipogenesis, lipid metabolism, mitochondrial biology and splicing itself (the latter ones including *Hnrnpu*, *Clk1* and *Rbm4*). Splicing factor HNRNPU has been described as interaction partner of brown fat regulatory lncRNAs *lncBATE1* and *Blnc1* that is required for brown adipogenesis (Alvarez-Dominguez *et al.*, 2015a; Zhao *et al.*, 2014); CLK1 is responsible for splicing factor SRp40 phosphorylation in white adipogenesis (Cooper *et al.*, 2014), and RBM4 acts as versatile splicing and transcription modulator itself that regulates an entire network of splicing events in brown adipogenesis (Chi & Lin, 2018; Lin, 2015b; Lin *et al.*, 2014). The instance that *Ctcflos* affects the splicing machinery and splicing associated factors themselves by means of transcription and splicing, puts a further level of complexity to the activity of *Ctcflos*. Further investigation is needed to clarify in which way *Ctcflos*-dependent splicing of the named factors shapes their functionality. Overlaps between *Ctcflos* and RBM4-dependent splicing modulations further raise the question whether RBM4 is involved in the mediation of *Ctcflos* splicing effects.

Importantly, *Prdm16* and *Neat1* that are targets of *Ctcflos* transcriptional regulation were experimentally identified to be also *Ctcflos* dependently spliced. *Ctcflos* is required for the switch of alternative splicing towards their thermogenesis promoting isoforms, which dominate during brite differentiation. The short isoforms of *Prdm16* and *Neat1* are required for full activation of essential thermogenic genes and *Ucp1*, as shown in the present thesis and previously reported for *Prdm16* (Chi & Lin, 2018). *Ctcflos* thus not only supports to increase the overall abundance of *Prdm16* and *Neat1* to induce the thermogenic gene program, but it enables additional fine adjustment of their functionality to even more effectively promote brite and brown adipogenesis.

Conclusively, *Prdm16* as protein coding master regulator and *Neat1* as lncRNA modulator in thermogenic adipogenesis exemplify the functionality of *Ctcflos* in both transcriptional and post-transcriptional alternative splicing regulation (Fig. 44). Global transcriptome analyses disclose that beyond this, *Ctcflos* orchestrates both processes on a broad scale.

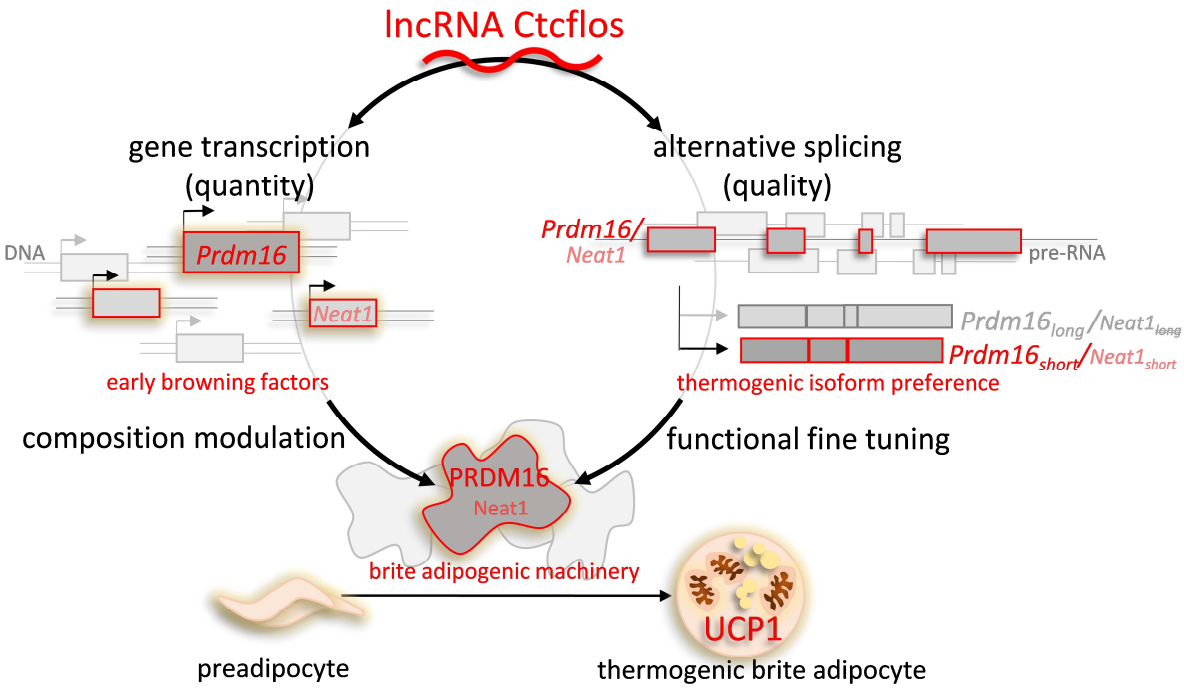

Figure 44: *Ctcflos* coordinates gene expression in brite adipogenesis on transcriptional and post-transcriptional alternative splicing level. Summary of the regulatory routes of *Ctcflos* in the regulation of gene expression in thermogenic adipogenesis. Modified from (Bast-Habersbrunner *et al.*, 2021).

4.5 EXPLORATIVE EXPERIMENTAL AND COMPUTATIONAL ANALYSES APPROACH THE MECHANISM OF *CTCFLOS* ACTIVITY

With transcription and alternative splicing identified as prominent regulatory routes of *Ctcflos*, the question arises how *Ctcflos* controls these two steps of gene expression on the molecular mechanistic level. Addressing this question, the following sections will discuss mechanisms of regulation of gene transcription and RNA splicing, investigate how lncRNAs can be involved in these processes and estimate whether *Ctcflos* could employ any of these mechanisms.

***Ctcflos* dependent transcription regulation might involve lncRNA guiding, hijacking or scaffolding function**

Gene transcription in eukaryotic cells is dominantly carried out by RNA polymerase II multiprotein complex. At sites of open chromatin it binds, guided by transcription factors, near the transcriptional start site of a gene, moves along the DNA, unwinds the double helix and catalyzes the assembly of the complementary RNA transcript (Cramer, 2019). To enable precise temporal coordination of induction and repression of defined gene sets during differentiation, the transcription process is controlled by several complementing mechanisms that in turn can be modulated by lncRNAs.

(I) At first instance, gene transcription is controlled on the level of chromatin. DNA in eukaryotic cells is tightly wound around histone protein complexes, forming a highly condensated chromatin structure that needs to be unpacked to enable access of the transcription machinery for gene expression. Chromatin modifying enzymes dynamically modulate condensation and decondensation of the DNA, thereby locally enhancing or repressing gene transcription (Grunstein, 1997; Lawrence *et al*, 2016). In this way, epigenetic

modifications present a strong tool to direct gene expression in early cell fate decisions and during cellular differentiation, as so in thermogenic adipocyte commitment and development. Accordingly, DNA methylation patterns vary between brown and brite adipocyte precursors (Sakamoto *et al*, 2007) and epigenetic signatures are dynamically changed during adipogenic differentiation (Mikkelsen *et al*, 2010; Sakamoto *et al*, 2008).

Chromatin modifiers in turn have been shown to be intensely controlled by lncRNAs. RNA co-immunoprecipitation with antibodies against chromatin modifying proteins in different human cell types revealed that as many as 38% of expressed lncRNAs associate with one of the complexes, proposing that epigenetic modulation is a common mechanism of lncRNA regulation (Bhat *et al*, 2016). LncRNAs can physically interact with one or more chromatin modifiers to modulate gene transcription *in cis* (e.g. *Adipogenic differentiation induced noncoding RNA* (*Adinr*), *Antisense lncRNA* (*Air*) and *inactive X specific transcripts* (*Xist*)) (Nagano *et al*, 2008; Plath *et al.*, 2002; Xiao *et al*, 2015) or *in trans*. LncRNAs acting *in trans*, can guide chromatin modifiers to distant loci by recognizing the surface of specific chromatin features or via complementary binding to the target DNA sequence, as exemplified by *Hox transcript antisense intergenic RNA* (*Hotair*) (Rinn *et al*, 2007).

Also for *Ctcflos*, an explorative analysis of its guidance potential to gene loci *in trans* provoked interest in further investigation. Overlapping genome wide alignment of the *Ctcflos* tr1 sequence with *Ctcflos* KD-induced transcriptional changes revealed six putative *Ctcflos* binding sites that co-localized with strong positive or negative *Ctcflos*-dependent transcription. *Ctcflos* might thus be envisioned to interact with a regulatory protein and to guide it to one or more of its putative binding sites, where it shapes transcription of the adjacent genes (Fig. 45). The fact that transcriptional modulation in the vicinity of the assumed binding sites affects several genes at once and mostly follows the same direction of regulation, argues for changes on chromatin level that broadly affect a larger gene region in the same manner (i.e. repression or induction). The identified regulated genes are predominantly oppositely modulated in *Ctcflos* KD and during regular brite adipogenesis, suggesting that their transcriptional regulation by *Ctcflos* is of importance in brite adipogenesis. *Klf4*, *Ybx1* and some further adipose or mitochondrial related genes (*Ndufaf5*, *Nbea*, *Aks*) next to *Ctcflos* blast hits might be of further interest (Birsoy *et al*, 2008; Burkart *et al*, 2011; Park *et al*, 2013; Su *et al*, 2004). Moreover, going beyond established regulatory circuits, this approach might provide the opportunity to detect novel *Ctcflos*-dependent browning regulators and warrant follow up investigation.

Ctcflos interactions with DNA and protein partners could be examined in future by antisense biotinylated oligonucleotide-mediated capture of *Ctcflos*, followed by extraction and analysis of crosslinked chromatin or proteins. Introducing point mutations into the identified putative *Ctcflos* DNA binding sites by CRISPR Cas and comparing the resulting phenotype with that of *Ctcflos* KD could help to further explore the functional relevance of *Ctcflos* DNA binding. When following up on this question, however, it should also be considered that the guidance function to a DNA locus might depend on the secondary structure of the lncRNA and that the screen for primary sequence alignments might not be sufficient. Looping and base pairing within the RNA molecule can bring distant sequence parts into spatial proximity, creating a binding module that is not evident in the primary sequence, as exemplified by lncRNA *Hotair*

(Hung & Chang, 2010; Kalwa *et al*, 2016). In this respect, it might additionally be fruitful to approach the question from a different angle, by screening loci of regulated genes for common DNA sequence motifs (Wang *et al*, 2006).

(II) On second level, gene transcription is largely regulated by the binding of transcription activators, repressors and their cofactors to regulatory sequences in promoters or enhancers upstream of target genes to locally induce or repress gene transcription (Cramer, 2019). The local availability of transcription factors is also subjected to intense modulation by lncRNAs. Sequences within lncRNAs can mimic transcription factor (TF) binding sites and act as decoys to prevent TF binding to their actual target sites on DNA (e.g. within lncRNA *Growth arrest specific 5* (*Gas5*) (Kino *et al.*, 2010)). Here, we observed that *Ctcflos* also hosts supposed binding matrices for several TFs. Notably, they included factors that operate as negative regulators in thermogenic gene expression and counter brite adipogenesis: ATF4, NR4A1, RBPJ and ZFP423. ATF4, which is decreased in cold stress, competes with cAMP Response Element Binding protein (CREB) for binding at the cAMP response element (CRE) of the *Pgc1α* promoter, reducing its transcription and thus impeding mitochondrial biogenesis (Wang *et al.*, 2013a), a trait that is also characteristic for *Ctcflos* KD cells. The orphan nuclear receptor NR4A1 is suggested to heterodimerize with RXRα, which is followed by their export from the nucleus into the cytosol. Limited nuclear availability of RXRα for interaction with PPARγ impedes its function in general adipogenesis and thermogenic gene expression (Kanzleiter *et al.*, 2005). RBPJ, as part of NOTCH signaling in thermogenic adipocytes, mediates repression of *Pgc1α* and most interestingly of *Prdm16* gene transcription (Bi *et al.*, 2014). Finally ZFP423, which is essential for the maintenance of white adipocyte identity and suppression of thermogenic gene programming in early cell fate decision, interacts with and inhibits members of the EBF family to prevent *Prdm16* gene transcription (Shao *et al.*, 2016). *Ctcflos*-mediated disruption of one of these pathways through TF hijacking could thus promote brite adipogenesis by regulating early cell fate decision via modulating PPARγ activity, *Prdm16* and *Pgc1α* transcription, well suiting the observed *Ctcflos* KD phenotype (Fig. 45). Again, pulldown and mass spectrometric analysis of *Ctcflos* crosslinked proteins would help in future investigations to test this hypothesis. Alternatively, the presence of *Ctcflos* could be tested in antibody mediated pulldown of the predicted trapped TFs.

(III) Thirdly, in gene transcription regulation, promoters and enhancers are targeted by several transcription factors at once, not only as monomers but also as homo- and heterodimers. It is thus their combined impact and interaction with each other that finally governs the transcription rate of the targeted gene, allowing precise adjustment of cellular gene transcription with a limited number of transcription factors (Funnell & Crossley, 2012). In this context, lncRNAs can additionally serve as scaffolds for several TFs to enable their interaction or to join them in space and time (Fig. 45). Among the TFs that possess binding sites within *Ctcflos*, there were previously proposed interaction partners. ATF4 might dimerize with NFE2L1 that controls proteasomal activity to ensure cellular protein quality in thermogenic conditions (Bartelt *et al*, 2018; Kim *et al.*, 2016). Most interestingly, in the predicted secondary structure of *Ctcflos*, the binding sites of the two factors are proposed to partially hybridize to each other. Binding of ATF4 and NFE2L1 to *Ctcflos* would thus position them into direct

neighborhood. Whether a putative ATF4-NFE2L1 heterodimer, scaffolded by *Ctcflos*, plays a role in thermogenic adipogenesis, would require further investigation.

Conclusively, lncRNA mediated guidance of chromatin modifiers, hijacking of TFs or scaffolding of transcription regulator interactions present effective mechanisms to comprehensively shape gene transcription. The exploratory approaches towards the question whether *Ctcflos* acts via any of these mechanisms in brite adipogenesis remain preliminary but arouse interest to further follow up on these concepts.

Compositional modulations of the splicing machinery and direct *Ctcflos*-splicing regulator interactions might mediate *Ctcflos*-dependent alternative splicing

The splicing process is conducted by a large ribonucleoprotein (RNP) assembly, the spliceosome, that is guided by splicing factors to bind to 5' and 3' splice sites at exon-intron boundaries and to catalyze the excision of the interstitial sequence (Chen & Manley, 2009). Similar as gene transcription, also the splicing process is tightly controlled by different means. LncRNAs can operate as effective modulators in these regulatory mechanisms.

(I) At first instance, splicing largely depends on the highly dynamic compositional adaptations of the spliceosome during the splicing process. The spliceosome is composed of multiple RNA and protein subunits that, in contrast to other preformed static RNP complexes, sequentially assemble and disassemble at the site of action and interact with regulatory factors (Chen & Manley, 2009). Compositional changes of the splicing machinery (as they occur in response to *Ctcflos* deficiency) could thus interfere with the splicing process and shape alternative splicing (Fig. 45). In *Drosophila melanogaster* and human cells, for instance, changing levels of core spliceosomal proteins (including U1, U2, U4, U6, U2AF, U2AF35 and others) led to changes in alternative splicing, affecting a defined subset of transcripts (Chen & Manley, 2009; Pacheco *et al*, 2006; Park *et al*, 2004). Furthermore, snRNP subunits of the spliceosome can be differentially expressed in varying tissues, suggesting cell type specific spliceosome compositions (Chen & Manley, 2009; Grosso *et al*, 2008). Accordingly, brite adipocyte differentiation is accompanied by decreased abundance of multiple spliceosomal subunits on transcriptional level. *Ctcflos* deficiency, in contrast, entailed opposed upregulation of several spliceosome components. These compositional changes might thus affect the splicing procedure and contribute to the observed shift in alternative splicing in *Ctcflos* deficiency.

(II) The early phase of splice site recognition and selection is dominantly coordinated by splicing factors that can bind to *cis*-regulatory sequence elements in the pre-mRNA to induce or repress the interaction between spliceosome and nearby splice sites. The RNA sequence elements are located within exons or introns and can function as splicing activating or repressing elements (exonic splicing enhancers (ESE) or silencers (ESS), intronic splicing enhancers (ISE) or silencers (ISS)). SR-proteins and HNRNPs constitute the two dominant families of splicing factors. Canonically, the two groups of splicing factors are attributed antagonistic activities, with SR-proteins preferentially binding to ESEs, recruiting the spliceosome to the nearby splice site for splicing induction. HNRNPs, in contrast, mostly bind to ISS or ESS sites to locally repress splicing by sterically blocking access of the spliceosome or splicing activators. The relative abundance of splicing enhancers and silencers thus influences

whether splicing is activated or inhibited at a given site. Slight changes in their overall stoichiometry can entail broadly altered splicing behavior and might help to establish cell type specific splicing patterns during cellular differentiation (Fig. 45) (Chen & Manley, 2009). Accordingly, each cell type has a unique repertoire of splicing factors (Black, 2003; Chen & Manley, 2009). In the present thesis, brite adipogenesis is characterized by comprehensive downregulation of *SR-proteins* and *Hnrnps* with more *Hnrnps* being affected. This regulation seems to be *Ctcflos*-dependent, as its KD had exactly the opposite effect, slightly more *Hnrnps* compared to *SR-proteins* were transcriptionally induced. The general upregulation of splicing factors and the shift towards *Hnrnp* splicing silencers in *Ctcflos* deficiency might thus further contribute to the observed altered splicing behavior and could be regarded in line with abundant exon skipping observed in differentially spliced transcripts in *Ctcflos* KD cells.

(III) Beyond the overall cellular stoichiometry of splicing enhancers and repressors, it is their local availability at sites of splicing activity that finally governs the splicing decision. Besides SR-proteins and HNRNPs, further RNA binding factors (RBPs) can associate with intronic or 3' untranslated regions and also modulate pre-mRNA processing, splicing and stability in a cell type specific manner (Chen & Manley, 2009). In this context, lncRNAs are abundantly reported to interact with splicing factors and RBPs, acting either as decoys to prevent their activity or recruiting them to nuclear regions or defined pre-mRNAs to regulate their local availability (Fig. 45) (Bai *et al.*, 2017; Romero-Barrios *et al*, 2018; Singer *et al.*, 2019). In the present thesis, this possibility was approached by computational predictions of *Ctcflos* protein interaction partners on the one hand and of overrepresented RNA binding protein motifs in differentially spliced transcripts on the other hand. This drew attention to RNA binding protein ELAVL1. It was predicted with high probability to interact with *Ctcflos*, and its binding motifs were among those overrepresented in the 3' UTRs and mRNA sequences of transcripts with altered splicing. ELAVL1 was described as negative regulator of adipogenesis, while its knockout promoted brown fat development and iWAT browning (Siang *et al.*, 2020). Binding to 3' UTRs and intronic sequences, ELAVL1 stabilizes the targeted RNA, facilitates its processing and can thereby also modulate its splicing profile (Mukherjee *et al.*, 2011; Siang *et al.*, 2020). The proposed interaction between *Ctcflos* and ELAVL1 could thus be hypothesized as hijacking mechanism that relieves ELAVL1-dependent alternative splicing and its repressive impact on browning.

The described computational predictions additionally highlighted RBM41 with highly overrepresented motifs, as well as RBP-FUS, PTBP1 and SRSF1, as further splicing associated putative interaction partners of *Ctcflos*.

Predicting splicing modulation from RNA sequence features, however, remains challenging, since the same binding motif can be recognized by different RBPs and alternative splicing events are usually controlled by multiple RBPs that mutually modulate their binding specificities (Fu & Ares, 2014). Nonetheless, computational predictions may provide initial indications towards the mechanistic activity of *Ctcflos* that could be pursued in follow up experiments.

Transcription and alternative splicing might be co-regulated *Ctcflos*-dependently within nuclear speckles

The investigations into *Ctcflos*-dependent transcription and alternative splicing raise the question of cause or consequence, independent or coordinated regulation of these processes. Different scenarios are possible: The splicing modulations could occur as consequence of *Ctcflos*-dependently altered transcription, e.g. mediated by the observed altered transcript levels of spliceosome components and splicing factors. Alternatively, altered transcription could be conditioned by splicing changes, e.g. through modulated isoform profiles of major thermogenic transcription factors or co-regulators. Both processes, however, occur synchronously, in direct response to *Ctcflos* KD, rather than in chronological order. Additionally, transcriptional and splicing changes do not target entirely distinct gene sets. Like *Prdm16* and *Neat1*, more genes are regulated on both levels. These observations rather suggest a coordinated regulation of the two processes by *Ctcflos*. Indeed, transcription and alternative splicing are tightly associated and should not be regarded as independent consecutive procedures (Tilgner *et al.*, 2012). This is supported by previous findings, showing that the sensitivity to splicing factors and the splicing pattern of a transcript can be modified by changes in the gene promoter region and thus altered TF binding (Cramer *et al*, 1997). Accordingly, RNA Pol II itself, TFs or their cofactors (such as PGC1) are able to interact with splicing factors, recruiting them to sites of active gene expression to concomitantly modulate the transcription rate and the splicing profile of the targeted gene (Auboeuf *et al*, 2004; Cramer *et al*, 1999; Das *et al*, 2007; Monsalve *et al*, 2000).

Notably, nuclear speckles present important points of contact for transcription and splicing factor activity regulation. Nuclear speckles are granule clusters, located in the interchromatin space, that are assumed to act as storage, assembly and modification compartments of transcription and splicing associated factors (SR-proteins, kinases and phosphatases, spliceosomal components, TFs and RNA Pol II subunits could be found within these structures) (Spector & Lamond, 2011). Nuclear speckles are often observed close to regions of highly active transcription and are dynamically regulated in size, shape and number in relation to the level of gene expression and in response to signals that modulate splicing activity (Spector *et al*, 1983). Splicing factors and transcription factors, in an inactive state, are supposed to reside within nuclear speckles, upon demand, phosphorylation by inherent kinases (CLK- and SRPK-kinases) signals their assembly to higher order complexes and triggers their transfer to sites of active gene expression. After modulating the transcription and splicing process, during which they are dephosphorylated, they shuttle back to the nuclear speckle storages (Fig. 45) (Cáceres *et al*, 1997; Misteli *et al*, 1998; Misteli & Spector, 1999).

In *Ctcflos* deficient brite adipocytes, *Srpk*-kinases are downregulated, while *Clk*-kinases are upregulated in normal brite adipogenesis. The lack of kinases in *Ctcflos* deficiency might impede activation and translocation of splicing factors and transcription factors out of nuclear speckles to sites of gene expression. The observed alterations in gene transcription and alternative splicing, as well as the increased abundance of nuclear speckles, could be considered as consequence thereof. Similarly, it was previously observed that enlarged and

rounded nuclear speckles occurred upon transcription inhibition, which entailed SR-protein accumulation in the speckles (Spector *et al.*, 1983).

Besides transcription and splicing associated protein factors, nuclear speckles also host a population of poly-adenylated RNAs (Carter *et al*, 1991; Huang *et al*, 1994; Spector & Lamond, 2011; Visa *et al*, 1993). This includes the long noncoding RNA *Malat1* (Hutchinson *et al*, 2007) that is involved in alternative splicing regulation in human HeLa cells through modulation of SR-protein phosphorylation and intra-nuclear translocation (Tripathi *et al*, 2010). This principally demonstrates the regulatory capacity of lncRNAs in these events. Despite strong sequence conservation of *Malat1* across mammalian species, there is a discrepancy in its function between human and mouse (Nakagawa *et al.*, 2012; Tripathi *et al.*, 2010). In contrast to its role in human cells, it was not essential for alternative splicing, splicing factor phosphorylation or nuclear speckle organization in the mouse (Galganski *et al*, 2017), proposing the presence of other, yet undefined RNA components, coordinating nuclear speckle functions in murine cells. Integrating the regulatory impact of *Ctcflos* on transcription and splicing with the effects on SR-protein kinase and nuclear speckle abundance, a role of *Ctcflos* in the coordination of nuclear speckle processes could be envisioned (Fig. 45). For experimental evaluation, sub-nuclear localization of *Ctcflos* should be specified by fluorescent *in situ* hybridization in a first step. Investigation of *Ctcflos*-dependent changes in the phosphorylation states of speckle-associated splicing and transcription factors would further inform about a putative function of *Ctcflos* in brite adipocyte nuclear speckle biology.

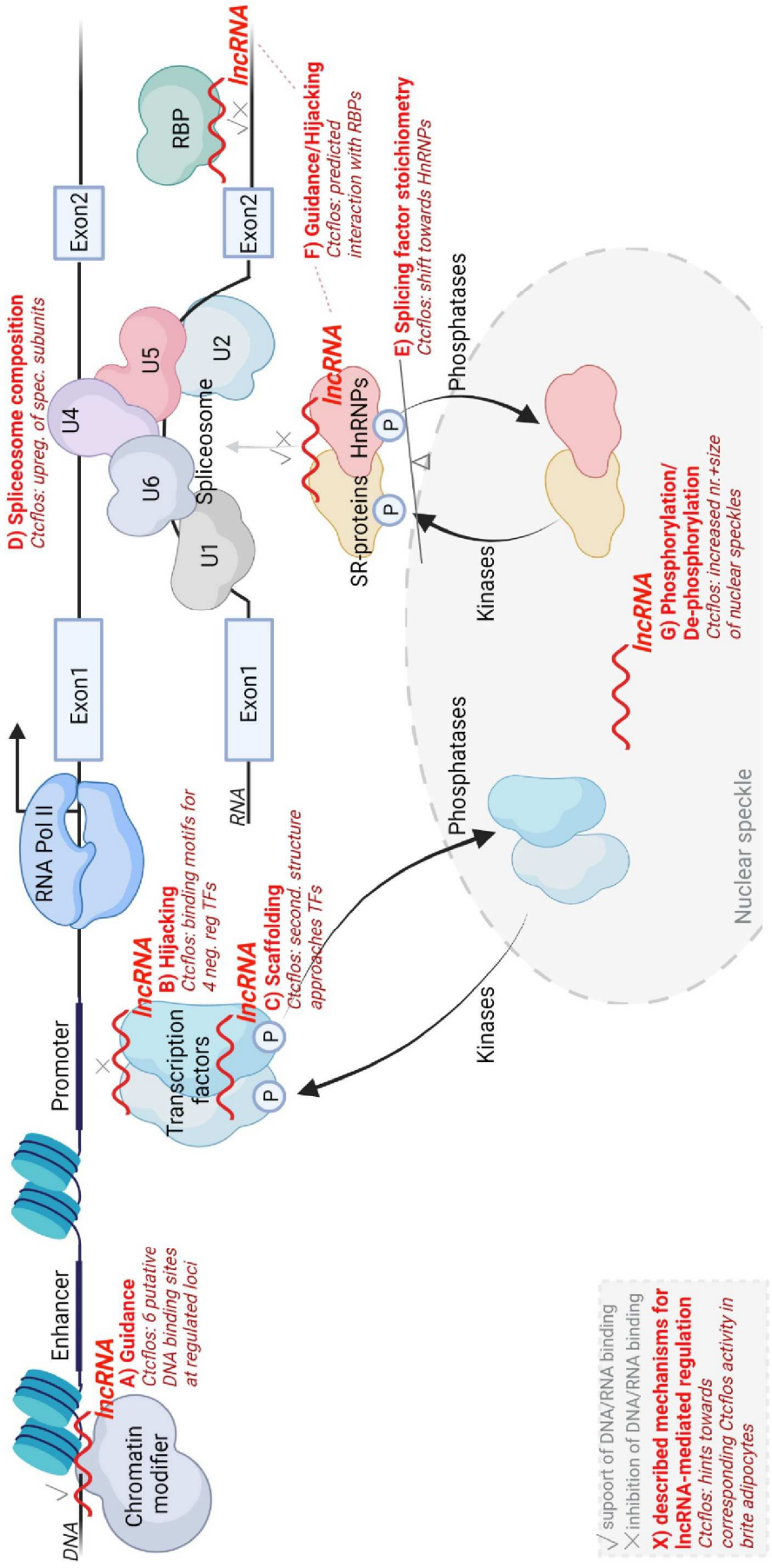

Figure 45: Explorative experimental and computational analyses raise interest in several possible mechanistic activities of *Ctcflos*. Illustration of the processes of transcription and alternative splicing and how they are regulated by chromatin modifiers, transcription factors and splicing factors. Possibilities of modulatory influences of lncRNAs on these processes are highlighted in red. Hints towards corresponding activities of *Ctcflos* are provided in dark red. Created with BioRender.com.

4.6 CONCLUSION AND OUTLOOK

In the present thesis we addressed a persisting gap in the understanding of regulatory pathways in thermogenic adipogenesis by investigating the role of the longtime neglected, yet regulatory powerful class of lncRNAs. The varied regulatory capacity of lncRNAs is increasingly recognized in a myriad of cellular processes, tissues and diseases and started to enter the field of adipose biology. Though their contribution in brown and especially in brite adipogenesis still remains only marginally investigated. Here we applied a model of genetically diverging browning capacities among inbred mouse strains in order to filter among the large range of adipocyte expressed lncRNAs those that act as functional regulators in brite adipocyte differentiation. This revealed *Ctcflos* as adipose tissue enriched lncRNA that directs early cell programming towards the thermogenic adipocyte lineage. *Ctcflos* thereby exemplifies the versatility of lncRNA mediated regulation by acting synchronously at two levels of gene expression. It shapes transcription and alternative splicing of thermogenesis associated genes, including established brite master regulators such as *Prdm16*, as well as novel browning modulators like lncRNA *Neat1*. With these functionalities, *Ctcflos* was characterized as an essential component in brite adipogenesis, involved in the induction of the brite/brown-selective gene program and functional fine-tuning of the cellular machinery towards thermogenesis.

Preliminary computational approaches towards the mechanism of *Ctcflos* activity opened a whole range of further research questions that could be the subject of future investigation. In this context, *Ctcflos* could be envisioned as guide or hijacker of chromatin modifiers, transcription and splicing factors or other RNA binding proteins. Alternatively, a coordinating role of *Ctcflos* in transcription and splicing regulation as lncRNA component within nuclear speckles might present a promising hypothesis to follow up. In future experiments it would therefore be of prime importance to determine protein interaction partners of *Ctcflos*, its putative DNA or RNA binding sites, clarify its isoform sequences and its exact localization in the nucleus.

Conclusively, the present thesis underlines the multi-dimensional nature of brite adipogenesis and the coordinative regulatory potential of lncRNAs in this process. In this respect, it provides an impulse to rethink our established view on thermogenic adipogenesis and to include lncRNAs as manifold orchestrators in cellular differentiation.

5 REFERENCES

Alpern D, Gardeux V, Russeil J, Mangeat B, Meireles-Filho ACA, Breysse R, Hacker D, Deplancke B (2019) BRB-seq: ultra-affordable high-throughput transcriptomics enabled by bulk RNA barcoding and sequencing. *Genome biology* 20: 71

Alvarez-Dominguez JR, Bai Z, Xu D, Yuan B, Lo KA, Yoon MJ, Lim YC, Knoll M, Slavov N, Chen S *et al* (2015a) De Novo Reconstruction of Adipose Tissue Transcriptomes Reveals Long Non-coding RNA Regulators of Brown Adipocyte Development. *Cell metabolism* 21: 764-776

Alvarez-Dominguez JR, Bai Z, Xu D, Yuan B, Lo KA, Yoon MJ, Lim YC, Knoll M, Slavov N, Chen S *et al* (2015b) De Novo Reconstruction of Adipose Tissue Transcriptomes Reveals Long Non-coding RNA Regulators of Brown Adipocyte Development. *Cell metabolism* 21: 764-776

Anders S, Reyes A, Huber W (2012) Detecting differential usage of exons from RNA-seq data. *Genome research* 22: 2008-2017

Anderson DM, Anderson KM, Chang CL, Makarewich CA, Nelson BR, McAnally JR, Kasaragod P, Shelton JM, Liou J, Bassel-Duby R *et al* (2015) A micropeptide encoded by a putative long noncoding RNA regulates muscle performance. *Cell* 160: 595-606

Auboeuf D, Dowhan DH, Kang YK, Larkin K, Lee JW, Berget SM, O'Malley BW (2004) Differential recruitment of nuclear receptor coactivators may determine alternative RNA splice site choice in target genes. *Proceedings of the National Academy of Sciences of the United States of America* 101: 2270-2274

Bai Z, Chai XR, Yoon MJ, Kim HJ, Lo KA, Zhang ZC, Xu D, Siang DTC, Walet ACE, Xu SH *et al* (2017) Dynamic transcriptome changes during adipose tissue energy expenditure reveal critical roles for long noncoding RNA regulators. *PLoS biology* 15: e2002176

Baralle FE, Giudice J (2017) Alternative splicing as a regulator of development and tissue identity. *Nature reviews Molecular cell biology* 18: 437-451

Barbatelli G, Murano I, Madsen L, Hao Q, Jimenez M, Kristiansen K, Giacobino JP, De Matteis R, Cinti S (2010) The emergence of cold-induced brown adipocytes in mouse white fat depots is determined predominantly by white to brown adipocyte transdifferentiation. *American journal of physiology Endocrinology and metabolism* 298: E1244-1253

Bartelt A, Bruns OT, Reimer R, Hohenberg H, Ittrich H, Peldschus K, Kaul MG, Tromsdorf UI, Weller H, Waurisch C *et al* (2011) Brown adipose tissue activity controls triglyceride clearance. *Nature medicine* 17: 200-205

Bartelt A, Heeren J (2014) Adipose tissue browning and metabolic health. *Nature reviews Endocrinology* 10: 24-36

Bartelt A, Widenmaier SB, Schlein C, Johann K, Goncalves RLS, Eguchi K, Fischer AW, Parlakgül G, Snyder NA, Nguyen TB *et al* (2018) Brown adipose tissue thermogenic adaptation requires Nrf1-mediated proteasomal activity. *Nature medicine* 24: 292-303

Bast-Habersbrunner A, Kiefer C, Weber P, Fromme T, Schießl A, Schwalie PC, Deplancke B, Li Y, Klingenspor M (2021) LncRNA Ctcflos orchestrates transcription and alternative splicing in thermogenic adipogenesis. *EMBO reports* 22: e51289

Bhat SA, Ahmad SM, Mumtaz PT, Malik AA, Dar MA, Urwat U, Shah RA, Ganai NA (2016) Long non-coding RNAs: Mechanism of action and functional utility. *Non-coding RNA research* 1: 43-50

Bi P, Shan T, Liu W, Yue F, Yang X, Liang XR, Wang J, Li J, Carlesso N, Liu X *et al* (2014) Inhibition of Notch signaling promotes browning of white adipose tissue and ameliorates obesity. *Nature medicine* 20: 911-918

Birsoy K, Chen Z, Friedman J (2008) Transcriptional regulation of adipogenesis by KLF4. *Cell metabolism* 7: 339-347

Black DL (2003) Mechanisms of alternative pre-messenger RNA splicing. *Annual review of biochemistry* 72: 291-336

Blüher M (2019) Neuregulin 4: A "Hotline" Between Brown Fat and Liver. *Obesity (Silver Spring, Md)* 27: 1555-1557

Bordicchia M, Liu D, Amri EZ, Ailhaud G, Dessi-Fulgheri P, Zhang C, Takahashi N, Sarzani R, Collins S (2012) Cardiac natriuretic peptides act via p38 MAPK to induce the brown fat thermogenic program in mouse and human adipocytes. *The Journal of clinical investigation* 122: 1022-1036

Bridges MC, Daulagala AC, Kourtidis A (2021) LNCcation: lncRNA localization and function. *The Journal of cell biology* 220

Burkart A, Shi X, Chouinard M, Corvera S (2011) Adenylate kinase 2 links mitochondrial energy metabolism to the induction of the unfolded protein response. *The Journal of biological chemistry* 286: 4081-4089

Cabili MN, Trapnell C, Goff L, Koziol M, Tazon-Vega B, Regev A, Rinn JL (2011) Integrative annotation of human large intergenic noncoding RNAs reveals global properties and specific subclasses. *Genes & development* 25: 1915-1927

Cáceres JF, Misteli T, Screaton GR, Spector DL, Krainer AR (1997) Role of the modular domains of SR proteins in subnuclear localization and alternative splicing specificity. *The Journal of cell biology* 138: 225-238

Cannon B, Nedergaard J (2004) Brown adipose tissue: function and physiological significance. *Physiological reviews* 84: 277-359

Carter KC, Taneja KL, Lawrence JB (1991) Discrete nuclear domains of poly(A) RNA and their relationship to the functional organization of the nucleus. *The Journal of cell biology* 115: 1191-1202

Cederberg A, Gronning LM, Ahren B, Tasken K, Carlsson P, Enerback S (2001) FOXC2 is a winged helix gene that counteracts obesity, hypertriglyceridemia, and diet-induced insulin resistance. *Cell* 106: 563-573

Cesana M, Cacchiarelli D, Legnini I, Santini T, Sthandier O, Chinappi M, Tramontano A, Bozzoni I (2011) A long noncoding RNA controls muscle differentiation by functioning as a competing endogenous RNA. *Cell* 147: 358-369

Chen K, Xie S, Jin W (2019) Crucial lncRNAs associated with adipocyte differentiation from human adipose-derived stem cells based on co-expression and ceRNA network analyses. *PeerJ* 7: e7544

Chen L, Zhang S (2016) Long noncoding RNAs in cell differentiation and pluripotency. *Cell and tissue research* 366: 509-521

Chen LL (2016) Linking Long Noncoding RNA Localization and Function. *Trends in biochemical sciences* 41: 761-772

Chen M, Manley JL (2009) Mechanisms of alternative splicing regulation: insights from molecular and genomics approaches. *Nature reviews Molecular cell biology* 10: 741-754

Chi YL, Lin JC (2018) RBM4a modulates the impact of PRDM16 on development of brown adipocytes through an alternative splicing mechanism. *Biochimica et biophysica acta Molecular cell research* 1865: 1515-1525

Chondronikola M, Volpi E, Børsheim E, Porter C, Annamalai P, Enerbäck S, Lidell ME, Saraf MK, Labbe SM, Hurren NM *et al* (2014) Brown adipose tissue improves whole-body glucose homeostasis and insulin sensitivity in humans. *Diabetes* 63: 4089-4099

Chondronikola M, Volpi E, Børsheim E, Porter C, Saraf MK, Annamalai P, Yfanti C, Chao T, Wong D, Shinoda K *et al* (2016) Brown Adipose Tissue Activation Is Linked to Distinct Systemic Effects on Lipid Metabolism in Humans. *Cell metabolism* 23: 1200-1206

Cohen P, Levy JD, Zhang Y, Frontini A, Kolodin DP, Svensson KJ, Lo JC, Zeng X, Ye L, Khandekar MJ *et al* (2014) Ablation of PRDM16 and beige adipose causes metabolic dysfunction and a subcutaneous to visceral fat switch. *Cell* 156: 304-316

Cooper DR, Carter G, Li P, Patel R, Watson JE, Patel NA (2014) Long Non-Coding RNA NEAT1 Associates with SRp40 to Temporally Regulate PPARgamma2 Splicing during Adipogenesis in 3T3-L1 Cells. *Genes* 5: 1050-1063

Costanzo M, Kuzmin E, van Leeuwen J, Mair B, Moffat J, Boone C, Andrews B (2019) Global Genetic Networks and the Genotype-to-Phenotype Relationship. *Cell* 177: 85-100

Cousin B, Cinti S, Morroni M, Raimbault S, Ricquier D, Penicaud L, Casteilla L (1992) Occurrence of brown adipocytes in rat white adipose tissue: molecular and morphological characterization. *Journal of cell science* 103 (Pt 4): 931-942

Cramer P (2019) Organization and regulation of gene transcription. *Nature* 573: 45-54

Cramer P, Cáceres JF, Cazalla D, Kadener S, Muro AF, Baralle FE, Kornblihtt AR (1999) Coupling of transcription with alternative splicing: RNA pol II promoters modulate SF2/ASF and 9G8 effects on an exonic splicing enhancer. *Molecular cell* 4: 251-258

Cramer P, Pesce CG, Baralle FE, Kornblihtt AR (1997) Functional association between promoter structure and transcript alternative splicing. *Proceedings of the National Academy of Sciences of the United States of America* 94: 11456-11460

Cui X, You L, Li Y, Zhu L, Zhang F, Xie K, Cao Y, Ji C, Guo X (2016) A transcribed ultraconserved noncoding RNA, uc.417, serves as a negative regulator of brown adipose tissue thermogenesis. *FASEB journal : official publication of the Federation of American Societies for Experimental Biology* 30: 4301-4312

Cypess AM, Lehman S, Williams G, Tal I, Rodman D, Goldfine AB, Kuo FC, Palmer EL, Tseng YH, Doria A *et al* (2009) Identification and importance of brown adipose tissue in adult humans. *The New England journal of medicine* 360: 1509-1517

Das R, Yu J, Zhang Z, Gygi MP, Krainer AR, Gygi SP, Reed R (2007) SR proteins function in coupling RNAP II transcription to pre-mRNA splicing. *Molecular cell* 26: 867-881

De Matteis R, Lucertini F, Guescini M, Polidori E, Zeppa S, Stocchi V, Cinti S, Cuppini R (2013) Exercise as a new physiological stimulus for brown adipose tissue activity. *Nutrition, metabolism, and cardiovascular diseases : NMCD* 23: 582-590

Dempersmier J, Sambeat A, Gulyaeva O, Paul SM, Hudak CS, Raposo HF, Kwan HY, Kang C, Wong RH, Sul HS (2015) Cold-inducible Zfp516 activates UCP1 transcription to promote browning of white fat and development of brown fat. *Molecular cell* 57: 235-246

Derrien T, Johnson R, Bussotti G, Tanzer A, Djebali S, Tilgner H, Guernec G, Martin D, Merkel A, Knowles DG *et al* (2012) The GENCODE v7 catalog of human long noncoding RNAs: analysis of their gene structure, evolution, and expression. *Genome research* 22: 1775-1789

Divakaruni AS, Brand MD (2011) The regulation and physiology of mitochondrial proton leak. *Physiology (Bethesda, Md)* 26: 192-205

Djebali S, Davis CA, Merkel A, Dobin A, Lassmann T, Mortazavi A, Tanzer A, Lagarde J, Lin W, Schlesinger F *et al* (2012) Landscape of transcription in human cells. *Nature* 489: 101-108

Entingh AJ, Taniguchi CM, Kahn CR (2003) Bi-directional regulation of brown fat adipogenesis by the insulin receptor. *The Journal of biological chemistry* 278: 33377-33383

Faghihi MA, Zhang M, Huang J, Modarresi F, Van der Brug MP, Nalls MA, Cookson MR, St-Laurent G, 3rd, Wahlestedt C (2010) Evidence for natural antisense transcript-mediated inhibition of microRNA function. *Genome biology* 11: R56

Fatica A, Bozzoni I (2014) Long non-coding RNAs: new players in cell differentiation and development. *Nature reviews Genetics* 15: 7-21

Fayyad AM, Khan AA, Abdallah SH, Alomran SS, Bajou K, Khattak MNK (2019) Rosiglitazone Enhances Browning Adipocytes in Association with MAPK and PI3-K Pathways During the Differentiation of Telomerase-Transformed Mesenchymal Stromal Cells into Adipocytes. *International journal of molecular sciences* 20

Feng J, Bi C, Clark BS, Mady R, Shah P, Kohtz JD (2006) The Evf-2 noncoding RNA is transcribed from the Dlx-5/6 ultraconserved region and functions as a Dlx-2 transcriptional coactivator. *Genes & development* 20: 1470-1484

Firmin FF, Oger F, Gheeraert C, Dubois-Chevalier J, Vercoutter-Edouart AS, Alzaid F, Mazuy C, Dehondt H, Alexandre J, Derudas B *et al* (2017) The RBM14/CoAA-interacting, long intergenic non-coding RNA Paral1 regulates adipogenesis and coactivates the nuclear receptor PPARγ. *Scientific reports* 7: 14087

Frankish A, Diekhans M, Ferreira AM, Johnson R, Jungreis I, Loveland J, Mudge JM, Sisu C, Wright J, Armstrong J *et al* (2019) GENCODE reference annotation for the human and mouse genomes. *Nucleic acids research* 47: D766-d773

Fu XD, Ares M, Jr. (2014) Context-dependent control of alternative splicing by RNA-binding proteins. *Nature reviews Genetics* 15: 689-701

Funnell AP, Crossley M (2012) Homo- and heterodimerization in transcriptional regulation. *Advances in experimental medicine and biology* 747: 105-121

Galganski L, Urbanek MO, Krzyzosiak WJ (2017) Nuclear speckles: molecular organization, biological function and role in disease. *Nucleic acids research* 45: 10350-10368

Geisler S, Coller J (2013) RNA in unexpected places: long non-coding RNA functions in diverse cellular contexts. *Nature reviews Molecular cell biology* 14: 699-712

Gernapudi R, Wolfson B, Zhang Y, Yao Y, Yang P, Asahara H, Zhou Q (2016) MicroRNA 140 Promotes Expression of Long Noncoding RNA NEAT1 in Adipogenesis. *Molecular and cellular biology* 36: 30-38

Gerngroß C, Schretter J, Klingenspor M, Schwaiger M, Fromme T (2017) Active Brown Fat During (18)F-FDG PET/CT Imaging Defines a Patient Group with Characteristic Traits and an Increased Probability of Brown Fat Redetection. *Journal of nuclear medicine : official publication, Society of Nuclear Medicine* 58: 1104-1110

Gharanei S, Shabir K, Brown JE, Weickert MO, Barber TM, Kyrou I, Randeva HS (2020) Regulatory microRNAs in Brown, Brite and White Adipose Tissue. *Cells* 9

Giordano A, Smorlesi A, Frontini A, Barbatelli G, Cinti S (2014) White, brown and pink adipocytes: the extraordinary plasticity of the adipose organ. *European journal of endocrinology* 170: R159-171

Giralt M, Villarroya F (2013) White, brown, beige/brite: different adipose cells for different functions? *Endocrinology* 154: 2992-3000

Goldfarb KC, Cech TR (2017) Targeted CRISPR disruption reveals a role for RNase MRP RNA in human preribosomal RNA processing. *Genes & development* 31: 59-71

Goldstein LD, Cao Y, Pau G, Lawrence M, Wu TD, Seshagiri S, Gentleman R (2016) Prediction and Quantification of Splice Events from RNA-Seq Data. *PloS one* 11: e0156132

Grosso AR, Gomes AQ, Barbosa-Morais NL, Caldeira S, Thorne NP, Grech G, von Lindern M, Carmo-Fonseca M (2008) Tissue-specific splicing factor gene expression signatures. *Nucleic acids research* 36: 4823-4832

Gruber AR, Lorenz R, Bernhart SH, Neuböck R, Hofacker IL (2008) The Vienna RNA websuite. *Nucleic acids research* 36: W70-74

Grunstein M (1997) Histone acetylation in chromatin structure and transcription. *Nature* 389: 349-352

Guerra C, Koza RA, Yamashita H, Walsh K, Kozak LP (1998) Emergence of brown adipocytes in white fat in mice is under genetic control. Effects on body weight and adiposity. *The Journal of clinical investigation* 102: 412-420

Hanssen MJ, Hoeks J, Brans B, van der Lans AA, Schaart G, van den Driessche JJ, Jorgensen JA, Boekschoten MV, Hesselink MK, Havekes B *et al* (2015) Short-term cold acclimation improves insulin sensitivity in patients with type 2 diabetes mellitus. *Nature medicine* 21: 863-865

Harms M, Seale P (2013) Brown and beige fat: development, function and therapeutic potential. *Nature medicine* 19: 1252-1263

Harms MJ, Ishibashi J, Wang W, Lim HW, Goyama S, Sato T, Kurokawa M, Won KJ, Seale P (2014) Prdm16 is required for the maintenance of brown adipocyte identity and function in adult mice. *Cell metabolism* 19: 593-604

Herz CT, Kiefer FW (2019) Adipose tissue browning in mice and humans. *The Journal of endocrinology* 241: R97-r109

Hezroni H, Koppstein D, Schwartz MG, Avrutin A, Bartel DP, Ulitsky I (2015) Principles of long noncoding RNA evolution derived from direct comparison of transcriptomes in 17 species. *Cell reports* 11: 1110-1122

Himms-Hagen J, Melnyk A, Zingaretti MC, Ceresi E, Barbatelli G, Cinti S (2000) Multilocular fat cells in WAT of CL-316243-treated rats derive directly from white adipocytes. *American journal of physiology Cell physiology* 279: C670-681

Hondares E, Mora O, Yubero P, Rodriguez de la Concepción M, Iglesias R, Giralt M, Villarroya F (2006) Thiazolidinediones and rexinoids induce peroxisome proliferator-activated receptor-coactivator (PGC)-1alpha gene transcription: an autoregulatory loop controls PGC-1alpha expression in

adipocytes via peroxisome proliferator-activated receptor-gamma coactivation. *Endocrinology* 147: 2829-2838

Huang S, Deerinck TJ, Ellisman MH, Spector DL (1994) In vivo analysis of the stability and transport of nuclear poly(A)+ RNA. *The Journal of cell biology* 126: 877-899

Hung CS, Lin JC (2020) Alternatively spliced MBNL1 isoforms exhibit differential influence on enhancing brown adipogenesis. *Biochimica et biophysica acta Gene regulatory mechanisms* 1863: 194437

Hung T, Chang HY (2010) Long noncoding RNA in genome regulation: prospects and mechanisms. *RNA biology* 7: 582-585

Hutchinson JN, Ensminger AW, Clemson CM, Lynch CR, Lawrence JB, Chess A (2007) A screen for nuclear transcripts identifies two linked noncoding RNAs associated with SC35 splicing domains. *BMC genomics* 8: 39

Javary J, Allain-Courtois N, Saucisse N, Costet P, Heraud C, Benhamed F, Pierre R, Bure C, Pallares-Lupon N, Do Cruzeiro M *et al* (2018) Liver Reptin/RUVBL2 controls glucose and lipid metabolism with opposite actions on mTORC1 and mTORC2 signalling. *Gut* 67: 2192-2203

Johnsson P, Lipovich L, Grandér D, Morris KV (2014) Evolutionary conservation of long non-coding RNAs; sequence, structure, function. *Biochimica et biophysica acta* 1840: 1063-1071

Kajimura S, Seale P, Tomaru T, Erdjument-Bromage H, Cooper MP, Ruas JL, Chin S, Tempst P, Lazar MA, Spiegelman BM (2008) Regulation of the brown and white fat gene programs through a PRDM16/CtBP transcriptional complex. *Genes & development* 22: 1397-1409

Kalwa M, Hänzelmann S, Otto S, Kuo CC, Franzen J, Joussen S, Fernandez-Rebollo E, Rath B, Koch C, Hofmann A *et al* (2016) The lncRNA HOTAIR impacts on mesenchymal stem cells via triple helix formation. *Nucleic acids research* 44: 10631-10643

Kang YJ, Yang DC, Kong L, Hou M, Meng YQ, Wei L, Gao G (2017) CPC2: a fast and accurate coding potential calculator based on sequence intrinsic features. *Nucleic acids research* 45: W12-w16

Kanzleiter T, Schneider T, Walter I, Bolze F, Eickhorst C, Heldmaier G, Klaus S, Klingenspor M (2005) Evidence for Nr4a1 as a cold-induced effector of brown fat thermogenesis. *Physiological genomics* 24: 37-44

Katayama S, Tomaru Y, Kasukawa T, Waki K, Nakanishi M, Nakamura M, Nishida H, Yap CC, Suzuki M, Kawai J *et al* (2005) Antisense transcription in the mammalian transcriptome. *Science (New York, NY)* 309: 1564-1566

Kershaw EE, Flier JS (2004) Adipose tissue as an endocrine organ. *The Journal of clinical endocrinology and metabolism* 89: 2548-2556

Kim HM, Han JW, Chan JY (2016) Nuclear Factor Erythroid-2 Like 1 (NFE2L1): Structure, function and regulation. *Gene* 584: 17-25

Kino T, Hurt DE, Ichijo T, Nader N, Chrousos GP (2010) Noncoding RNA gas5 is a growth arrest- and starvation-associated repressor of the glucocorticoid receptor. *Science signaling* 3: ra8

Kleiner S, Mepani RJ, Laznik D, Ye L, Jurczak MJ, Jornayvaz FR, Estall JL, Chatterjee Bhowmick D, Shulman GI, Spiegelman BM (2012) Development of insulin resistance in mice lacking PGC-1α in adipose tissues. *Proceedings of the National Academy of Sciences of the United States of America* 109: 9635-9640

Klingenspor M, Bast A, Bolze F, Li Y, Maurer S, Schweizer S, Willershäuser M, Fromme T (2017) Brown Adipose Tissue. In: *Adipose Tissue Biology*, M. S. (ed.)Springer, Cham.:

Konermann S, Brigham MD, Trevino AE, Joung J, Abudayyeh OO, Barcena C, Hsu PD, Habib N, Gootenberg JS, Nishimasu H *et al* (2015) Genome-scale transcriptional activation by an engineered CRISPR-Cas9 complex. *Nature* 517: 583-588

Kornienko AE, Guenzl PM, Barlow DP, Pauler FM (2013) Gene regulation by the act of long non-coding RNA transcription. *BMC biology* 11: 59

Koza RA, Hohmann SM, Guerra C, Rossmeisl M, Kozak LP (2000) Synergistic gene interactions control the induction of the mitochondrial uncoupling protein (Ucp1) gene in white fat tissue. *The Journal of biological chemistry* 275: 34486-34492

Kozak LP, Koza RA (2010) The genetics of brown adipose tissue. *Progress in molecular biology and translational science* 94: 75-123

Krismer K, Varmeh S, Bird MA, Gattinger A, Kong YW, Handly ED, Bernwinkler T, Anderson DA, Heinzel A, Joughin BA *et al* (2019) Transite: A computational motif-based analysis platform that identifies RNA-binding proteins modulating changes in gene expression. *bioRxiv*: 416743

Krystal GW, Armstrong BC, Battey JF (1990) N-myc mRNA forms an RNA-RNA duplex with endogenous antisense transcripts. *Molecular and cellular biology* 10: 4180-4191

Kung JT, Colognori D, Lee JT (2013) Long noncoding RNAs: past, present, and future. *Genetics* 193: 651-669

Lagarde J, Uszczynska-Ratajczak B, Carbonell S, Pérez-Lluch S, Abad A, Davis C, Gingeras TR, Frankish A, Harrow J, Guigo R *et al* (2017) High-throughput annotation of full-length long noncoding RNAs with capture long-read sequencing. *Nature genetics* 49: 1731-1740

Lawrence M, Daujat S, Schneider R (2016) Lateral Thinking: How Histone Modifications Regulate Gene Expression. *Trends in genetics : TIG* 32: 42-56

Lebedeva S, Jens M, Theil K, Schwanhäusser B, Selbach M, Landthaler M, Rajewsky N (2011) Transcriptome-wide analysis of regulatory interactions of the RNA-binding protein HuR. *Molecular cell* 43: 340-352

Lee YH, Petkova AP, Konkar AA, Granneman JG (2015) Cellular origins of cold-induced brown adipocytes in adult mice. *FASEB journal : official publication of the Federation of American Societies for Experimental Biology* 29: 286-299

Li Y, Bolze F, Fromme T, Klingenspor M (2014a) Intrinsic differences in BRITE adipogenesis of primary adipocytes from two different mouse strains. *Biochimica et biophysica acta* 1841: 1345-1352

Li Y, Fromme T, Klingenspor M (2017) Meaningful respirometric measurements of UCP1-mediated thermogenesis. *Biochimie* 134: 56-61

Li Y, Fromme T, Schweizer S, Schottl T, Klingenspor M (2014b) Taking control over intracellular fatty acid levels is essential for the analysis of thermogenic function in cultured primary brown and brite/beige adipocytes. *EMBO reports* 15: 1069-1076

Li Y, Schnabl K, Gabler SM, Willershauser M, Reber J, Karlas A, Laurila S, Lahesmaa M, M UD, Bast-Habersbrunner A *et al* (2018) Secretin-Activated Brown Fat Mediates Prandial Thermogenesis to Induce Satiation. *Cell* 175: 1561-1574.e1512

Li Y, Schwalie PC, Bast-Habersbrunner A, Mocek S, Russeil J, Fromme T, Deplancke B, Klingenspor M (2019) Systems-Genetics-Based Inference of a Core Regulatory Network Underlying White Fat Browning. *Cell reports* 29: 4099-4113.e4095

Li Y SP, Bast-Habersbrunner A, Mocek S, Russeil J, Fromme T, Deplancke B, Klingenspor M RNA-seq of mouse subcutaneous SVF cells before and after differentiation with a brown fat differentiation cocktail (https://www.ebi.ac.uk/arrayexpress/experiments/E-MTAB-8344/). (2019) [DATASET]

Lin JC (2015a) Impacts of Alternative Splicing Events on the Differentiation of Adipocytes. *International journal of molecular sciences* 16: 22169-22189

Lin JC (2015b) RBM4-MEF2C network constitutes a feed-forward circuit that facilitates the differentiation of brown adipocytes. *RNA biology* 12: 208-220

Lin JC, Chi YL, Peng HY, Lu YH (2016a) RBM4-Nova1-SRSF6 splicing cascade modulates the development of brown adipocytes. *Biochimica et biophysica acta* 1859: 1368-1379

Lin JC, Lu YH, Liu YR, Lin YJ (2016b) RBM4a-regulated splicing cascade modulates the differentiation and metabolic activities of brown adipocytes. *Scientific reports* 6: 20665

Lin JC, Tarn WY, Hsieh WK (2014) Emerging role for RNA binding motif protein 4 in the development of brown adipocytes. *Biochimica et biophysica acta* 1843: 769-779

Liu C, Bai B, Skogerbø G, Cai L, Deng W, Zhang Y, Bu D, Zhao Y, Chen R (2005) NONCODE: an integrated knowledge database of non-coding RNAs. *Nucleic acids research* 33: D112-115

Liu J, Zhang C, Zhang B, Sheng Y, Xu W, Luo Y, He X, Huang K (2020) Comprehensive Analysis of the Characteristics and Differences in Adult and Newborn Brown Adipose Tissue (BAT): Newborn BAT Is a More Active/Dynamic BAT. *Cells* 9

Loncar D (1991) Convertible adipose tissue in mice. *Cell and tissue research* 266: 149-161

Lundh M, Pluciñska K, Isidor MS, Petersen PSS, Emanuelli B (2017) Bidirectional manipulation of gene expression in adipocytes using CRISPRa and siRNA. *Molecular metabolism* 6: 1313-1320

Major GC, Doucet E, Trayhurn P, Astrup A, Tremblay A (2007) Clinical significance of adaptive thermogenesis. *International journal of obesity (2005)* 31: 204-212

Marcher AB, Loft A, Nielsen R, Vihervaara T, Madsen JG, Sysi-Aho M, Ekroos K, Mandrup S (2015) RNA-Seq and Mass-Spectrometry-Based Lipidomics Reveal Extensive Changes of Glycerolipid Pathways in Brown Adipose Tissue in Response to Cold. *Cell reports* 13: 2000-2013

Marchese FP, Raimondi I, Huarte M (2017) The multidimensional mechanisms of long noncoding RNA function. *Genome biology* 18: 206

Mariner PD, Walters RD, Espinoza CA, Drullinger LF, Wagner SD, Kugel JF, Goodrich JA (2008) Human Alu RNA is a modular transacting repressor of mRNA transcription during heat shock. *Molecular cell* 29: 499-509

Martianov I, Ramadass A, Serra Barros A, Chow N, Akoulitchev A (2007) Repression of the human dihydrofolate reductase gene by a non-coding interfering transcript. *Nature* 445: 666-670

Maurer S FT, Klingenspor M Gene Expression Omnibus GSE119452 (https://www.ncbi.nlm.nih.gov/geo/query/acc.cgi?acc=GSE119452). (2018) [DATASET]

Melé M, Mattioli K, Mallard W, Shechner DM, Gerhardinger C, Rinn JL (2017) Chromatin environment, transcriptional regulation, and splicing distinguish lincRNAs and mRNAs. *Genome research* 27: 27-37

Mi L, Zhao XY, Li S, Yang G, Lin JD (2017) Conserved function of the long noncoding RNA Blnc1 in brown adipocyte differentiation. *Molecular metabolism* 6: 101-110

Miao H, Wang L, Zhan H, Dai J, Chang Y, Wu F, Liu T, Liu Z, Gao C, Li L *et al* (2019) A long noncoding RNA distributed in both nucleus and cytoplasm operates in the PYCARD-regulated apoptosis by coordinating the epigenetic and translational regulation. *PLoS genetics* 15: e1008144

Mikkelsen TS, Xu Z, Zhang X, Wang L, Gimble JM, Lander ES, Rosen ED (2010) Comparative epigenomic analysis of murine and human adipogenesis. *Cell* 143: 156-169

Milet C, Bléher M, Allbright K, Orgeur M, Coulpier F, Duprez D, Havis E (2017) Egr1 deficiency induces browning of inguinal subcutaneous white adipose tissue in mice. *Scientific reports* 7: 16153

Misteli T, Cáceres JF, Clement JQ, Krainer AR, Wilkinson MF, Spector DL (1998) Serine phosphorylation of SR proteins is required for their recruitment to sites of transcription in vivo. *The Journal of cell biology* 143: 297-307

Misteli T, Spector DL (1999) RNA polymerase II targets pre-mRNA splicing factors to transcription sites in vivo. *Molecular cell* 3: 697-705

Modrek B, Lee CJ (2003) Alternative splicing in the human, mouse and rat genomes is associated with an increased frequency of exon creation and/or loss. *Nature genetics* 34: 177-180

Monsalve M, Wu Z, Adelmant G, Puigserver P, Fan M, Spiegelman BM (2000) Direct coupling of transcription and mRNA processing through the thermogenic coactivator PGC-1. *Molecular cell* 6: 307-316

Mukherjee N, Corcoran DL, Nusbaum JD, Reid DW, Georgiev S, Hafner M, Ascano M, Jr., Tuschl T, Ohler U, Keene JD (2011) Integrative regulatory mapping indicates that the RNA-binding protein HuR couples pre-mRNA processing and mRNA stability. *Molecular cell* 43: 327-339

Müller TD, Clemmensen C, Finan B, DiMarchi RD, Tschöp MH (2018) Anti-Obesity Therapy: from Rainbow Pills to Polyagonists. *Pharmacological reviews* 70: 712-746

Nagano T, Mitchell JA, Sanz LA, Pauler FM, Ferguson-Smith AC, Feil R, Fraser P (2008) The Air noncoding RNA epigenetically silences transcription by targeting G9a to chromatin. *Science (New York, NY)* 322: 1717-1720

Nakagawa S, Ip JY, Shioi G, Tripathi V, Zong X, Hirose T, Prasanth KV (2012) Malat1 is not an essential component of nuclear speckles in mice. *RNA (New York, NY)* 18: 1487-1499

Nicholls DG, Locke RM (1984) Thermogenic mechanisms in brown fat. *Physiological reviews* 64: 1-64

Nicholls DG, Rial E (1999) A history of the first uncoupling protein, UCP1. *Journal of bioenergetics and biomembranes* 31: 399-406

Noh JH, Kim KM, Abdelmohsen K, Yoon JH, Panda AC, Munk R, Kim J, Curtis J, Moad CA, Wohler CM *et al* (2016) HuR and GRSF1 modulate the nuclear export and mitochondrial localization of the lncRNA RMRP. *Genes & development* 30: 1224-1239

Oeckl J, Bast-Habersbrunner A, Fromme T, Klingenspor M, Li Y (2020) Isolation, Culture, and Functional Analysis of Murine Thermogenic Adipocytes. *STAR protocols* 1: 100118

Ohno H, Shinoda K, Ohyama K, Sharp LZ, Kajimura S (2013) EHMT1 controls brown adipose cell fate and thermogenesis through the PRDM16 complex. *Nature* 504: 163-167

Ohno H, Shinoda K, Spiegelman BM, Kajimura S (2012) PPARγ agonists induce a white-to-brown fat conversion through stabilization of PRDM16 protein. *Cell metabolism* 15: 395-404

Olsen JM, Åslund A, Bokhari MH, Hutchinson DS, Bengtsson T (2019) Acute β-adrenoceptor mediated glucose clearance in brown adipose tissue; a distinct pathway independent of functional insulin signaling. *Molecular metabolism* 30: 240-249

Ouellet V, Labbe SM, Blondin DP, Phoenix S, Guerin B, Haman F, Turcotte EE, Richard D, Carpentier AC (2012) Brown adipose tissue oxidative metabolism contributes to energy expenditure during acute cold exposure in humans. *The Journal of clinical investigation* 122: 545-552

Ouellet V, Routhier-Labadie A, Bellemare W, Lakhal-Chaieb L, Turcotte E, Carpentier AC, Richard D (2011) Outdoor temperature, age, sex, body mass index, and diabetic status determine the prevalence, mass, and glucose-uptake activity of 18F-FDG-detected BAT in humans. *The Journal of clinical endocrinology and metabolism* 96: 192-199

Pacheco TR, Moita LF, Gomes AQ, Hacohen N, Carmo-Fonseca M (2006) RNA interference knockdown of hU2AF35 impairs cell cycle progression and modulates alternative splicing of Cdc25 transcripts. *Molecular biology of the cell* 17: 4187-4199

Pan Q, Shai O, Lee LJ, Frey BJ, Blencowe BJ (2008) Deep surveying of alternative splicing complexity in the human transcriptome by high-throughput sequencing. *Nature genetics* 40: 1413-1415

Park JH, Kang HJ, Kang SI, Lee JE, Hur J, Ge K, Mueller E, Li H, Lee BC, Lee SB (2013) A multifunctional protein, EWS, is essential for early brown fat lineage determination. *Developmental cell* 26: 393-404

Park JW, Parisky K, Celotto AM, Reenan RA, Graveley BR (2004) Identification of alternative splicing regulators by RNA interference in Drosophila. *Proceedings of the National Academy of Sciences of the United States of America* 101: 15974-15979

Paz I, Kosti I, Ares M, Jr., Cline M, Mandel-Gutfreund Y (2014) RBPmap: a web server for mapping binding sites of RNA-binding proteins. *Nucleic acids research* 42: W361-367

Peng HY, Liang YC, Tan TH, Chuang HC, Lin YJ, Lin JC (2018) RBM4a-SRSF3-MAP4K4 Splicing Cascade Constitutes a Molecular Mechanism for Regulating Brown Adipogenesis. *International journal of molecular sciences* 19

Peng L, Liu F, Yang J, Liu X, Meng Y, Deng X, Peng C, Tian G, Zhou L (2019) Probing lncRNA-Protein Interactions: Data Repositories, Models, and Algorithms. *Frontiers in genetics* 10: 1346

Petrovic N, Walden TB, Shabalina IG, Timmons JA, Cannon B, Nedergaard J (2010) Chronic peroxisome proliferator-activated receptor gamma (PPARgamma) activation of epididymally derived white adipocyte cultures reveals a population of thermogenically competent, UCP1-containing adipocytes molecularly distinct from classic brown adipocytes. *The Journal of biological chemistry* 285: 7153-7164

Plath K, Mlynarczyk-Evans S, Nusinow DA, Panning B (2002) Xist RNA and the mechanism of X chromosome inactivation. *Annual review of genetics* 36: 233-278

Pradhan RN, Zachara M, Deplancke B (2017) A systems perspective on brown adipogenesis and metabolic activation. *Obesity reviews : an official journal of the International Association for the Study of Obesity* 18 Suppl 1: 65-81

Puigserver P, Wu Z, Park CW, Graves R, Wright M, Spiegelman BM (1998) A cold-inducible coactivator of nuclear receptors linked to adaptive thermogenesis. *Cell* 92: 829-839

Qiang L, Wang L, Kon N, Zhao W, Lee S, Zhang Y, Rosenbaum M, Zhao Y, Gu W, Farmer SR *et al* (2012) Brown remodeling of white adipose tissue by SirT1-dependent deacetylation of Pparγ. *Cell* 150: 620-632

Quandt K, Frech K, Karas H, Wingender E, Werner T (1995) MatInd and MatInspector: new fast and versatile tools for detection of consensus matches in nucleotide sequence data. *Nucleic acids research* 23: 4878-4884

Rajakumari S, Wu J, Ishibashi J, Lim HW, Giang AH, Won KJ, Reed RR, Seale P (2013) EBF2 determines and maintains brown adipocyte identity. *Cell metabolism* 17: 562-574

Rinn JL, Kertesz M, Wang JK, Squazzo SL, Xu X, Brugmann SA, Goodnough LH, Helms JA, Farnham PJ, Segal E *et al* (2007) Functional demarcation of active and silent chromatin domains in human HOX loci by noncoding RNAs. *Cell* 129: 1311-1323

Romero-Barrios N, Legascue MF, Benhamed M, Ariel F, Crespi M (2018) Splicing regulation by long noncoding RNAs. *Nucleic acids research* 46: 2169-2184

Rosen ED, MacDougald OA (2006) Adipocyte differentiation from the inside out. *Nature reviews Molecular cell biology* 7: 885-896

Rosenwald M, Perdikari A, Rülicke T, Wolfrum C (2013) Bi-directional interconversion of brite and white adipocytes. *Nature cell biology* 15: 659-667

Saito M, Okamatsu-Ogura Y, Matsushita M, Watanabe K, Yoneshiro T, Nio-Kobayashi J, Iwanaga T, Miyagawa M, Kameya T, Nakada K *et al* (2009) High incidence of metabolically active brown adipose tissue in healthy adult humans: effects of cold exposure and adiposity. *Diabetes* 58: 1526-1531

Sakamoto H, Kogo Y, Ohgane J, Hattori N, Yagi S, Tanaka S, Shiota K (2008) Sequential changes in genome-wide DNA methylation status during adipocyte differentiation. *Biochemical and biophysical research communications* 366: 360-366

Sakamoto H, Suzuki M, Abe T, Hosoyama T, Himeno E, Tanaka S, Greally JM, Hattori N, Yagi S, Shiota K (2007) Cell type-specific methylation profiles occurring disproportionately in CpG-less regions that delineate developmental similarity. *Genes to cells : devoted to molecular & cellular mechanisms* 12: 1123-1132

Schmidt E, Dhaouadi I, Gaziano I, Oliverio M, Klemm P, Awazawa M, Mitterer G, Fernandez-Rebollo E, Pradas-Juni M, Wagner W *et al* (2018) LincRNA H19 protects from dietary obesity by constraining expression of monoallelic genes in brown fat. *Nature communications* 9: 3622

Schmitz SU, Grote P, Herrmann BG (2016) Mechanisms of long noncoding RNA function in development and disease. *Cellular and molecular life sciences : CMLS* 73: 2491-2509

Schulz TJ, Tseng YH (2013) Brown adipose tissue: development, metabolism and beyond. *The Biochemical journal* 453: 167-178

Seale P, Bjork B, Yang W, Kajimura S, Chin S, Kuang S, Scime A, Devarakonda S, Conroe HM, Erdjument-Bromage H *et al* (2008) PRDM16 controls a brown fat/skeletal muscle switch. *Nature* 454: 961-967

Seale P, Conroe HM, Estall J, Kajimura S, Frontini A, Ishibashi J, Cohen P, Cinti S, Spiegelman BM (2011) Prdm16 determines the thermogenic program of subcutaneous white adipose tissue in mice. *The Journal of clinical investigation* 121: 96-105

Seale P, Kajimura S, Yang W, Chin S, Rohas LM, Uldry M, Tavernier G, Langin D, Spiegelman BM (2007) Transcriptional control of brown fat determination by PRDM16. *Cell metabolism* 6: 38-54

Shabalina IG, Petrovic N, de Jong JM, Kalinovich AV, Cannon B, Nedergaard J (2013) UCP1 in brite/beige adipose tissue mitochondria is functionally thermogenic. *Cell reports* 5: 1196-1203

Shalem O, Sanjana NE, Hartenian E, Shi X, Scott DA, Mikkelson T, Heckl D, Ebert BL, Root DE, Doench JG *et al* (2014) Genome-scale CRISPR-Cas9 knockout screening in human cells. *Science (New York, NY)* 343: 84-87

Shao M, Ishibashi J, Kusminski CM, Wang QA, Hepler C, Vishvanath L, MacPherson KA, Spurgin SB, Sun K, Holland WL *et al* (2016) Zfp423 Maintains White Adipocyte Identity through Suppression of the Beige Cell Thermogenic Gene Program. *Cell metabolism* 23: 1167-1184

Shapira SN, Lim HW, Rajakumari S, Sakers AP, Ishibashi J, Harms MJ, Won KJ, Seale P (2017) EBF2 transcriptionally regulates brown adipogenesis via the histone reader DPF3 and the BAF chromatin remodeling complex. *Genes & development* 31: 660-673

Sharp LZ, Shinoda K, Ohno H, Scheel DW, Tomoda E, Ruiz L, Hu H, Wang L, Pavlova Z, Gilsanz V *et al* (2012) Human BAT possesses molecular signatures that resemble beige/brite cells. *PloS one* 7: e49452

Siang DTC, Lim YC, Kyaw AMM, Win KN, Chia SY, Degirmenci U, Hu X, Tan BC, Walet ACE, Sun L *et al* (2020) The RNA-binding protein HuR is a negative regulator in adipogenesis. *Nature communications* 11: 213

Singer RA, Arnes L, Cui Y, Wang J, Gao Y, Guney MA, Burnum-Johnson KE, Rabadan R, Ansong C, Orr G *et al* (2019) The Long Noncoding RNA Paupar Modulates PAX6 Regulatory Activities to Promote Alpha Cell Development and Function. *Cell metabolism*

Slocum N, Durrant JR, Bailey D, Yoon L, Jordan H, Barton J, Brown RH, Clifton L, Milliken T, Harrington W *et al* (2013) Responses of brown adipose tissue to diet-induced obesity, exercise, dietary restriction and ephedrine treatment. *Experimental and toxicologic pathology : official journal of the Gesellschaft fur Toxikologische Pathologie* 65: 549-557

Spector DL, Lamond AI (2011) Nuclear speckles. *Cold Spring Harbor perspectives in biology* 3

Spector DL, Schrier WH, Busch H (1983) Immunoelectron microscopic localization of snRNPs. *Biology of the cell* 49: 1-10

Stanford KI, Middelbeek RJ, Townsend KL, An D, Nygaard EB, Hitchcox KM, Markan KR, Nakano K, Hirshman MF, Tseng YH *et al* (2013) Brown adipose tissue regulates glucose homeostasis and insulin sensitivity. *The Journal of clinical investigation* 123: 215-223

Statello L, Guo CJ, Chen LL, Huarte M (2021) Gene regulation by long non-coding RNAs and its biological functions. *Nature reviews Molecular cell biology* 22: 96-118

Stine RR, Shapira SN, Lim HW, Ishibashi J, Harms M, Won KJ, Seale P (2016) EBF2 promotes the recruitment of beige adipocytes in white adipose tissue. *Molecular metabolism* 5: 57-65

Su Y, Balice-Gordon RJ, Hess DM, Landsman DS, Minarcik J, Golden J, Hurwitz I, Liebhaber SA, Cooke NE (2004) Neurobeachin is essential for neuromuscular synaptic transmission. *The Journal of neuroscience : the official journal of the Society for Neuroscience* 24: 3627-3636

Sun L, Goff LA, Trapnell C, Alexander R, Lo KA, Hacisuleyman E, Sauvageau M, Tazon-Vega B, Kelley DR, Hendrickson DG *et al* (2013) Long noncoding RNAs regulate adipogenesis. *Proceedings of the National Academy of Sciences of the United States of America* 110: 3387-3392

Sun L, Xie H, Mori MA, Alexander R, Yuan B, Hattangadi SM, Liu Q, Kahn CR, Lodish HF (2011) Mir193b-365 is essential for brown fat differentiation. *Nature cell biology* 13: 958-965

Taft RJ, Pheasant M, Mattick JS (2007) The relationship between non-protein-coding DNA and eukaryotic complexity. *BioEssays : news and reviews in molecular, cellular and developmental biology* 29: 288-299

The-ENCODE-Project-Consortium (2012) An integrated encyclopedia of DNA elements in the human genome. *Nature* 489: 57-74

Tilgner H, Knowles DG, Johnson R, Davis CA, Chakrabortty S, Djebali S, Curado J, Snyder M, Gingeras TR, Guigó R (2012) Deep sequencing of subcellular RNA fractions shows splicing to be predominantly co-transcriptional in the human genome but inefficient for lncRNAs. *Genome research* 22: 1616-1625

Tiraby C, Tavernier G, Lefort C, Larrouy D, Bouillaud F, Ricquier D, Langin D (2003) Acquirement of brown fat cell features by human white adipocytes. *The Journal of biological chemistry* 278: 33370-33376

Tran KV, Brown EL, DeSouza T, Jespersen NZ, Nandrup-Bus C, Yang Q, Yang Z, Desai A, Min SY, Rojas-Rodriguez R *et al* (2020) Human thermogenic adipocyte regulation by the long noncoding RNA LINC00473. *Nature metabolism* 2: 397-412

Tripathi V, Ellis JD, Shen Z, Song DY, Pan Q, Watt AT, Freier SM, Bennett CF, Sharma A, Bubulya PA *et al* (2010) The nuclear-retained noncoding RNA MALAT1 regulates alternative splicing by modulating SR splicing factor phosphorylation. *Molecular cell* 39: 925-938

Tsai MC, Manor O, Wan Y, Mosammaparast N, Wang JK, Lan F, Shi Y, Segal E, Chang HY (2010) Long noncoding RNA as modular scaffold of histone modification complexes. *Science (New York, NY)* 329: 689-693

van Marken Lichtenbelt WD, Vanhommerig JW, Smulders NM, Drossaerts JM, Kemerink GJ, Bouvy ND, Schrauwen P, Teule GJ (2009) Cold-activated brown adipose tissue in healthy men. *The New England journal of medicine* 360: 1500-1508

Van Nguyen TT, Vu VV, Pham PV (2020) Transcriptional Factors of Thermogenic Adipocyte Development and Generation of Brown and Beige Adipocytes From Stem Cells. *Stem cell reviews and reports* 16: 876-892

Vernia S, Edwards YJ, Han MS, Cavanagh-Kyros J, Barrett T, Kim JK, Davis RJ (2016) An alternative splicing program promotes adipose tissue thermogenesis. *eLife* 5

Villanueva CJ, Vergnes L, Wang J, Drew BG, Hong C, Tu Y, Hu Y, Peng X, Xu F, Saez E *et al* (2013) Adipose subtype-selective recruitment of TLE3 or Prdm16 by PPARγ specifies lipid storage versus thermogenic gene programs. *Cell metabolism* 17: 423-435

Villegas VE, Zaphiropoulos PG (2015) Neighboring gene regulation by antisense long non-coding RNAs. *International journal of molecular sciences* 16: 3251-3266

Virtanen KA, Lidell ME, Orava J, Heglind M, Westergren R, Niemi T, Taittonen M, Laine J, Savisto NJ, Enerback S *et al* (2009) Functional brown adipose tissue in healthy adults. *The New England journal of medicine* 360: 1518-1525

Visa N, Puvion-Dutilleul F, Harper F, Bachellerie JP, Puvion E (1993) Intranuclear distribution of poly(A) RNA determined by electron microscope in situ hybridization. *Experimental cell research* 208: 19-34

Volders PJ, Anckaert J, Verheggen K, Nuytens J, Martens L, Mestdagh P, Vandesompele J (2019) LNCipedia 5: towards a reference set of human long non-coding RNAs. *Nucleic acids research* 47: D135-d139

Wang C, Xia T, Du Y, Meng Q, Li H, Liu B, Chen S, Guo F (2013a) Effects of ATF4 on PGC1α expression in brown adipose tissue and metabolic responses to cold stress. *Metabolism: clinical and experimental* 62: 282-289

Wang L, Park HJ, Dasari S, Wang S, Kocher JP, Li W (2013b) CPAT: Coding-Potential Assessment Tool using an alignment-free logistic regression model. *Nucleic acids research* 41: e74

Wang X, Arai S, Song X, Reichart D, Du K, Pascual G, Tempst P, Rosenfeld MG, Glass CK, Kurokawa R (2008) Induced ncRNAs allosterically modify RNA-binding proteins in cis to inhibit transcription. *Nature* 454: 126-130

Wang Y, Hu SB, Wang MR, Yao RW, Wu D, Yang L, Chen LL (2018) Genome-wide screening of NEAT1 regulators reveals cross-regulation between paraspeckles and mitochondria. *Nature cell biology* 20: 1145-1158

Wang Y, Hua S, Cui X, Cao Y, Wen J, Chi X, Ji C, Pang L, You L (2020) The Effect of FOXC2-AS1 on White Adipocyte Browning and the Possible Regulatory Mechanism. *Frontiers in endocrinology* 11: 565483

Wang Z, Willard HF, Mukherjee S, Furey TS (2006) Evidence of influence of genomic DNA sequence on human X chromosome inactivation. *PLoS computational biology* 2: e113

Willingham AT, Orth AP, Batalov S, Peters EC, Wen BG, Aza-Blanc P, Hogenesch JB, Schultz PG (2005) A strategy for probing the function of noncoding RNAs finds a repressor of NFAT. *Science (New York, NY)* 309: 1570-1573

Wrzodek C, Eichner J, Buchel F, Zell A (2013) InCroMAP: integrated analysis of cross-platform microarray and pathway data. *Bioinformatics (Oxford, England)* 29: 506-508

Wu C, Orozco C, Boyer J, Leglise M, Goodale J, Batalov S, Hodge CL, Haase J, Janes J, Huss JW, 3rd *et al* (2009) BioGPS: an extensible and customizable portal for querying and organizing gene annotation resources. *Genome biology* 10: R130

Wu J, Bostrom P, Sparks LM, Ye L, Choi JH, Giang AH, Khandekar M, Virtanen KA, Nuutila P, Schaart G *et al* (2012) Beige adipocytes are a distinct type of thermogenic fat cell in mouse and human. *Cell* 150: 366-376

Wu J, Cohen P, Spiegelman BM (2013) Adaptive thermogenesis in adipocytes: is beige the new brown? *Genes & development* 27: 234-250

Wulf A, Harneit A, Kröger M, Kebenko M, Wetzel MG, Weitzel JM (2008) T3-mediated expression of PGC-1alpha via a far upstream located thyroid hormone response element. *Molecular and cellular endocrinology* 287: 90-95

Xiao T, Liu L, Li H, Sun Y, Luo H, Li T, Wang S, Dalton S, Zhao RC, Chen R (2015) Long Noncoding RNA ADINR Regulates Adipogenesis by Transcriptionally Activating C/EBPα. *Stem cell reports* 5: 856-865

Xiong Y, Yue F, Jia Z, Gao Y, Jin W, Hu K, Zhang Y, Zhu D, Yang G, Kuang S (2018) A novel brown adipocyte-enriched long non-coding RNA that is required for brown adipocyte differentiation and sufficient to drive thermogenic gene program in white adipocytes. *Biochimica et biophysica acta Molecular and cell biology of lipids* 1863: 409-419

Xu B, Gerin I, Miao H, Vu-Phan D, Johnson CN, Xu R, Chen XW, Cawthorn WP, MacDougald OA, Koenig RJ (2010) Multiple roles for the non-coding RNA SRA in regulation of adipogenesis and insulin sensitivity. *PloS one* 5: e14199

Xue B, Coulter A, Rim JS, Koza RA, Kozak LP (2005) Transcriptional synergy and the regulation of Ucp1 during brown adipocyte induction in white fat depots. *Molecular and cellular biology* 25: 8311-8322

Yap KL, Li S, Muñoz-Cabello AM, Raguz S, Zeng L, Mujtaba S, Gil J, Walsh MJ, Zhou MM (2010) Molecular interplay of the noncoding RNA ANRIL and methylated histone H3 lysine 27 by polycomb CBX7 in transcriptional silencing of INK4a. *Molecular cell* 38: 662-674

Yoneshiro T, Aita S, Matsushita M, Kayahara T, Kameya T, Kawai Y, Iwanaga T, Saito M (2013) Recruited brown adipose tissue as an antiobesity agent in humans. *The Journal of clinical investigation* 123: 3404-3408

You L, Zhou Y, Cui X, Wang X, Sun Y, Gao Y, Wang X, Wen J, Xie K, Tang R *et al* (2018) GM13133 is a negative regulator in mouse white adipocytes differentiation and drives the characteristics of brown adipocytes. *Journal of cellular physiology* 233: 313-324

Young P, Arch JR, Ashwell M (1984) Brown adipose tissue in the parametrial fat pad of the mouse. *FEBS letters* 167: 10-14

Zeng C, Fukunaga T, Hamada M (2018) Identification and analysis of ribosome-associated lncRNAs using ribosome profiling data. *BMC genomics* 19: 414

Zhang P, Wu W, Chen Q, Chen M (2019) Non-Coding RNAs and their Integrated Networks. *Journal of integrative bioinformatics* 16

Zhang W, Yue X, Tang G, Wu W, Huang F, Zhang X (2018) SFPEL-LPI: Sequence-based feature projection ensemble learning for predicting LncRNA-protein interactions. *PLoS computational biology* 14: e1006616

Zhang Y, Ma Y, Gu M, Peng Y (2020) lncRNA TUG1 promotes the brown remodeling of white adipose tissue by regulating miR-204-targeted SIRT1 in diabetic mice. *International journal of molecular medicine* 46: 2225-2234

Zhao J, Song X, Wang K (2016) lncScore: alignment-free identification of long noncoding RNA from assembled novel transcripts. *Scientific reports* 6: 34838

Zhao XY, Li S, Wang GX, Yu Q, Lin JD (2014) A long noncoding RNA transcriptional regulatory circuit drives thermogenic adipocyte differentiation. *Molecular cell* 55: 372-382

Zhao XY, Lin JD (2015) Long Noncoding RNAs: A New Regulatory Code in Metabolic Control. *Trends in biochemical sciences* 40: 586-596

Zhu E, Zhang J, Li Y, Yuan H, Zhou J, Wang B (2019) Long noncoding RNA Plnc1 controls adipocyte differentiation by regulating peroxisome proliferator-activated receptor gamma. *FASEB journal : official publication of the Federation of American Societies for Experimental Biology* 33: 2396-2408

Ziegler C, Kretz M (2017) The More the Merrier-Complexity in Long Non-Coding RNA Loci. *Frontiers in endocrinology* 8: 90

Zuckerman B, Ulitsky I (2019) Predictive models of subcellular localization of long RNAs. *RNA (New York, NY)* 25: 557-572

6 APPENDIX

6.1 SUPPLEMENT DATA

Table S1: Protocol for Seahorse respirometry.

process	time
calibration of probes	
equilibration	12 min
loop (3 times)	
mixing	2 min
time delay	2 min
measurement	3 min
injection of port A	
loop (3 times)	
mixing	2 min
time delay	2 min
measurement	3 min
injection of port B	
loop (5 times)	
mixing	2 min
time delay	2 min
measurement	3 min
injection of port C	
loop (3 times)	
mixing	2 min
time delay	2 min
measurement	3 min
injection of port D	
loop (3 times)	
mixing	2 min
time delay	2 min
measurement	3 min

Table S2: GO term analysis of regulated genes 10 Mbs downstream of *Ctcflos* blast hits of interest. GO term analysis performed by InCroMAP software (Wrzodek et al, 2013).

#	GO-term	P-value
1	protein ubiquitination	1,01E-10
2	cytoplasmic stress granule	2,09E-09
3	protein phosphatase 1 binding	3,73E-08
4	**ribonucleoprotein complex**	4,22E-08
5	**mRNA binding**	2,54E-07
6	ubiquitin-dependent protein catabolic process	3,36E-07
7	cellular response to laminar fluid shear stress	4,35E-07
8	**transcription regulator complex**	5,39E-07
9	**fat cell differentiation**	9,70E-07
10	heart process	1,04E-06
11	double-stranded RNA binding	1,43E-06
12	RNA polymerase II-specific DNA-binding transcription factor binding	2,50E-06
13	transcription coregulator binding	3,47E-06
14	ear development	4,42E-06
15	regulation of embryonic development	4,94E-06
16	regulation of apoptotic process	7,01E-06
17	protein stabilization	8,39E-06
18	production of miRNAs involved in gene silencing by miRNA	8,67E-06
19	magnesium ion binding	9,81E-06
20	angiogenesis	2,37E-05
21	positive regulation of intrinsic apoptotic signaling pathway	2,48E-05
22	mRNA stabilization	2,72E-05
23	microtubule binding	3,13E-05
24	nuclear body	3,29E-05
25	negative regulation of G1/S transition of mitotic cell cycle	3,38E-05
26	ATP metabolic process	3,52E-05
27	collagen-containing extracellular matrix	4,00E-05
28	positive regulation of protein-containing complex assembly	4,27E-05
29	chromatin	4,58E-05
30	gene silencing by RNA	5,25E-05

Table S3: Regulation of genes 10 Mbs up- and downstream of *Ctcflos* blast hits of interest.
Regulated genes 10 Mbs up- and downstream of *Ctcflos* DNA-blast hits of interest. Regulation by *Ctcflos* KD (left) and regulation during brite adipocyte differentiation (right), green color indicates downregulation, red color indicates upregulation.

2:76225865-76225883		reg. by Ctcflos KD	reg. by browning
upstream			
AK004093	Scn7a	down	up
AK148698	AK148698	down	down
AK081657	AK081657	down	up
AK160605	AK160605	down	up
NM_001110512	Mettl8	down	up
AK037504	A130022F02Rik	down	up
AK083717	Itga6	down	up
NM_177784	Klhl23	up	down
AK149068	AK149068	up	up
ENSMUST00000152371	Nfe2l2	up	up
downstream			
NM_011871	Prkra	down	up
ENSMUST00000099944	Calcrl	down	up
ENSMUST00000111641	Serping1	down	up
AK089975	Rbm45	up	down
AK017712	Ssfa2	up	up
NM_175514	Fam171b	up	down

2:132465636-132465674			
upstream			
AK005218	1500011K16Rik	down	up
AK011959	Tmem87b	down	up
AK048328	1700037H04Rik	down	up
NM_001004174	AA467197	up	up
AK166116	Dut	up	down
AK011490	Bcl2l11	up	down
AK014355	AK014355	up	down
AK042594	Gm4430	up	down
ENSMUST00000110277	Pced1a	up	down
AK008279	Itpa	up	down
ENSMUST00000151143	Smox	up	down
AK018504	Rassf2	up	down
downstream			
AK086966	E030016H06Rik	down	up
AK032753	AK032753	down	up
AK045691	AK045691	down	up
ENSMUST00000147744	Plcb4	down	up
AK008406	Mkks	down	up
AK009123	Ndufaf5	down	up

2:173113379-173114093			
upstream			
AK032033	Elmo2	down	up
ENSMUST00000059826	Kcnb1	down	up
AK013774	Tshz2	down	up
NM_029761	Dok5	down	down
ENSMUST00000164863	ENSMUST00000164863	up	up
ENSMUST00000149287	Dbndd2	up	up
AK005002	Stau1	up	down
NM_008968	Ptgis	up	down
AK003584	Rnf114	up	up
downstream			
AK149415	AK149415	down	up
ENSMUST00000120437	ENSMUST00000120437	down	up
AK011539	Ppp1r3d	down	up
AK079276	Znf512b	down	down
ENSMUST00000168292	ENSMUST00000168292	up	down
AK075846	Ythdf1	up	down

3:49082197-49082227		reg. by Ctcflos KD	reg. by browning
upstream			
AK045813	D3Ertd751e	down	up
AK049332	Phf17	up	up
downstream			
NM_030595	Nbea	down	down
AK036560	Pcdh18	up	down
AK149340	Ccrn4l	up	up
AK163846	Naa15	up	down
ENSMUST00000182246	Rfxap	up	up
AK043552	Mab21l1	up	down
AK134603	Tm4sf1	up	down
AK011504	Wwtr1	up	up
AK017449	Tsc22d2	up	down

4:45679551-45679582			
upstream			
AK150864	Mob3b	down	up
ENSMUST00000117696	ENSMUST00000117696	down	up
AK005286	Aptx	down	up
AK076642	Aqp7	down	up
AK042005	AK042005	up	up
AK005099	Dcaf12	up	up
AK083821	Vcp	up	down
ENSMUST00000140005	Ccdc107	up	down
NM_027511	Hrct1	up	up
downstream			
AK020313	Slc25a51	down	up
AK134030	Col15a1	down	up
ENSMUST00000140008	Fbxo10	up	down
ENSMUST00000121512	ENSMUST00000121512	up	up
AK011381	Msantd3	up	down
AK043792	Tmeff1	up	down
ENSMUST00000117914	ENSMUST00000117914	up	down
AK141244	Klf4	up	down

4:121001232-121001269			
upstream			
AK040809	Trabd2b	down	down
AK078882	Cyp4b1	down	up
AK004728	Mast2	down	down
NM_146256	Hpdl	down	up
AK136442	St3gal3	down	up
AK047461	Lurap1	up	up
AK172415	Rnf220	up	down
AK083459	Cdc20	up	down
AK010418	Ccdc23	up	down
ENSMUST00000145976	Ybx1	up	down
AK006290	Ppcs	up	up
ENSMUST00000144114	Exo5	up	down
downstream			
ENSMUST00000106150	Eva1b	down	down
ENSMUST00000152762	Ak2	down	up
AK146959	Mycl	up	down
AK160589	Pabpc4	up	down
AK132422	AK132422	up	down
ENSMUST00000067277	D130007C19Rik	up	down
NM_010213	Fhl3	up	down
AK078163	Snip1	up	down
AK076962	Sh3d21	up	up
AK149904	Adprhl2	up	up
AK141219	Ago1	up	down
ENSMUST00000143632	Phc2	up	down
AK015966	Rnf19b	up	down
AK079390	Marcksl1	up	down
ENSMUST00000105998	Tinagl1	up	down

Table S4: Predicted RBM41 binding sites within *Ctcflos* isoform 1. RBM41 binding site prediction within *Ctcflos* tr1 using RBPmap (Paz *et al*, 2014).

Position in *Ctcflos*	Motif	K-mer	Z-score	P-value
595	uacuu	gacuu	1.962	2.49e-02
599	uacuu	uccuu	1.962	2.49e-02
861	wuacwuk	auacaua	3.099	9.71e-04
862	uacuu	uacau	2.865	2.09e-03
865	wuacwuk	auacauu	3.321	4.48e-04
866	uacuu	uacau	2.865	2.09e-03
869	wuacwuk	auucuuu	2.667	3.83e-03
870	uacuu	uucuu	2.183	1.45e-02

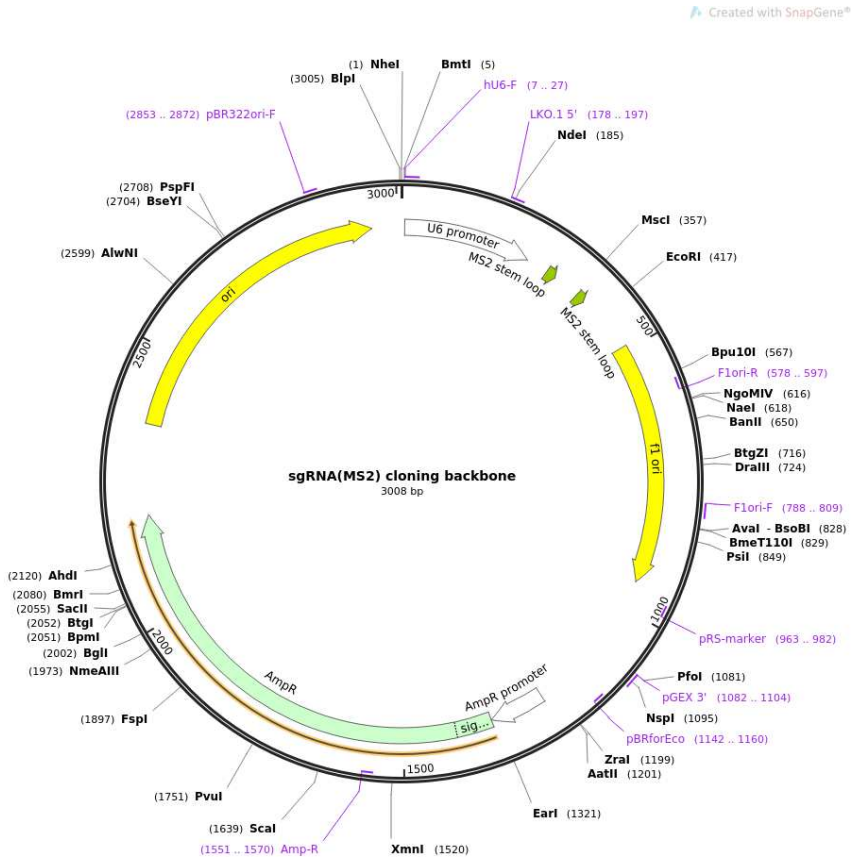

Figure S1: Vector card of sgRNA(MS2) cloning backbone (Addgene 61424).

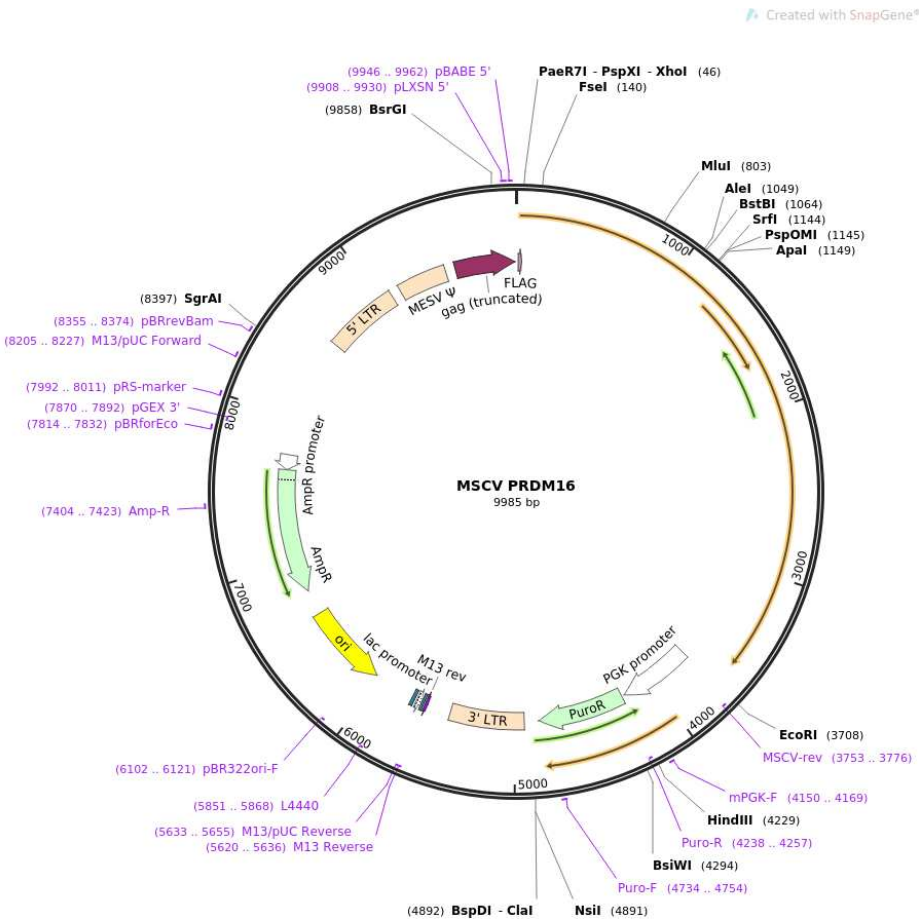

Figure S2: Vector card of MSCV-Prdm16 vector (Addgene 15504).

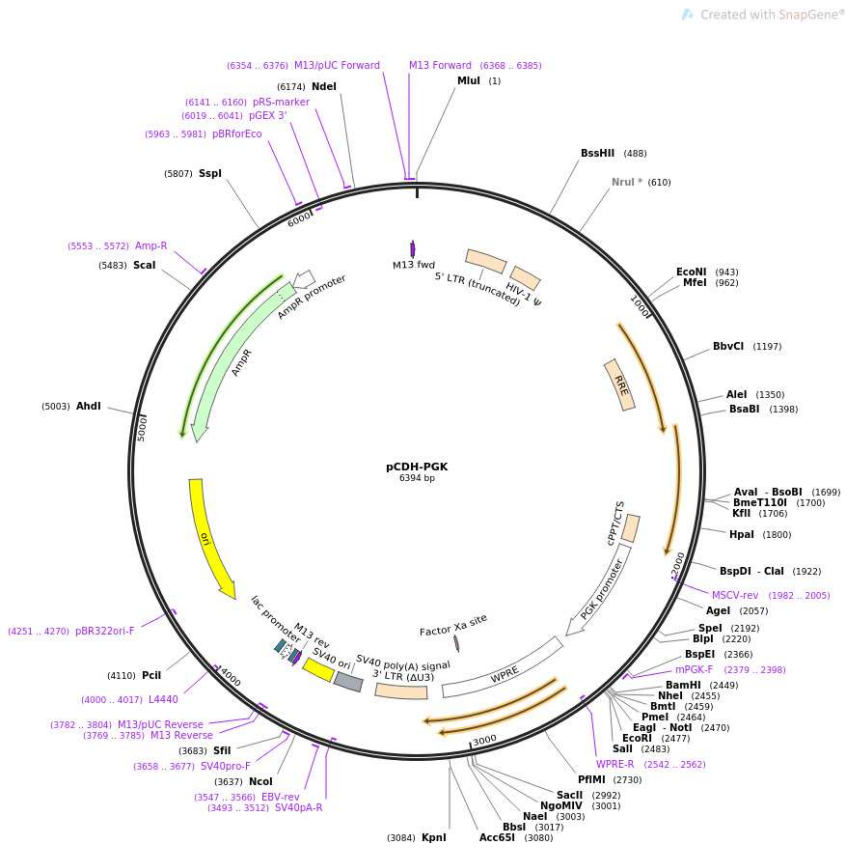

Figure S3: Vector card of pCDH-PGK lentiviral overexpression vector (Addgene 72268).

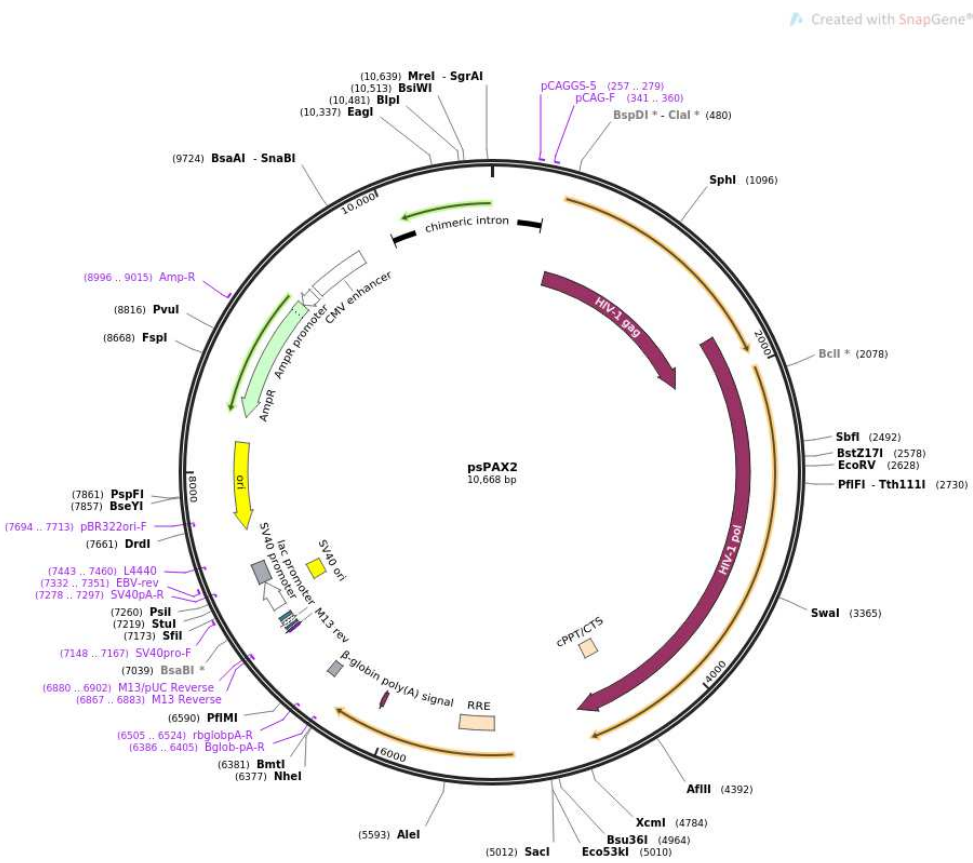

Figure S4: Vector card of psPAX2 packaging plasmid (Addgene 12260).

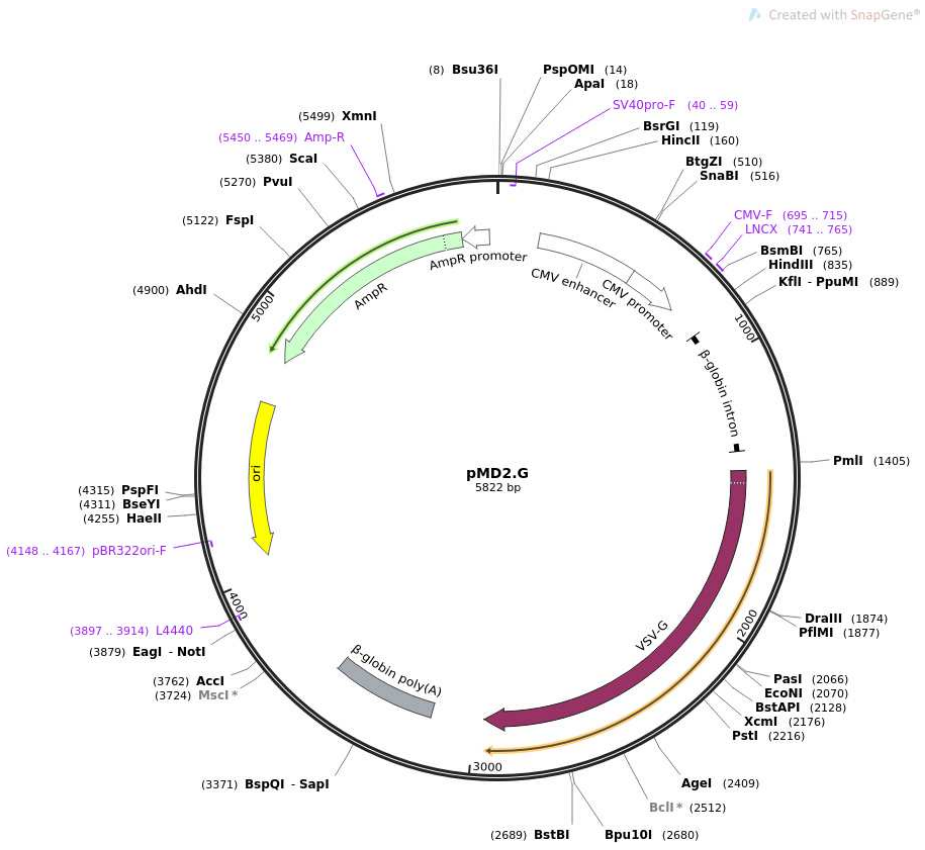

Figure S5: Vector card of pMD2.G envelope plasmid (Addgene 12259).

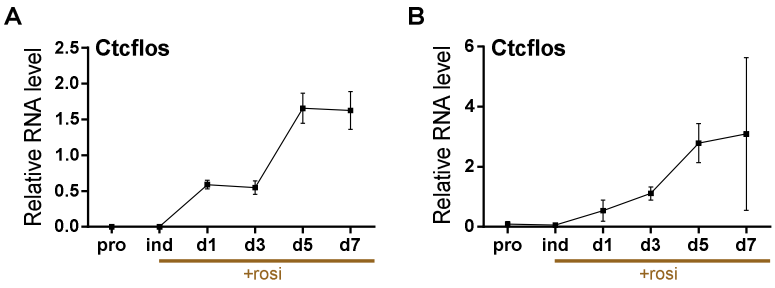

Figure S6: Time course of *Ctcflos* expression during brite adipogenesis. (A, B) Time course of relative *Ctcflos* expression across proliferation, induction and differentiation of primary brite adipocytes derived from iWAT of 129S6 mice (transcript levels relative to *Gtf2b*), assessed by qPCR. Mean ± SD, n=2-3 (technical replicates). The experiment was conducted in total for three times. For the third replicate see (Fig. 13. A).

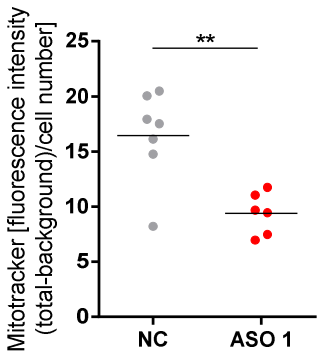

Figure S7: Mitochondrial staining of *Ctcflos* KD and control cells. Quantification of Mito Tracker staining as whole image fluorescence intensity subtracted by background and normalized to cell number. Mean and individual values, n=6-7 (technical replicates), this experiment represents the second biological replicate of mitochondrial staining, for the first biological replicate see (Fig. 21 F), unpaired t test. Modified from (Bast-Habersbrunner *et al.*, 2021).

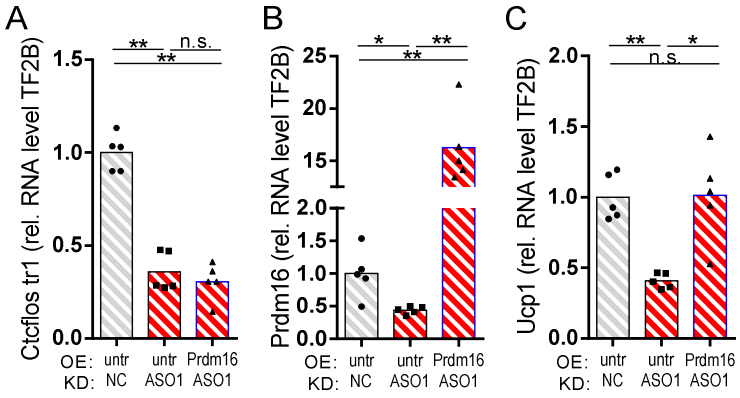

Figure S8: Comparison of *Prdm16* overexpressing with virus-untreated control cells. (A) *Ctcflos* tr1, **(B)** *Prdm16* and **(C)** *Ucp1* transcript levels relative to *Gtf2b* in primary iWAT cells infected with *Prdm16*-expressing viral particles at the second day of proliferation or untreated, followed by reverse transfection at the first day of differentiation using non-targeting control or *Ctcflos* tr1-targeting ASO1. Gene expression analyzed 72 hours later by qPCR. Mean and individual values. Each graph presents

pooled data from two experiments with slightly varying virus titers. RM One-way ANOVA (Tukey-test). N.s. p>0.05, *p<0.05, **p<0.01. Modified from (Bast-Habersbrunner *et al.*, 2021).

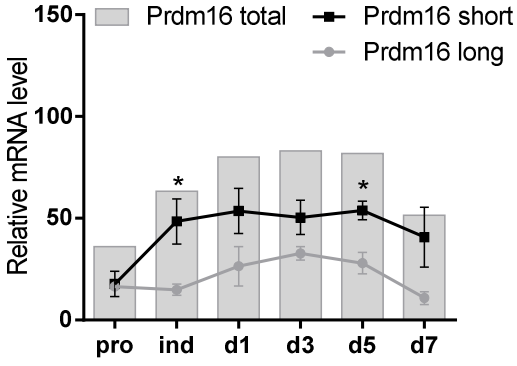

Figure S9: Time course of *Prdm16* short and long isoform expression during brite adipogenesis. Time course of *Prdm16* total, long and short isoform expression relative to *Gtf2b* during brite adipogenesis, assessed by qPCR using isoform specific primers. Mean values ± SD, the experiment was performed twice, for the second biological replicate see (Fig. 25 B), Two-way ANOVA (Šídák-test). *p< 0.05.

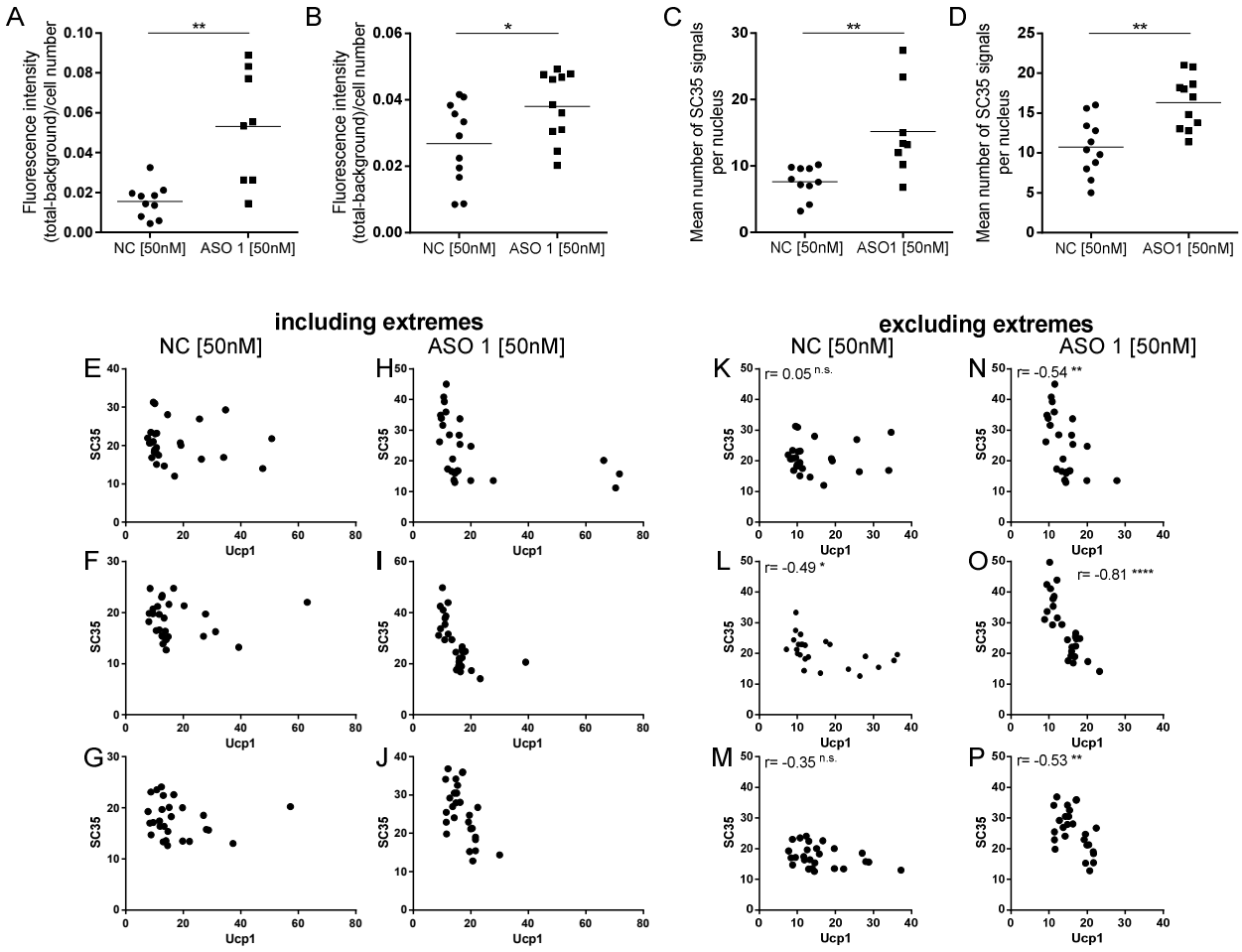

Figure S10: Immunocytochemical analysis of SC35. (A, B) Quantification of SC35 fluorescence signal from immunocytochemistry as whole image fluorescence intensity subtracted by background and normalized to total cell number. Mean and individual values, n=8-11 (technical replicates) the

experiment was performed for a total of three times, for the third experiment see (Fig. 43 C), unpaired t tests. **(C, D)** Quantification of nuclear speckle number from immunocytochemistry as mean number of SC35 signals per nucleus. Mean and individual values, n=8-11 (technical replicates) the experiment was performed for a total of three times, for the third experiment see (Fig. 43 D), unpaired t tests. **(E-P)** Correlation of SC35 and UCP1 fluorescence signals in immunocytochemistry across individual cells in (E-G, K-M) control and (H-J, N-P) Ctcflos tr1 KD (ASO1) cells. (E-J) Extreme values are included. (K-D) Extreme values were excluded to avoid distortion of correlation analysis. The experiment was performed for a total of four times, for the fourth experiment see (Fig. 43 E, F). Pearson correlation. N.s. $p>0.05$, *$p<0.05$, **$p<0.01$, ****$p<0.0001$. Modified from (Bast-Habersbrunner *et al.*, 2021)

6.2 KEY RESOURCES TABLE

LNA Gapmer ASOs and siRNAs	Sequence	Source
LNA Gapmer ASO1 (Ctcflos tr 1)	5'- GCTTGGGTGGAGGATT -3'	Qiagen
LNA Gapmer ASO2 (Ctcflos tr 3+4)	5'- ATTTGACAACCACTG - 3'	Qiagen
LNA Gapmer ASO3 (Ctcflos tr 1)	5'- GCTTGGGTGGAGGATT -3'	Qiagen
LNA Gapmer ASO4 (Ctcflos tr 1)	5'- CTGGCTTGGGTGGAGG -3'	Qiagen
LNA Gapmer ASO5 (Ctcflos tr 3+4)	5'- AGTCAGACACCTTTTA -3'	Qiagen
LNA Gapmer ASO6 (Ctcflos tr 3+4	5'- AGACTAATTGCTAGCG -3'	Qiagen
LNA Gapmer Negative control	5'- AACACGTCTATACGC -3'	Qiagen
LNA Gapmer ASO all (Neat1 tr long)	5'- TCTAGAGAGTGGTGTA -3'	Qiagen
LNA Gapmer ASO all (Neat1 tr long+short)	5'- AGAAGATGCAGCAGTC -3'	Qiagen
dsiRNA (Ctcfl)	5'- GAATTCTAAAGTCAACCTGAGAATC -3'	IDT
siRNA (Pck1)	5'- GGAAGTTCGTGGAAGGCAA -3'	Eurofins Genomics
siRNA (Rrdm16)	5'- GAAGAGCGTGAGTACAAATTT -3'	Eurofins Genomics
Primers used for qPCR		
Gtf2b for	F: 5'- TGGAGATTTGTCCACCATGA -3'	Eurofins Genomics
Gtf2b rev	R: 5'- GAATTGCCAAACTCATCAAAACT -3'	Eurofins Genomics
Ctcflos tr1 for	F: 5'- ACTGTCCAGGTCCCTAACCC -3'	Eurofins Genomics
Ctcflos tr1 rev	R: 5'- GACTCCCTGCTTGGAGAAGA -3'	Eurofins Genomics
Ctcflos tr3+4b for	F: 5'- CCCCAGAACAAGAAGAGCTG -3'	Eurofins Genomics
Ctcflos tr3+4b rev	R: 5'- CGAGTATTGGAGAAGGACAGC -3'	Eurofins Genomics
Ucp1 for	F: 5'- GTACACCAAGGAAGGACCGA -3'	Eurofins Genomics
Ucp1 rev	R: 5'- TTTATTCGTGGTCTCCCAGC -3'	Eurofins Genomics
pre-Ucp1 for	F: 5'- GGATTGGCCTCTACGACTCA -3'	Eurofins Genomics
pre-Ucp1 rev	R: 5'- TAAGCTTCTCTGGGACCGTG -3'	Eurofins Genomics
45SrRNA for	F: 5'- CTTGACCATGTCCCCAGAGT -3'	Eurofins Genomics
45SrRNA rev	R: 5'- AGGCACCTAGGAGACAAACC -3'	Eurofins Genomics
12SrRNA for	F: 5'- ACACGACAGCTAAGACCCAA -3'	Eurofins Genomics
12SrRNA rev	R: 5'- GGTAGAGCGGGGTTTATCGA -3'	Eurofins Genomics
Cidea for	F: 5'- TGCTCTTCTGTATCGCCCAGT -3'	Eurofins Genomics
Cidea rev	R: 5'- GCCGTGTTAAGGAATCTGCTG -3'	Eurofins Genomics
Cox7a1 for	F: 5'- CCGACAATGACCTCCCAGTA -3'	Eurofins Genomics
Cox7a1 rev	R: 5'- TGTTTGTCCAAGTCCTCCAA -3'	Eurofins Genomics
Atgl for	F: 5'- GGAAATTGGGTGACCATCTG -3'	Eurofins Genomics
Atgl rev	R: 5'- AAGGCCACATTGGTGCAG -3'	Eurofins Genomics
Hsl for	F: 5'- GCTTGGTTCAAGTGGAGAGC -3'	Eurofins Genomics
Hsl rev	R: 5'- GCCTAGTGCCTTCTGGTCTG -3'	Eurofins Genomics
Fabp4 for	F: 5'- GATGGTGACAAGCTGGTGGT -3'	Eurofins Genomics
Fabp4 rev	R: 5'- TTTATTTAATCAACATAACCATATCCA -3'	Eurofins Genomics
Leptin for	F: 5'- TTCACACACGCAGTCGGTATC -3'	Eurofins Genomics
Leptin rev	R: 5'- TGGTCCATCTTGGACAAACTCA -3'	Eurofins Genomics
Prdm16 short for	F: 5'- GTACCCTGGCTTTGGACTCT -3',	Eurofins Genomics
Prdm16 short rev	R: 5'- GTACCCTGGCTTTGGACTCT -3'	Eurofins Genomics
Prdm16 long for	F: 5'- CTTTGGGAAGGGGCTGGAT -3'	Eurofins Genomics
Prdm16 long rev	R: 5'- GGTTAAAGGCTCCGGACTCT -3'	Eurofins Genomics
Prdm16 total for	F: 5'- GTCAGAGGAGAAATTTGATGG -3'	Eurofins Genomics

Prdm16 total rev	R: 5’- AGAAGGAATGCTGTGAGTAG -3’	Eurofins Genomics
Ctcfl for	F: 5’- AGAGGACCCACAAGAACGAG -3’	Eurofins Genomics
Ctcfl rev	R: 5’- AGTAGCTGCTTCTGTCGGAA -3’	Eurofins Genomics
Pck1 for	F: 5’- GTGAGGAAGTTCGTGGAAGG -3’	Eurofins Genomics
Pck1 rev	R: 5'- AGTGAGAGCCAGCCAACAGT -3’	Eurofins Genomics
Neat1 long and short for	F: 5'- CTGTCTGCTGGCACTTGAC -3'	Eurofins Genomics
Neat1 long and short rev	R: 5'- TCCAGCACCGACTCTACATC -3'	Eurofins Genomics
Neat1 long for	F: 5'- TGCTTTGTTTGCCTGACTCC -3'	Eurofins Genomics
Neat1 long rev	R: 5'- TGAAACTACCAGGCTGAGGG -3'	Eurofins Genomics
Primers used for PCR		
Ctcflos tr1 for	F: 5’- GAGCTTGGAGGAAGTGAACG -3’	Eurofins Genomics
Ctcflos tr1 rev	R: 5’- TCAAGGGACGATCTTTCCAG -3’	Eurofins Genomics
Ctcflos tr2 for	F: 5’- GCAGTGAAACCTTCCAGAGC-3’	Eurofins Genomics
Ctcflos tr2 rev	R: 5’- AAGTGATTCCAAGTGTCACCA -3’	Eurofins Genomics
Ctcflos tr3+4a for	F: 5’- GCTGTCCTTCTCCAATACTCG-3’	Eurofins Genomics
Ctcflos tr3+4a rev	R: 5’- GGGGTTAGGACAAAGAAGCTC -3’	Eurofins Genomics
Ctcflos tr3+4b for	F: 5’- CCCCAGAACAAGAAGAGCTG -3’	Eurofins Genomics
Ctcflos tr3+4b rev	R: 5’- CGAGTATTGGAGAAGGACAGC -3’	Eurofins Genomics
Ctcflos tr4 for	F: 5’- CCCCAGAACAAGAAGAGCTG -3‘	Eurofins Genomics
Ctcflos tr4 rev	R: 5’- TTCTCTTCTCCCCACCCTTG -3’	Eurofins Genomics
Prdm16 s+l for	F: 5’- GAGCCCCAAGGAGTCTATGA -3’	Eurofins Genomics
Prdm16 s+l rev	R: 5’- CGAGGGTCCTGTGATGTTCAA -3’	Eurofins Genomics
Insr +/-exon11 for	F: 5’- GAGGATTACCTGCACAACG -3’	Eurofins Genomics
Insr +/-exon11 rev	R: 5’- TTCCTTTGGCTCTTGCCAC -3’	Eurofins Genomics
sgRNAs for CRISPRa(SAM)-mediated OE		
Ctcflos sgRNA 1	5'- AACACACTTGCGTCATTACT -3'	Eurofins Genomics
Ctcflos sgRNA 2	5'- ATTCTTTCTGTGTTTATTC -3'	Eurofins Genomics
Ctcflos sgRNA 3	5'- AAAATAGCCACAGCAGAAAG -3'	Eurofins Genomics
Ctcflos sgRNA 4	5'- GGAGTGACGCGCGGCTGGG -3'	Eurofins Genomics

Antibodies	**Cat. Nr.**	**Source**
rabbit anti-UCP1 (for immunoblot)	Cat# AB23841	Abcam
rabbit anti-COX4 (for immunoblot)	Cat# 4844	Cell Sign. Technology
mouse anti-Actinb (for immunoblot)	Cat# MAB1501	EMD Millipore
goat anti-rabbit IRDye 800 CW (for immunoblot)	Cat# 926-32211	Li-Cor
donkey anti-mouse IRDye 680 CW (for immunoblot)	Cat# 926-68072	Li-Cor
rabbit anti-UCP1 (for ICC)	Cat# AB10983	Abcam
mouse anti-SC35 (for ICC)	Cat# AB11826	Abcam
Alexa Fluor 647 donkey anti-mouse IgG (for ICC)	Cat# A-31571	Invitrogen
Alexa Fluor 546 donkey anti-rabbit IgG (for ICC)	Cat# A-10040	Life Technologies

Chemicals	Cat. Nr.	Source
100 bp-DNA Ladder	Cat# T833	Carl Roth
1k bp-DNA Ladder	Cat# Y014	Carl Roth
Acetic acid	Cat# 6755.1	Carl Roth
Amphotericine B	Cat# A2612	Biochrom
AMPure magnetic beads	Cat# A63881	Beckman Coulter
Antimycin A	Cat# A8674	Sigma-Aldrich
BbsI-HF restriction enzyme	Cat# R3539S	NEB
β-mercaptoethanol	Cat# M3148	Sigma-Aldrich
Bovine serum al+A8:C52bumin (BSA) fraction V	Cat# 8076	Carl Roth
Bovine serum albumin (BSA) Fatty Acid Free	Cat# A3803-100G	Sigma-Aldrich
Bromphenol blue	Cat# B0126	Sigma-Aldrich
Chloroform p.a.	Cat# Y015.1	Carl Roth
Collagenase A	Cat# C 1-22	Biochrom
Cover glasses, Menzel Gläser	Cat# MENZBB024060M113	VWR
DEPC	Cat# D5758	Sigma-Aldrich
Dexamethasone	Cat# D4902	Sigma-Aldrich
DME (base)	Cat# D5030-10x1L	Sigma-Aldrich
DMEM	Cat# D5796	Sigma-Aldrich
DMSO	Cat# 4720	Carl Roth
Donkey serum	Cat# D9663	Sigma-Aldrich
EcoRI-HF restriction enzyme	Cat# R3101S	NEB
EDTA	Cat# V432B	Promega
Ethanol 70%, denatured	Cat# T913	Carl Roth
Ethanol 96%, denatured	Cat# T171	Carl Roth
Ethanol 99.8% p.a.	Cat# 9065	Carl Roth
Exonuclease I	Cat# M0293S	NEB
FCCP	Cat# C2920-10MG	Sigma-Aldrich
Fetal bovine serum (FBS)	Cat# S0615	Biochrom
Free Glycerol reagent	Cat# F6428	Sigma-Aldrich
Gentamycin	Cat# A2712	Biochrom
Glucose	Cat# HN06	Biochrom
Glutamax	Cat# 35050-061	Life Technologies
Glycerin	Cat# 3783	Carl Roth
Hank's balanced salt solution (HBSS) w/Mg;Ca	Cat# 14025-050	Invitrogen
HCl	Cat# 0281	Carl Roth
HDGreen Plus	Cat# ISII-HDGreen Plus	Intas
Indomethacin	Cat# I7378	Sigma-Aldrich
Insulin	Cat# I9278-5ML	Sigma-Aldrich
Isobutylmethylxanthine	Cat# I5879	Sigma-Aldrich
Isoginkgetin	Cat# 6483	Tocris
Isoproterenol	Cat# I6504-100MG	Sigma-Aldrich
Lipofectamin RNAiMax	Cat# 13778150	Thermo Scientific
Magnesium cloride	Cat# M8266	Sigma-Aldrich
Mitotracker Deep Red 633	Cat# M22426	Invitrogen
Nitrocellulose	Cat# 926-31092	Li-Cor
NP-40	Cat# NP40S	Sigma-Aldrich
Nuclease-free water	Cat# 129114	Qiagen

Oil Red O	Cat# O0625	Sigma-Aldrich
Oligomycin	Cat# O4876-5mg	Sigma-Aldrich
OptiMEM	Cat# 31985062	Thermo Fisher
PEG-it Virus precipitation solution	Cat# LV810A-1	System Biosciences
Penecillin/Streptomycin	Cat# A2212	Biochrom
Phenol red	Cat# P3532	Sigma-Aldrich
Phosphate Buffered Saline (PBS) Tablets	Cat# 18912-014	Gibco
Phusion High-Fidelity DNA polymerase	Cat# F530S	Thermo Scientific
PmeI restriction enzyme	Cat# R0560S	NEB
Polybrene	Cat# TR-1003-G	Sigma-Aldrich
PolyFext transfection reagent	Cat# 301105	Qiagen
Potassium chloride	Cat# P9541	Sigma-Aldrich
Rapid ligase buffer (2x)	Cat# B101	Enzymatics
Rosiglitazone	Cat# Cay71740	Biomol
SensiMix SYBR no Rox	Cat# QT650-20	BioLine
Sodium chloride	Cat# 3957	Carl Roth
Sodium deoxycholat	Cat# D6750	Sigma-Aldrich
Sodium pyruvate solution 100 mM	Cat# 11360-070	Gibco
Sucrose	Cat# 84097	Sigma-Aldrich
SuperScriptTM II Reverse Transcriptase	Cat# 18064014	Lifetech
T3	Cat# T6397	Sigma-Aldrich
T4 DNA ligase	Cat# M0202S	NEB
T4 ligase buffer	Cat# B0202S	NEB
T4 PNK	Cat# M0201S	NEB
T7 ligase	Cat# L6020L	Enzymatics
TEMED	Cat# 2367	Carl Roth
Tris	Cat# 4855	Carl Roth
TRISure	Cat# BIO-38033	Bioline
Triton X-100	Cat# 85111	Thermo Scientific
Trypsin	Cat# 59417C	Sigma-Aldrich
Vectashield Mounting Medium	Cat# VEC-H-1000	Biozol
XF calibrant buffer	Cat# 100840-000	Agilent technologies

Commercial Kit Systems	**Cat#**	**Source**
DNA clean and concentrator kit	Cat# D4014	Zymo Research
High Output v2 kit	Cat# FC-404-2005	Illumina
High Sensitivity NGS Fragment Analysis kit	Cat# DNF-474	Advanced Analytical
ImmoMix	Cat# BIO-25020	Bioline
One-Wash Lentivirus Titer Kit HIV-1 p24 Elisa Assay	Cat# TR30038	Origene
Pierce BCA Protein Assay Kit	Cat# 23225	Thermo Scientific
PolyATract mRNA isolation system	Cat# Z5310	Promega
PureYield Plasmid Miniprep System	Cat# A1223	Promega
Qubit dsDNA HS Assay kit	Cat# Q32851	Invitrogen
RNA 6000 Nano kit	Cat# 5067-1511	Agilent
SensiFast cDNA Synthesis Kit	Cat# BIO-65054	BioLine
SensiMix Sybr no Rox	Cat# QT650-20	BioLine
Seahorse XF96 fluxPak	Cat# 102310-001	Agilent
SV Total RNA Isolation System	Cat# Z3105	Promega
Wizard SV Gel and PCR Clean-Up system	Cat# A9281	Promega

Equipment, Devices, Disposals	Cat#	Source
Cell strainer, 40 µM	Cat# 352340	BD Biosciences
Dounce Homogenizer (type B pestle) 0.0005-0.0025 in	Cat# 885300-0001	DWK Life Sciences
Falcon tube (50 ml)	Cat# 62.547.254	Sarstedt
Falcon tube (15 ml)	Cat# 62.554.502	Sarstedt
FlexiPERM slide	Cat# 94.6032.039	Sarstedt
Illumina HighSeq4000	N/A	Illumina
Illumina NextSeq500	N/A	Illumina
Infinite M200 Microplate reader	Cat# 30016056	Tecan
LI-COR Odyssey Infrared Imaging System	Ody-2197	Li-Cor
Lightcycler 480 (384 well)	5015243001	Roche
Matrix Electronic 384 Equalizer Pipette	Cat# 2139-11	Thermo Scientific
Micro 96 well plate nunc	Cat# 260895	VWR
Microvettes coated with lithium heparin	Cat# 16.443	Sarstedt
neoVortex Vortex Mixer	Cat# D-6012	neoLAB
Nitrocellulose membrane	Cat# 926-31092	Li-Cor
Nylon Mesh 250 µm	Cat# 510-9526	VWR
Olympus FluoView FV10i	N/A	Olympus
PCR tubes	Cat# 72.991.992	Sarstedt
Pipette tips (0.5-10, 10-100, 100-1000 µl)	Cat# 70.1130, 70.760.002, 70.762	Sarstedt
Precise shaking incubator	N/A	WiseCube®WIS-20
SuperFrost Microscope slides	Cat# 12372098	Thermo Scientific
Thermomixer comfort	Cat# 926-31092	Eppendorf
Trans-Blot SD Semi-Dry Transfer Cell	170-3940	BioRad
Tubes (1.5 ml, 2 ml)	Cat# 72.690.001, 72.691	Sarstedt
Ultra-Turrax D-1 disperser	N/A	Miccra GmbH
XF96 Extracellular Flux Analyzer	N/A	Agilent

Cell Lines and Bacteria	Cat#	Source
C3H10T1/2-CRISPRa(SAM)	N/A	prov. by B. Emanuelli (Lundh et al, 2017)
NEB5α competent E. coli	Cat# C2988J	NEB
NEB Stable competent E. coli	Cat# C3040I	NEB
HEK 293T	N/A	N/A

Plasmids	Cat#	Source
sgRNA(MS2) cloning backbone	Cat# 61424	Addgene
MSCV-Prdm16	Cat# 15504	Addgene
pCDH-PGK vector	Cat# 72268	Addgene
psPAX	Cat# 12260	Addgene
pMD2.G	Cat# 12259	Addgene

Deposited Data	Accession	Source
Ctcflos KD BRB-seq data	GSE169150	Gene Expression Omnibus
Ctcflos KD deep RNA-seq data	GSE169151	Gene Expression Omnibus

Software, Algorithms	Availability	Source
BLAT	(http://www.ensembl.org/Multi/Tools/Blast)	Ensembl
BLASTX	(https://blast.ncbi.nlm.nih.gov/Blast.cgi)	NCBI
Digital Image analysis	(https://www.wimasis.com/en/)	Wimasis
Genomatix Software Suite	N/A	Genomatix AG
GraphPad Prism 6	N/A	GraphPad Software
Image J	N/A	Image J
InCroMAP software	(http://www.ra.cs.uni-tuebingen.de/software/InCroMAP/index.htm)	(Wrzodek *et al*, 2013)
DEXSeq algorithm	N/A	(Anders *et al*, 2012)
SGSeq algiorithm	N/A	(Goldstein *et al.*, 2016)
Web based analysis tools		
Transite	(https://transite.mit.edu/, 06.11.2019)	(Krismer et al., 2019)
RBPmap	(http://rbpmap.technion.ac.il/ 03.03.2020)	(Paz et al, 2014)
CPC2	(http://cpc2.cbi.pku.edu.cn.)	(Kang *et al*, 2017)
CPAT	(http://lilab.research.bcm.edu/cpat/index.php)	(Wang *et al*, 2013b)
lncScore	(https://github.com/WGLab/lncScore)	(Zhao *et al*, 2016)
RNAfold web server	(http://rna.tbi.univie.ac.at/cgi-bin/RNAWebSuite/RNAfold.cgi)	(Gruber *et al*, 2008)
Transite	(https://transite.mit.edu)	(Krismer *et al*, 2019)
SFPEL-LPI	(www.bioinfotech.cn/SFPEL-LPI)	(Zhang *et al*, 2018)
R packages		
R package Factoextra	(https://cran.r-project.org/web/packages/factoextra/index.html)	CRAN.R-Project
R package GeneNet	(https://cran.r-project.org/web/packages/GeneNet/index.html)	CRAN.R-Project
R package Igraph	(https://cran.r-project.org/web/packages/igraph/index.html)	CRAN.R-Project
R package TopGO	(https://bioconductor.org/packages/release/bioc/html/topGO.html)	Bioconductor
R package tostpaired.raw	(https://cran.r-project.org/web/packages/TOSTER/index.html)	CRAN.R-Project

7 ACKNOWLEDGMENT

This work would not have been possible without the great help and support of several people, to whom I would like to express a big thank you at this point.

First of all, I want to thank Prof. Dr. Martin Klingenspor, who gave me the opportunity to do my PhD at his chair, who inspired me with his encouraging enthusiasm for science and research and who always supported me with great ideas and helpful advices.

A big thank you goes to Dr. Yongguo Li, a great scientist, who laid the basis for this project and who supported me in every step of my PhD. With his brilliant mind he always provided me with new ideas, concepts and hypothesis to think about. He guided me as colleague and mentor through project conceptualization, lab work, paper writing and a nerve-racking publication process. I learned a lot.

I also want to express a special thank you to PD Dr. Tobias Fromme, a brilliant, incredibly patient and helpful person, who not only provides great support in all scientific questions, but also does a great job as motivational coach. The same great thank you goes to Dr. Katharina Schnabl, from whom I have learned a lot, both professionally and personally, who supported me in every issue and who has become a really good friend. I am also very happy, that I could share office and lab with wonderful PhD colleagues and technicians in a great working atmosphere. I enjoyed/am enjoying the numerous constructive discussions and exchange with my office mates Josef, Thomas, Hui and Johanna and the nice company by Eva, Gloria and all other past and present colleagues in the lab. Thanks also again to Dr. Florian Bolze, who accompanied my first steps into science.

Thank you also to our collaboration partners Dr. Petra Catalina Schwalie, Prof. Dr. Bart Deplancke (EPFL Lausanne) and Dr. Peter Weber (Helmholtz Zentrum München) for their support in transcriptome sequencing and analysis, and thank you also to the students, who contributed to this work.

Zu guter Letzt gebührt ein riesiges Dankeschön natürlich meiner Familie: meinen Eltern und meiner Schwester, die immer hinter mir stehen, die mich unterstützen, mich ermutigen meinen Weg zu machen und ohne deren Rückhalt diese Arbeit nicht möglich gewesen wäre, und meinem Mann, für seine Liebe und Geduld und dass er seit 14 Jahren mit mir durch alle Höhen und Tiefen geht, mir Halt und Freude gibt und wenn nötig Seite an Seite mit mir die Nächte durcharbeitet.

8 PUBLICATIONS

Bast-Habersbrunner A, Kiefer C, Weber P, Fromme T, Schießl A, Schwalie PC, Deplancke B, Li Y, Klingenspor M (2021) LncRNA Ctcflos orchestrates transcription and alternative splicing in thermogenic adipogenesis. EMBO reports 22: e51289

Bast-Habersbrunner A, Fromme T (2020) Purine Nucleotides in the Regulation of Brown Adipose Tissue Activity. Frontiers in endocrinology 11: 118

Oeckl J, Bast-Habersbrunner A, Fromme T, Klingenspor M, Li Y (2020) Isolation, Culture, and Functional Analysis of Murine Thermogenic Adipocytes. STAR protocols 1: 100118

Fromme T, Dieckmann S, Bast-Habersbrunner A, Musiol E, Kirchinger K, Gillere R, Klemm U, Karlas A, Ntziachristos V, Scholz J, Birnbacher L, Herzen J, Simonnet S, Brecht M (2021) Filling the Gap: Entirely Beige/Brite Adipose Tissues in One of the Smallest Mammals, Suncus etruscus. The FASEB Journal 35: S1

Wang H, Willershäuser M, Li Y, Fromme T, Schnabl K, Bast-Habersbrunner A, Ramisch S, Mocek S, Klingenspor M (2020) Uncoupling protein 1 expression does not protect mice from diet-induced obesity. American journal of physiology Endocrinology and metabolism 320: E333-345

Li Y, Schwalie PC, Bast-Habersbrunner A, Mocek S, Russeil J, Fromme T, Deplancke B, Klingenspor M (2019) Systems-Genetics-Based Inference of a Core Regulatory Network Underlying White Fat Browning. Cell reports 29: 4099-4113.e4095

Li Y, Schnabl K, Gabler SM, Willershauser M, Reber J, Karlas A, Laurila S, Lahesmaa M, M UD, Bast-Habersbrunner A, Virtanen K, Fromme T, Bolze F, O'Farrell L, Alsina-Fernandez J, Coskun T, Ntziachristos V, Nuutila P, Klingenspor M (2018) Secretin-Activated Brown Fat Mediates Prandial Thermogenesis to Induce Satiation. Cell 175: 1561-1574.e1512

Klingenspor M, Bast A, Bolze F, Li Y, Maurer S, Schweizer S, Willershäuser M, Fromme T (2017) Brown Adipose Tissue. In: Adipose Tissue Biology, M. S. (ed.)Springer, Cham.:

Bolze F, Bast A, Mocek S, Morath V, Yuan D, Rink N, Schlapschy M, Zimmermann A, Heikenwalder M, Skerra A, Klingenspor M (2016a) Treatment of diet-induced lipodystrophic C57BL/6J mice with long-acting PASylated leptin normalises insulin sensitivity and hepatic steatosis by promoting lipid utilisation. Diabetologia 59: 2005-2012

Bolze F, Morath V, Bast A, Rink N, Schlapschy M, Mocek S, Skerra A, Klingenspor M (2016b) Long-Acting PASylated Leptin Ameliorates Obesity by Promoting Satiety and Preventing Hypometabolism in Leptin-Deficient Lep(ob/ob) Mice. Endocrinology 157: 233-244